Universidad de Valladolid

ESDUVa
Escuela de Doctorado Universidad de Valladolid

PROGRAMA DE DOCTORADO EN INVESTIGACIÓN BIOMÉDICA

TESIS DOCTORAL:

NOVEL HYDROGEL-FORMING ELASTIN-LIKE RECOMBINAMERS FOR BIOMEDICAL APPLICATIONS

Presentada por Arturo Ibáñez Fonseca para optar al grado de
Doctor por la Universidad de Valladolid

Dirigida por:

Dr. Francisco Javier Arias Vallejo
Dra. Matilde Alonso Rodrigo

INDEX

ABSTRACT 15

Abstract **17**

Hypotheses **22**

Objectives **24**

RESUMEN 29

1. HIPÓTESIS **31**

2. OBJETIVOS **33**

3. INTRODUCCIÓN **36**

3.1. Biomedicina y biomateriales 36

3.1.1. Biocompatibilidad 37

3.1.2. Ingeniería de tejidos y medicina regenerativa 38

3.1.2.1. Regeneración ósea 39

3.2. Recombinámeros tipo elastina (ELRs) 40

3.2.1. Diseño de ELRs con características avanzadas 40

3.2.2. Hidrogeles basados en ELRs 43

4. MATERIALES Y MÉTODOS **47**

4.1. Materiales 47

4.1.1. Reactivos 47

4.1.2. Otros materiales.....50

4.1.3. Tipos celulares.....50

4.1.4. Modelos animales 51

4.1.5. Recombinámeros tipo elastina (ELRs).....51

4.2. Métodos.....54

4.2.1. Síntesis de ELRs 54

4.2.2. Modificación química de ELRs.....55

4.2.3. Caracterización físico-química general de ELRs.....56

4.2.3.1. Análisis del nivel de endotoxinas..... 56

4.2.3.2. Electroforesis en gel de poliacrilamida con SDS (en condiciones desnaturalizantes, SDS-PAGE)..... 56

4.2.3.3. Espectrometría de masas (MALDI-TOF) 57

4.2.3.4. Análisis de aminoácidos (HPLC) 57

4.2.3.5. Calorimetría diferencial de barrido (DSC)..... 57

4.2.3.6. Resonancia magnética nuclear de protón (^{1}H-NMR) 58

4.2.4. Caracterización mecánica de hidrogeles basados en ELRs mediante medidas reológicas 58

4.2.5. Caracterización de SELRs fusionados a proteínas fluorescentes (SELR-FPs) por espectroscopía.....59

4.2.6. Caracterización de la interacción FRET entre SELR-FPs 60

4.2.6.1. Espectroscopía de fluorescencia ("quencheo" del donador) 60

4.2.6.2. Microscopía confocal ("quemado" del aceptor) 61

4.2.7. Ensayos de biodegradación enzimática *in vitro* 62

4.2.8. Cultivos celulares 63

4.2.8.1. Determinación del número de células vivas 63

4.2.9. Experimentos *in vivo* 64

4.2.9.1. Preparación e inyección subcutánea de disoluciones de ELRs en ratones 64

4.2.9.2. Medida de bioluminiscencia de Luc-hMSCs embebidas en hidrogeles basados en ELRs inyectados en ratones 66

4.2.9.3. Medida de la concentración de citoquinas en sangre de ratones 67

4.2.9.4. Extracción y procesamiento histológico de hidrogeles inyectados subcutáneamente en ratones 68

4.2.9.5. Técnicas quirúrgicas e inyección de disoluciones de ELRs en conejos 69

4.2.9.6. Tomografía computerizada multi-corte (MSCT) de fémures de conejos 70

4.2.9.7. Extracción y procesamiento histológico de tejido óseo 70

4.2.10. Análisis estadístico 71

5. RESULTADOS Y DISCUSIÓN 72

5.1. Biosíntesis y caracterización físico-química de ELRs 72

5.2. Estudio de las propiedades mecánicas de hidrogeles basados en ELRs 74

5.3. Biodegradación enzimática *in vitro* de ELRs sensibles a elastasa 76

5.4. Citocompatibilidad de ELRs 79

5.4.1. Viabilidad celular *in vitro* 79

5.4.2. Adhesión celular sobre sustratos de ELR 80

5.4.3. Proliferación celular sobre sustratos de ELR 81

5.4.4. Viabilidad celular en hidrogeles basados en ELRs inyectados *in vivo* 84

5.5. Evaluación de la biocompatibilidad *in vivo* de hidrogeles basados en ELRs 86

5.5.1. Determinación de la respuesta inflamatoria sistémica mediante la cuantificación de citoquinas en sangre 86

5.5.2. Valoración macroscópica de la estabilidad a largo plazo de los hidrogeles y de inducción de la respuesta a cuerpo extraño 88

5.5.3. Evaluación histológica de hidrogeles basados en ELRs inyectados *in vivo* 89

5.6. Evaluación de la regeneración ósea mediada por hidrogeles bioactivos basados en ELRs..... 91

5.6.1. Tomografía computerizada multi-corte (MSCT) 91

5.6.2. Resultados histológicos..... 93

5.7. Caracterización de la fluorescencia de SELR-FPs 95

5.8. Caracterización de la eficiencia de la interacción FRET entre dos SELR-FPs diferentes..... 98

6. CONCLUSIONES 104

6.1. Diseño, bioproducción y caracterización de ELRs formadores de hidrogeles 104

6.2. Biocompatibilidad de hidrogeles basados en ELRs..... 105

6.3. Regeneración ósea mediada por hidrogeles bioactivos y biodegradables basados en ELRs 106

6.4. Evaluación de la fluorescencia y de la interacción FRET entre dos SELR-FPs diferentes..... 107

7. REFERENCIAS 109

CHAPTER 1: ELASTIN-LIKE POLYMERS: PROPERTIES, SYNTHESIS AND APPLICATIONS 119

1. INTRODUCTION 121

2. ELASTIN-LIKE RECOMBINAMERs ENGINEERING, BIOPRODUCTION AND DESIGN 125

2.1. History and evolution of the synthesis of elastin-like recombinamers 125

2.1.1. Ancient times (the "chemistry ages")..... 125

2.1.2. Modern times (the "recombinant ages")..... 126

2.1.3. Contemporary times (the "seamless recursive ages")..... 127

2.2. Hosts for the expression of elastin-like recombinamers..... 131

2.2.1. Prokaryotic hosts..... 131

2.2.1.1. The gold standard: Escherichia coli 131

2.2.2. Eukaryotic hosts 133

2.2.2.1. Aspergillus nidulans fungus 133

2.2.2.2. Yeast.....134

2.2.2.3. Plants 135

2.3. Novel design of elastin-like recombinamers with different features..... 138

2.3.1. Substitution of the guest amino acid 139

2.3.2. Fusion of other protein polymers..... 140

2.3.3. Fusion of bioactive domains 141

2.3.4. Fusion of full-length proteins..... 142

3. STRUCTURES AND PHYSICAL CHARACTERISTICS OF ELASTIN-LIKE RECOMBINAMERs 144

3.1. Micelles and nanoparticles..... 145

3.2. ELR-coatings and films..... 147

3.3. ELR-based hydrogels..... 149

4. ELASTIN-LIKE RECOMBINAMERS: APPLICATIONS..... 156

4.1. ELRs for gene delivery applications..... 156

4.2. ELRs as vaccine delivery systems 158

4.3. ELR-based hydrogels for tissue engineering applications..... 162

4.4. ELRs for surface bio-functionalization 167

Abbreviations 170

References 171

CHAPTER 2: BIOCOMPATIBILITY OF TWO MODEL ELASTIN-LIKE RECOMBINAMER-BASED HYDROGELS FORMED THROUGH PHYSICAL OR CHEMICAL CROSSLINKING FOR VARIOUS APPLICATIONS IN TISSUE ENGINEERING AND REGENERATIVE MEDICINE..... 193

Abstract 195

1. INTRODUCTION..... 197

2. MATERIALS AND METHODS 200

2.1. Ethical approval..... 200

2.2. ELR biosynthesis, characterization and modification 200

2.3. Gel formation 202

2.4. Cell cultures 203

2.5. Cell proliferation experiments 204

2.6. Determination of hMSC bioluminescence *in vivo* . 205

2.7. Subcutaneous implantation and ELISA *in vivo* 206

2.8. Long-term hydrogel stability *in vivo* 207

2.9. Histological processing 208

2.10. Statistical analysis 209

3. RESULTS AND DISCUSSION 209

3.1. ELR bioproduction and characterization 209

3.2. HUVEC proliferation on ELR substrates 210

3.3. *In vivo* cell tracking and viability of hMSCs in ELR-based hydrogels 212

3.4. Evaluation of the inflammatory response mediated by ELR hydrogels *in vivo* 215

3.5. Macroscopic evaluation of the long-term stability of ELR-based hydrogels *in vivo* 218

3.6. Histological evaluation of ELR-based hydrogels injected subcutaneously 220

4. CONCLUSIONS 223

Conflict of interest **224**

Acknowledgments **224**

References **224**

Supporting information **228**

5. SUPPORTING INFORMATION **229**

CHAPTER 3: BONE REGENERATION MEDIATED BY A BIOACTIVE AND BIODEGRADABLE ECM-LIKE HYDROGEL BASED ON ELASTIN-LIKE RECOMBINAMERS.. 235

Abstract **237**

1. INTRODUCTION **239**

2. MATERIALS AND METHODS **241**

2.1. Ethical approval 241

2.2. ELR biosynthesis and characterization 242

2.3. Elastase-mediated cleavage of the ELR in solution 243

2.4. *In vitro* cell culture 244

2.5. Cell viability 244

2.6. Cell adhesion on ELR-coated tissue culture plates 245

2.7. Dissolution of the ELRs for the *in vivo* experiments 245

2.8. *In vivo* experiments 246

2.9. Multi-slice computed tomography (MSCT) 246

2.10. Bone histopathology 246

2.11. Statistical analysis 247

3. RESULTS 248

3.1. ELR biosynthesis and characterization 248

3.2. Enzymatic cleavage of ELR molecules by elastase digestion 249

3.3. hMSCs viability and integrin-mediated cell adhesion 252

3.4. Biochemical and clinical results 254

3.5. MSCT studies 254

3.6. Histopathology results 256

4. DISCUSSION 258

Acknowledgements 264

Author disclosure statement 264

References 264

5. SUPPLEMENTARY INFORMATION 272

5.1. Supplementary Methods 272

5.1.1. ELR biosynthesis and characterization 272

5.1.2. Elastase-mediated cleavage of the ELR in solution 273

5.1.3. *In vivo* experiments 273

5.1.3.1. Pre-surgical preparation *273*

5.1.3.2. Surgical procedure *274*

5.1.3.3. Post-surgical clinical studies *275*

5.2. Supplementary Figures and Tables 275

CHAPTER 4: FÖRSTER RESONANCE ENERGY TRANSFER-PAIRED HYDROGEL FORMING SILK-ELASTIN-LIKE RECOMBINAMERS BY RECOMBINANT CONJUGATION OF FLUORESCENT PROTEINS 285

Abstract 287

1. INTRODUCTION 289

2. RESULTS AND DISCUSSION 292

2.1. Fluorescent SELRs design, bioproduction and physicochemical characterization 292

2.2. Mechanical properties of hydrogels based on SELR-FPs 294

2.3. Fluorescence characterization of SELR-FPs by spectroscopy 296

2.4. Calculation of FRET efficiency in SELR-FPs mixtures by spectroscopy (donor quenching) 299

2.5. Calculation of FRET efficiency in a SELR-FP mixture by confocal microscopy (acceptor photobleaching) 302

3. CONCLUSIONS 304

4. MATERIALS AND METHODS 306

4.1. SELR-FPs design and bioproduction 306

4.2. Physicochemical characterization of pure SELR-FPs 306

4.3. Rheology of SELR-FP-based hydrogels 307

4.4. Fluorescence spectroscopy of SELR-FPs..... 308

4.5. FRET efficiency calculation through spectroscopy (donor quenching)..... 309

4.6. FRET efficiency calculation through confocal microscopy (acceptor photobleaching) 310

Acknowledgments 311

Supporting Information..... 312

Conflicts of interest..... 312

List of abbreviations 312

References 314

5. SUPPORTING INFORMATION 319

Table of contents 319

FUTURE DIRECTIONS AND CONCLUSIONS 331

Future directions 333

1. ELR-based hydrogels for skeletal muscle regeneration..... 333

2. Investigation of pore dynamics in SELR-based hydrogels 337

References 343

Conclusions 345

1. Genetic engineering, bioproduction and characterization of hydrogel-form ing ELRs 345

2. Biocompatibility of ELR-based hydrogels 346

3. Bone regeneration mediated by bioactive and biodegradable hydrogels based on ELRs 347

4. Fluorescence and FRET evaluation of two different SELR-FPs 348

APPENDIX 351

Abbreviations 353

Table of standard amino acid abbreviations 355

Publications 356

Congresses and conferences 359

Other contributions 362

ABSTRACT

Abstract

There is an increasing interest in developing advanced biomaterials with improved biocompatibility and functionality that might find uses in the field of biomedicine, for example in tissue engineering and regenerative medicine (TERM). Nowadays, recombinant polypeptides or polymers are one of the most prominent types of biomaterials, due to their nature. They are obtained through recombinant DNA technology, which allows the controlled biosynthesis of tailored polypeptides that may be designed to include combinations of polymeric amino acid sequences and/or bioactive domains. Within this type of biomaterials we can find elastin-like polypeptides (ELPs), which have also been recently termed elastin-like recombinamers (ELRs), according to their recombinant origin. These ELRs are composed of repetitions of the VPGXG (Val-Pro-Gly-X-Gly) pentapeptide, in which X (guest residue) can be any amino acid expect L-Proline. This composition confers the ELRs a smart behaviour of thermoresponsiveness defined by the so-called Inverse Temperature Transition (ITT) occurring above the Transition Temperature (T_t), which implies a phase transition of the dissolved ELR when this T_t is reached. Therefore, this thermal response is of great interest, since it has been shown to promote the formation of different structures, such as hydrogels that mimic the extracellular matrix, at the physiological temperature, whereas an ELR solution can be easily handled (e.g. injected *in vivo*) below the T_t. Furthermore, the T_t can be modulated depending on the polarity of the side chain of the amino acid chosen as guest residue. Moreover,

if this residue contains functional goups, it can also be used for further chemical modifications in order to achieve, for instance, chemically (covalently) cross-linked hydrogels.

Lately, different types of ELRs have shown potential applications in TERM. However, the general biocompatibility of these ELRs and of the hydrogels based on them has not been extensively studied to date. Thus, it is one of the aims of this Thesis to evaluate whether two types of hydrogels based on ELRs (physically or chemically cross-linked) are biocompatible or not by use of wide-ranging methods, hence being suitable for TERM applications. For this purpose, the *in vitro* cytocompatibility was studied by culturing endothelial cells on ELR substrates, showing optimal proliferation up to 9 days. Regarding *in vivo* cytocompatibility, luciferase-expressing human mesenchymal stem cells (Luc-hMSCs) were viable for at least 4 weeks in terms of bioluminescence emission when embedded in ELR-based hydrogels and injected subcutaneously into immunosuppressed mice. Furthermore, both types of ELR-based hydrogels were injected subcutaneously in immunocompetent mice and serum TNFα, IL-1β, IL-4, IL-6 and IL-10 concentrations were measured by ELISA, confirming the lack of inflammatory response, as also observed upon macroscopic and histological evaluation. All these findings suggest that both types of ELRs possess broad biocompatibility, thus making them very promising for TERM-related applications.

Once the biocompatibility of ELR-based hydrogels was confirmed, novel ELRs were specifically designed and bioproduced to promote optimal bone regeneration, taking into account the

increasing morbidity of bone fractures and defects due to changes in the age pyramid, and the limitations in the use of auto-, allo-, and xenografts. In order to assess this hypothesis, an ELR containing RGD (Arg-Gly-Asp) cell-adhesion sequences and another one fused to the osteogenic bone morphogenetic protein-2 (BMP-2) were used to form injectable physically cross-linked hydrogels. Moreover, elastase-sensitive domains were included in both ELR molecules, thereby conferring biodegradation as a result of enzymatic cleavage and avoiding the need for scaffold removal after bone regeneration. Both ELRs and their combination showed excellent *in vitro* cytocompatibility, and the culture of cells on RGD-containing ELRs resulted in optimal cell adhesion. In addition, hydrogels based on a mixture of both ELRs were implanted in a pilot study involving a femoral bone injury model in New Zealand White rabbits, showing complete regeneration in six out of seven cases, with the other showing partial closure of the defect. Moreover, bone neo-formation was confirmed using different techniques, such as radiography, computed tomography and histology. Therefore, this hydrogel system therefore displays significant potential in the regeneration of bone defects, promoting self-regeneration by the surrounding tissue with no involvement of stem cells or osteogenic factors other than BMP-2, which is released in a controlled manner by elastase-mediated cleavage from the ELR backbone.

On the other hand, it was also proposed that the fusion of fluorescent proteins (FPs) to ELRs that include silk-like domains (thus termed silk-elastin-like recombinamers or SELRs), which further stabilize the ELR-based hydrogels, would confer fluorescence to the hydrogels, hence improving their traceability if

used to produce biomedical devices for potential TERM applications. In this Thesis, we fused two different fluorescent proteins (FPs), i.e. the green *Aequorea coerulescens* EGFP (AcEGFP) and the near-infrared eqFP650, to a SELR able to form irreversible hydrogels through physical cross-linking. These recombinamers showed an emission of fluorescence similar to the single FPs, and they were capable of forming hydrogels with different stiffness (G' = 60-4000 Pa), by varying the concentration of the SELR-FPs. These results support the hypothesis, suggesting that a combination of these SELRs with other SELRs including different bioactivities, such as cell adhesion, may provide a biomimetic scaffold that is also liable to be tracked *in vivo* by non-invasive fluorescence measurements, which is a starting point for further work in this regard. In addition, the absorption spectrum of SELR-eqFP650 showed a peak greatly overlapping the emission spectrum of the SELR-AcEGFP. New possibilities arose from this finding, since this overlap could enable Förster resonance energy transfer (FRET) upon the interaction between two SELR molecules, each one containing a different FP. FRET has been defined to take place at a distance of less than 10 nm between the donor (in this case SELR-AcEGFP) and the acceptor (SELR-eqFP650), the latter inducing the quenching of the donor. The interaction between both SELR-FPs (i.e. reducing the distance below 10 nm) might be driven by the self-assembly of the elastin-like domains above the T_t, and by the stacking of silk domains at any temperature. This effect was studied by different methods and a FRET efficiency of 0.06-0.2 was observed, depending on the technique used for its calculation. Therefore, biosensing applications may derive by taking advantage

of the FRET occurring between both SELR-FPs through the development of ratiometric biosensors by including amino acid sequences that bind to different targets using genetic engineering methods.

In summary, the work showed in this Thesis provides new insights about hydrogel-forming ELRs designed to be used in biomedical applications. Specifically, it describes the physico-chemical characterization of several novel ELRs, and confirms the biocompatibility of two types of hydrogels based on these ELRs. Furthermore, bone regeneration has shown to be optimized by the use of ELR-based hydrogels. On the other hand, basic characterization of the fluorescence emitted by SELR-FPs provide evidence about the feasibility of constructing biomedical devices that include them, in order to improve their traceability *in vivo*. Moreover, the finding of a FRET interaction sets the basis for further use as ratiometric biosensors upon improvement of the SELR functionality through incorporation of target-binding domains by recombinant DNA technology.

Hypotheses

1. The use of genetic engineering techniques and recombinant expression in *Escherichia coli* allows the biosynthesis of elastin-like recombinamers (ELRs), which, if specifically designed, are able to form hydrogels that possess potential biomedical applications, taking advantage of their thermosensitivity.

2. Hydrogels based on specifically designed ELRs show functionalities that promote their biocompatibility, such as interaction with cells via adhesion domains that improve the biomimetic features of these scaffolds.

3. The genetic fusion of growth factors, like the bone morphogenetic protein-2 (BMP-2), to hydrogel-forming ELRs, in combination with ELRs that comprise cell adhesion motifs, induce the repair of a bone defect. The inclusion of amino acid sequences sensitive to proteases, such as elastase, permits the replacement of the hydrogels for regenerated tissue.

4. The design and recombinant bioproduction of silk-elastin-like recombinamers (SELRs) genetically bioconjugated to fluorescent proteins (FPs) adds new features to those SELRs, and also to the hydrogels based on them, improving their *in vivo* traceability by non-invasive methods. On the other hand, the combination of a donor FP (e.g. the enhanced green fluorescent protein or EGFP) and an acceptor one (e.g. the far-red fluorescent protein eqFP650) in the same scaffold promotes the interaction through Förster resonance energy transfer

(FRET), increasing the number of potential applications in the fields of biomedicine and biosensing.

Objectives

1. The general objective of this Thesis is the development of novel smart biomaterials that allow the formation of bioactive hydrogels, which may be used in various biomedical applications. For this purpose, we intend to employ different elastin-like recombinamers (ELRs) with features inherent to advanced biomaterials, such as thermosensitivity. Moreover, their physicochemical and biological properties can be easily modulated through changes in the amino acid sequence, due to their recombinant origin.

2. The first specific aim of the Thesis is to design and bioproduce novel hydrogel-forming bioactive ELRs through recombinant DNA technology, using *Escherichia coli* as heterologous host. Furthermore, they will be characterized by different methods, such as mass spectrometry and differential scanning calorimetry. Specifically, we will try to obtain ELR-based hydrogels that simulate the extracellular matrix in terms of cytocompatibility by the inclusion of cell adhesion motifs through genetic engineering. On the other hand, we expect to form osteogenic hydrogels that induce bone regeneration by fusing the gene of the bone morphogenetic protein-2 (BMP-2) into the ELR one, being also sensitive to elastasa-mediated biodegradation. Likewise, we intend to get fluorescent hydrogels that may improve the traceability of biomedical devices made by them, and that may be also used in the development of biosensors.

3. Secondly, we aim to evaluate the biocompatibility of different types of ELR-based hydrogels, being stabilized either by chemical (covalent bonds) or by physical cross-linking (non-covalent interactions triggered by a physical stimulus, such as a temperature increase). To that end, it will be necessary to use animal models that permit to elucidate the interaction between ELR-based hydrogels and living tissues. In addition, we will perform cell culture experiments to test cytocompatibility, both *in vitro* and *in vivo*, in this case embedding cells within the hydrogels.

4. On the other hand, once the biocompatibility has been evaluated, we intend to assess the bone regeneration of a well-established bone defect in an animal model, promoted by ELR-based hydrogels. In this case, two different ELRs will be used for hydrogel formation, namely an ELR fused to BMP-2 and the other one including cell adhesion (RGD) domains. First, the biodegradation of both bioactive ELRs, which include elastase-sensitive motifs, together with their cytocompatibility, will be verified *in vitro*. Then, it will be necessary to confirm the improved bone regeneration mediated by ELR-based hydrogels *in vivo*, by the use of different techniques, such as computed tomography or histopathology.

5. Finally, we aim to determine the fluorescent properties of two SELRs, one fused to the *Aequorea coerulescens* green fluorescent protein (AcEGFP) and the other one to the far-red fluorescent protein named eqFP650. This study will be performed by spectroscopy, comparing both fluorescent SELRs

with their single FP counterparts. Furthermore, we want to evaluate the feasibility of Förster resonance energy transfer (FRET) between both SELRs at different concentrations and temperatures. For this purpose, we will use hydrogels (high SELR concentration) and solutions (low SELR concentration) based on a combination of the fluorescent SELRs. Then, they will be measured by different methods, such as spectroscopy and confocal microscopy, taking advantage of a FRET consequence, namely the "quenching" of the donor fluorophore in the presence of the acceptor one. In this study, the donor would be the SELR fused to AcEGFP, while the acceptor would be the one that includes eqFP650.

RESUMEN

1. HIPÓTESIS

1. El uso de técnicas de ingeniería genética estandarizadas, así como de métodos de bioproducción en *Escherichia coli*, permiten la biosíntesis de recombinámeros tipo elastina ("elastin-like recombinamers", ELRs, en inglés), capaces de formar hidrogeles con potenciales aplicaciones biomédicas, aprovechando su termosensibilidad.

2. Los hidrogeles formados a partir de ELRs con diseños específicos presentan funcionalidades que promueven su biocompatibilidad, tales como la interacción con células y tejidos a través de secuencias de adhesión celular, que mejoran las características biomiméticas de estos "scaffolds".

3. La fusión de factores de crecimiento, como la proteína morfogenética de hueso-2 (BMP-2), a ELRs formadores de hidrogeles, en combinación con ELRs que incluyen secuencias de adhesión celular, induce la reparación de un tejido óseo dañado. La inserción de secuencias de aminoácidos que son reconocidas por proteasas, como la elastasa, permite la sustitución de los hidrogeles por tejido regenerado.

4. El diseño y bioproducción recombinante de recombinámeros tipo elastina y seda ("silk-elastin-like recombinamers", SELRs, en inglés) fusionados a proteínas fluorescentes ("fluorescent proteins", FPs, en inglés) añade nuevas propiedades a los mismos, así como a los hidrogeles formados a partir de ellos, mejorando su trazabilidad *in vivo* mediante técnicas poco invasivas. Por otro lado, la combinación de una FP donadora

(por ejemplo, la proteína verde fluorescente mejorada ó EGFP) y una aceptora (como la proteína roja fluorescente eqFP650) en la misma estructura promueve la interacción mediante transferencia de energía por resonancia de Förster (FRET), incrementando el número de potenciales aplicaciones en el campo de la biomedicina y de los biosensores.

2. OBJETIVOS

1. El objetivo general de esta tesis es el desarrollo de nuevos biomateriales inteligentes que permitan la formación de hidrogeles bioactivos que puedan ser utilizados en diversas aplicaciones en el campo de la biomedicina. Para ello, se pretende hacer uso de diversos recombinámeros tipo elastina ("elastin-like recombinamers", ELRs, en inglés), con características propias de biomateriales avanzados, tales como la sensibilidad a cambios de temperatura y/o de pH, y la posibilidad de modular fácilmente sus propiedades físico-químicas y biológicas a través de modificaciones en la secuencia primaria de aminoácidos, debido a su naturaleza recombinante.

2. El primer objetivo específico consiste en el diseño y bioproducción de nuevos ELRs bioactivos formadores de hidrogeles, mediante técnicas de ingeniería genética y expresión heteróloga en *Escherichia coli*, y la caracterización de todos los ELRs utilizados en esta tesis. En concreto, se pretende obtener hidrogeles basados en ELRs que simulen la matriz extracelular en términos de citocompatibilidad y distintas funcionalidades a través de la fusión genética de secuencias de adhesión celular. Por otro lado, se quiere conseguir hidrogeles osteogénicos que promuevan la regeneración de tejido óseo por la inclusión de la proteína morfogenética de hueso (BMP-2), y que además sean susceptibles de ser degradados por acción de la enzima elastasa. Asimismo, se persigue lograr la formación de hidrogeles fluorescentes que permitan una mejor

trazabilidad de dispositivos biomédicos en los que se incluyan, además del desarrollo de biosensores.

3. En segundo lugar, se pretende evaluar la biocompatibilidad de distintos tipos de hidrogeles basados en ELRs, uno estabilizado mediante entrecruzamiento químico (enlaces covalentes) y otro por entrecruzamiento físico (interacciones no covalentes desencadenadas por un estímulo físico, en este caso la temperatura). En este apartado, es necesario el uso de modelos animales que permitan elucidar la interacción entre los hidrogeles formados por ELRs y los tejidos vivos, así como la utilización de cultivos celulares, tanto *in vitro* como *in vivo*, que faciliten un estudio sistemático de la citocompatibilidad de los ELRs y los hidrogeles biofuncionales derivados de los mismos.

4. Por otro lado, una vez determinada la biocompatibilidad, se quiere determinar la regeneración ósea mediada por hidrogeles basados en ELRs en un modelo animal preestablecido de defecto femoral controlado. En primer lugar, se requiere comprobar la biodegradación de una mezcla de dos ELRs diseñados para promover la formación de hueso que contienen secuencias sensibles a elastasa, así como su citocompatibilidad *in vitro*. A continuación, es necesaria la aplicación *in vivo* del hidrogel generado a partir de dos ELRs bioactivos, uno con secuencias de adhesión celular y otro con la BMP-2, para certificar la mejora en la regeneración, gracias a este hidrogel, mediante diversas técnicas, como la tomografía computerizada o la histología.

5. Por último, se pretende evaluar las propiedades de fluorescencia de dos SELRs, uno de ellos fusionado a una proteína verde fluorescente (AcEGFP) y el otro a una roja (eqFP650). Dicha evaluación se llevará a cabo mediante espectroscopía, realizándose una comparación de las mismas con las de las proteínas fluorescentes originales. Además, se quiere determinar la posible existencia de un efecto de transferencia de energía de resonancia de Förster (FRET), entre ambos SELRs a distintas concentraciones y temperaturas. Para ello se trabajará tanto en forma de hidrogeles mixtos como en disolución, y mediante distintos métodos como espectroscopía y microscopía confocal, aprovechando un fenómeno observado en FRET, denominado "quencheo" del fluoróforo donador en presencia del aceptor. En este estudio, el donador sería el SELR que incluye la AcEGFP, mientras que el aceptor sería el que contiene la eqFP650.

3. INTRODUCCIÓN

3.1. Biomedicina y biomateriales

El continuo afán del ser humano por encontrar tratamientos más efectivos frente a las distintas enfermedades que le afectan, así como la ingente cantidad de conocimiento generado en las últimas décadas, ha promovido la aparición de nuevos campos de investigación derivados de la medicina, englobando muchas otras ramas de la ciencia, tales como la bioquímica, la inmunología y la biotecnología, traduciéndose en lo que hoy denominamos biomedicina (1). Esta emergente área de investigación pretende desarrollar sistemas que permitan una mejora, tanto en el diagnóstico como en el tratamiento, de distintos problemas de salud. De este modo, en los últimos años ha existido una ferviente búsqueda de dispositivos biomédicos que sean capaces de, por ejemplo, mejorar la regeneración de defectos tisulares (2), permitir su trazabilidad *in vivo* mediante técnicas mínimamente invasivas (3), o ser utilizados como biosensores para un diagnóstico más avanzado de diversas enfermedades (4).

Dentro de las distintas estrategias destinadas al desarrollo de aplicaciones biomédicas, se puede encontrar el uso de biomateriales, cuya definición ha evolucionado desde su concepción primigenia, hasta llegar a la propuesta por D.F. Williams en 2009, que tiene en cuenta los avances conseguidos en los últimos tiempos (5):

> "Un biomaterial es una sustancia que ha sido diseñada para adquirir una forma tal que, por sí misma o como

> parte de un sistema complejo, es utilizada para dirigir, mediante el control de las interacciones con los componentes de los sistemas vivos, el curso de cualquier procedimiento terapéutico o diagnóstico, en medicina de humanos o veterinaria".

Sin embargo, tradicionalmente se han utilizado biomateriales que podrían considerarse básicos a nivel de funcionalidad, entre los cuales cabe mencionar distintos metales (6) y cerámicas (7), que vienen siendo aplicados en clínica desde las primeras grandes civilizaciones (8). Posteriormente, a mediados del siglo XX, la ciencia de los (bio)materiales experimentó un gran impulso con el desarrollo de polímeros sintéticos, como el ácido poli(láctico-co-glicólico) (PLGA) o el ácido poliláctico (PLLA) (9, 10), y naturales, como por ejemplo el alginato o la seda (11, 12), que, pese a presentar un gran avance, seguían teniendo carencias a nivel de funcionalidad y biocompatibilidad. Por estos motivos, en los últimos años, el esfuerzo de muchos investigadores se ha dirigido al desarrollo de nuevos biomateriales, incluyendo polímeros proteicos obtenidos mediante la tecnología del ADN recombinante, los cuales ofrecen una mejora significativa en su funcionalidad al poder regularse de forma muy controlada la inclusión de secuencias bioactivas (13).

3.1.1. Biocompatibilidad

La definición más reciente del término "biocompatibilidad" hace referencia a "la capacidad de un biomaterial de llevar a cabo la función deseada referida a una terapia médica, sin promover ningún efecto local o sistémico no deseado en el que recibe dicha

terapia, sino generando la respuesta tisular o celular beneficiosa más apropiada en esa situación específica, y optimizando el desempeño clínicamente relevante de esa terapia" (14). Sin embargo, existe cierta tendencia en el campo de los biomateriales a definir la biocompatibilidad de un modo más general, entendiendo que un material es biocompatible si cumple ciertos requisitos, como ser citocompatible (tanto *in vitro* como *in vivo*), no promover una respuesta inflamatoria aguda o crónica grave, interaccionar con los tejidos circundantes de manera similar a como los tejidos interaccionan entre sí, y no inducir una respuesta a cuerpo extraño (que conlleva la formación de tejido fibrótico), entre otras propiedades. Por tanto, todos los nuevos biomateriales que pretendan ser aplicados en ingeniería de tejidos y/o medicina regenerativa, como los hidrogeles basados en ELRs, deben demostrar no sólo su funcionalidad *in vitro*, sino también cierto grado de biocompatibilidad en los términos generales definidos aquí.

3.1.2. Ingeniería de tejidos y medicina regenerativa

La ingeniería de tejidos está íntimamente relacionada con la ciencia de los biomateriales, enmarcándose, además, dentro de la biomedicina. Puede definirse como la generación de sustitutos funcionales de tejidos dañados, mediante la aplicación de principios de biología e ingeniería, como, por ejemplo, la combinación de andamiajes o matrices sintéticas, células vivas y moléculas biológicamente activas o fármacos, que permitan la formación de un tejido lo más similar posible al que debe ser sustituido (15). Por otro lado, la medicina regenerativa englobaría a la ingeniería de

tejidos, pero a menudo se relaciona más con el uso de biomateriales para la promoción de los sistemas de regeneración endógenos del organismo, mediante el implante de biomateriales, células, factores, o combinaciones de ellos, que induzcan un proceso de regeneración tisular óptimo, sin utilizar tales medios como sustitutos del tejido dañado (16).

3.1.2.1. Regeneración ósea

Los cambios producidos en los últimos años en la pirámide poblacional, hacia un mayor número de personas de edad avanzada, ha aumentado la morbilidad de enfermedades óseas, como las fracturas de hueso (17) o la osteoporosis (18). Sin embargo, pese al creciente número de biomateriales disponibles, el uso de hueso autólogo es hoy la primera opción para el reemplazamiento de tejido óseo dañado. El inconveniente principal reside en la dificultad de conseguir un biomaterial que sea ostoinductivo, es decir, que induzca la diferenciación de células progenitoras a osteoblastos; osteoconductivo, favoreciendo el crecimiento del tejido óseo sano circundante, y osteointegrativo, esto es, que el tejido regenerado sea capaz de integrarse con el pre-existente (19). Además, en el caso de aplicar un biomaterial para medicina regenerativa, este debe ser capaz de estimular una respuesta celular óptima (bioactivo) y de ser reemplazado por el tejido formado *de novo*, siendo, por tanto, biodegradable, y actuando como un sustituto provisional (20, 21).

3.2. Recombinámeros tipo elastina (ELRs)

Dentro de esta nueva clase de biomateriales recombinantes podemos encontrar los recombinámeros tipo elastina ("elastin-like recombinamers", ELRs, en inglés) (22), cuya composición, inspirada en la secuencia de aminoácidos de la elastina natural, una proteína de la matriz extracelular que confiere elasticidad a los tejidos, está basada en la repetición del pentapéptido L-Valina-L-Prolina-Glicina-X-Glicina (VPGXG, usando la terminología de una letra para aminoácidos), en el que X (denominado aminoácido invitado) puede ser cualquier residuo, excepto L-Prolina. La propiedad más característica de los ELRs es la termosensibilidad, que conlleva un cambio reversible en la conformación espacial de estos polipéptidos, sufriendo una transición de temperatura inversa ("Inverse Temperature Transition", ITT, en inglés) (23) por encima de la denominada Temperatura de Transición (T_t), la cual depende de la polaridad de la cadena lateral del aminoácido invitado (24). En un medio acuoso, las moléculas de ELR se mantendrán solubles por debajo de la T_t, mientras que por encima de esa temperatura se auto-ensamblarán en estructuras supramoleculares por interacciones hidrofóbicas, dando lugar a distintos tipos de estructuras, desde partículas (25) a hidrogeles (26). Puede encontrarse una explicación más detallada del mecanismo de transición de los ELRs en el Capítulo 1 de esta tesis.

3.2.1. Diseño de ELRs con características avanzadas

Debido a su carácter recombinante, es posible fusionar secuencias de ADN que codifican distintos péptidos y proteínas

presentes en las secuencias propias de los ELRs, así como combinar secuencias de pentapéptidos con distintos aminoácidos invitados en la misma molécula de ELR, obteniendo así un biomaterial con funcionalidad avanzada, de una forma sencilla, mediante técnicas de ingeniería genética (27). De este modo, se puede hablar de ELRs "hechos a medida" para aplicaciones específicas.

Dentro de las múltiples posibilidades, la inclusión de secuencias repetitivas derivadas de otras proteínas poliméricas, como la fibroína de la seda del gusano *Bombyx mori*, permite combinar la rigidez y alta estabilidad de esta proteína con la elasticidad inherente a los ELRs, dando lugar a los recombinámeros tipo elastina y seda ("silk-elastin-like recombinamers", SELRs, en inglés). Además, de este modo se obteniene una mejora en las propiedades estructurales de las distintas formas derivadas del auto-ensamblaje, como, por ejemplo, hidrogeles (28).

Por otro lado, en aras de una mejora en la funcionalidad, es posible añadir distintas secuencias bioactivas que induzcan una determinada interacción con las células que componen el "nicho" o microambiente en el cual se pretenden implantar los ELRs. En este sentido, la fusión del tripéptido Arginina-Glicina-Aspártico (RGD), presente en la fibronectina y en otras proteínas de la matriz extracelular (29, 30), permitiría la adhesión celular a los ELRs de forma general en múltiples tipos celulares, preferentemente vía integrinas del tipo $\alpha_5\beta_1$ y $\alpha_v\beta_3$ (31). Así, las distintas estructuras basadas en ELRs tendrían una mejor interacción con las células, promoviendo su adhesión y, por tanto, su proliferación celular, de un modo mucho más biomimético, simulando las características de la matriz extracelular (32).

Con el objetivo de utilizar los ELRs en aplicaciones más específicas, se pueden fusionar factores de crecimiento, como la proteína morfogénetica de hueso-2 ("bone morphogenetic protein-2", BMP-2, en inglés) (33), la cual ha demostrado su capacidad de promover la regeneración de tejido óseo dañado (34), confiriendo así propiedades osteoinductivas a los ELRs.

Del mismo modo, la inclusión de secuencias de degradación enzimática, como las que son reconocidas por la elastasa, que contienen el hexapéptido L-Valina-Glicina-L-Valina-L-Alanina-L-Prolina-Glicina (VGVAPG), y cuya L-Alanina le confiere la sensibilidad enzimática (35), permitiría mejorar la biodegradabilidad de los ELRs, lo cual debería suceder en paralelo al proceso terapéutico, como por ejemplo, el de regeneración tisular.

Asimismo, la fusión de proteínas fluorescentes ("fluorescent proteins", FPs, en inglés) mejoraría la trazabilidad de los ELRs una vez implantados en el organismo a lo largo del tiempo, permitiendo su visualización con equipos específicos de medida de fluorescencia *in vivo*. Dentro de las FPs, el caso más utilizado en biología molecular es el de la proteína verde fluorescente ("green fluorescent protein", GFP, en inglés) y sus derivadas, como, por ejemplo, la GFP mejorada de *Aequorea coerulescens* (AcEGFP) (36, 37). Sin embargo, el uso de esta proteína en aplicaciones *in vivo* está muy limitada por el hecho de que existe una auto-fluorescencia en el rango de longitudes de onda de emisión de la GFP/AcEGFP, producida por moléculas endógenas, como la hemoglobina, presentes en los distintos tejidos de los organismos vivos, produciéndose una relación señal-ruido muy baja (38). Por tanto,

es de gran utilidad la utilización de FPs que emitan en el rango del rojo lejano (a partir de 600-650 nm), en el cual no se da esta auto-fluorescencia. Dentro de este tipo de FPs podemos encontrar la eqFP650, expresada por la anémona *Entacmaea quadricolor*, y que ha sido descrita como la FP más brillante por encima de los 635 nm (39).

No obstante, la fusión de FPs a las secuencias de ELR (dando lugar a ELR-FPs) no sólo permite una mejora en la trazabilidad del biomaterial, sino que añade otras posibilidades de aplicación, teniendo en cuenta la versatilidad de las técnicas de espectroscopía y microscopía de fluorescencia. En este sentido, se podría explorar la interacción entre dos moléculas de ELR que expresen dos FPs diferentes, mediante transferencia de energía de resonancia de Förster ("Förster resonance energy transfer", FRET, en inglés), cuya eficiencia es alta cuando se cumplen tres supuestos: 1) distancia de 1-10 nm entre el fluoróforo (en este caso una FP) donador y el aceptor, 2) alineamiento dipolo-dipolo favorable, y 3) solapamiento del espectro de emisión de la FP donadora y el de excitación de la aceptora (40). A efectos prácticos, el fenómeno FRET supone una disminución en la intensidad de fluorescencia emitida por la FP donadora en presencia de la aceptora, lo cual se puede medir tanto por métodos espectrométricos ("quencheo" del donador o "donor quenching", en inglés) como de microscopía confocal ("quemado" del aceptor o "acceptor photobleaching", en inglés) (41).

3.2.2. Hidrogeles basados en ELRs

Los hidrogeles son estructuras tridimensionales capaces de retener altos porcentajes de agua, basados en materiales

poliméricos cuyas moléculas se entrecruzan mediante uno o varios tipos de interacciones intermoleculares, estabilizando la red que los conforma (42). En los últimos años, estas estructuras han sido el foco de un gran interés por parte de la comunidad científica dedicada a la investigación en los campos de la ingeniería de tejidos y la medicina regenerativa debido a sus características, entre las cuales cabe reseñar la capacidad de inmovilizar y liberar de forma controlada células, genes, y fármacos en general, así como de proveer un andamiaje similar a la matriz extracelular, con un contenido en agua similar a la misma, en el cual las células son capaces de migrar y en el que los tejidos pueden integrarse (43). Además, el hecho de que existan hidrogeles inyectables, es decir, que permiten ser introducidos en el organismo mediante un método mínimamente invasivo como es una inyección, hace que tengan un potencial enorme en el campo de la regeneración tisular, al evitar intervenciones quirúrgicas para su implantación (43). Dentro de los hidrogeles inyectables se incluyen aquellos basados en ELRs, puesto que al mantener la temperatura por debajo de la T_t las moléculas de ELR permanecen solubles y esa disolución puede ser inyectada. Una vez en contacto con el organismo, y suponiendo que en su diseño se haya tenido en cuenta una T_t menor a la temperatura corporal, las moléculas de ELR transicionarán formando un hidrogel estabilizado por interacciones hidrofóbicas (26).

De este modo, se han diseñado nuevos ELRs, todos ellos con una estructura de bloques, por lo cual son usualmente denominados co-recombinámeros tipo elastina en bloques (“elastin-like block co-combinamers”, ELbcR, en inglés). Este diseño permite combinar repeticiones de pentapéptidos VPGXG con distintos aminoácidos

invitados. Concretamente, en este trabajo se han utilizado ELbcRs anfifílicos, es decir, que combinan bloques hidrofílicos (polares) e hidrofóbicos (apolares). En el primer caso, el aminoácido elegido como residuo invitado ha sido el L-Ácido glutámico (E, en código de una letra), que, además, confiere carga negativa al pentapéptido, al contener un grupo carboxilo en su cadena lateral. Por otro lado, en el bloque hidrofóbico se ha sustituido el aminoácido en cuarta posición por una L-Isoleucina (I), con una cadena lateral apolar. Por consiguiente, en el ELbcR final se encuentran dos dominios marcados, uno hidrofílico cuya T_t estará por encima de la temperatura fisiológica, y otro hidrofóbico con una T_t menor a 37 ºC. Esta construcción ha sido diseñada previamente, demostrando la capacidad de formar hidrogeles (44). En un trabajo posterior, se demostró que la estabilidad de estos hidrogeles aumentaba considerablemente mediante la fusión de secuencias repetitivas derivadas de la fibroína de la seda de *B. mori*, específicamente el hexapéptido Gly-L-Ala-Gly-L-Ala-Gly-L-Ser (GAGAGS), por lo que se han incluido en algunos de los ELbcRs utilizados en este trabajo, pasándose a denominar SELRs (28).

Por tanto, con el objetivo de comprobar las hipótesis planteadas en esta tesis doctoral, se han desarrollado nuevos ELRs avanzados, derivados de un ELbcR y un SELR (resultado de la modificación del primero) generados previamente, capaces de formar hidrogeles, mediante la fusión de secuencias bioactivas de adhesión celular, concretamente el “loop” de 12 aminoácidos que contiene el tripéptido RGD que promueve la adhesión celular, como se ha comentado anteriormente; de osteogénesis (BMP-2), y la

inclusión de proteínas fluorescentes, en particular la proteína verde AcEGFP y la roja eqFP650.

Por otro lado, la inclusión de aminoácidos invitados con grupos funcionales en su cadena lateral, susceptibles de ser modificados para una mayor reactividad, tales como la lisina, que contiene un grupo ε-amino, permite la formación de hidrogeles con entrecruzamiento químico, es decir, estabilizados por enlaces covalentes entre las cadenas que lo componen (45), tal y como se encuentra en la naturaleza, por la acción de las distintas isoformas de la enzima lisil oxidasa (46).

4. MATERIALES Y MÉTODOS

4.1. Materiales

4.1.1. Reactivos

Los reactivos utilizados en el transcurso de esta tesis se pueden observar en la **Tabla 1**.

Tabla 1. Reactivos utilizados en el transcurso de la presente tesis doctoral.

Reactivo	Proveedor
AcGFP1	Clontech
Ácido clorhídrico	Fisher Scientific
Ácido etilendiaminatetraacético (EDTA)	Sigma-Aldrich
Acrilamida/Bis-acrilamida 37,5:1 40% (p/v)	Amresco
AEBSF	Apollo Scientific
Agar	BD
Agarosa Seakem	Cambrex
Agua ultra-pura (MilliQ)	Millipore
Antiespumante 204	Sigma-Aldrich
Ampicilina	Apollo Scientific
Azul de bromofenol	Sigma-Aldrich
Calceína-AM	Invitrogen

Cloruro de cobre	Sigma-Aldrich
Cloruro de sodio (NaCl)	Fisher Scientific
Dimetilsulfóxido deuterado (DMSO-d_6)	Sigma-Aldrich
Dodecilsulfato sódico (SDS)	Sigma-Aldrich
E-64	Apollo Scientific
Elastasa pancreática porcina (Ref. E1250)	Sigma-Aldrich
Enzimas de restricción (*Sap*I, *Ear*I, *Eco*RI, *Dpn*I) y otras enzimas (T4 DNA ligasa, FastAP, SAP)	Thermo Scientific
Etanol	Panreac
Fluoruro de fenilmetilsulfato (PMSF)	Apollo Scientific
Gentamicina/Anfotericina	Gibco
Glicerol	Fisher Scientific
Glicina	Sigma-Aldrich
Glucosa	Panreac
Hematoxilina-eosina	Sigma-Aldrich
Hidróxido de sodio (NaOH)	Fisher Scientific
Kit de purificación de plásmidos "NucleoSpin Plasmid"	Macherey-Nagel
Kit de extracción de ADN en geles de agarosa "PureLink Quick Gel Extraction"	Invitrogen
Kits ELISA (TNFα, IL-1β, IL-4, IL-6, IL-10)	Thermo Scientific
Leupeptina	Apollo Scientific

Lipopolisacárido bacteriano (LPS)	Sigma-Aldrich
Marcador de ADN 1kb Plus Ladder	Invitrogen
Marcador de proteínas "Pierce Unstained"	Thermo Scientific
Medio de cultivo de auto-inducción "Terrific" (TB)	Formedium
Medio de cultivo de lisogenia (Luria Bertani, LB)	Conda
Medios de cultivo (DMEM 1g/L glucosa, Medium 200)	Gibco
Parafina	Sigma-Aldrich
Paraformaldehído	Sigma-Aldrich
Penicilina/Estreptomicina	Gibco
Pepstatina A	Apollo Scientific
Persulfato de amonio	Sigma-Aldrich
Suero fetal bovino (FBS)	Gibco
Sulfato de amonio	Fisher Scientific
Suplemento de crecimiento con bajo suero (LSGS)	Gibco
Tampón fosfato salino (PBS)	Gibco
Tetrametiletilendiamina (TEMED)	Sigma-Aldrich
Tinción de ADN "SimplySafe"	Eurx
Tripsina/EDTA 0.05%	Gibco

Tris(hidroximetil)aminometano (Tris)	Sigma-Aldrich
Tritón X-100	Sigma-Aldrich
Trypan blue	Invitrogen
TurboFP650	Evrogen
Xilol	Sigma-Aldrich
β-Mercaptoetanol	Sigma-Aldrich

4.1.2. Otros materiales

Todo el material de plástico desechable (puntas de pipeta, pipetas, tubos de centrífuga, tubos de microcentrífuga, etc.) se obtuvo estéril o se esterilizó por autoclavado (Autotester E-75) a 121ºC y 1 atmósfera de presión durante 20 minutos. El material de vidrio (vasos, matraces, pipetas, etc.) se lavó adecuadamente para su uso y se esterilizó del mismo modo, en su caso.

4.1.3. Tipos celulares

- Células primarias mesenquimales humanas ("human mesenchymal stem cells", hMSCs, en inglés; Citospin/Hospital Clínico Universitario de Salamanca)
- Células primarias endoteliales humanas de vena de cordón umbilical ("human umbilical vein endothelial cells", HUVECs, en inglés; ATCC CRL-1730)

4.1.4. Modelos animales

- Conejo New Zealand hembra adulto con un peso medio de 3,5 kg (granja privada)
- Ratón Swiss nude nu/nu inmunodeprimido (Charles River Laboratories)
- Ratón Swiss WT (Servicio de Investigación y Bienestar Animal de la Universidad de Valladolid)

4.1.5. Recombinámeros tipo elastina (ELRs)

Los ELRs empleados en el transcurso de esta tesis doctoral se describen en la **Tabla 2**, y un esquema de los mismos se presenta en la **Figura 1**.

Tabla 2. ELRs utilizados en este trabajo, obtenidos en los laboratorios del G.I.R. BIOFORGE de la Universidad de Valladolid. Las secuencias correspondientes a las proteínas fluorescentes, verde y roja, aparecen coloreadas respectivamente en dichos colores.

ELR	Secuencia de aminoácidos abreviada	Peso molecular (Da)
HRGD6 (usado para la formación de ELR-CFCGs en el Capítulo 2)	MGSSHHHHHHSSGLVPRGSHMESLLP-{[(VPGIG)$_2$-(VPGKG)-(VPGIG)$_2$]$_2$-AVTGRGDSPASS-[(VPGIG)$_2$-(VPGKG)-(VPGIG)$_2$]$_2$}$_6$V	60660
(EIS)$_2$-RGD6 (SELR en el Capítulo 2)	MESLLP-{[(VPGVG)$_2$-VPGEG-(VPGVG)$_2$]$_{10}$-(VGIPG)$_{60}$-[V(GAGAGSG)$_5$]$_2$G}-[(VPGIG)$_5$-AVTGRGDSPASS]$_6$V	121012

(EI)$_2$ (ELR no sensible a elastasa) (44)	MESLLP-[(VPGVG)$_2$-VPGEG-(VPGVG)$_2$]$_{10}$-(VGIPG)$_{60}$-[(VPGVG)$_2$-VPGEG-(VPGVG)$_2$]$_{10}$-(VGIPG)$_{60}$-V	93158
ELR-E-RGD	MESLLP-[(VPGVG)$_2$-VPGEG-(VPGVG)$_2$]$_{10}$-(VGIPG)$_{60}$-(VGVAPG)$_3$-[(VPGVG)$_2$-VPGEG-(VPGVG)$_2$]$_{10}$-(VGIPG)$_{60}$-[(VPGIG)$_{10}$-AVTGRGDSPASS-(VPGIG)$_{10}$]$_2$V	113556
ELR-E-BMP-2	MESLLP-[(VPGVG)$_2$-VPGEG-(VPGVG)$_2$]$_{10}$-(VGIPG)$_{60}$-(VGVAPG)$_3$-[(VPGVG)$_2$-VPGEG-(VPGVG)$_2$]$_{10}$-(VGIPG)$_{60}$-(VGVAPG)$_3$-VKSSCKRHPLYVDFSDVGWND WIVAPPGYHAFYCHGECPFPLA DHLNSTNHAIVQTLVNSVNSKIP KACCVPTELSAISMLYLDENEKV VLKNYQDMVVEGCGCRV	107752
SELR-AcEGFP	MESLLP-{[(VPGVG)$_2$-VPGEG-(VPGVG)$_2$]$_{10}$-(VGIPG)$_{60}$-[V(GAGAGSG)$_5$]$_2$G}-VMASKGEELFTGVVPILVELDGDV NGHKFSVSGEGEGDATYGKLTLKF ICTTGKLPVPWPTLVTTLTYGVQCF SRYPDHMKQHDFFKSAMPEGYIQE RTIFFEDDGNYKSRAEVKFEGDTLV NRIELTGTDFKEDGNILGNKMEYNY NAHNVYIMTDKAKNGIKVNFKIRH NIEDGSVQLADHYQQNTPIGDGPVL LPDNHYLSTQSALSKDPNEKRDHMI LLEFVTAAGITHGMDELYKV	128737
SELR-eqFP650	MESLLP-{[(VPGVG)$_2$-VPGEG-(VPGVG)$_2$]$_{10}$-(VGIPG)$_{60}$-[V(GAGAGSG)$_5$]$_2$G}-VMGEDSELISENMHMKLYMEGTVNG HHFKCTSEGEGKPYEGTQTAKIKVVEGG PLPFAFDILATSFMYGSKTFINHTQGIPDF FKQSFPEGFTWERITTYEDGGVLTATQDT	128048

	SLQNGCLIYNVKINGVNFPSNGPVMQKK TLGWEASTEMLYPADSGLRGHSQMALKL VGGGYLHCSLKTTYRSKKPAKNLKMPGFY FVDRKLERIKEADKETYVEQHEMAVARYC DLPSKLGHSV	

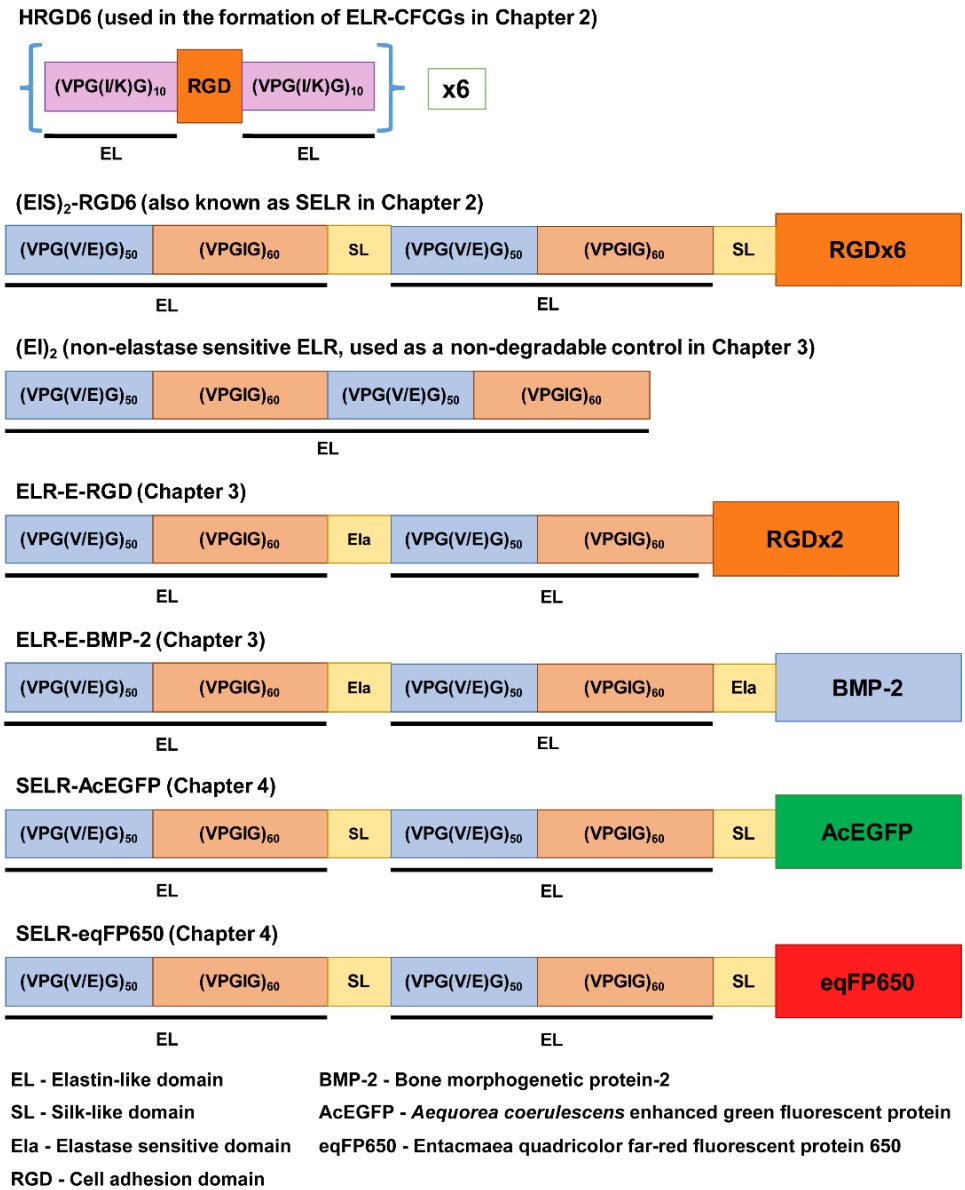

Figura 1. Esquema de todos los ELRs utilizados en esta tesis.

4.2. Métodos

4.2.1. Síntesis de ELRs

Todos los genes que codifican los ELRs utilizados en este trabajo, exceptuando los de los ELRs HRGD6, ELR-E-RGD y $(EI)_2$, han sido obtenidos de forma exclusiva para el desarrollo del mismo, mediante técnicas de ingeniería genética descritas en la bibliografía (27). Brevemente, los genes que codifican los distintos polipétidos, tanto de ELR como secuencias bioactivas/otras proteínas, son sintetizados por un servicio externo (NZYTech) y clonados en el plásmido pDriveAll, obtenido a partir de diversas modificaciones del plásmido pDrive (Qiagen), según se ha descrito anteriormente (47). Las enzimas de restricción utilizadas para la clonación sin interrupciones ("seamless cloning") son *Ear*I y *Sap*I (Thermo Scientific), dos enzimas de restricción de tipo IIS que tienen actividad endonucleasa sobre una secuencia contigua a la de reconocimiento, por lo que resultan óptimas para este tipo de clonación. Una vez que se obtiene la construcción génica final, se extrae del plásmido de clonación y se realiza un subclonaje en el plásmido de expresión pET7, resultado de distintas modificaciones sobre el vector comercial pET-25b(+) (Novagen). Posteriormente, este plásmido se usa para transformar cepas de expresión de *Escherichia coli*, en concreto BLR(DE3) (Novagen), que se cultivan en un biorreactor de 15 L (Applikon Biotechnology) en condiciones de pH, temperatura, agitación y concentración de O_2 controladas, consiguiendo así la bioproducción de los distintos ELRs. Ulteriormente, tras la ruptura mecánica de la pared celular y la membrana bacteriana por disrupción (modelo TS 0.75KW, Constant

Systems), estos son purificados aprovechando su característica de termosensibilidad mediante sucesivos ciclos de enfriamiento y calentamiento (lo que se denomina, en inglés, "Inverse Transition Cycling", ITC), seguidos de centrifugaciones en cada paso (48). Así, finalmente, se obtiene un producto puro que se dializa y se filtra a través de filtros de 0,22 μm (Nalgene) para conseguir una disolución de ELR estéril que se liofiliza (FreeZone 1, LABCONCO) para una mejor conservación del producto a largo plazo. Para eliminar las endotoxinas, se introdujo un paso de precipitación ácida del resto de proteínas (pH 3,5) previo al ITC, y se utilizó sulfato de amonio como sal para conseguir la precipitación de los ELRs en cada paso.

4.2.2. Modificación química de ELRs

La modificación química del ELR denominado HRGD6 se llevó a cabo según el procedimiento establecido con anterioridad (45). De forma simplificada, se modificó el grupo ε-amino de las lisinas que contiene dicho ELR para obtener grupos azida o ciclooctino (en moléculas diferentes), dando lugar al HRGD6-N_3 y al HRGD6-ciclo. Estos grupos forman un enlace covalente entre sí al mezclar las disoluciones que contienen los ELRs modificados, en lo que se conoce como química "click", permitiendo la formación de hidrogeles con entrecruzamiento químico en condiciones fisológicas (solvente acuoso) y sin que se libere ningún producto intermedio que pueda ser citotóxico.

4.2.3. Caracterización físico-química general de ELRs

4.2.3.1. Análisis del nivel de endotoxinas

El nivel de endotoxinas se determinó para todos los ELRs utilizados *in vivo* mediante el ensayo del lisado de amebocitos de *Limulus* (LAL) con el sistema Endosafe-PTS (Charles River Laboratories).

4.2.3.2. Electroforesis en gel de poliacrilamida con SDS (en condiciones desnaturalizantes, SDS-PAGE)

La electroforesis en geles de poliacrilamida con SDS (49), que desnaturaliza las proteínas y las aporta carga negativa homogénea para una migración dependiente de su tamaño (y no de la carga), permite conocer el peso molecular (Mw) de los ELRs, así como el nivel de pureza y de degradación de los mismos. En este trabajo, se ha utilizado el sistema de electroforesis vertical "MiniVE" de Hoefer (Amersham Pharmacia Biotec). Para el análisis por electroforesis, se cargaron entre 1,92 y 3,2 μg de ELR, según el tamaño del pocillo.

Los geles de poliacrilamida se tiñen con una disolución de 0,3 M de cloruro de cobre una vez finalizada la electroforesis. Se trata de una tinción negativa, que no tiñe las proteínas, sino que el cobre interacciona electrostáticamente con el SDS que contiene el propio gel, dejando las zonas que contienen proteínas sin teñir, observándose, por tanto, como bandas oscuras (50). Las imágenes de los geles se tomaron con el sistema Gel Logic 100 Imaging System (Eastman Kodak) y se analizaron con el programa Kodak 1D Image Analysis (Eastman Kodak).

4.2.3.3. Espectrometría de masas (MALDI-TOF)

La espectrometría de masas del tipo "Matrix-assisted laser desorption/ionization–Time-of-flight" (MALDI-TOF) permite conocer de forma exacta el Mw, por lo que se puede considerar complementaria a la técnica SDS-PAGE. Esta técnica ha sido llevada a cabo en el Laboratorio de Técnicas Instrumentales (LTI) de la Universidad de Valladolid (UVa) en el equipo MALDI-TOF Voyager STR (Applied Biosystems).

4.2.3.4. Análisis de aminoácidos (HPLC)

El análisis de muestras de ELR previamente hidrolizadas mediante "High-Performance Liquid Chromatography" (HPLC) permite conocer la composición de aminoácidos de las moléculas de ELR. Este método se llevó a cabo en el LTI de la UVa con el equipo de HPLC en gradiente Waters 600 acoplado a un detector de UV Waters 2487 (Waters).

4.2.3.5. Calorimetría diferencial de barrido (DSC)

La calorimetría diferencial de barrido (DSC) es una técnica que mide la diferencia en la cantidad de energía (calor) necesaria para aumentar la temperatura de una muestra con respecto a una referencia. En nuestro caso, se utiliza para medir la T_t de los ELRs, puesto que, cuando ocurra un cambio de fase o transición, la cantidad de calor que será necesario aportar a la disolución de ELR para aumentar la temperatura será mayor que para la referencia (disolvente sin ELR), al tratarse de un proceso endotérmico y consumirse parte de la energía aportada al sistema durante la

transición. Para este trabajo, se utilizó el equipo Mettler Toledo 822e con refrigeración mediante nitrógeno líquido. Los experimentos consistieron en una primera etapa isotérmica a 0ºC durante 5 minutos, seguida de una etapa de calentamiento, desde 0 a 60ºC, a una velocidad de 5ºC/min. Los ELRs se disolvieron a 50 mg/mL en agua o en PBS, midiendo, en el primer caso, la T_t a distintos valores de pH.

4.2.3.6. Resonancia magnética nuclear de protón (^{1}H-NMR)

La resonancia magnética nuclear ("nuclear magnetic resonance", NMR, en inglés) permite estudiar el comportamiento de los núcleos de los átomos, cuando tienen spin diferente de cero, en presencia de un campo magnético externo. Este produce una orientación determinada de los spines, cuya relajación depende de la estructura molecular y, por tanto, es diferente para cada molécula, pudiéndose obtener una "huella dactilar" de la misma, incluso para las que dan lugar a espectros complejos, como las proteínas, concretamente los ELRs. En este trabajo se ha obtenido el espectro de NMR de protón (^{1}H-NMR) para todos los lotes de ELRs bioproducidos con el equipo NMR 500 (Agilent Technologies) del LTI de la Uva, lo que nos permite comprobar la ausencia de impurezas para cada uno de ellos y la conformidad de los espectros con respecto a los valores teóricos esperados.

4.2.4. Caracterización mecánica de hidrogeles basados en ELRs mediante medidas reológicas

La reología es una rama de la física que estudia la capacidad de los materiales de fluir y de deformarse. Por tanto, esta técnica

puede utilizarse para estudiar el comportamiento viscoelástico (propiedades viscosas y elásticas en respuesta a una deformación) de los hidrogeles, obteniendo una medida de su rigidez/dureza. En este trabajo, se ha utilizado un reómetro de esfuerzo controlado (AR200ex, TA Instruments), equipado con una placa Peltier para controlar la temperatura. Se utilizó una geometría de platos paralelos de 12 mm de diámetro y se utilizó un volumen de muestra de 200 μL depositado directamente sobre la Peltier fría (a 5ºC) para pasar rápidamente a 37ºC y formar un hidrogel *in situ*. Con el objetivo de obtener medidas del módulo de almacenamiento (G'), que después se utilizaron para comparar distintas muestras entre sí a distintas concentraciones, se realizó un barrido en el tiempo con una deformación constante del 0,5% y una frecuencia de 1 Hz.

4.2.5. Caracterización de SELRs fusionados a proteínas fluorescentes (SELR-FPs) por espectroscopía

Con el objetivo de obtener datos concretos que permitan definir las propiedades fluorescentes de los SELR-FPs diseñados en esta tesis y poder compararlos con los de las FPs nativas, se realizaron medidas de absorbancia y emisión de fluorescencia en un lector de placas y cubetas multi-modo (SpectraMax M2e, Molecular Devices), el cual permite el análisis de múltiples muestras en una misma lectura, controlando, además, la temperatura (todas las medidas se llevaron a cabo a 37ºC). De este modo, en primer lugar, se calculó el coeficiente de extinción molar (ε) mediante la medida de la absorbancia (A), en este caso en una cubeta de plástico y en el mismo equipo, teniendo en cuenta que estos dos factores están relacionados entre sí por la ley de Lambert-Beer (ecuación 1):

$$(1)\ A = \varepsilon \cdot l \cdot C$$

Así, conociendo el paso de luz (l) de 1 cm, se puede calcular ε para una concentración conocida (C) del SELR-FP, en este caso 10 mg/mL en PBS. Se utilizó una disolución de SELR sin ninguna FP fusionada a la misma concentración como blanco.

Por otro lado, se obtuvo el espectro de emisión, y, por tanto, la longitud de onda de emisión máxima, midiendo la intensidad de fluorescencia de 50 μL de una disolución de cada SELR-FP por separado, en placas de 96 pocillos, ajustando la longitud de onda de excitación en el máximo (λ_{max}) de absorción obtenido previamente.

Para calcular el rendimiento cuántico ("quantum yield", QY, en inglés), se compararon los espectros de emisión de los SELR-FPs con los de las FPs nativas (AcGFP1 y eqFP650 o TurboFP650), cuyos valores de QY son conocidos y se usaron como referencia, con el programa a|e - UV-Vis-IR Spectral Software 2.2 (FluorTools, www.fluortools.com). El brillo de los SELR-FPs se calculó mediante el producto de ε y el QY, y se expresó normalizado al de la AcGFP1.

4.2.6. Caracterización de la interacción FRET entre SELR-FPs

4.2.6.1. Espectroscopía de fluorescencia ("quencheo" del donador)

Una de las técnicas utilizadas para evaluar la eficiencia del efecto FRET es la espectroscopía de fluorescencia, mediante el método denominado "quencheo" del donador ("donor quenching", en inglés). Éste se basa en el fenómeno comentado anteriormente, por el que la proteína donadora, en este caso el recombinámero SELR-AcEGFP, ve reducida su intensidad de fluorescencia en

presencia de la proteína aceptora, esto es, SELR-eqFP650. Por tanto, a través de la medida de la intensidad de fluorescencia de SELR-AcEGFP en la λ_{max} de emisión en presencia (F_{DA}) y en ausencia (F_D) de SELR-eqFP650, se puede calcular la eficiencia de la interacción FRET con la siguiente fórmula (ecuación 2) (51):

$$(2)\ E = 1 - \frac{F_{DA}}{F_D}$$

Esta técnica se llevó a cabo con el equipo descrito anteriormente (4.2.5), con disoluciones preparadas a distintas concentraciones de SELR-FPs (10, 50, 100 y 200 mg/mL, en agua ultra-pura), manteniendo siempre una relación molar de 1:1 para las dos SELR-FPs. Además, las medidas se realizaron por debajo (15ºC) y por encima (37ºC) de la T_t.

4.2.6.2. Microscopía confocal ("quemado" del aceptor)

Otra técnica mediante la cual se puede calcular la eficiencia FRET es la microscopía confocal (microscopio confocal Leica TCS SP5 controlado por el programa informático LAS, y acoplado a un láser de Argón (499-559 nm) y a una lámpara de luz blanca con monocromador), utilizando el método denominado "quemado" del aceptor ("acceptor photobleaching", en inglés), cuyo fundamento es el mismo que en el caso del "quenching" del donador usado en espectroscopía de fluorescencia. En este caso, se "quema" la fluorescencia del aceptor (SELR-eqFP650) con un láser de alta intensidad en un hidrogel (200 mg/mL, en agua ultra-pura) compuesto de ambos SELR-FPs (relación molar de 1:1), por lo que, tras el paso de "quemado", la intensidad de fluorescencia (I_{post}) del donador (SELR-AcEGFP) será mayor que antes del "quemado"

(I_{pre}). Teniendo en cuenta que el "quemado" del aceptor puede conllevar también un mínimo "quemado" del donador, se midió la intensidad de fluorescencia dentro (I_p) y fuera (I_{np}) de la región "quemada" para contrarrestar esta fuente de error en la medida final. Por tanto, la eficiencia FRET se puede calcular con la siguiente fórmula (ecuación 3, correspondiente a "Equation 4" en el Capítulo 4 de esta tesis):

$$(4)\ E = 1 - \frac{\left(\frac{I_p}{I_{np}}\right)_{pre}}{\left(\frac{I_p}{I_{np}}\right)_{post}}$$

4.2.7. Ensayos de biodegradación enzimática *in vitro*

Los ensayos de biodegradación enzimática se llevaron a cabo con los ELRs sensibles a elastasa, concretamente el ELR-E-RGD y el ELR-E-BMP-2, ambos utilizados en el Capítulo 3 de esta tesis. Para ello, se disolvió una mezcla de ambos, en la misma proporción a la que se utilizaron en los subsiguientes experimentos (98% (p/p) de ELR-E-RGD y 2% (p/p) de ELR-E-BMP-2), a una concentración de 1 mg/mL en agua ultra-pura. Posteriormente, se añadieron distintas cantidades de elastasa pancreática porcina (1,2; 1,8 y 2,4 U) y las muestras se incubaron a 37ºC, tomando alícuotas a distintos tiempos (10, 20, 30, 45, 60, 90 y 120 minutos). Se utilizó un ELR (con estructura similar) sin secuencias sensibles a elastasa como control. El análisis de las muestras se realizó mediante SDS-PAGE, según se ha descrito anteriormente (4.2.3.2).

4.2.8. Cultivos celulares

Las células endoteliales (HUVEC) utilizadas en este estudio se cultivaron con el medio de cultivo Medium 200 suplementado con antibióticos (gentamicina/anfotericina al 1%) y con el suplemento de crecimiento con bajo suero (LSGS). Estas células se mantuvieron en cultivo en un incubador a 37ºC y 5% CO_2.

Las células mesenquimales humanas (hMSCs) utilizadas en el Capítulo 2 de esta tesis fueron obtenidas en el Servicio de Hematología (Laboratorio de Terapia Celular) del Hospital Universitario de Salamanca a partir de médula ósea de donantes sanos. Estas células fueron transducidas mediante lentivirus con el plásmido pLV-CMV-Luc2-IRES-GFP para conseguir la expresión constitutiva de luciferasa. En cuanto a las hMSCs utilizadas en el Capítulo 3, fueron gentilmente donadas por Citospin S.L (Valladolid, España).

Todos los tipos celulares fueron cultivados hasta 80-90% de confluencia, momento en el cual se tripsinizaron para su pasaje. Además, se realizaron cambios de medio cada 2-3 días en todos los casos.

4.2.8.1. Determinación del número de células vivas

Para calcular el número de células vivas presentes en el cultivo, se utilizó el ensayo de Calceína AM, por el cual sólo las células vivas, con esterasas activas, son capaces de hidrolizar el grupo acetoximetil éster que evita que la calceína sea fluorescente, pasando a emitir fluorescencia verde cuando esto ocurre. Esta emisión de fluorescencia puede ser medida cuantitativamente con

un lector de placas (SpectraMax M2e) a λ_{max} de excitación y emisión de la calceína (485 y 530 nm, respectivamente). De este modo, habiendo realizado una recta patrón con un número de células conocido, es posible calcular el número de células en un cultivo con unas condiciones determinadas, por ejemplo, con células cultivadas sobre sustratos de ELR, para estudiar las propiedades adherentes y la consiguiente proliferación celular estudiando el número de células vivas a distintos tiempos, o en cultivos realizados con medio suplementado con uno o varios ELRs en disolución para estudiar su citotoxicidad.

4.2.9. Experimentos *in vivo*

4.2.9.1. Preparación e inyección subcutánea de disoluciones de ELRs en ratones

Para los estudios de bioluminiscencia *in vivo* se utilizaron 3 ratones Swiss nude nu/nu por grupo (n = 3). En primer lugar, se disolvieron los ELRs en medio de cultivo DMEM a distintas concentraciones, dejándolos 24 h a 4ºC. Para formar los hidrogeles con entrecruzamiento químico, se disolvieron los ELRs denominados HRGD6-N_3 y el HRGD6-ciclo a las concentraciones de 25, 50, 75 y 100 mg/mL, siendo referidas como concentración (C) 1, 2, 3 y 4, respectivamente. En el caso de la formación de hidrogeles con entrecruzamiendo físico, el $(EIS)_2$-RGD6 (también denominado SELR en el Capítulo 2 de esta tesis) se disolvió a 75, 100, 125 y 150 mg/mL, denominándose, como en el caso anterior, concentración 1, 2, 3 y 4, respectivamente. Posteriormente, se mezclaron las hMSCs que expresan la luciferasa (Luc-hMSCs) con estas disoluciones, a una concentración final de células de

10^6 células/mL. Por último, se inyectaron subcutáneamente 100 μL de la disolución de SELR o de la mezcla de HRGD6-N_3 y HRGD6-ciclo, con una jeringuilla de 20G, respectivamente. Cada concentración (1, 2, 3 y 4) fue inyectada en distintos puntos de la zona dorsal del animal, según se indica en la Figura 2. En el caso de los hidrogeles con entrecruzamiento químico, se mezclaron previamente 50 μL de cada componente, manteniendo una proporción de 1:1 en volumen. Todos los procedimientos se llevaron a cabo en condiciones de esterilidad en salas con presión positiva y equipadas con campanas de flujo laminar.

Con respecto a la inyección de ELRs formadores de hidrogeles para la cuantificación de citoquinas y el estudio macroscópico e histológico a distintos tiempos, se utilizaron tres ratones Swiss WT por grupo (n = 3). Primero, se prepararon las disoluciones de ELR, en concreto los dos componentes derivados de HRGD6 a 75 mg/mL, y el SELR a 150 mg/mL, ambos en PBS (24 h, 4ºC). La diferencia en las concentraciones se debe al tipo de entrecruzamiento que estabiliza los hidrogeles formados con cada ELR. En el primer caso, el entrecruzamiento es químico (mediante la formación de enlaces covalentes), por lo que la concentración necesaria para formar hidrogeles es más baja que en el caso de los hidrogeles físicos, estabilizados por interacciones hidrofóbicas y puentes de hidrógeno (SELR). Posteriormente, se anestesiaron los animales y se inyectaron las disoluciones de ELR, de manera similar a la descrita en el párrafo anterior. En este caso, se incluyó un grupo control negativo (inyección de PBS) y otro positivo, al que se le inyectó lipopolisacárido bacteriano (LPS) a una concentración de 3 mg/kg (52), con el objetivo de promover una respuesta

inflamatoria aguda que resultase en un incremento de los niveles de citoquinas en sangre.

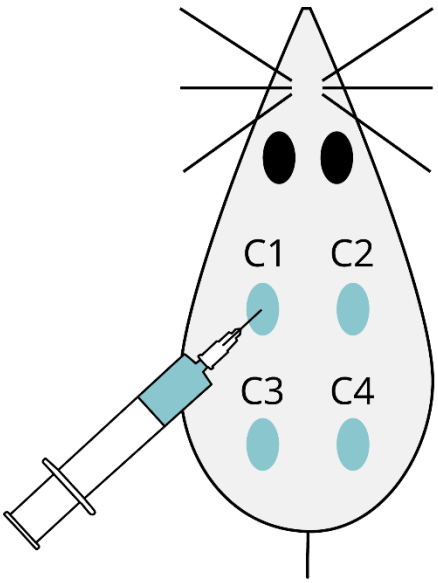

C (mg/mL)	SELR	ELR-CFCGs
C1	75	25
C2	100	50
C3	125	75
C4	150	100

Figura 2. Esquema que ilustra la inyección de distintas concentraciones de hidrogeles basados en SELR y ELR-CFCGs, incluyendo Luc-hMSCs embebidas, en distintas partes de ratones nu/nu.

4.2.9.2. Medida de bioluminiscencia de Luc-hMSCs embebidas en hidrogeles basados en ELRs inyectados en ratones

Con el objetivo de estudiar la viabilidad celular en el interior de hidrogeles basados en ELRs inyectados subcutáneamente en ratones, se utilizaron las Luc-hMSCs descritas en la sección 4.2.8. De este modo, es posible utilizar un método mínimamente invasivo como es la inyección de luciferina y la observación de la bioluminiscencia emitida al ser oxidada por la actividad de la luciferasa, expresada solamente por las células viables y metabólicamente activas que se encuentren embebidas en el

hidrogel. Estos fueron inyectados según se describe en el epígrafe 4.2.9.1.

La medida de la bioluminiscencia se llevó a cabo con el equipo Xenogen IVIS 50 (Xenogen Corporation, Caliper Life Science). Los ratones se anestesiaron con isoflurano y se les inyectaron 15 μg de luciferina por g de peso. Posteriormente, se les introdujo en la cámara del equipo IVIS 10 minutos después de la inyección y se obtuvieron imágenes que fueron ulteriormente analizadas con el programa Living Image 2.50.1 (Xenogen Corporation, Caliper Life Science), calculando el número de fotones emitidos por segundo en una región de interés determinada. Este procedimiento se realizó a día 1 y después de forma semanal hasta las 4 semanas.

4.2.9.3. Medida de la concentración de citoquinas en sangre de ratones

Tras la inyección subcutánea de las disoluciones frías de ELRs, según lo especificado en el apartado 4.2.9.1 para ratones Swiss WT, se extrajeron aproximadamente 250 μL de sangre de todos los ratones de cada grupo en tubos capilares Microvette CB 300 K2E (Sarsted) a distintos tiempos: 1, 2 y 7 días post-inyección. Posteriormente, las muestras se cetrifugaron a 2000 rcf durante 10 minutos y se separó el suero, que se utilizó en los ensayos "enzyme-linked immunosorbent assay" (ELISA), que permitieron conocer la concentración de las distintas citoquinas evaluadas: TNFα, IL-1β, IL-4, IL-6 y IL-10 (referencia de productos EMTNFA, EM2IL1B, EMIL4, EM2IL6 y EM2IL10, respectivamente; Thermo Scientific). Estos ensayos fueron realizados de acuerdo a las

directrices de cada kit, utilizando citoquinas recombinantes para la obtención de una recta de calibrado, en cada caso. La medida colorimétrica se llevó a cabo en un lector de placas (SpectraMax M2e).

4.2.9.4. Extracción y procesamiento histológico de hidrogeles inyectados subcutáneamente en ratones

En primer lugar, se llevó a cabo la eutanasia de los animales mediante dislocación cervical. Seguidamente, se extrajeron los hidrogeles alojados debajo de la piel para su posterior análisis macroscópico y microscópico, utilizando material quirúrgico apropiado (tijeras, bisturí, pinzas, etc.). Los hidrogeles fueron fijados en un volumen de paraformaldehído al 4% en PBS 10 veces mayor al del hidrogel, durante al menos 24 horas a 4ºC. Posteriormente, las muestras se deshidrataron por inmersión en soluciones de etanol de concentración creciente (75%, 95% y 100%) con un paso final en xilol. Finalmente, los hidrogeles se incluyeron en parafina y se realizaron cortes de 10 μm, que se colocaron sobre portaobjetos y se desparafinaron y rehidrataron mediante inmersión en xilol, disoluciones de etanol de concentración decreciente (100%, 95% y 75%) y agua.

La tinción hematoxilina-eosina se llevó a cabo siguiendo métodos descritos en la bibliografía (53). Específicamente, los portaobjetos se introdujeron en la solución de hematoxilina por 30 segundos y se lavaron en agua durante 1 minuto. Después, se usó una disolución de eosina al 1% para la tinción, manteniendo los portaobjetos durante 30 segundos en la misma. Por último, las muestras se deshidrataron de nuevo, según el procedimiento

descrito anteriormente, y se añadió medio de montaje sobre cada una de ellas para colocar el cubreobjetos. Las imágenes de los cortes fueron obtenidas con un microscopio óptico de campo claro (Nikon Eclipse 80i) equipado con una cámara a color (Nikon Digital Sight DS-Fi1).

4.2.9.5. Técnicas quirúrgicas e inyección de disoluciones de ELRs en conejos

Con el objetivo de evaluar la capacidad de regeneración ósea de hidrogeles bioactivos basados en ELRs, se utilizaron 7 conejos New Zealand hembra adultos para la creación y el tratamiento de defectos óseos, según se ha descrito anteriormente (54). Brevemente, los animales fueron anestesiados con una inyección intramuscular de una combinación de ketamina (35 mg/kg), xilacina al 2% (18 mg/kg) y acepromazina al 1% (1 mg/kg). Tras el rasurado, lavado e incisión de la rodilla, se procedió al taladrado del cóndilo femoral, primero con una broca de 3 mm de diámetro, continuando después con una de 6 mm para obtener un defecto de ese diámetro final, con una profundidad de 3 mm. El defecto se lavó con suero fisiológico para eliminar restos de hueso y se realizó hemostasia sobre la lesión con gasas. Posteriormente, se inyectaron 100 μL de una disolución de una mezcla de ELRs (98% (p/p) de ELR-E-RGD y 2% (p/p) de ELR-E-BMP-2) previamente disuelta a 4ºC durante 24 horas. Finalmente, se suturó el plano aponeurótico con hilo reabsorbible 3/0, y la piel con Nylon 3/0, lavando la herida con povidona yodada. Todos los animales siguieron un análisis diario de su estado general, movilidad e ingesta de comida. Asimismo, se evaluaron parámetros bioquímicos tras 0, 2, 30 y

90 días desde el inicio del estudio para comprobar el bienestar animal.

4.2.9.6. Tomografía computerizada multi-corte (MSCT) de fémures de conejos

La tomografía computerizada multi-corte permite realizar una reconstrucción tridimensional de los huesos analizados, además de poder observar cada corte, coronal, longitudinal y axial, por separado. Esta técnica se empleó para analizar los siete fémures extraídos de los conejos utilizados en los experimentos de regeneración ósea sobre los que se realizaron los defectos. Para ello, se utilizó el equipo Alexion (Toshiba), y las imágenes se procesaron con el programa Alexion Advance Edition, concretamente con el algoritmo Adaptive Iterative Dose Reduction (AIDR 3D).

4.2.9.7. Extracción y procesamiento histológico de tejido óseo

Tras la eutanasia de los animales con tres dosis de anestesia (54), 3 meses después de la operación, se extrajeron los fémures de los mismos para su análisis histológico. Para ello, se cortó la epífisis femoral 4 cm por debajo de la metáfisis. Posteriormente, las muestras se descalcificaron con solución de Morse y se incluyeron en parafina siguiendo protocolos preestablecidos (55). Las muestras se cortaron en serie (grosor de 7 μm) usando un microtomo manual (Micron-Zeiss) y se tiñeron con hematoxilina-eosina. Las imágenes se obtuvieron con un microscopio óptico (Olympus CH30) acoplado a una cámara digital (Sony) Todas las muestras fueron observadas por dos histopatólogos independientes mediante un análisis ciego.

4.2.10. Análisis estadístico

Los datos presentados en esta tesis se presentan como la media ± desviación estándar (n = 3-4, según lo especificado en cada apartado concreto). El análisis estadístico ha sido realizado mediante un análisis de la varianza de una vía con la prueba post-hoc de Holm-Sidak. Se ha considerado significativo un p-valor menor de 0,05. Las diferencias significativas se exponen del siguiente modo: (*) $p < 0,05$; (**) $p < 0,01$; (***) $p < 0,001$; $p > 0,05$ indica ausencia de diferencias significativas ("no significant differences", n.s.d., en inglés).

5. RESULTADOS Y DISCUSIÓN

5.1. Biosíntesis y caracterización físico-química de ELRs

Los genes completos de todos los ELRs utilizados en esta tesis se obtuvieron satisfactoriamente, según los análisis llevados a cabo mediante electroforesis en gel de agarosa y secuenciación de ADN. Del mismo modo, la biosíntesis de los ELRs dio lugar a rendimientos que van desde los 120 a los 400 mg/L de medio de cultivo.

En cuanto a la caracterización, en todos los casos se utilizaron las siguientes técnicas: SDS-PAGE y MALDI para la determinación del peso molecular y la pureza de los ELRs, DSC para el cálculo de la T_t, ^{1}H-NMR para obtener una "huella dactilar" de los recombinámeros y descartar la presencia de contaminantes, y HPLC para el análisis de la composición de aminoácidos. Los resultados de peso molecular obtenidos por SDS-PAGE y MALDI-TOF fueron similares a los esperados en todos los casos, con pequeñas variaciones de hasta el 1,4% (sólo en el caso del SELR-AcEGFP), y con una media de variación del 0,6%. Esto probablemente se debe a las limitaciones del aparato y de la técnica, al tratarse de proteínas de alto peso molecular (de 108 a 129 kDa, exceptuando el HRGD6) y calcularse este parámetro a partir del dicación, esto es, del valor de m/2z. Por otro lado, la T_t se situó siempre por debajo de la temperatura fisiológica, permitiendo el uso de estos ELRs para la formación de hidrogeles una vez inyectados *in vivo*. Además, la T_t resultó ser mayor cuando se

fusionaron otras secuencias polares al ELR, lo cual está en concordancia con lo descrito en la bibliografía (56). En lo que respecta al espectro obtenido por ^{1}H-NMR, éste fue muy similar para todos los lotes, dando picos muy similares a los predichos.

Los niveles de endotoxinas de los ELRs utilizados *in vivo* fueron medidos, dando como resultado un máximo de 2 unidades de endotoxinas/mg ELR, para los ELRs utilizados a menor concentración. Los ELRs utilizados a mayores concentraciones (hasta 300 mg/mL) contenían menos de 0,01 UE/mg de ELR. De este modo, incluso a las concentraciones de ELR más altas, los niveles de endotoxinas se mantuvieron por debajo del límite marcado por la FDA (20 UE/dispositivo biomédico).

Todos los datos correspondientes a la caracterización de los ELRs utilizados en esta tesis pueden encontrarse en los distintos capítulos de la misma, así como en la **Tabla 3**.

Tabla 3. Resumen de los rendimientos, pesos moleculares (Mw) teóricos y experimentales, y de las Temperaturas de Transición (T_t) de los distintos ELRs bioproducidos en el desarrollo de esta tesis.

ELR	Rendimiento (mg/L)	Mw teórico (kDa)	Mw experimental (kDa)	T_t (ºC) en PBS (pH 7.2-7.4)
$(EIS)_2$-RGD6 (SELR en el Capítulo 2)	400	121,0	120,4	16,8
ELR-E-RGD	200	113,6	113,4	15,8
ELR-E-BMP-2	200	107,8	107,5	15,3

SELR-AcEGFP	133	128,7	126,9 (m/2z)	16,8
SELR-eqFP650	120	128,1	128,9 (m/2z)	17,2

5.2. Estudio de las propiedades mecánicas de hidrogeles basados en ELRs

Las propiedades viscoelásticas de los hidrogeles basados en ELRs se obtuvieron mediante medidas reológicas, según lo detallado en la sección 4.2.4. En el caso de los hidrogeles resultado de la mezcla de ELRs bioactivos (ELR-E-RGD y ELR-E-BMP-2), utilizados para regeneración ósea (Capítulo 3), puede observarse un módulo de almacenamiento (G') de 1600 Pa a 300 mg/mL (2,64 mM), el cual es muy bajo en comparación con las propiedades mecánicas del hueso (G' = 3,3 GPa (57)). Sin embargo, en el ámbito de la medicina regenerativa, en muchos casos se pretende el uso de hidrogeles blandos que permitan la invasión y proliferación celular en su interior, actuando como un tejido blando temporal que se sustituirá por hueso regenerado con el paso del tiempo. En cambio, los hidrogeles basados en ELRs que incluyen secuencias derivadas de la fibroína de la seda (SELRs) tienen un G' mayor a concentraciones menores, como es el caso del SELR-AcEGFP y del SELR-eqFP650: a 1,94 mM poseen un G' de 4055 y 3354 Pa, respectivamente. Este resultado resalta la capacidad de las secuencias tipo seda ("silk", en inglés) de reforzar la estructura de los hidrogeles basados en SELRs, tal y como se ha descrito anteriormente (28).

Por otro lado, la comparación de las propiedades mecánicas de los SELR-FPs y el SELR simple mostró que para este último G' era 2,6; 2,3 y 2,4 veces más alto que para el SELR-AcEGFP, SELR-eqFP650 y la mezcla 1:1 molar de ambos, respectivamente, a una concentración de 1,13 mM (Figura 3). Este resultado demuestra que la inclusión de proteínas más o menos grandes puede promover efectos estéricos que impiden la interacción de los grupos que estabilizan la estructura mediante interacciones hidrofóbicas, en el caso de los dominios tipo elastina, y enlaces de hidrógeno, entre motivos tipo seda. Esta hipótesis se ve reforzada por el hecho de que en el caso del SELR que incluye la eqFP650, que es una proteína dimérica, G' es menor que para el SELR-AcEGFP a 1,94 mM. La formación de estos dímeros, conllevaría la ocupación de un mayor volumen, por lo cual aumentarían los impedimentos estéricos, explicando la reducción de G'.

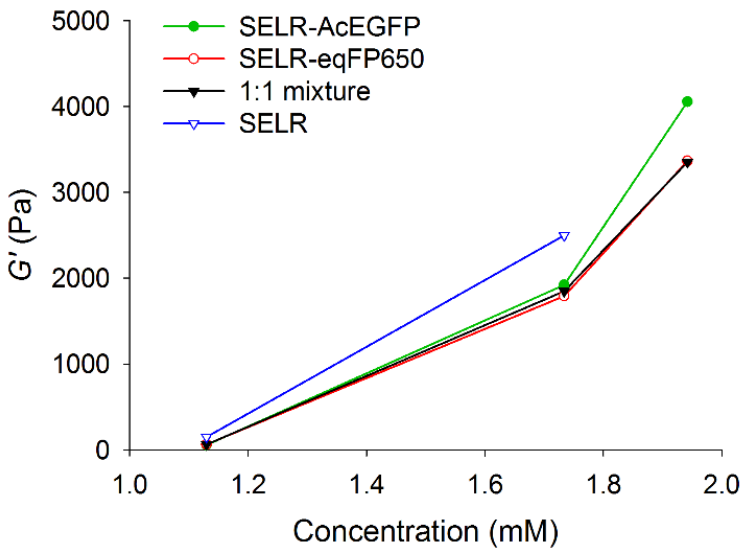

Figura 3. Gráfica comparativa de G' para el SELR simple y los SELR-FPs a distintas concentraciones.

5.3. Biodegradación enzimática *in vitro* de ELRs sensibles a elastasa

Teniendo en cuenta la incorporación de secuencias sensibles a degradación por elastasa (hexapéptido VGVAPG) en ELRs bioactivos, que contienen la secuencia de adhesión celular RGD y el factor osteogénico BMP-2, se llevó a cabo un análisis de biodegradación de estos ELRs *in vitro* mediante el uso de dicha proteasa, según lo especificado en el apartado 4.2.7. De este modo, se observó una degradación dependiente de la cantidad de elastasa utilizada, siendo mucho más rápida para la cantidad más alta (2,4 U) (Figura 4). Por el contrario, no se observó degradación en el control negativo (ELR sin secuencias sensibles a elastasa, denominado $(EI)_2$ en la Tabla 2) a ningún tiempo.

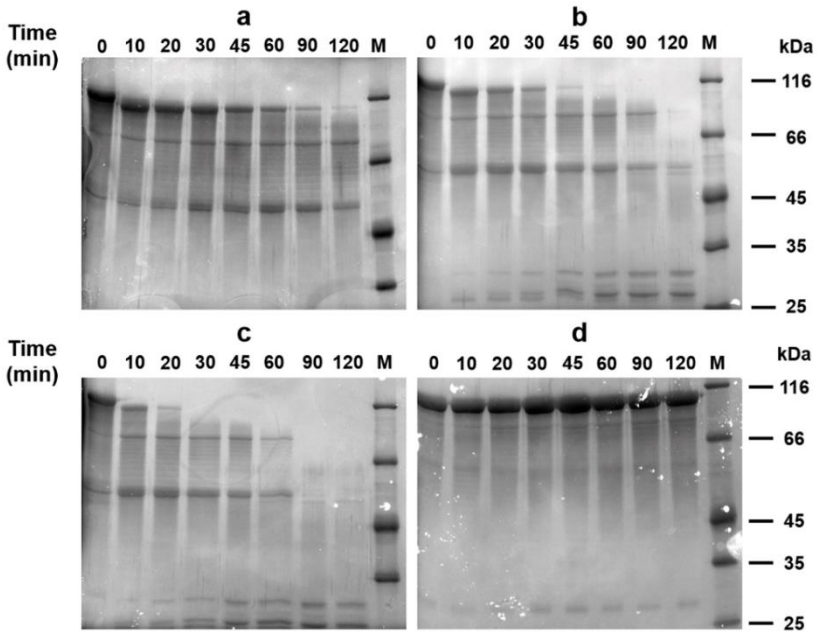

Figura 4. Imágenes de SDS-PAGE mostrando la degradación de la mezcla de ELRs (98% (p/p) de ELR-E-RGD y 2% (p/p) de ELR-E-BMP-2) a

distintos tiempos con a) 1,2 U; b) 1,8 U y c) 2,4 U de elastasa. La imagen d) corresponde al $(EI)_2$, no sensible a elastasa (**Tabla 2**) (44) (1,2 U de enzima).

Asimismo, el análisis de la desaparición de las bandas correspondientes a las moléculas íntegras de ELRs mostró de una forma cuantitativa las diferencias en la cinética de degradación para cada una de las cantidades de elastasa utilizadas (**Figura 5**).

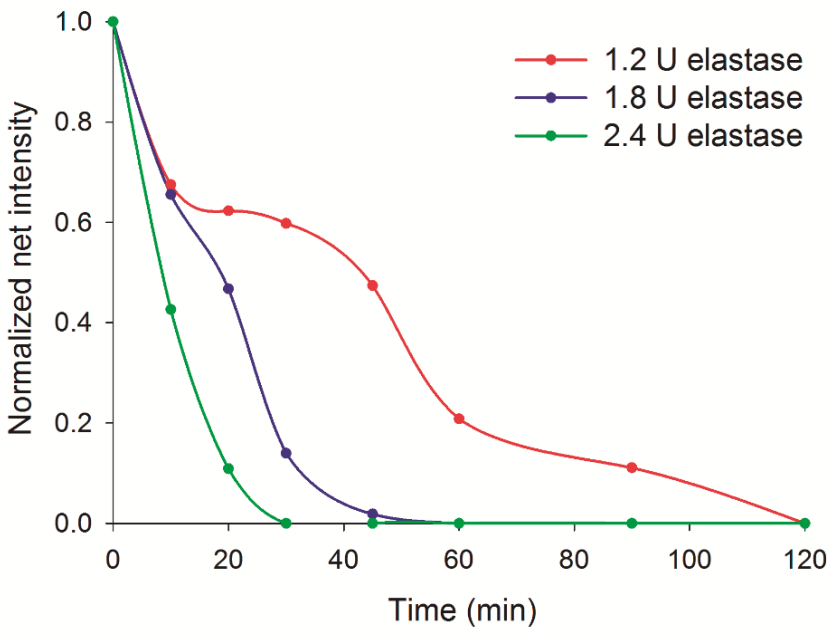

Figura 5. Cinética de degradación por elastasa de la mezcla de ELRs (98% (p/p) de ELR-E-RGD y 2% (p/p) de ELR-E-BMP-2) con distintas cantidades de enzima, estudiando la desaparición de la banda correspondiente a las moléculas completas de ELRs.

Por otro lado, las bandas que aparecen experimentalmente como consecuencia de la degradación se corresponden con las esperadas teóricamente, teniendo en cuenta que, según exponen otros estudios previos (58, 59), los ELRs tienden a migrar

electroforéticamente con un aumento del 20% en el peso molecular aparente con respecto al esperado, debido a sus características hidrofóbicas (Tabla 4).

Tabla 4. Peso molecular esperado, peso molecular + 20%, y peso molecular calculado de las bandas que aparecen a consecuencia de la degradación mediada por elastasa de los ELRs.

Bandas aparecidas	Peso molecular esperado (kDa)	Peso molecular esperado + 20% (kDa)	Peso molecular aparente *Mw* (kDa)
Banda 1	66,5-65,5	79,8-78,6	80,8
Banda 2	48,2-46,7	57,8-56,0	54,2

La presencia de estos dominios de degradación por elastasas conlleva el corte de las moléculas de ELR justo después de cada punto de entrecruzamiento (dominios tipo elastina hidrofóbicos, conteniendo isoleucina como aminoácido invitado), lo que supone, a nivel macroscópico, la ruptura de la red que estabiliza el hidrogel, facilitando su desintegración Figura 6. Por otro lado, el ELR-E-BMP-2 dispone de secuencias sensibles a elastasas entre los bloques de elastina y la BMP-2, por lo que la actividad de dichas proteasas supone la liberación de esta proteína osteogénica.

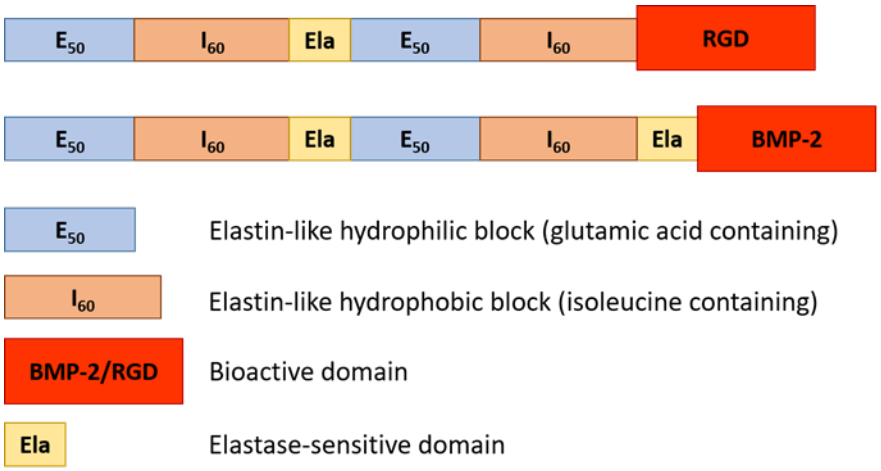

Figura 6. Esquema del diseño de los ELRs bioproducidos para promover la regeneración ósea, siendo el ELR-E-RGD y el ELR-E-BMP-2, respectivamente.

5.4. Citocompatibilidad de ELRs

5.4.1. Viabilidad celular *in vitro*

Para determinar la citocompatibilidad de los ELRs en términos de viabilidad celular, se utilizaron hMSCs que fueron cultivadas con medio suplementado con ELRs (a 10 mg/mL), en concreto con ELR-E-RGD, ELR-E-BMP-2 y la mezcla de ambos (98% (p/p) ELR-E-RGD y 2% (p/p) ELR-E-BMP-2). Tras 3 días de cultivo, se calculó la viabilidad celular mediante el ensayo de calceína AM 4.2.8.1, observándose una ausencia de diferencias significativas entre las distintas condiciones, incluyendo el control negativo, con medio no suplementado con ELRs (Figura 7).

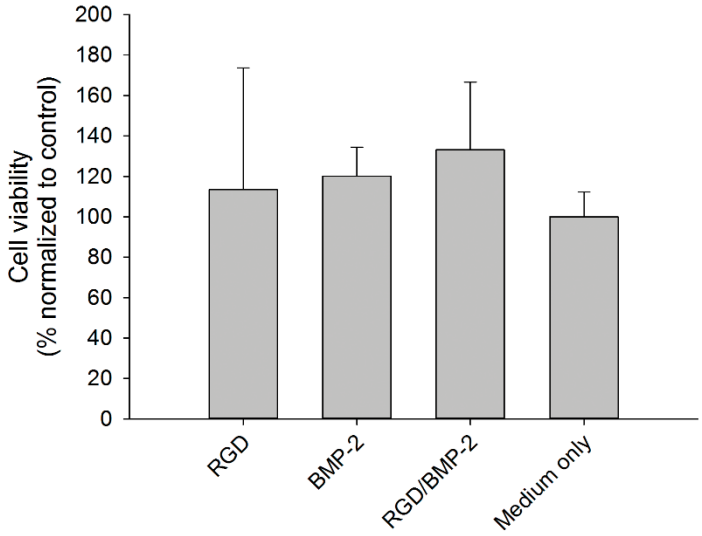

Figura 7. Resultados de viabilidad celular en cada condición, normalizados frente al control.

5.4.2. Adhesión celular sobre sustratos de ELR

En primer lugar, se adsorbieron los ELRs (ELR-E-RGD, ELR-E-BMP-2 y la mezcla de ambos) en placas de 96 pocillos y se utilizó una disolución de BSA al 5% para bloquear las posibles zonas del pocillo no recubiertas por los ELRs (ver Capítulo 3 para una descripción más detallada del procedimiento). Posteriormente, se sembraron hMSCs y se determinó la adhesión a las 24 horas tras realizar los correspondientes lavados para retirar las células en suspensión, mediante el ensayo de calceína AM. Así, se observó que no existían diferencias significativas entre los grupos ELR-E-RGD, mezcla y control negativo (placa de cultivo), mientras que estas sí se observaban entre estos grupos y el de ELR-E-BMP-2 (Figura 8). Este resultado concuerda con lo esperado, puesto que la BMP-2 no contiene secuencias de adhesión celular.

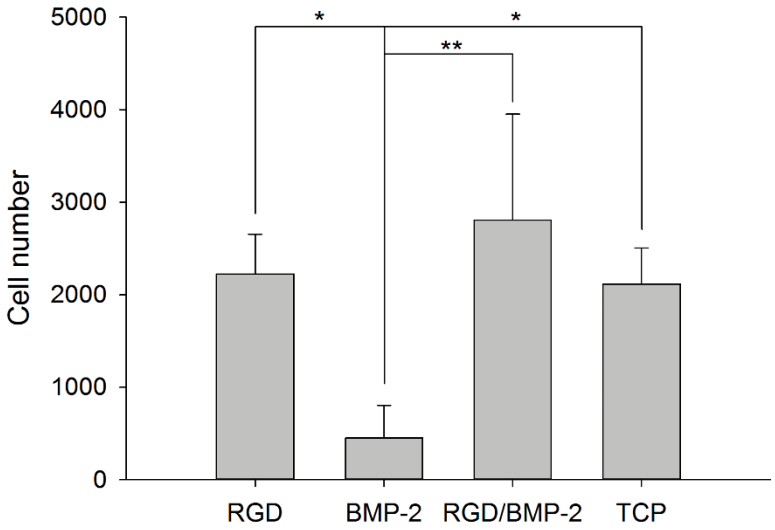

Figura 8. Número de hMSCs adheridas a las placas recubiertas con ELRs para cada condición.

5.4.3. Proliferación celular sobre sustratos de ELR

La proliferación celular sobre sustratos de ELR se evaluó cultivando células endoteliales (HUVECs) sobre el SELR (también denominado $(EIS)_2$-RGD6), adsorbido en placas de cultivo no adherentes, y sobre "ELR-catalyst free click gels" (ELR-CFCGs) formados por entrecruzamiento químico de moléculas de HRGD6 modificadas para contener grupos azida y ciclooctino (HRGD6-N_3 y HRGD6-ciclo, respectivamente). El uso de este tipo de células (HUVECs) viene justificado por estudios previos en los que se propone la utilización de hidrogeles basados en ELRs n aplicaciones cardiovasculares (60). Ambos ELRs contienen secuencias de adhesión celular, que contienen el tripéptido RGD, por lo que pueden aportar, *a priori*, un ambiente favorable para la adhesión y la proliferación celular. Así, las HUVECs se encontraron adheridas

a los sustratos de ELR-CFCGs, de forma similar al control (placa de cultivo; “tissue culture plate”, TCP, en inglés), como puede observarse en la Figura 9. Además, se observó una rápida proliferación para las células cultivadas en esta condición, dándose un número de células elevado a día 4, similar al encontrado a los 9 días. Por otro lado, se observó un número de células menor sobre los sustratos de SELR a día 1 ($p < 0,001$). Por tanto, el número de células sobre este sustrato a los 4 días, también mostró diferencias significativas con respecto a los ELR-CFCGs y el control ($p < 0,001$), aunque el valor obtenido es muy similar al número de células esperado (aproximadamente 2400), teniendo en cuenta el número de divisiones celulares entre el día 1 y el 4 (dos divisiones celulares como mucho). Por último, no se observaron diferencias significativas entre las distintas condiciones tras 9 días de cultivo, lo que indica que las HUVECs son capaces de proliferar hasta llegar a confluencia sobre sustratos de ELR-CFCGs y de SELR, de manera similar a lo que ocurre en el control (TCP).

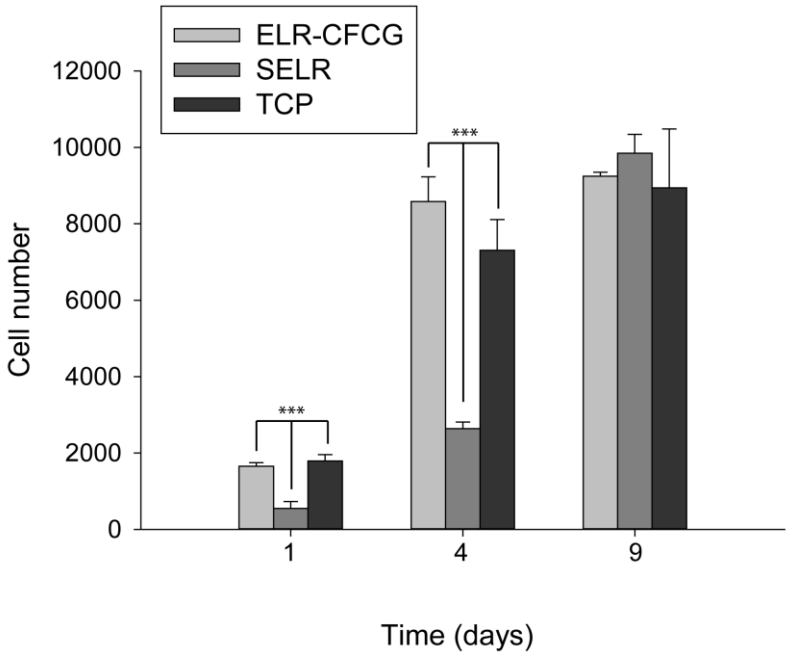

Figura 9. Número de HUVECs cultivadas sobre distintos sustratos de ELR a distintos tiempos. (***) $p < 0{,}001$ ($n = 3$).

Las diferencias en el número de HUVECs sobre el SELR y el ELR-CFCG pueden deberse a la variación en la densidad superficial de RGD de los sustratos (61, 62). En el caso del HRGD6, el ELR utilizado para la formación de ELR-CFCGs, su peso molecular es de 66 kDa y contiene 6 dominios RGD, mientras que el SELR mantiene el mismo número de motivos RGD, pero con un peso molecular de 121 kDa. Esto quiere decir que una superficie recubierta con SELR expondrá un menor número de dominios RGD que una con ELR-CFCG para la misma área. Esto podría influir también en la velocidad de proliferación, según sugieren estudios previos (63, 64).

5.4.4. Viabilidad celular en hidrogeles basados en ELRs inyectados *in vivo*

Con el objetivo de comprobar la viabilidad de Luc-hMSCs embebidas en el interior de hidrogeles basados en ELRs inyectados subcutáneamente en ratones, se midió la bioluminiscencia emitida por la oxidación de la luciferina en presencia de la luciferasa. Las células viables, metabólicamente activas, que no hayan migrado fuera del hidrogel expresarán esta enzima y podrá observarse bioluminiscencia. Este método es, además, mínimamente invasivo, por lo que permite reducir el número de animales utilizados en el experimento.

Los hidrogeles con hMSCs inyectados se formaron instantáneamente, lo cual se pudo comprobar por la aparición de una protuberancia debajo de la piel. Posteriormente, se midió la bioluminiscencia a distintos tiempos, observándose una señal en los animales con hidrogeles basados en SELR de concentraciones de 100 y 125 mg/mL después de 3 semanas, mientras que a las cuatro semanas sólo se observó señal para la concentración de 100 mg/mL (Figura 10). En cambio, para los ELR-CFCGs se detectó una señal de bioluminiscencia para todas las concentraciones usadas hasta el final del experimento a las 4 semanas.

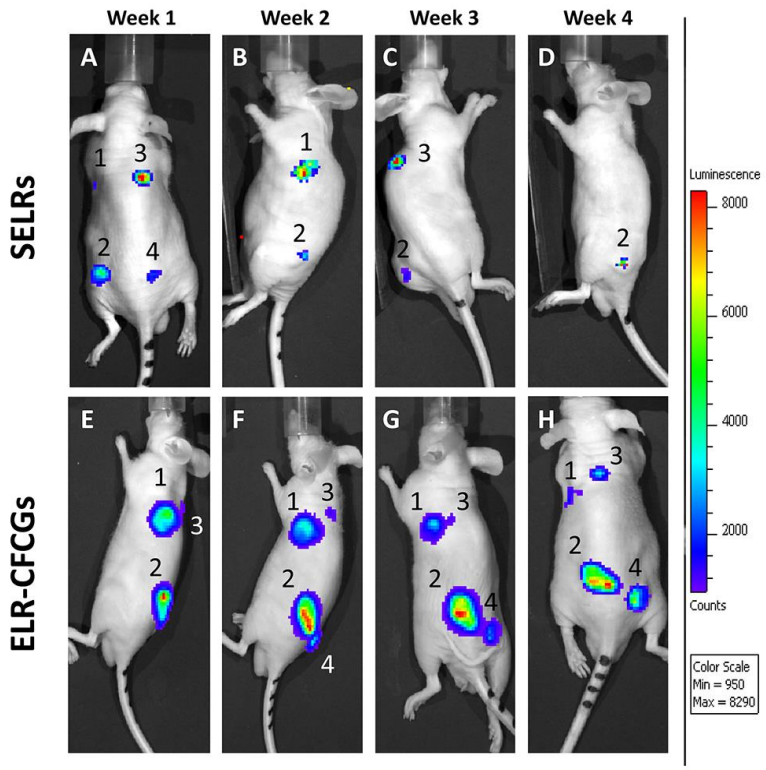

Figura 10. Imágenes de bioluminiscencia mediada por Luc-hMSCs embebidas en hidrogeles basados en SELR (A-D) y ELR-CFCGs (E-H) a distintos tiempos. Las concentraciones 1, 2, 3 y 4 corresponden a 75, 100, 125 y 150 mg/mL para el SELR y a 25, 50, 75 y 100 mg/mL para el ELR-CFCG, respectivamente.

Las diferencias entre ambos tipos de hidrogeles podrían deberse a que la migración de células desde dentro del hidrogel hacia fuera estaría más facilitada en el caso de aquellos constituidos por el SELR, puesto que están estabilizados por interacciones no covalentes que podrían ser contrarrestadas por las fuerzas ejercidas por la célula en su desplazamiento, mientras que esto no sería posible en hidrogeles estabilizados por entrecruzamiento químico, residiendo en el hidrogel durante más tiempo. Sin embargo, la presencia de hMSCs viables en ambos tipos de hidrogeles hasta 4

semanas después de haber sido inyectados, al menos en una de las concentraciones probadas, demuestra su citocompatibilidad, presentándose como candidatos a su utilización en aplicaciones de terapia celular.

5.5. Evaluación de la biocompatibilidad *in vivo* de hidrogeles basados en ELRs

5.5.1. Determinación de la respuesta inflamatoria sistémica mediante la cuantificación de citoquinas en sangre

La medida de la concentración de distintas citoquinas relacionadas con la respuesta inflamatoria (TNFα, IL-1β, IL-4, IL-6 e IL-10) en sangre a distintos tiempos, mediante ELISA (según lo descrito en el apartado 4.2.9.3), reveló la existencia de diferencias significativas entre los niveles de citoquinas encontrados en los grupos con hidrogeles basados en SELRs y ELR-CFCGs y el control positivo, LPS ($p < 0.05$), en todos los casos, con la excepción de IL-6 (Figura 11). Para los niveles de esta citoquina, no se encontraron diferencias significativas entre el grupo SELR y el LPS a los 2 días post-inyección, y tampoco a los 7 días entre ninguno de los grupos. Además, no hubo diferencias significativas entre las concentraciones de citoquinas medidas para el control negativo (PBS) y para ambos tipos de hidrogeles, exceptuando los niveles de IL-6 para el grupo SELR a día 1.

Por tanto, a tenor de estos resultados, podemos concluir que los hidrogeles basados en SELR (15 mg/hidrogel) y los ELR-CFCGs (7,5 mg/hidrogel) no inducen una respuesta inflamatoria mediada

por citoquinas al ser inyectados *in vivo*, constatando, igualmente, la ausencia de endotoxinas en los ELRs.

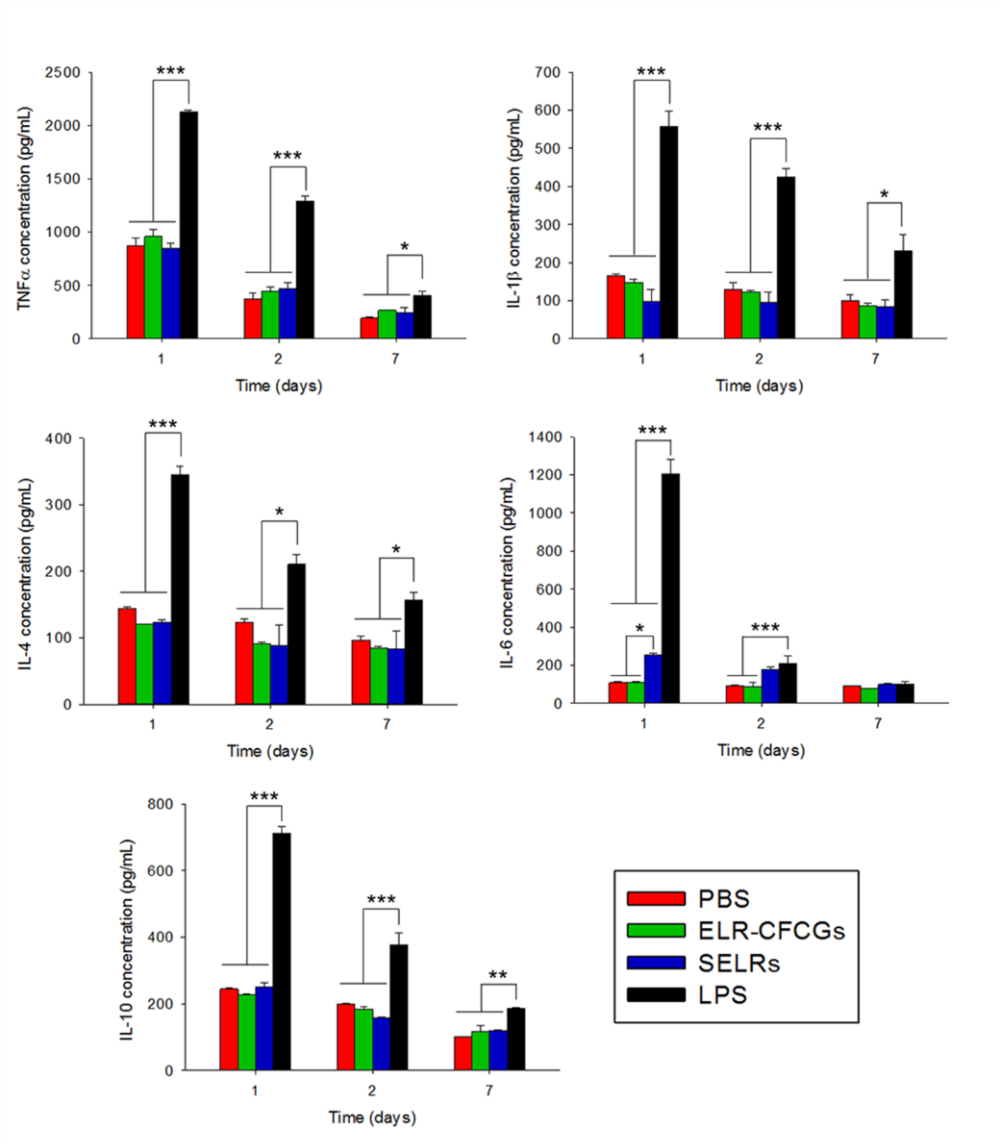

Figura 11. Concentraciones de citoquinas en sangre medidas por ELISA a distintos tiempos. (*) $p < 0,05$; (**) $p < 0,01$; (***) $p < 0,001$ (n = 3).

5.5.2. Valoración macroscópica de la estabilidad a largo plazo de los hidrogeles y de inducción de la respuesta a cuerpo extraño

Los hidrogeles inyectados se extrajeron a distintos tiempos post-inyección, en concreto 1, 3 y 6 meses. Ambos tipos fueron encontrados ligeramente adheridos a la hipodermis en todos los ratones de cada grupo, a todos los tiempos (Figura 12). Este resultado subraya la alta estabilidad de los hidrogeles al ser implantados subcutáneamente *in vivo*, lo cual está en concordancia con los resultados obtenidos *in vitro* previamente (28, 45). Esta estabilidad permitiría el uso de estos sistemas en ingeniería de tejidos y para la liberación de fármacos, teniendo en cuenta que sería necesario incluir secuencias sensibles a proteasas para conseguir su biodegradación.

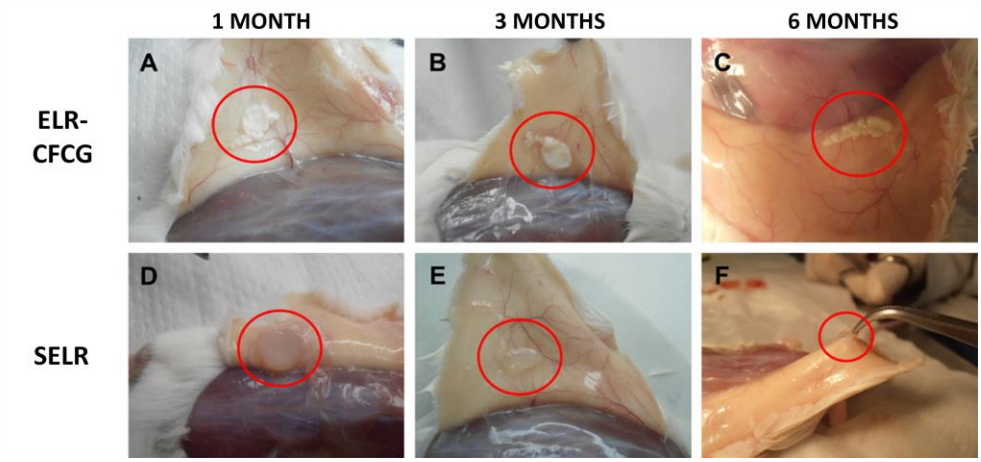

Figura 12. ELR-CFCGs (A-C) e hidrogeles basados en SELR (D-F) adheridos a la hipodermis de los ratones, extraídos a distintos tiempos post-inyección.

Por otro lado, no se observó encapsulación ni enrojecimiento de los tejidos en contacto con los hidrogeles. En cuanto a la

morfología, se observan diferencias en el color y en el aspecto general, siendo más homogéneos los hidrogeles basados en SELRs. La explicación de este fenómeno está en la distinta composición de las moléculas de ELR que componen cada tipo de hidrogel, y puede encontrarse con más detalle en el Capítulo 2 de esta tesis.

5.5.3. Evaluación histológica de hidrogeles basados en ELRs inyectados *in vivo*

La evaluación histológica de los distintos tipos de hidrogeles basados en ELRs, extraídos 6 meses después de su inyección subcutánea *in vivo*, y teñidos con hematoxilina-eosina, reveló la ausencia de macrófagos o células gigantes alrededor o dentro de los hidrogeles, indicando que no indujeron una respuesta inmune celular (Figura 13). Además, se observó la presencia de una fina capa de tejido conectivo alrededor de los dos tipos de hidrogeles, considerándose una reacción benigna por la que las células interaccionan con las células de un modo biocompatible, muy lejos de lo que se observaría en caso de haberse producido una encapsulación o fibrosis a consecuencia de una respuesta a cuerpo extraño.

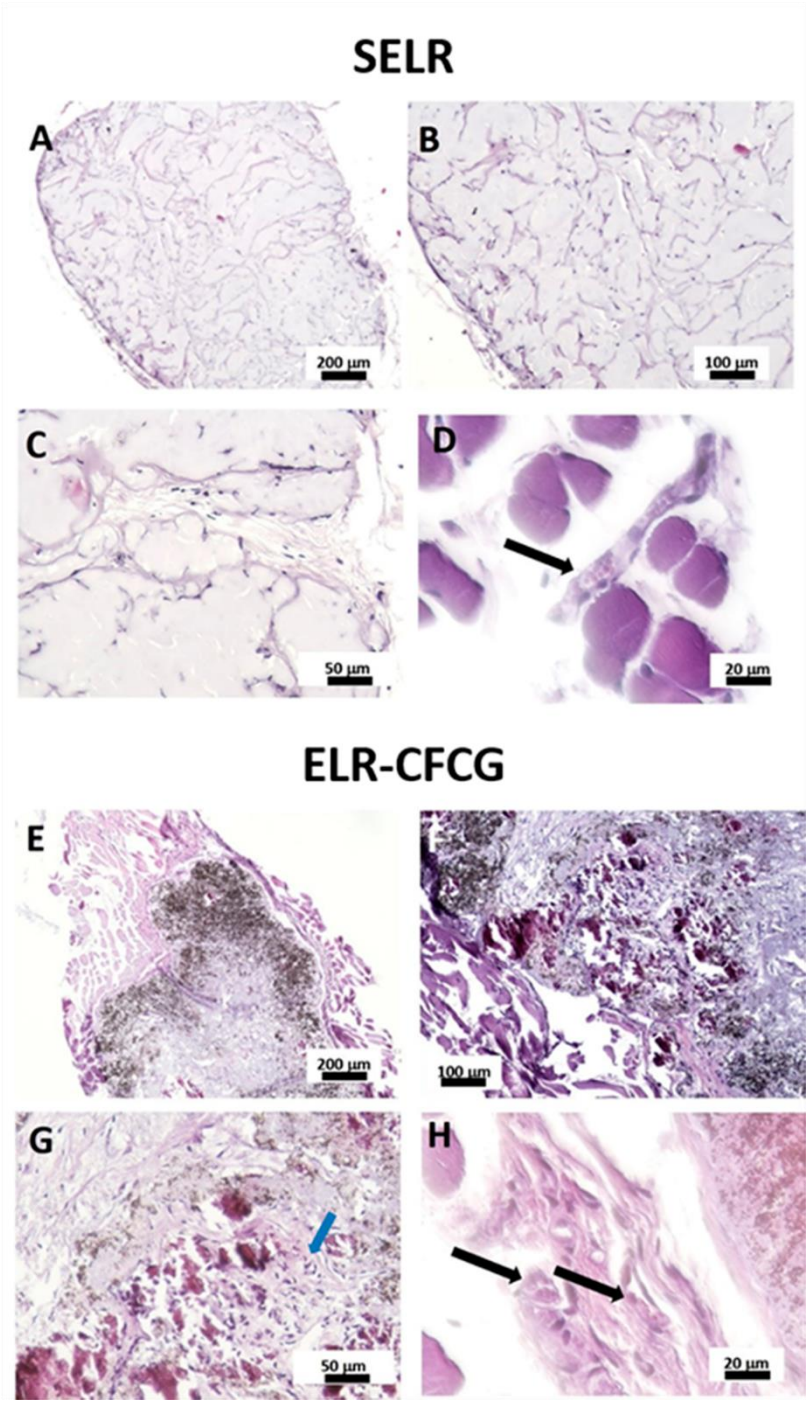

Figura 13. Secciones de hidrogeles basados en SELR (A-D) y de ELR-CFCGs (E-H) extraídos a los 6 meses post-inyección, teñidos con hematoxilina-eosina. Las flechas negras indican vasos sanguíneos.

Asimismo, pudo observarse la infiltración de células del propio animal dentro de los hidrogeles basados en SELR, mientras que este hecho no era tan obvio para los ELR-CFCGs, aunque pueden verse algunos núcleos celulares en el interior de estos últimos. Estas diferencias pueden explicarse del mismo modo que en el apartado 5.4.4. La colonización celular está probablemente promovida por la presencia de dominios de adhesión celular (RGD) en los hidrogeles. Además, se observaron vasos sanguíneos (flechas negras) alrededor de los hidrogeles, identificados por la presencia de glóbulos rojos dentro de estructuras tipo vaso, indicando una interacción biocompatible entre el organismo y los hidrogeles. En cuanto a la morfología microscópica, concuerda bien con lo observado en la evaluación macroscópica.

5.6. Evaluación de la regeneración ósea mediada por hidrogeles bioactivos basados en ELRs

5.6.1. Tomografía computerizada multi-corte (MSCT)

En cuanto a la reparación de hueso dañado, los estudios realizados por tomografía computerizada mostraron una buena regeneración ósea en la zona del defecto (Figura 14). De forma pormenorizada, la región distal de la metaepífisis mostró el cierre total del defecto en los planos coronales y sagitales para todas las muestras analizadas (n = 7), exceptuando una en la que se podía identificar un pequeño defecto de 1 mm en el sitio de la lesión, pudiendo ser, simplemente, una consecuencia de las diferencias entre animales en la velocidad de regeneración. De estos resultados puede deducirse que los hidrogeles basados en los recombinámeros

ELR-E-RGD y ELR-E-BMP-2 tienen un alto potencial osteogénico para restituir un defecto óseo de 6 mm de diámetro, probablemente debido a la bioactividad de la BMP-2.

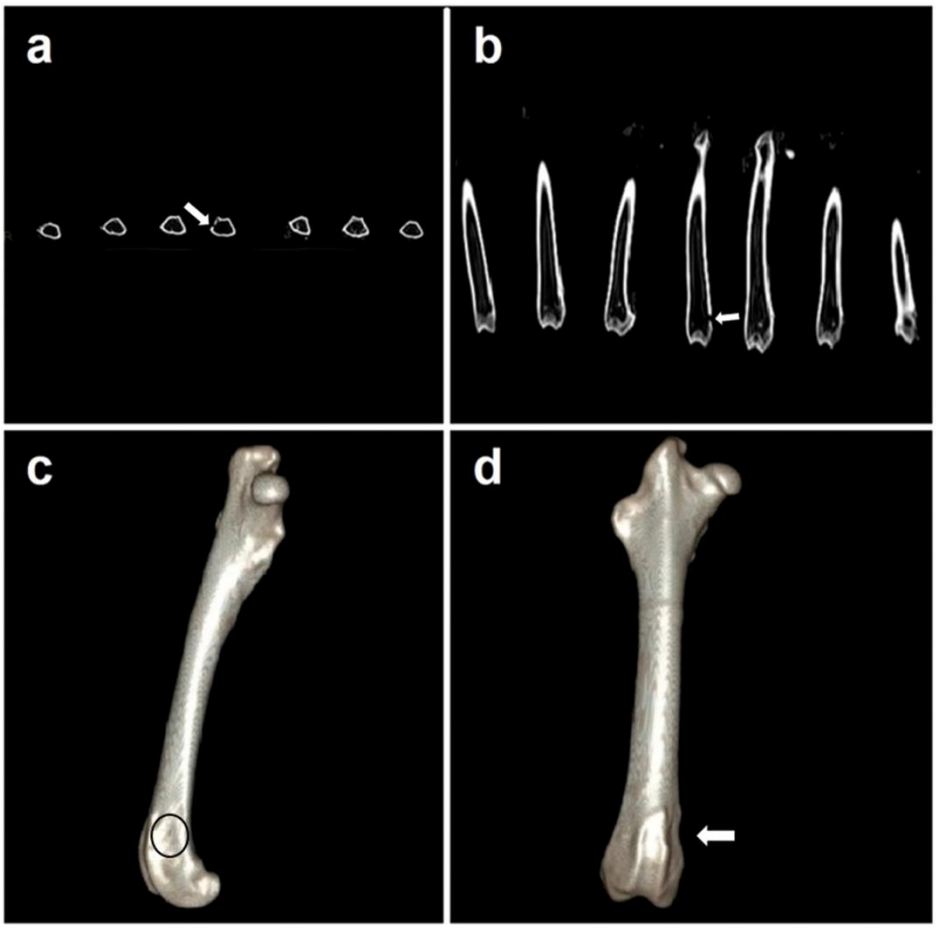

Figura 14. a) Tomografía axial computerizada. La flecha blanca señala la muestra parcialmente regenerada. b) Cortes coronales de la tomografía computerizada. La flecha blanca señala la muestra parcialmente regenerada. c) Reconstrucción 3D de uno de los fémures regenerados. La circunferencia negra indica la zona del defecto. d) Reconstrucción 3D del fémur parcialmente regenerado. La flecha blanca señala la zona donde persiste el defecto. Obsérvese que tal defecto es sólo una hendidura con continuidad en las capas subyacentes.

5.6.2. Resultados histológicos

Las muestras de los fémures utilizadas en el análisis histológico mostraron la formación de hueso regenerado en la zona del defecto. Este hueso neo-formado era grueso y contenía hueso lamelar o compacto. Además, se pudieron observar numerosos canales vasculares de distintos calibres, rodeados de varias capas de osteoblastos (Figura 15a). Cada capa de hueso se depositó sobre los restos del hidrogel basado en ELRs de una forma desorganizada (Figura 15b), pareciéndose al hueso pagetoide (Figura 15c), en el que las células producen un patrón en forma de mosaico en vez de un patrón lineal lamelar de hueso compacto. Además, se pudieron observar restos de los hidrogeles de ELR dentro de la zona del defecto, mostrando una forma de malla. Se observaron también estructuras redondas, triangulares, romboides o incluso amorfas en dicha malla, mostrando un patrón eosinófilo granular mineralizado. Estas estructuras mineralizadas se encontraron rodeadas de células tipo osteoblastos, con células similares a osteocitos dentro de ellas, observándose también angiogénesis (Figura 15d). Asimismo, se pueden observar zonas correspondientes a médula ósea hematopoyética alrededor de la zona del defecto rellenada con hueso trabecular (Figura 15e). Este hueso trabecular neo-formado se encontró cubierto por dos, tres o incluso más capas de osteoblastos. Además, se observaron osteocitos en la región interna del defecto (Figura 15f).

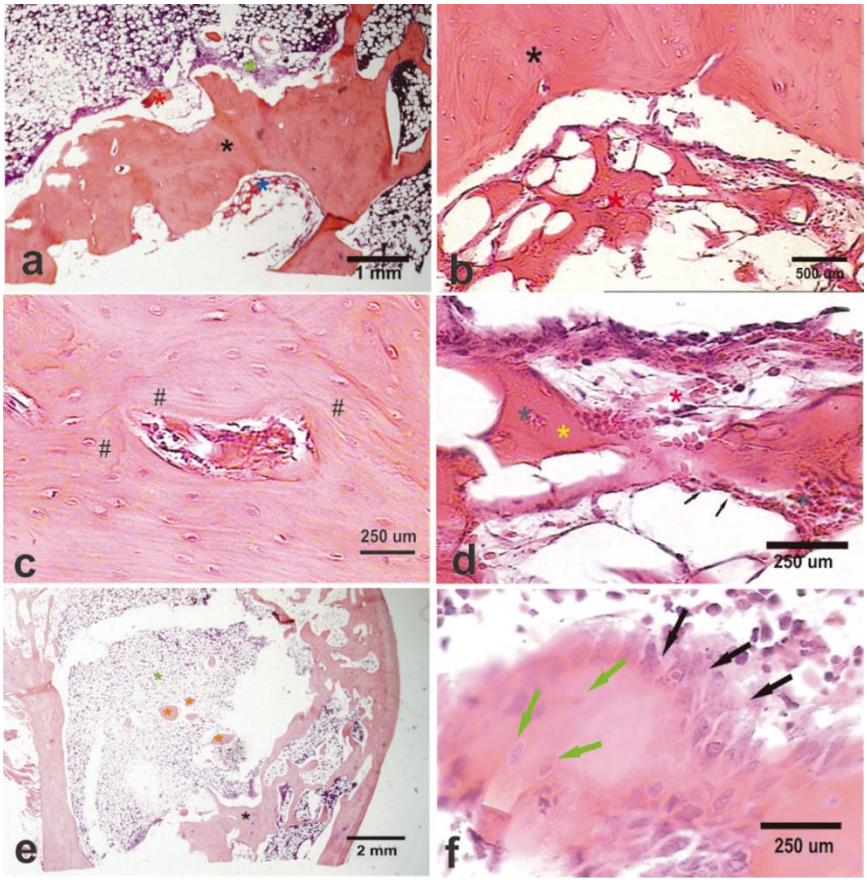

Figura 15. Microfotografías tomadas de secciones de hueso femoral descalcificado teñidas con hematoxilina-eosina. a) Zona del defecto regenerado en la que se observa hueso lamelar con numerosos vasos sanguíneos (asterisco negro), restos de hidrogel (asterisco azul), médula ósea hematopoyética y capas de osteoblastos (asterisco verde). b) Interfase entre el hueso lamelar (asterisco negro) y el hidrogel de ELR (asterisco rojo), con un aspecto de red. c) Zona del defecto en la que se observan canales vasculares en hueso lamelar neo-formado. Cada capa de hueso se encuentra depositada en forma de "mosaico", pareciéndose al hueso pagetoide. d) Zona del defecto en la que se observan regiones amorfas mineralizadas dentro de los restos del hidrogel, rodeadas de células similares a osteoblastos (flechas negras). También se observan zonas de micro-hemorragia (asterisco rojo) y vasos sanguíneos dilatados (asterisco gris). e) Microfotografía panorámica de la epífisis femoral y la metáfisis que muestra hueso neo-formado en la zona del defecto (asterisco negro). El hueso está rodeado por médula ósea hematopoyética (asterisco verde) con trabéculas óseas (asterisco naranja). f) Nódulos óseos alrededor de la región del defecto con múltiples capas de osteoblastos (flechas negras). También se pueden ver osteocitos dentro de un nódulo (flechas verdes).

Este análisis histológico muestra que la zona del defecto femoral fue reemplazada por hueso lamelar denso neo-formado. Aunque aún se podían observar algunos restos de los hidrogeles basados en ELRs 90 días después de la implantación, estos estaban rodeados por vasos sanguíneos dilatados y hueso denso, lo cual está en concordancia con el precepto aceptado de que sólo se forma hueso *de novo* en presencia de irrigación de sangre (65). Este hueso se dispone de forma aleatoria, irregularmente, en distintas direcciones, sugiriendo que la organización en forma de red en el interior del hidrogel dirige el depósito de la matriz ósea y la mineralización llevada a cabo por las células progenitoras que lo colonizan (66). Las nuevas trabéculas formadas muestran una forma peculiar, como si se hubieran obtenido por la confluencia de formaciones óseas redondeadas aisladas. Las numerosas capas de osteoblastos y las distintas formas observadas, que parecen simular una pseudo-estratificación, podrían ser resultado de la actividad de la BMP-2 liberada por el hidrogel por acción de la elastasa (67, 68).

5.7. Caracterización de la fluorescencia de SELR-FPs

El coeficiente de extinción molar (ε) se calculó a partir de la absorbancia medida en el máximo del espectro, utilizando la ecuación 1 (4.2.5), la cual fue A = 0,548 para el SELR-AcEGFP a 488 nm y A = 0,800 para el SELR-eqFP650 a 589 nm. De este modo, se obtuvo que el valor de ε corresponde al 21,7% y al 15,8% de los valores de ε de las FPs nativas para el SELR-AcEGFP y SELR-eqFP650, respectivamente. El resto de parámetros que completan la caracterización de la fluorescencia de los SELR-FPs se pueden observar en la Tabla 5.

Tabla 5. Parámetros característicos de la fluorescencia emitida por los dos SELR-FPs comparados con los de las FPs nativas.

Properties	AcGFP1 (Clontech)	SELR-AcEGFP	eqFP650 (TurboFP650, Evrogen)	SELR-eqFP650
Excitation peak (nm)	475	475	592	Peak 1 – 516 Peak 2 – 587
Emission peak (nm)	505	510	650	Peak 1 – 540 Peak 2 – 636
Molar extinction coefficient (ε, M^{-1} cm^{-1}) at excitation maximum	32500	7046	65000	10243
Fluorescence quantum yield (QY)	0.82	0.34	0.24	0.10
Brightness[a] (a.u.)	26650	2396	15600	1024
Brightness related to AcGFP1	1	0.09	0.59	0.04
Reference	Commercial brochure	This work	18	This work

En lo que respecta a los espectros de excitación y de emisión de los SELR-FPs (Figura 16), estos fueron muy similares a los descritos para las FPs nativas (36, 37, 39). Sin embargo, los máximos de excitación y de emisión para el SELR-eqFP650 se encontraron ligeramente desplazados, lo que sugiere que la fusión del SELR a la FP puede impedir la correcta maduración o dimerización de la misma, modificando la conformación del

cromóforo y, por tanto, el comportamiento de excitación y de emisión de fluorescencia.

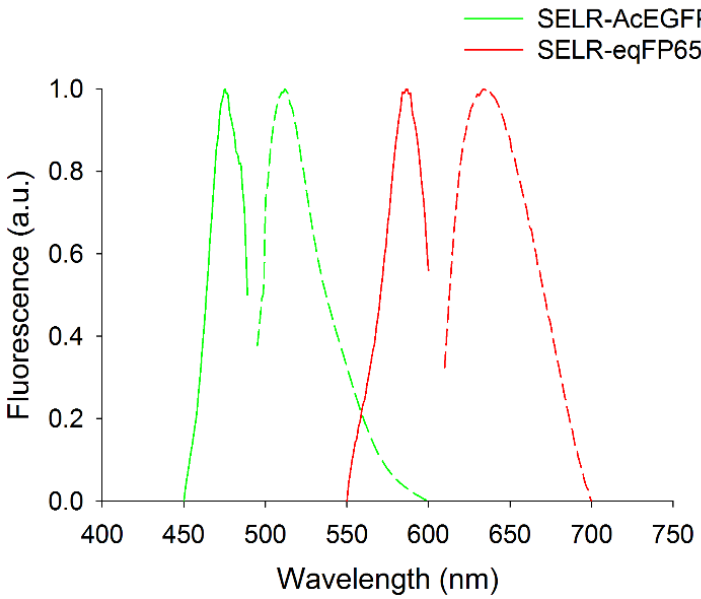

Figura 16. Espectros de excitación (líneas continuas) y de emisión (líneas discontinuas) para el SELR-AcEGFP y el SELR-eqFP650.

Por otro lado, se encontró un pico a 521 nm en el espectro de absorbancia del SELR-eqFP650 que no estaba descrito para la FP nativa. La aparición del mismo puede ser debida a la dimerización incompleta o al plegamiento incorrecto de la FP al estar fusionada al SELR. Sin embargo, este pico se solapa ampliamente con el pico de emisión del SELR-AcEGFP (**Figura 17**), mejorando potencialmente la eficiencia de la interacción FRET entre ambos SELR-FPs.

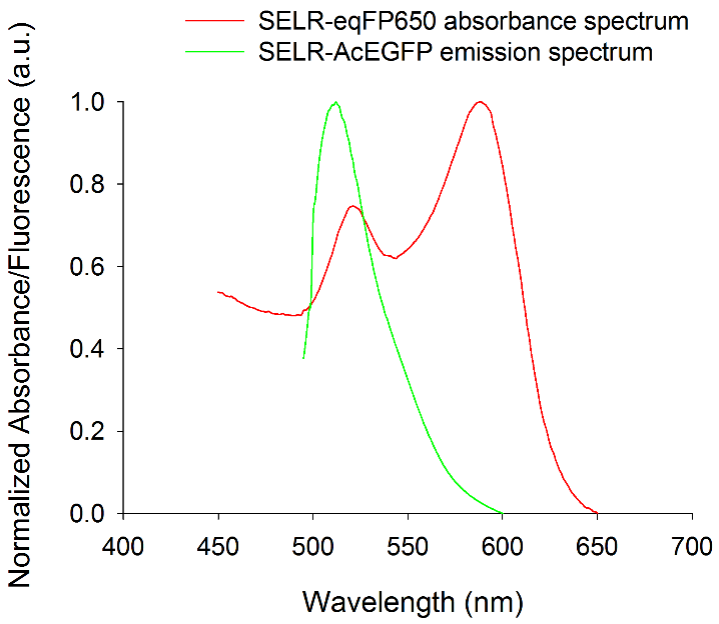

Figura 17. Solapamiento del espectro de absorbancia de SELR-eqFP650 y el espectro de emisión del SELR-AcEGFP.

5.8. Caracterización de la eficiencia de la interacción FRET entre dos SELR-FPs diferentes

La determinación experimental de la eficiencia de FRET (E) mediante espectroscopía se llevó a cabo según lo descrito en la sección 4.2.6.1. De este modo, se obtuvieron los espectros de emisión de disoluciones de SELR-AcEGFP y de una mezcla de una relación 1:1 molar de ambos SELR-FPs a distintas concentraciones. Como se puede observar en la Figura 18, la intensidad de fluorescencia del SELR-AcEGFP descendió en presencia del SELR-eqFP650 en todos los casos, excepto para la concentración más baja (10 mg/mL). Este último caso puede explicarse por el hecho de que la distancia entre el SELR-AcEGFP y el SELR-eqFP650 a esa

concentración probablemente es demasiado alta, no pudiendo ocurrir el efecto FRET.

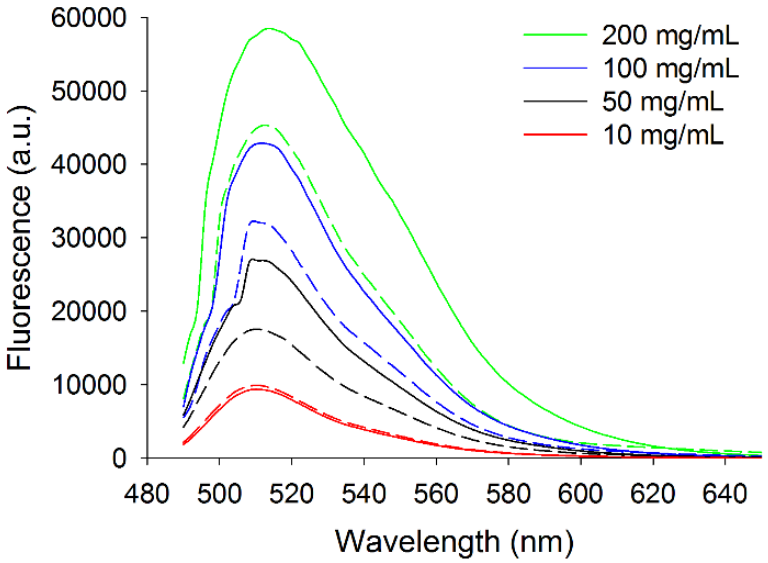

Figura 18. Espectros de emisión (λ_{ex} = 475 nm) de disoluciones de SELR-AcEGFP (líneas sólidas) y de una mezcla 1:1 molar de ambos SELR-FPs (líneas discontínuas) a distintas concentraciones.

Con estos datos, se calculó el valor de la eficiencia de FRET (*E)* para cada caso, a dos temperaturas diferentes, por debajo (15ºC) y por encima (37ºC) de la T_t, como se ha descrito anteriormente (4.2.6.1). Los resultados, según se observa en la Figura 19, muestran que a 10 mg/mL la *E* es despreciable o nula, a diferencia del resto de concentraciones. Por otro lado, no existen diferencias significativas entre los valores obtenidos a distintas temperaturas para ninguna concentración (los valores exactos se pueden observar en la Tabla 6).

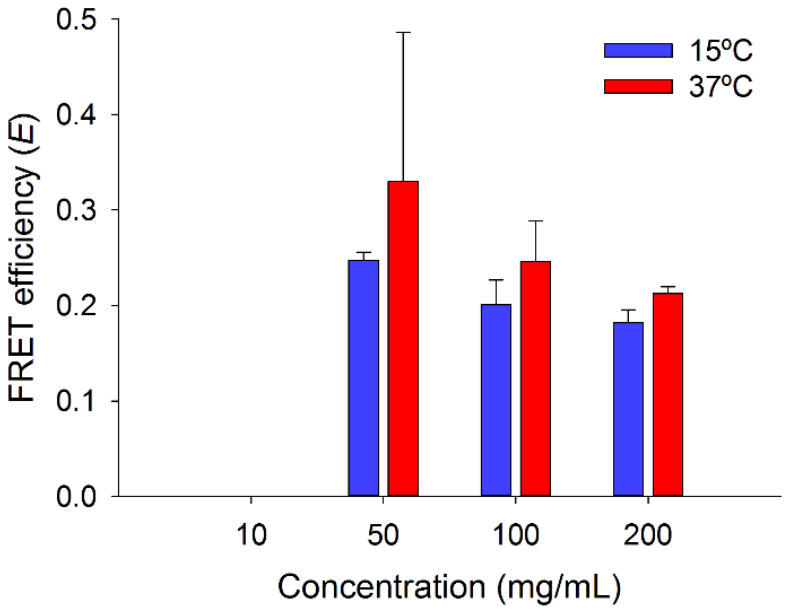

Figura 19. Eficiencias de FRET calculadas por espectroscopía ("quencheo" del donador) a distintas temperaturas y concentraciones.

Tabla 6. Eficiencias de FRET para la mezcla 1:1 molar de SELR-FPs a distintas concentraciones y temperaturas (n=2).

Concentration (mg/mL)	Temperature (ºC)	FRET efficiency (mean ± SD)
	15	0
	37	0
	15	0.247 ± 0.008
	37	0.330 ± 0.156
	15	0.201 ± 0.026
	37	0.246 ± 0.043
	15	0.182 ± 0.014
	37	0.212 ± 0.007

La ausencia de diferencias entre las distintas concentraciones y temperaturas utilizadas en el experimento sugiere que una vez que se alcanza una concentración mínima (entre 10 y 50 mg/mL), la distancia entre las moléculas de SELR-FPs es suficientemente pequeña para permitir el FRET (1-10 nm), independientemente de la agregación de los bloques tipo elastina por encima de la T_t. En este punto, es necesario tener en cuenta que los dominios tipo seda son capaces de establecer interacciones entre ellos a cualquier temperatura, lo que podría ayudar a las moléculas a apilarse y a permanecer a una distancia menor a temperaturas menores a la T_t. Además, puede observarse un incremento en E por encima de la T_t, probablemente debido a la interacción hidrofóbica de los bloques tipo elastina de los SELR-FPs.

Por otro lado, se calculó E por microscopía confocal, según lo especificado en el apartado 4.2.6.2. En la Figura 20 se pueden observar las imágenes correspondientes a un campo ("field of view", FOV, en inglés) dentro del hidrogel formado a partir de una mezcla 1:1 molar de ambos SELR-FPs a 200 mg/mL. Para conseguir el "quemado" del aceptor se eligió una región de interés ("region of interest", ROI, en inglés) sobre la cual se hizo incidir el láser de alta intensidad. De ese ROI, se tomaron imágenes antes y después del "quemado", pudiendo observarse claramente un aumento en la intensidad de fluorescencia en el canal verde (correspondiente al SELR-AcEGFP) en la imagen Post, con respecto a la Pre, mientras que en el canal rojo se puede ver una disminución drástica de la fluorescencia (93,8 ± 0,3%). Este resultado puede observarse aún más claramente en la imagen FRET, obtenida de la substracción de la imagen Pre de la Post.

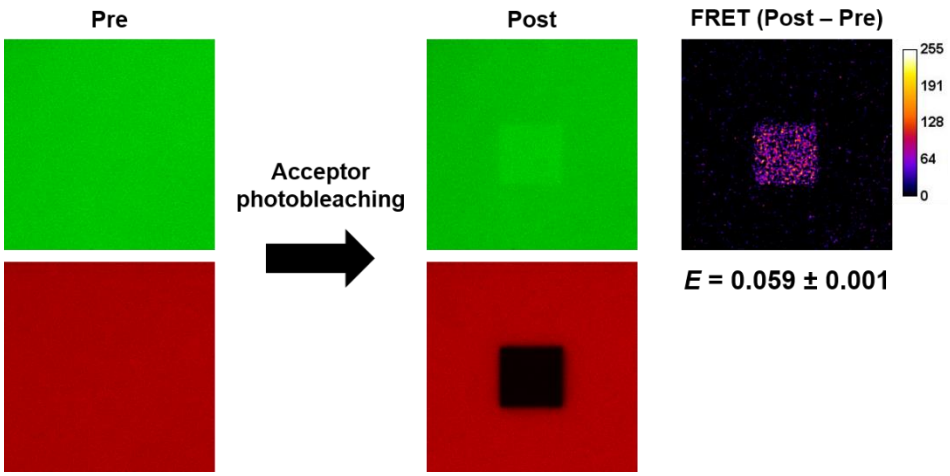

Figura 20. Diagrama que muestra los resultados del "desquencheo" de SELR-AcEGFP al "quemar" el SELR-eqFP650 mediante microscopía confocal.

Posteriormente, se calculó la intensidad de los píxeles en el canal verde dentro del ROI en la imagen Pre y Post, lo cual sirvió para la obtención de la *E*. Para ello, se hizo uso de la ecuación 4, que tiene en cuenta la corrección de los datos experimentales, como se explica en la sección 4.2.6.2. De este modo, se obtuvo que E = 0,059 ± 0,001. Este valor contrasta con el determinado por espectroscopía de fluorescencia. La discrepancia entre ambos valores de E puede explicarse por los métodos usados para la determinación de cada uno de ellos. En concreto, en el cálculo de E por espectroscopía, se utiliza la ecuación 2, que resulta de la simplificación de otras fórmulas más complejas, asumiendo que la intensidad de la excitación del donador (SELR-AcEGFP), y todos los parámetros de medida, son idénticos para las disoluciones de SELR-AcEGFP y de la mezcla 1:1 molar de ambos SELR-FPs (69). Puesto que ambas medidas se realizaron a la vez, los parámetros son iguales. Sin embargo, la primera asunción no se pudo confirmar, debido al

solapamiento de los espectros del SELR-AcEGFP y el SELR-eqFP650. Por tanto, se confió en una preparación de la muestra precisa y en el uso de duplicados para evitar este tipo de errores, que podrían no haber sido erradicados completamente. Además, en lo que respecta a la microscopía confocal, no se consiguió un "quemado" del aceptor al 100% (la reducción en la intensidad de emisión de fluorescencia en el canal rojo, correspondiente al SELR-eqFP650, fue del 93,8 ± 0,3%), por lo que la *E* calculada mediante esta técnica podría no ser tan alta como realmente es.

Por último, cabe reseñar que la aparición de este fenómeno FRET entre dos SELR-FPs permitiría, por ejemplo, el desarrollo de biosensores fluorescentes ratiométricos, en los que se mide el cambio de la fluorescencia de la FP donadora en presencia de la aceptora en respuesta a un estímulo, siendo más sensibles que los sensores intensiométricos (70). Estos biosensores requerirían la fusión a los SELR-FPs de secuencias de unión a distintas moléculas diana, como glucosa (71) o iones metálicos (72).

6. CONCLUSIONES

6.1. Diseño, bioproducción y caracterización de ELRs formadores de hidrogeles

En esta tesis, se han desarrollado ELRs formadores de hidrogeles novedosos, con una bioactividad mejorada en términos de adhesión celular, osteogenesis y emisión de fluorescencia. Con respecto a la adhesión celular, se ha diseñado y bioproducido un SELR con dominios RGD, con el objetivo de formar hidrogeles biomiméticos. Por otro lado, se ha fusionado la BMP-2 a un ELR sensible a elastasa y, por tanto, biodegradable, para conseguir un biomaterial osteogénico. Por último, para conseguir una emisión de fluorescencia por parte de los hidrogeles basados en ELRs, se han fusionado dos FPs a un SELR (por separado). Una de esas FPs, en concreto la AcEGFP, deriva de la GFP, y, por tanto, emite en el rango de longitudes de onda correspondientes al verde en el espectro visible. En cambio, la otra FP utilizada, denominada eqFP650, emite fluorescencia en el rojo lejano. Todas estas construcciones génicas fueron obtenidas satisfactoriamente, tal y como se comprobó por electroforesis en geles de agarosa y secuenciación de ADN. Los ELRs se expresaron en *Escherichia coli* para su bioproducción, obteniendo rendimientos de 120 a 400 mg/L de medio de cultivo.

Las técnicas de caracterización, tales como SDS-PAGE y MALDI-TOF, determinaron una buena concordancia entre el peso molecular experimental y el teórico o esperado. Por otro lado, la T_t de los ELRs se comprobó mediante medidas de DSC, confirmando

que estaba por debajo de la temperatura fisiológica en todos los casos, pudiendo ser utilizados para formar hidrogeles al ser inyectados *in vivo*. Otros métodos, como ^{1}H-NMR y HPLC aportaron resultados aceptables para confirmar la pureza de todos los lotes de los distintos ELRs. Además, las propiedades mecánicas demostraron ser fácilmente modificables según la concentración de los ELRs.

6.2. Biocompatibilidad de hidrogeles basados en ELRs

La biocompatibilidad en términos generales de hidrogeles basados en ELRs entrecruzados física o químicamente ha sido evaluada en este trabajo mediante distintos métodos, tanto *in vitro* como *in vivo*. Concretamente, se ha mostrado cómo las células endoteliales (HUVECs) fueron capaces de proliferar al ser sembradas en superficies recubiertas con ELR a lo largo de 9 días de cultivo. Además, se inyectaron subcutáneamente en ratones Luc-hMSCs embebidas en el interior de hidrogeles basados en ELRs, y su viabilidad fue confirmada por bioluminiscencia, tras la inyección de luciferasa, hasta un tiempo de 4 semanas. Por otro lado, la inyección subcutánea de hidrogeles basados en ELRs no indujo una respuesta inflamatoria, según los resultados obtenidos en la determinación de la concentración de distintas citoquinas (TNFα, IL-1β, IL-4, IL-6 and IL-10), en comparación con los controles negativo (PBS) y positivo (LPS). La observación macroscópica e histológica de estos hidrogeles inyectados *in vivo* corroboró los resultados obtenidos en los experimentos anteriores, mostrando una gran estabilidad de los hidrogeles después de 6 meses.

Asimismo, se observó una reacción leve, mostrando la ausencia de respuesta a cuerpo extraño para ambos tipos de hidrogeles, viéndose también una infiltración y colonización celular de los hidrogeles, de una forma biocompatible.

En resumen, este trabajo confirma la biocompatibilidad de dos tipos de hidrogeles multi-propósito basados en ELRs, siendo este el primer paso hacia el uso de estos hidrogeles en distintas aplicaciones en los campos de la ingeniería de tejidos y la medicina regenerativa.

6.3. Regeneración ósea mediada por hidrogeles bioactivos y biodegradables basados en ELRs

Una vez conocida la biocompatibilidad de los hidrogeles basados en ELRs, se evaluó la capacidad de un hidrogel bioactivo y biodegradable basado en ELRs de promover la regeneración de un defecto óseo. En primer lugar, se biosintetizaron dos ELRs sensibles a elastasa y formadores de hidrogeles, uno de ellos conteniendo secuencias de adhesión celular (RGD) y el otro incluyendo el factor de crecimiento BMP-2. Posteriormente, se evaluó *in vitro* la biodegradación de una mezcla de ambos ELRs, mediante la digestión enzimática con elastasa, confirmando la sensibilidad a esta enzima. Además, la ausencia de citotoxicidad de los ELRs se comprobó cultivando hMSCs en medio suplementado con los mismos, mientras que la adhesión celular sobre sustratos de ELR también fue demostrada. Por último, se creó un defecto en el hueso femoral de conejos New Zealand, que fueron rellenados con el hidrogel formado a partir de una mezcla de ELRs. Tras 3 meses, los huesos fueron extraídos y la regeneración fue evaluada mediante

distintos métodos. La tomografía computerizada en 3D mostró una reparación completa del defecto, con calcificación de hueso, en 6 de 7 muestras, estando la restante casi completamente regenerada. El análisis histológico mostró la formación *de novo* de hueso lamelar (compacto), junto con zonas similares al hueso pagetoide con una estructura menos organizada, probablemente debido a la disposición de la matriz neo-formada siguiendo la red del hidrogel. Se podían observar todavía algunos fragmentos de los hidrogeles basados en ELRs, pero estaban casi completamente degradados por la acción de la elastasa secretada dentro de la fase de remodelación ocurrida durante el proceso de regeneración.

En conclusión, este trabajo confirma la capacidad de un hidrogel bioactivo y biodegradable basado en ELRs de regenerar tejido óseo, siendo osteoinductivo y osteoconductivo.

6.4. Evaluación de la fluorescencia y de la interacción FRET entre dos SELR-FPs diferentes

Dos SELRs fluorescentes capaces de formar hidrogeles han sido desarrollados durante esta tesis, mediante la bioconjugación genética de dos proteínas fluorescentes diferentes: AcEGFP y eqFP650, dando lugar a dos SELRs distintos. En lo que respecta a las propiedades de fluorescencia, el espectro de excitación y de emisión de ambos recombinámeros fueron similares a los de las FPs nativas, excepto por algunas diferencias en el máximo de excitación y de emisión de la eqFP650, así como en los espectros globales, probablemente debido a una maduración incompleta del plegamiento y/o de la dimerización. Concretamente, se encontró un pico desplazado hacia luz verde en el espectro de absorción del

SELR-eqFP650, no descrito en la bibliografía para la FP nativa, y que se solapaba en gran medida con el espectro de emisión del SELR-AcEGFP, lo cual motivó la evaluación de la interacción FRET entre ambos SELR-FPs. Por tanto, se calculó la eficiencia FRET (E) mediante distintos métodos dando resultados diferentes, posiblemente por la existencia de errores derivados de las distintas técnicas. Además, los valores de E fueron similares para todas las condiciones probadas, siendo así independiente de la concentración (una vez que se ha llegado a una concentración mínima) y de la temperatura (por encima o por debajo de la T_t).

Este trabajo muestra la evidencia de cómo SELRs fusionados a FPs diferentes pueden utilizarse en el estudio de E para nuevas parejas de FRET. Por otro lado, pueden deducirse múltiples aplicaciones de este trabajo, como el estudio de estructuras auto-ensambladas basadas en ELRs (p. ej., partículas o hidrogeles), y el desarrollo de hidrogeles para ingeniería de tejidos con trazabilidad mejorada. Del mismo modo, los SELR-FPs descritos aquí pueden llegar a emplearse como biosensores, por sí mismos o como pareja de FRET, gracias a la posibilidad de incluir dominios de unión a metales u otros ligandos, debido a su naturaleza recombinante.

7. REFERENCIAS

1. Berger J. The age of biomedicine: current trends in traditional subjects. Journal of Applied Biomedicine. 2011;9(2):57-61.
2. Khademhosseini A, Langer R. A decade of progress in tissue engineering. Nat Protocols. 2016;11(10):1775-81.
3. Appel AA, Anastasio MA, Larson JC, Brey EM. Imaging challenges in biomaterials and tissue engineering. Biomaterials. 2013;34(28):6615-30.
4. Yellen G, Mongeon R. Quantitative two-photon imaging of fluorescent biosensors. Current Opinion in Chemical Biology. 2015;27:24-30.
5. Williams DF. On the nature of biomaterials. Biomaterials. 2009;30(30):5897-909.
6. Frydman A, Simonian K. Review of models for titanium as a foreign body. Journal of the California Dental Association. 2014;42(12):829-33.
7. Denry I, Kelly JR. Emerging ceramic-based materials for dentistry. Journal of dental research. 2014;93(12):1235-42.
8. Migonney V. History of Biomaterials. Biomaterials: John Wiley & Sons, Inc.; 2014. p. 1-10.
9. Pan Z, Ding J. Poly(lactide-co-glycolide) porous scaffolds for tissue engineering and regenerative medicine. Interface Focus. 2012;2(3):366-77.
10. Hu J, Sun X, Ma H, Xie C, Chen YE, Ma PX. Porous nanofibrous PLLA scaffolds for vascular tissue engineering. Biomaterials. 2010;31(31):7971-7.
11. Lee KY, Mooney DJ. Alginate: Properties and biomedical applications. Progress in Polymer Science. 2012;37(1):106-26.
12. Melke J, Midha S, Ghosh S, Ito K, Hofmann S. Silk fibroin as biomaterial for bone tissue engineering. Acta Biomaterialia. 2016;31:1-16.
13. Girotti A, Orbanic D, Ibáñez-Fonseca A, Gonzalez-Obeso C, Rodríguez-Cabello JC. Recombinant Technology in the Development of Materials and

Systems for Soft-Tissue Repair. Advanced healthcare materials. 2015;4(16):2423-55.

14. Williams DF. On the mechanisms of biocompatibility. Biomaterials. 2008;29(20):2941-53.

15. Langer R, Vacanti J. Tissue engineering. Science. 1993;260(5110):920-6.

16. Mao AS, Mooney DJ. Regenerative medicine: Current therapies and future directions. Proceedings of the National Academy of Sciences. 2015;112(47):14452-9.

17. Melton LJ, Achenbach SJ, Atkinson EJ, Therneau TM, Amin S. Long-term mortality following fractures at different skeletal sites: a population-based cohort study. Osteoporosis International. 2013;24(5):1689-96.

18. Compston J. Osteoporosis: Social and Economic Impact. Radiologic Clinics. 2010;48(3):477-82.

19. Alghazali KM, Nima ZA, Hamzah RN, Dhar MS, Anderson DE, Biris AS. Bone-tissue engineering: complex tunable structural and biological responses to injury, drug delivery, and cell-based therapies. Drug Metabolism Reviews. 2015;47(4):431-54.

20. Amini AR, Laurencin CT, Nukavarapu SP. Bone Tissue Engineering: Recent Advances and Challenges. Critical reviews in biomedical engineering. 2012;40(5):363-408.

21. Detsch R, Boccaccini AR. The role of osteoclasts in bone tissue engineering. Journal of Tissue Engineering and Regenerative Medicine. 2015;9(10):1133-49.

22. Rodríguez-Cabello JC, Martín L, Alonso M, Arias FJ, Testera AM. "Recombinamers" as advanced materials for the post-oil age. Polymer. 2009;50(22):5159-69.

23. Urry DW. What Sustains Life? Consilient Mechanisms for Protein-Based Machines and Materials. Boston (USA): Birkhäuser Boston; 2006.

24. Ribeiro A, Arias FJ, Reguera J, Alonso M, Rodríguez-Cabello JC. Influence of the Amino-Acid Sequence on the Inverse Temperature Transition of Elastin-Like Polymers. Biophysical Journal. 2009;97(1):312-20.

25. Herrero-Vanrell R, Rincón AC, Alonso M, Reboto V, Molina-Martinez IT, Rodríguez-Cabello JC. Self-assembled particles of an elastin-like polymer as vehicles for controlled drug release. Journal of Controlled Release. 2005;102(1):113-22.

26. Martín L, Castro E, Ribeiro A, Alonso M, Rodríguez-Cabello JC. Temperature-Triggered Self-Assembly of Elastin-Like Block Co-Recombinamers:The Controlled Formation of Micelles and Vesicles in an Aqueous Medium. Biomacromolecules. 2012;13(2):293-8.

27. Rodríguez-Cabello JC, Girotti A, Ribeiro A, Arias FJ. Synthesis of Genetically Engineered Protein Polymers (Recombinamers) as an Example of Advanced Self-Assembled Smart Materials. In: Navarro M, Planell JA, editors. Nanotechnology in Regenerative Medicine: Methods and Protocols. Totowa, NJ: Humana Press; 2012. p. 17-38.

28. Fernandez-Colino A, Arias FJ, Alonso M, Rodriguez-Cabello JC. Self-organized ECM-mimetic model based on an amphiphilic multiblock silk-elastin-like corecombinamer with a concomitant dual physical gelation process. Biomacromolecules. 2014;15(10):3781-93.

29. Ruoslahti E, Pierschbacher MD. Arg-Gly-Asp: A versatile cell recognition signal. Cell. 1986;44(4):517-8.

30. Ruoslahti E. RGD and other recognition sequences for integrins. Annual Review of Cell and Developmental Biology. 1996;12(1):697-715.

31. Barczyk M, Carracedo S, Gullberg D. Integrins. Cell and Tissue Research. 2009;339(1):269.

32. Liu JC, Heilshorn SC, Tirrell DA. Comparative Cell Response to Artificial Extracellular Matrix Proteins Containing the RGD and CS5 Cell-Binding Domains. Biomacromolecules. 2004;5(2):497-504.

33. Chen D, Zhao M, Mundy GR. Bone Morphogenetic Proteins. Growth Factors. 2004;22(4):233-41.

34. Inoda H, Yamamoto G, Hattori T. Histological investigation of osteoinductive properties of rh-BMP2 in a rat calvarial bone defect model. Journal of Cranio-Maxillofacial Surgery. 2004;32(6):365-9.

35. Lombard C, Arzel L, Bouchu D, Wallach J, Saulnier J. Human leukocyte elastase hydrolysis of peptides derived from human elastin exon 24. Biochimie. 2006;88(12):1915-21.

36. Gurskaya NG, Fradkov AF, Pounkova NI, Staroverov DB, Bulina ME, Yanushevich YG, et al. A colourless green fluorescent protein homologue from the non-fluorescent hydromedusa Aequorea coerulescens and its fluorescent mutants. Biochemical Journal. 2003;373(2):403.

37. Cormack BP, Valdivia RH, Falkow S. FACS-optimized mutants of the green fluorescent protein (GFP). Gene. 1996;173(1):33-8.

38. Kobayashi H, Ogawa M, Alford R, Choyke PL, Urano Y. New Strategies for Fluorescent Probe Design in Medical Diagnostic Imaging. Chemical Reviews. 2010;110(5):2620-40.

39. Shcherbo D, Shemiakina II, Ryabova AV, Luker KE, Schmidt BT, Souslova EA, et al. Near-infrared fluorescent proteins. Nat Meth. 2010;7(10):827-9.

40. Day RN, Davidson MW. Fluorescent proteins for FRET microscopy: Monitoring protein interactions in living cells. BioEssays. 2012;34(5):341-50.

41. Obeng EM, Dullah EC, Danquah MK, Budiman C, Ongkudon CM. FRET spectroscopy-towards effective biomolecular probing. Analytical Methods. 2016;8(27):5323-37.

42. Kopeček J. Hydrogel biomaterials: A smart future? Biomaterials. 2007;28(34):5185-92.

43. Hunt JA, Chen R, van Veen T, Bryan N. Hydrogels for tissue engineering and regenerative medicine. Journal of Materials Chemistry B. 2014;2(33):5319-38.

44. Martin L, Arias FJ, Alonso M, Garcia-Arevalo C, Rodriguez-Cabello JC. Rapid micropatterning by temperature-triggered reversible gelation of a

recombinant smart elastin-like tetrablock-copolymer. Soft Matter. 2010;6(6):1121-4.

45. Gonzalez de Torre I, Santos M, Quintanilla L, Testera A, Alonso M, Rodriguez Cabello JC. Elastin-like recombinamer catalyst-free click gels: characterization of poroelastic and intrinsic viscoelastic properties. Acta biomaterialia. 2014;10(6):2495-505.

46. Kagan HM, Li W. Lysyl oxidase: Properties, specificity, and biological roles inside and outside of the cell. Journal of Cellular Biochemistry. 2003;88(4):660-72.

47. Girotti A. Desarrollo de una plataforma biotecnológica para la obtención de polímeros recombinantes tipo elastina. Valladolid: Universidad de Valladolid; 2007.

48. Meyer DE, Chilkoti A. Protein purification by inverse transition cycling. Protein Interactions. New York (USA): Cold Spring Harbor Laboratory Press; 2002. p. 329-43.

49. Laemmli UK. Cleavage of structural proteins during the assembly of the head of bacteriophage T4. Nature. 1970;227(5259):680-5.

50. Lee C, Levin A, Branton D. Copper staining: A five-minute protein stain for sodium dodecyl sulfate-polyacrylamide gels. Analytical Biochemistry. 1987;166(2):308-12.

51. Lakowicz JR. Principles of Fluorescence Spectroscopy. 3 ed: Springer US; 2006. XXVI, 954 p.

52. Lehner MD, Ittner J, Bundschuh DS, van Rooijen N, Wendel A, Hartung T. Improved Innate Immunity of Endotoxin-Tolerant Mice Increases Resistance to Salmonella enterica Serovar Typhimurium Infection despite Attenuated Cytokine Response. Infection and Immunity. 2001;69(1):463-71.

53. Fischer AH, Jacobson KA, Rose J, Zeller R. Hematoxylin and Eosin Staining of Tissue and Cell Sections. Cold Spring Harbor Protocols. 2008;2008(5):pdb.prot4986.

54. Coletta DJ, Lozano D, Rocha-Oliveira AA, Mortarino P, Bumaguin GE, Vitelli E, et al. Characterization of Hybrid Bioactive Glass-polyvinyl Alcohol Scaffolds Containing a PTHrP-derived Pentapeptide as Implants for Tissue Engineering Applications. The Open Biomedical Engineering Journal. 2014;8:20-7.

55. Shibata Y, Fujita S, Takahashi H, Yamaguchi A, Koji T. Assessment of decalcifying protocols for detection of specific RNA by non-radioactive in situ hybridization in calcified tissues. Histochemistry and cell biology. 2000;113(3):153-9.

56. Christensen T, Hassouneh W, Trabbic-Carlson K, Chilkoti A. Predicting Transition Temperatures of Elastin-Like Polypeptide Fusion Proteins. Biomacromolecules. 2013;14(5):1514-9.

57. Özkaya N, Nordin M, Goldsheyder D, Leger D. Fundamentals of Biomechanics. New York: Springer-Verlag New York; 2012. XVII, 275 p.

58. McPherson DT, Xu J, Urry DW. Product Purification by Reversible Phase Transition FollowingEscherichia coliExpression of Genes Encoding up to 251 Repeats of the Elastomeric Pentapeptide GVGVP. Protein Expression and Purification. 1996;7(1):51-7.

59. Meyer DE, Chilkoti A. Genetically Encoded Synthesis of Protein-Based Polymers with Precisely Specified Molecular Weight and Sequence by Recursive Directional Ligation: Examples from the Elastin-like Polypeptide System. Biomacromolecules. 2002;3(2):357-67.

60. de Torre IG, Wolf F, Santos M, Rongen L, Alonso M, Jockenhoevel S, et al. Elastin-like recombinamer-covered stents: Towards a fully biocompatible and non-thrombogenic device for cardiovascular diseases. Acta Biomaterialia. 2015;12:146-55.

61. Chollet C, Chanseau C, Remy M, Guignandon A, Bareille R, Labrugère C, et al. The effect of RGD density on osteoblast and endothelial cell behavior on RGD-grafted polyethylene terephthalate surfaces. Biomaterials. 2009;30(5):711-20.

62. Patel S, Tsang J, Harbers GM, Healy KE, Li S. Regulation of endothelial cell function by GRGDSP peptide grafted on interpenetrating polymers. Journal of Biomedical Materials Research Part A. 2007;83A(2):423-33.

63. Larsen CC, Kligman F, Kottke-Marchant K, Marchant RE. The effect of RGD fluorosurfactant polymer modification of ePTFE on endothelial cell adhesion, growth, and function. Biomaterials. 2006;27(28):4846-55.

64. Lin Y-S, Wang S-S, Chung T-W, Wang Y-H, Chiou S-H, Hsu J-J, et al. Growth of Endothelial Cells on Different Concentrations of Gly-Arg-Gly-Asp Photochemically Grafted in Polyethylene Glycol Modified Polyurethane. Artificial Organs. 2001;25(8):617-21.

65. Tomlinson RE, Silva MJ. Skeletal Blood Flow in Bone Repair and Maintenance. 2013;1:311.

66. Missana L, Nagai N, Kuboki Y. Comparative histological studies of bone and cartilage formations induced by various BMP-carrier composites. Journal of Oral Biosciences. 1994;36(1):9-19.

67. Issa JPM, Do Nascimento C, Lamano T, Iyomasa MM, Sebald W, De Albuquerque Jr RF. Effect of recombinant human bone morphogenetic protein-2 on bone formation in the acute distraction osteogenesis of rat mandibles. Clinical Oral Implants Research. 2009;20(11):1286-92.

68. Issa JPM, Defino HLA, Netto JC, Volpon JB, Regalo SCH, Iyomasa MM, et al. Evaluation of rhBMP-2 and Natural Latex as Potential Osteogenic Proteins in Critical Size Defects by Histomorphometric Methods. The Anatomical Record: Advances in Integrative Anatomy and Evolutionary Biology. 2010;293(5):794-801.

69. Hildebrandt N. How to Apply FRET: From Experimental Design to Data Analysis. FRET – Förster Resonance Energy Transfer: Wiley-VCH Verlag GmbH & Co. KGaA; 2013. p. 105-63.

70. Carlson HJ, Campbell RE. Genetically encoded FRET-based biosensors for multiparameter fluorescence imaging. Current Opinion in Biotechnology. 2009;20(1):19-27.

71. Hsieh HV, Sherman DB, Andaluz SA, Amiss TJ, Pitner JB. Fluorescence Resonance Energy Transfer Glucose Sensor from Site-Specific Dual Labeling of Glucose/Galactose Binding Protein Using Ligand Protection. Journal of Diabetes Science and Technology. 2012;6(6):1286-95.

72. Hussain SA, Dey D, Chakraborty S, Saha J, Roy AD, Chakraborty S, et al. Fluorescence Resonance Energy Transfer (FRET) sensor. Journal of Spectroscopy and Dynamics. 2015;5(7).

CHAPTER 1

ELASTIN-LIKE POLYMERS: PROPERTIES, SYNTHESIS AND APPLICATIONS

José Carlos Rodríguez-Cabello,[1] Arturo Ibáñez-Fonseca,[1] Filippo Cipriani,[2] Leander Poocza,[1] Israel González de Torre,[1,2] Matilde Alonso[1]

[1] Universidad de Valladolid, BIOFORGE, CIBER-BBN, Valladolid, Spain

[2] Technical Proteins NanoBioTechnology (TPNBT) S.L., Valladolid, Spain

J.C. Rodríguez-Cabello, A. Ibáñez-Fonseca, F. Cipriani, L. Poocza, I. González de Torre, M. Alonso. Elastin-like Polymers: Properties, Synthesis and Applications. *Encyclopedia of Polymer Science and Technology* (2017). In press. doi: 10.1002/0471440264.pst656

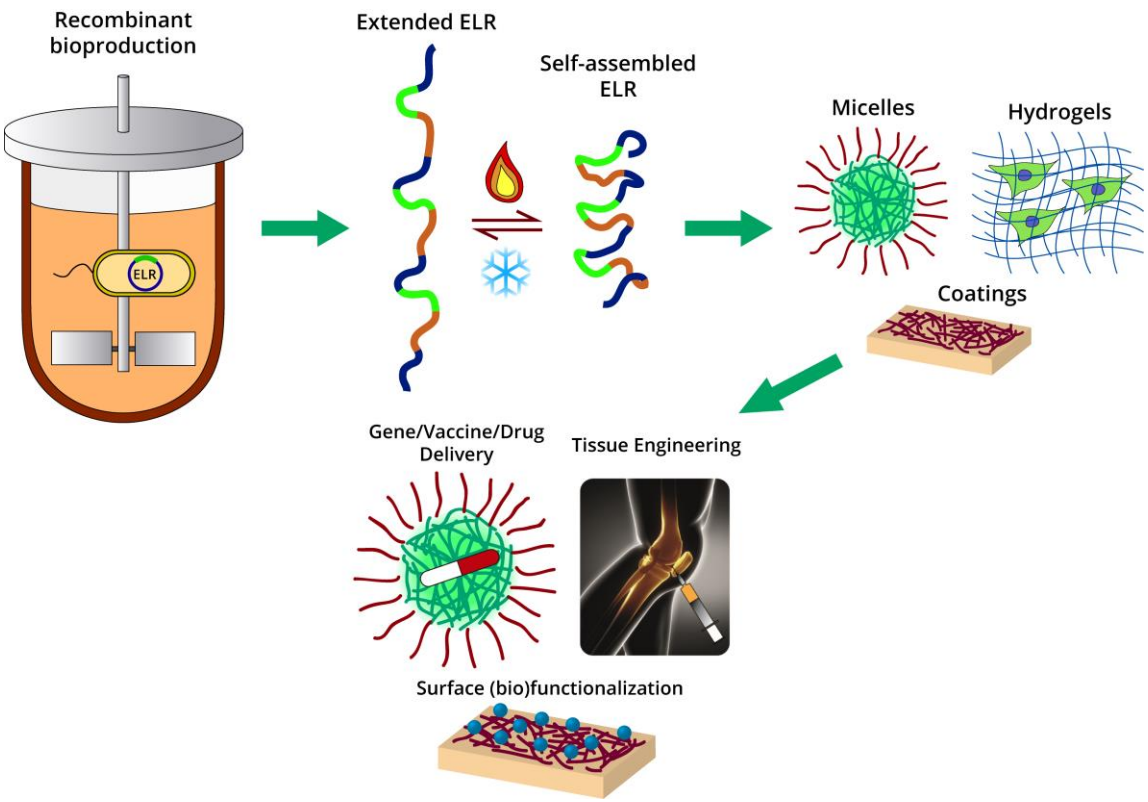

1. INTRODUCTION

Etymologically, the term protein comes from the Greek *proteios*, which means "holding first place", or could come from the god *Proteus* which name suggests "primal", "firstborn" and it is associated to the facility of this God to change his form and opinion. The name itself indicates the crucial role that proteins have in the living beings and the diverse forms in which we can find them in nature. If the importance of water is well known in the composition of the human beings, around 60% in adult males (1), proteins are not less important. In fact, more than 50% of the dry weight of our bodies is formed by proteins. They may have very different functionalities in the living systems, and some of them are large molecules that help to form the structure of our tissues irrespective of their location. In this way, we can find them forming really hard structures like bones, nails, horns or scales but they are also present in softer tissues like liver, muscles or connective tissue. Furthermore, proteins are not only involved in these structural tasks but they play a paramount role in the activation or deactivation of gene expression, or having regulatory functions helping to organize several processes or regulating metabolism or even taking part in muscle contractions.

Among these proteins, elastin is one of the most important proteins that can be found composing the extracellular matrix (ECM) which provides structural integrity to the organs and tissues in the living beings. Elastin is not only an important protein within the composition of the ECM, but it also possesses certain features that make it unique. For instance, it is extremely durable and with

a very low turnover in healthy tissues, the estimated half-life of this protein is around 70 years (2). Elastin confers elasticity and resilience to many tissues like ligaments, tendons, arteries or lungs among others (3). This elasticity is given by the presence of hydrophobic regions within the structure of the monomers of elastin that tend to aggregate and self-assemble contributing to the polymeric organization of the elastin (4). Along the last decades of the 20th century not few researchers were interested in this self-assemble property and started to explore the synthesis and production of artificial polypeptides based on these hydrophobic domains that conferred such properties to the elastin molecule (5-8). They found that the most frequent fragment of pentapeptides in the structure of the natural elastin was the sequence VPGVG, appearing up to 50 times in a single elastin molecule. It was discovered that synthetic polymers of $(VPGVG)_n$ ($n \leq 150$) were soluble in water below 25°C but they aggregated suffering a phase transition above this temperature (8). This change in the conformation of the protein leads to a viscoelastic state in which the amount of polymer is around 50% and the other 50% is water. This process is common to all the elastin-like polymers (ELPs) and it is accompanied by a halving of the length of the polymer and a release of a great amount of energy (9). All this process is driven by a change in the structure of the ELP, from an extended conformation below the transition temperature (T_t), to a β–spiral with three units of the basic pentamer VPGVG, forming a type II β–turn per turn of the spiral, above the T_t (5) (Figure 1). The T_t can be tuned by changing the fourth amino acid of the pentamer VPGXG, where X could be any amino acid except proline, because its structure destabilizes the

β–turn impeding the correct packing of the chains of the polymer. The T_t of an ELP is clearly influenced by the nature of the guest amino acid on the X position in the sequence $(VPGXG)_n$ (apolar residues decrease the T_t, while polar ones increase the value of the T_t) and by the overall polymer length (n). The effect of this two parameters has been deeply investigated and described by Urry and coworkers (10). Moreover, the T_t is sensitive to other external factors as for instance ionic strength, pH, pressure, light or chemical modifications (9).

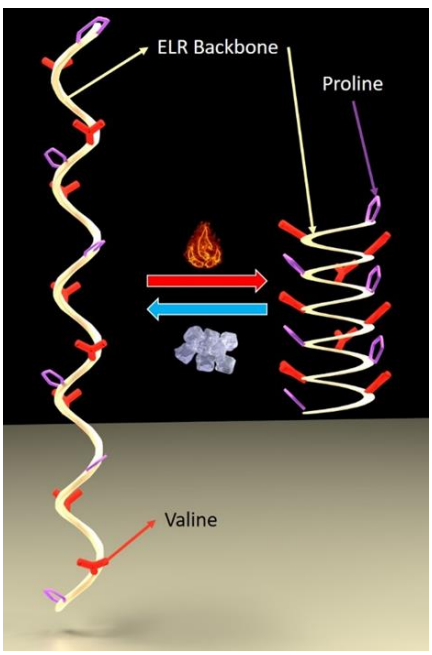

Figure 1. Schematic representation of the conformational change of the ELP and ELR backbone depending on the temperature.

Chemical synthesis of various polypeptides based on elastin were successfully obtained by using standard chemical processes as demonstrated by Urry, Prasad and others (11,12), but some problems arise when more complex structures or simply larger polymers want to be synthetized, like problems in purification and

polydispersity and, even if these amounts of mixture of products are obtained in small quantities, they can drastically affect the physical properties of the final product (13). The arrival of the recombinant DNA technology opened a new way to design and produce synthetic proteins. The old nomenclature of ELPs was changed to ELRs (elastin-like recombinamers) pointing out the recombinant origin of this new family of elastin-based polymers. With this new approach, some of the problems derived from the old chemical synthesis, like polydispersity, need for organic solvents and the further elimination of their residues, were overcome while a higher control over the amino acid sequence was obtained. Moreover, the purification process changed from classical chemical purification pathways to one based exclusively on the thermal behavior of the ELRs. After some inverse transition cycles (ITC), which imply heating and cooling of the suspension containing ELRs above and below their inverse temperature transition (ITT), they can be easily purified without the need of the addition of chemical agents or solvents that should be removed afterwards. During the last decade, a better control over the recombinant techniques and the use of more specific and accurate enzymes has led to the precise biotechnological processes that are nowadays applied in the production of the ELRs.

ELRs are biological polymers that due to their flexibility in the design, their self-assembly properties, easy chemical modification allowing the introduction of many interesting functionalities, versatility to be processed in many forms (aggregates, fibers, layers, nano-particles or hydrogels) and excellent cyto- and biocompatibility, have a high potential in many

fields, from drug-delivery to tissue engineering, including others such as protein purification, anti-cancer gene therapies or nano-vaccines.

In the next pages we will explore the evolution of ELRs from their ancient chemical origin to the most cutting-edge bioproduction techniques, exploring the several hosts that can be used to bioproduce them and their versatility in the design. We will also immerse in the several structures that ELRs can form and their possibilities in the numerous medical fields where they can be applied.

2. ELASTIN-LIKE RECOMBINAMERs ENGINEERING, BIOPRODUCTION AND DESIGN

2.1. History and evolution of the synthesis of elastin-like recombinamers

2.1.1. Ancient times (the "chemistry ages")

The finding of repetitive sequences in porcine elastin by Gray *et al.*, in 1973 (14), led to the chemical synthesis of different versions of some of these oligopeptides, being one of them the pentapeptide Val-Pro-Gly-Val-Gly (VPGVG in single-letter amino acid code). There was a lot of enthusiasm to study the conformational properties of these peptides in an attempt to shed light into the features of natural elastin, a polymeric protein that gathered a lot of attention due to its relationship with several diseases (15,16). Hence, Urry's laboratory began synthetizing elastin-derived

peptides and soon became one of the leading research groups in this field. However, the synthetic strategies required complex methods including the use of diverse precursors and solvents, while the overall yield and the length of the polypeptide were very limited (17). Despite the limitations, these synthetic approaches allowed the attaining of VPGVG (poly)pentapeptides to perform conformational studies (17,18), even by covalent cross-linking of these peptides, which also led to morphological studies by scanning electron microscopy (SEM) and to the determination of stress-strain curves (19). Finally, all these early studies resulted in the development of molecular dynamics calculations which gave more information about the secondary structure of the protein and about the backbone torsion angles ψ and φ of the amino acid residues in the polypeptide, both in its relaxed and extended state (20).

2.1.2. Modern times (the "recombinant ages")

By that time, the last years of the 80´s, recombinant DNA technology had arisen as a very promising tool for the biotechnological synthesis of proteins in heterologous hosts, mainly *Escherichia coli*. Therefore, researchers started to use this technology for the expression of polymeric proteins to overcome the disadvantages of both chemical synthesis and extraction from natural sources. The first biosynthetic strategy for the production of ELRs, in this case fused to silk-like sequences (repetitions of the GAGAGS hexapeptide), was reported by Cappello *et al.* in 1990 (21). Nevertheless, the molecular biology methods that led to the obtaining of the elastin-like gene were described two years before in a patent by Ferrari *et al.* (22). This document explains the head-to-

tail concatemerization of the elastin-like gene by self-ligation of cohesive DNA ends leading to a final gene encoding the amino acid sequence $(VPGVG)_{160}$. Hence, this self-ligation method allowed the synthesis of ELR genes with different lengths, although in an uncontrolled manner and without the guarantee of achieving a gene with the desired length. This process was further explained by Tirrell *et al*. for the genetic engineering and expression of protein polymers in general, also discussing the potential issues derived from the use of the recombinant DNA technology (23).

2.1.3. Contemporary times (the "seamless recursive ages")

After these first steps towards genetic engineering of ELRs, new methods were developed to overcome some disadvantages, like the low number of endonucleases recognizing non-palindromic cleavage sites needed for the self-ligation in a correct head-to-tail orientation. Hence, some procedures described for general cloning were used in the context of ELRs. This is the case of the "seamless cloning" technique that allowed the cleavage of DNA outside the recognition sequence by the use of the type IIs restriction endonuclease *Eam*1104I and, therefore, avoided the introduction of extraneous nucleotides (nts) in the cloned sequence (23). This method was first used successfully by Conticello and co-workers for the synthesis of ELR genes, suggesting that it could be a more rapid and efficient system for the bioproduction of protein polymers (25). Nonetheless, they still relied in concatemerization to achieve the desired length of the gene. To overcome this limitation, Meyer and Chilkoti proposed a new method termed "recursive directional ligation" (RDL) (26). In their work, they described the use of two

different restriction endonucleases with well-defined features, namely *Pfl*MI and *Bgl*I, to synthetize ELR genes. These two restriction enzymes leave single-stranded DNA ends upon cleavage that are cohesive one with the other, so one of them can be used to extract the ELR insert, while the other one is used to linearize the cloning vector. Both molecules were then mixed together for ligation to achieve the final construction. The plasmid vector was designed so the restriction sites were maintained after each cloning step, allowing subsequent insertions of ELR-coding genes. As an evolution of this method, Chilkoti and co-workers described a new RDL strategy termed plasmid reconstruction (PRe)-RDL (27). In this case, they introduced type IIs restriction endonucleases to RDL for a more efficient seamless cloning. Moreover, it avoided self-ligation of the vector and nonproductive circularization of the insert by cutting both the insert-donor plasmid and the receptor vector in halves with two different type IIs endonucleases that leave non-complementary overhangs. Therefore, a circular plasmid is only achieved when both insert and vector have been ligated.

Despite the great improvement in the genetic engineering of ELRs reached so far, there were still some limitations that should be overcome, like complexity in plasmid design. In this regard, Rodríguez-Cabello *et al.* described a new method for the easy and rapid generation of ELR gene constructs and their expression in heterologous hosts (28). For this purpose, they relied on the seamless cloning approach through two type IIs endonucleases, namely the aforementioned *Eam*1104I and *Sap*I. The only difference between them is that *Sap*I recognizes a 7-nt sequence, while *Eam*1104I recognizes a 6-nt one (GCTCTTC and CTCTTC,

respectively), being the latter included in the *Sap*I one. With this strategy, it is possible to engineer a plasmid so it can include two *Eam*1104I restriction sites, being one of them also a *Sap*I recognition sequence. For this purpose, two commercially available plasmids, one being the pDrive cloning vector and the other one the pET-25b(+) expression vector, were modified by site-directed mutagenesis to exclude inherent *Eam*1104I and *Sap*I restriction sites and only include the desired ones. On the other hand, it allows controlled concatemerization following the previous guidelines for RDL. Furthermore, it avoids self-ligation in a very simple way by treating the receptor plasmid with a shrimp alkaline phosphatase, hence eluding the need of cutting plasmids in halves as described above. This procedure, named iterative-recursive method, is a good example of how molecular biology methods can be fine-tuned to achieve well-defined repetitive genes coding for protein polymer sequences very efficiently.

A schematic representation of the multiple options in ELR design and genetic engineering can be observed in Figure 2.

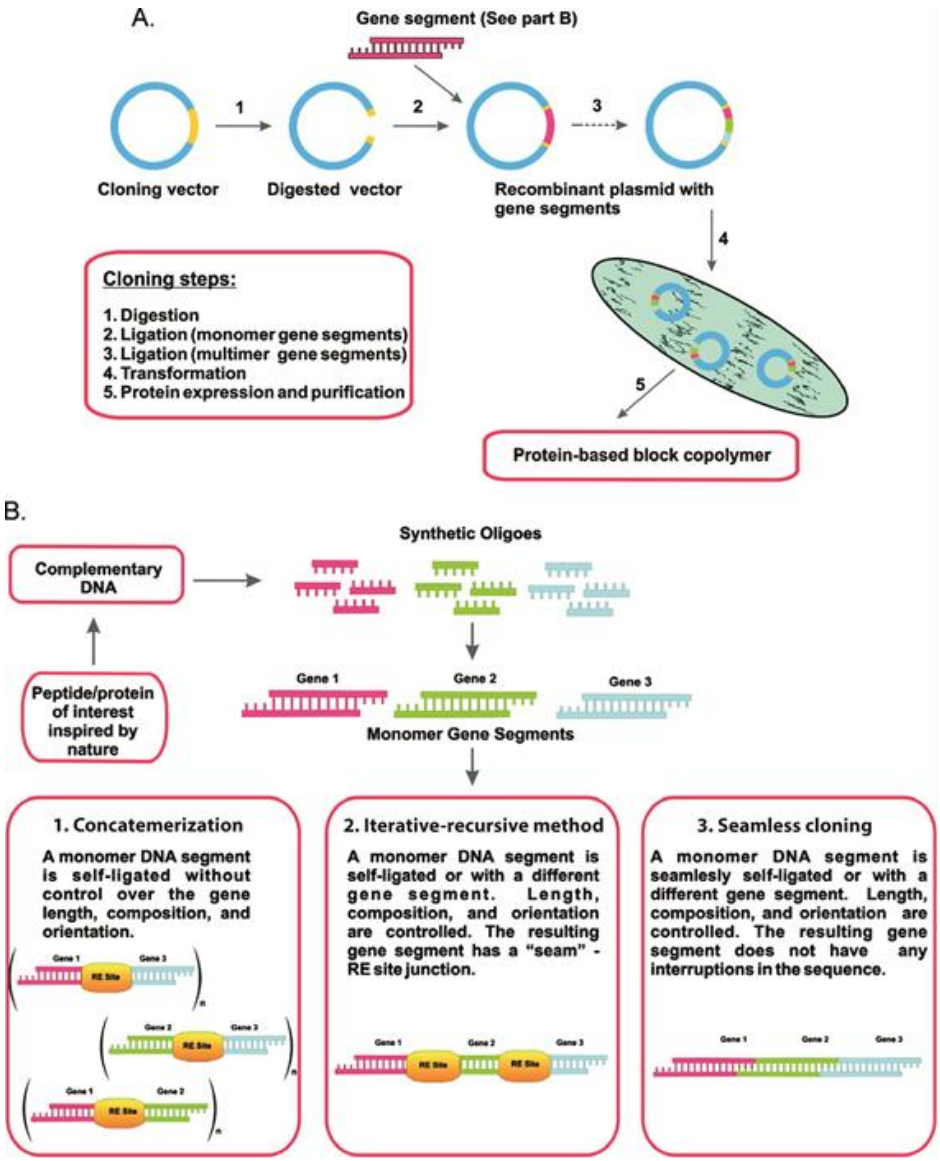

Figure 2. Schematic representation of the different approaches for the design and genetic engineering of protein polymers in general and ELRs in particular. Adapted with permission from (29).

2.2. Hosts for the expression of elastin-like recombinamers

2.2.1. Prokaryotic hosts

2.2.1.1. The gold standard: Escherichia coli

Like in the case of many other proteins produced by recombinant DNA technology, *E. coli* was used for the heterologous expression of ELRs in the first place, as is the case for all the works commented above. This is mainly due to the well-studied metabolism and culture conditions of this *Enterobacteriaceae*. Furthermore, ELRs do not undergo post-translational modifications and their folding is correctly achieved without the mediation of eukaryotic chaperones or any similar system. Hence, *E. coli* arose from the beginning as a good host to achieve an optimal expression and yield of ELR biosynthesis. However, although expression was easily achieved for short (30) and long ELRs (31), there was still plenty of room for optimization. First, Guda *et al.* compared the expression of the gene coding for G-$(VPGVG)_{119}$-VPGV in Luria Broth (LB) culture medium following induction with isopropylthio-β-D-galactoside (IPTG) and Terrific Broth (TB) without induction (32), and they found that the expression was very much higher in the case of TB culture after 24 hours. This TB medium had shown before a favorable effect on plasmid stability, while the use of lactose in TB made it a good auto-induction medium (33).

Other approaches regarding the optimization of ELR bioproduction explored the supplementation of *E. coli* culture

medium with amino acids that are highly repeated in the ELR sequence: glycine, valine, proline, and alanine. In this way, depletion of intracellular amino acid pools in *E. coli* could be avoided. Therefore, Chow *et al.* studied the expression of ELR and the final yield in terms of grams of ELR per liter of culture, both with LB culture medium followed by IPTG induction, and with TB medium (34). In this work, the authors showed that the use of glycerol, phosphate buffer and proline as supplements of TB medium enhanced 6-fold the ELR yield compared to the basal TB, from an initial 0.27 g/L to 1.6 g/L, with the subsequent reduction in cost. Furthermore, their results suggest that, surprisingly, supplementation of amino acids other than those abundant in ELRs (asparagine, aspartic acid, glutamine and glutamic acid) also enhanced protein yields, indicating that regulatory mechanisms in the control of intracellular amino acid pools that are more complicated than it could be expected in the first place may exist.

Other works have reported a high-level expression of ELRs fused to silk-like domains, hence making silk-elastin-like recombinamers (SELRs). Machado *et al.* showed a volumetric yield of 150 mg/L, being 6-fold higher than previously reported productivities, just by using auto-induction TB medium supplemented with lactose and controlling temperature at 37 ºC (35). However, cell densities were too low compared with lactose supplemented TB at the same conditions, so the process could still be optimized. Furthermore, it was a low-scale batch production and some parameters influencing bacterial culture were uncontrolled. Henceforth, a comprehensive and detailed study was carried out by Collins *et al.*, even though it was performed again in low-scale

fermentation systems (shake flasks) (35). Cultures were performed at different conditions by changing medium and medium composition, initial pH, incubation temperature, flask volume to culture volume ratio, agitation rate, IPTG induction concentration, elapsed fermentation time at induction and induction period. Though, the chosen approach was 'one-factor-at-a-time' and therefore the study had some limitations. Despite of these limitations, it was found that the best yield of 500 mg/L is achieved at 37 ºC with TB at pH 6-7.5, a 10:1 flask volume:culture volume ratio, agitation speed of 200 rpm and induction at the beginning of the stationary phase with 0.5 mM IPTG for 4 hours. Further studies were performed by the same group, in this case using a fed-batch approach and a 3 L bioreactor, allowing a more powerful and deeper experimental design (36). Then, they evaluated the effect of the pre-induction and post-induction growth rates, dissolved oxygen concentration, dry cell weight at induction, and IPTG concentration for induction. Furthermore, they could control pH, O_2 concentration and feeding of a glucose solution during all the fermentation process. With this experimental setting, they showed that they obtained a yield of 4.3 g/L of SELR in the best conditions. This is 9-fold higher than the data previously reported by them.

2.2.2. Eukaryotic hosts

2.2.2.1. Aspergillus nidulans fungus

One of the first attempts to produce ELRs in eukaryotic hosts was made by Herzog *et al.* in *Aspergillus nidulans* (*A. nidulans*) fungus (37). They inserted the gene encoding for G-$(VPGVG)_{119}$-

VPGV mentioned above into an expression vector designed for *A. nidulans* under the control of a constitutive promoter. Their results showed that they were able to isolate different fungus colonies that integrated the plasmid with varying copies into their own genome. However, the translational efficiency was low, and they suggest that this effect could be due to some codons found in the ELR gene (cloned from an *E. coli*-optimized plasmid) that are rarely used in *A. nidulans*. Despite the proposal made by the authors towards the optimization of ELR bioproduction through *A. nidulans*, no other examples have been found in the literature.

2.2.2.2. Yeast

On the other hand, the well-studied *Pichia pastoris* (*P. pastoris*) yeast has become a model eukaryotic organism for recombinant protein expression and there are some examples in the literature in which it has been chosen for the biosynthesis of ELRs. In the first case reported, Schipperus *et al.* produced secreted ELRs in *P. pastoris* with a yield of 255 mg of ELR per liter of culture medium (38). They suggest that this low-scale system is completely scalable, easily purifying ELRs without the need of cell disruption, even though times for culturing and inducing expression in yeast are substantially longer than in the case of *E. coli*. Furthermore, this expression host allows glycosylation and/or formation of disulfide bonds, so it is proposed as a good system for the expression of ELR fusion proteins that may undergo any of these post-translational modifications. Almost at the same time, Sallach *et al.* described the expression in *P. pastoris* of non-repetitive ELR genes with identical amino acid sequences, taking advantage of the degenerate genetic

code (39). They propose the same advantages than the previous work, but they also emphasize that in a yeast expression system there is no need to remove bacterial lipopolysaccharide, achieving an endotoxin-free product after simple ITC purification. In another study by Schipperus *et al.* comparing the secretion of ELRs with different transition temperatures (T_t) by *P. pastoris*, they found that higher yields are obtained for shorter and more hydrophilic ELRs (39). Therefore, they suggest that below T_t the ELRs are soluble and more easily secreted. However, the conclusion to this work seems too ambitious since only three ELRs were designed and produced for the comparison, and none of them was strongly hydrophilic.

2.2.2.3. Plants

As regards other expression systems, recombinant protein production in plants has been widely developed since the beginning of the recombinant DNA era and, hence, ELRs have been produced in this system too. In the first work describing ELR production in plant cells, Zhang *et al.* transformed tobacco cells physically by particle bombardment (biolistics) for the expression of the gene encoding $(GVGVP)_{121}$ (41). They showed integration of the ELR gene in the genome of the cells (2-5 copies) and expression of the elastomeric protein, although at very low quantities. As a next step, the following article by this group showed the feasibility to express the same ELR in transgenic tobacco (*Nicotiana tabacum*) plants (42). Nonetheless, only 0.5 to 5 μg per g of fresh weight of leaf tissues were obtained, being approximately 0.003 to 0.03% of total soluble proteins, while 0.01 to 0.05% was observed by Western blot prior to purification. Even though there are many other examples of

expression of ELRs in transgenic plants, they mostly use them as fusion tags to improve the stability of the expression and the purification efficiency of different recombinant proteins, which will be briefly described below. However, there is a very recent work by Heppner *et al*. that describes the bioproduction of a fusion protein comprising spider silk and ELR sequences in tobacco leaves (43). The spider silk block is not excised from the whole protein after purification, so it can be taken as an example of ELR expression in plants. Authors showed a yield of 400 mg per 6 kg of leaves (66.7 mg/kg or μg/g) which is more than a 13-fold increase when compared to the results commented above, although the comparison is limited because in this last case ELR is fused to spider silk.

The expression of ELRs in all the heterologous hosts described in this section is summarized in Table 1.

Table 1. Table describing the heterologous hosts used for the bioproduction of ELRs to date.

Host		**$(VPGXG)_n$ composition**	**Main achievements**	**Refs.**
		$(VPGVG)_{160}$	First recombinant production of an ELR combined with silk-like sequences	(22)
		$(VPGVG)_{20}$	First biotechnological production of an ELR by itself	(30)

		$(VPGVG)_{251}$	First reported expression of extremely long ELRs	(31)
		$(VPGVG)_{120}$	Comparison between culture media of different composition	(32)
		$[(VPGVG)_2$-VPGGG-VPGAG-$(VPGVG)_3$-VPGGG-VPGAG-$VPGGG]_9$ (also called ELP-90)	Supplementation of medium with amino acids highly repeated in ELRs to avoid depletion	(34)
		$(VPAVG)_{20}$ and $(VPAVG)_9$	SELR with high yield by using auto-induction medium	(35)
		$(VPAVG)_9$	'One-factor-at-a-time' optimization of the bioproduction of a SELR in shake flask cultures (low scale)	(36)
		$(VPAVG)_9$	Optimization of the bioproduction of a SELR in fed-batch culture in a bioreactor obtaining the highest yield reported to date	(37)
	Aspergillus nidulans fungus	$(VPGVG)_{120}$	Unique example of ELR expression in fungal hosts	(38)
		ELP-90	First reported expression of secreted ELRs in yeasts	(39)

		$[(VPGVG)_2$-VPGEG-$(VPGVG)_2]_{21}$	Suggestion of avoidance of LPS removal	(40)
		ELP-90 ELP-40 $[(VPGVG)_2$-VPGGG-VPGLG-$(VPGVG)_3$-VPGGG-VPGLG-VPGGG$]_4$	Higher yields for shorter and more hydrophilic ELRs	(41)
		$(VPGVG)_{121}$	First work describing ELR production in plant cells	(42)
		$(VPGVG)_{121}$	First expression of an ELR in plants	(43)
		ELP-100	ELR fused to a spider silk protein produced through a simple and scalable method	(44)

2.3. Novel design of elastin-like recombinamers with different features

Taking advantage of the genetic engineering, which may allow the inclusion of changes in the amino acid sequence of ELRs or even the fusion of different proteins, the features of ELRs can be tuned and/or improved, increasing the complexity of these protein polymers (44).

2.3.1. Substitution of the guest amino acid

One of the first choices regarding the modification of the ELR sequences is the amino acid in the fourth position (guest residue) of the elastin-derived pentapeptide, or the X in VPGXG, as described above. Since this choice may change completely the physicochemical properties of the ELR, the T_t above all, it is a common way to differently design ELRs and has been extensively evaluated (45). Moreover, the molecular biology methods used in the synthesis of ELR genes permit the construction of elastin-like block corecombinamers (ELbcR) that arise as a result of the combination of elastin-like sequences with different substitutions in the guest residue. This approach may confer different properties to a single ELR molecule (46), and also leads to more complex self-assemblies above the T_t as evaluated in different works (47,48). In addition, Meyer *et al.* studied the effect of the length and concentration on the T_t for different ELRs, showing that there is a higher decrease of T_t for ELRs with lower molecular weight (MW) when the concentration is increased, while this effect is lower for ELRs with higher MW (49). Furthermore, they proposed equations that may allow the prediction of the T_t for other ELRs. Some years later, the same group further evaluated the changes of T_t depending on alanine content as the guest residue, and on MW of the ELR and concentration, developing a model to predict T_t by changing these conditions (50). Through the combination of two different factors affecting T_t, i.e. the arrangement of blocks with different guest residues and the length of these blocks, Ribeiro *et al.* showed that it is not only the mean polarity what influences variations in T_t and

enthalpy (ΔH) of the transition, but also the distribution and length of the polar/apolar blocks within the ELbcR molecule (51).

2.3.2. Fusion of other protein polymers

Many studies have explored the possibility of using ELRs in combination to other protein polymers like silk, collagen or resilin to improve or change their properties in different applications, most of them within the field of tissue engineering (52).

The first examples of this section have already been shown above in relation to SELRs. Silk-like domains derive from the repetition of the GAGAGS hexapeptide found in *Bombyx mori* silk fibroin, which is known to self-assemble into *β*-sheet secondary structures, conferring high strength, toughness and ductile elongation to materials (21). They have been widely fused to elastin-like blocks by different groups. For example, Nagarsekar *et al.* described the design and production of different silk-elastin-like block co-recombinamers (SELbcRs) that showed sensitiveness to diverse stimuli like pH and temperature (53). In another study, Wang *et al.* developed a high-throughput for the screening of SELRs matching specific material functions (54). For this purpose, they expressed a library of different SELRs in *E. coli* cultured in 96-well plates and purified the recombinamers *in situ*. Then, they performed a physicochemical and mechanical characterization on those SELRs without taking them out of the plates, suggesting that it could be a rapid and powerful tool to elucidate the properties of recombinant materials.

In another work, Bracalello *et al.* designed and produced a chimeric resilin-elastin-collagen-like recombinamer that showed a different

self-assembling pattern than any of each protein polymer had shown separately, with great tendency to form higher order fibrillar structures (55).

2.3.3. Fusion of bioactive domains

In order to generate extracellular matrix-like materials, cell adhesion motifs have been fused to ELR sequences by genetic engineering as described by different groups. In a first example, Panitch *et al*. combined a VPGIG repeated sequence with the REDV peptide found in the CS5 region of fibronectin that promotes endothelial cell attachment and spreading, but not smooth muscle cells or platelets (56). In their work, they showed a successful attachment of cells on surfaces coated with the ELR, compared to the control surfaces. Similarly, Girotti *et al*. fused the REDV sequence to an ELR including lysine-containing blocks that could be cross-linked to form artificial matrices, as demonstrated (57).

Regarding other cell-adhesion sequences, Urry and co-workers used the RGD tripeptide (58) for the first time to successfully enhance cell attachment on ELR-based matrices cross-linked by γ-irradiation (59). However, this first case of RGD modification was performed with chemically synthetized polypeptides. On the other hand, the first example found in the literature of a recombinantly produced ELR including RGD sequences was reported by Liu *et al*. who compared the cell response between RGD and REDV sequences (60). In their study, they found that RGD promoted a faster attachment while being stronger than in the case of REDV. Most probably because of that

finding, many other groups have included RGD domains within ELR molecules since then to improve cell adhesion.

In addition to these works regarding cell-adhesion sequences, other motifs have been fused to ELRs to undergo dimerization, therefore modifying the structural properties of their supramolecular assembling. This is described in the work by Fernández-Colino *et al.*, where they showed the fusion of a leucine zipper domain, containing a cysteine residue, to an ELbcR (61). This domain was shown to be able to form dimers stabilized by a disulfide bond, hence allowing the cross-linking of hydrogels based on this zipper-containing ELbcR in a reversible manner, depending on the redox conditions of the system. On the other hand, Zhang *et al.* designed and bioproduced ELRs including either a SpyTag short polypeptide or a SpyCatcher protein (62). This protein is able to recognize the SpyTag polypeptide undergoing an autocatalytic bond formation between them. The combination of ELRs comprising these Spy sequences resulted in different supramolecular structures that were further characterized.

As can be deduced from the above paragraphs, many different sequences can be recombinantly introduced within the backbone of the ELRs depending on the physical, chemical and biological requirements of the final protein and the subsequent application.

2.3.4. Fusion of full-length proteins

In order to anticipate the properties of ELRs when fused to different proteins, Chilkoti and co-workers studied the effect of the arrangement of four proteins in the final fusion product, i.e. C-

terminus or N-terminus, on the expression levels and yields of purified protein (63). By their results, they could conclude that the yield was higher when the proteins were placed at the C-terminus, and that the specific activity of the fused proteins was higher in that case for three out of four proteins. However, as they comment themselves in the manuscript, these results are applicable only to an ELR with a specific sequence, and to four particular proteins. Additionally, the same group was able to develop a model to predict the effect of hydrophilic proteins on the thermal behavior of ELR fusion proteins, showing that the presence of charged residues is the most important parameter affecting the T_t of the ELR when compared to the ELR itself (64).

Many other proteins have been fused to ELRs to date. Some of them used ELRs as tags, taking advantage of their facile purification by ITC (31) to produce recombinant proteins (65) that are finally excised from the ELRs by different methods, namely intein self-cleavage (66), protease-mediated cleavage (67), or by including the self-processing module from *Neisseria meningitides* FrpC (68). There are many examples in which this approach has been employed in the expression of recombinant proteins in *Nicotiana tabacum* plants (69), like an anti-human TNF antibody (70), and in tobacco cell suspensions to produce human IL-10 (71). Furthermore, this strategy has been also shown to be successful to produce antimicrobial peptides in *E. coli* efficiently (72,73).

3. STRUCTURES AND PHYSICAL CHARACTERISTICS OF ELASTIN-LIKE RECOMBINAMERs

Materials based on ELRs underlie a high potential, characterized by the extraordinary biocompatibility, tunable mechanical properties and the variety of structures that can be generated (i.e. micelles, nanoparticles, hydrogels, films, and nanofibers). Besides the introduction of bioactive sequences into the ELR-based structures, ELRs can be designed to self-assemble into either micelles, physical hydrogels, nanoparticles, or solvent casted films (Figure 3). Furthermore, reactive cues can be introduced in the sequence to allow chemical modification.

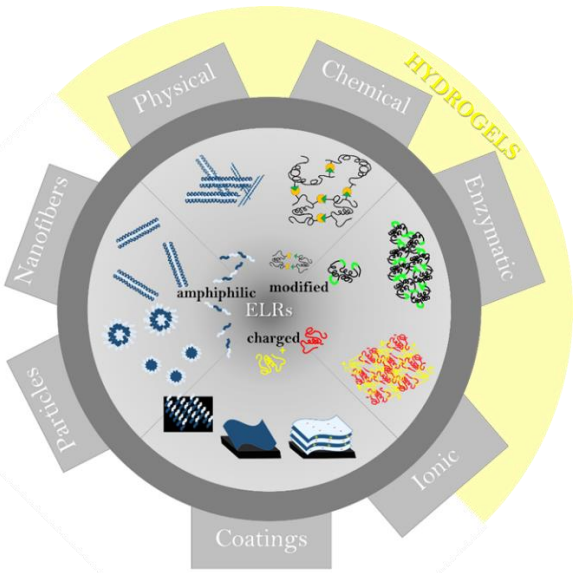

Figure 3. The diversity of ELR structures and their sequential origin.

3.1. Micelles and nanoparticles

The first self-assembling ELRs were achieved with polymers containing blocks of different polarity, inspired by block-copolymers and their related properties, like phase separation, micelle formation, etc. The difference between block-copolymers and amphiphilic ELRs, is that in amphiphilic ELRs the blocks of different polarity retain the ELR pentapeptide sequence (VPGXG), and the changes in polarity are introduced through the X amino acid. The influence of the X amino acid, has been methodically described by Urry (74). As well as block-copolymers, elastin-like block co-recombinamers (ELbcRs) showed the ability to form micelles in solution. The hydrophobic block tends to be embedded in the core, hidden from the water solution, while the hydrophilic block(s) forms the corona exposed to the outer part of the structure. It has been shown that the formation of stable nanoparticles requires a relatively high molecular weight of at least 48 pentapeptides. Furthermore, the particle size and the molecular weight of the ELR are directly related (75). The ITT of the ELRs, depending on the characteristics of the micelles, can either lead to coalescence of micelles into lyotropic gels (76), through polydisperse microparticles (77), or to a simple swelling and deswelling of the micelles, accompanied by size changes. Typical sizes of ELR nanoparticles reported are usually in the range of 10 to 100 nm (78-83), but due to the temperature sensitivity and related agglomeration, also micro sized particles have been reported (77,84). The ability to trigger the formation of nanoparticles by the swelling and shrinking kinetics, intensified the research on the tuning of the micelle sizes and the T_t related changes. Several

methods have been explored to either stabilize ELR-based micelles. For instance, the concentration of the ELR solution, which has been found to have a clear effect in the particle size (76); another method is the addition of surfactants that can stabilize or destabilize the ELR particles (85); salt concentration is crucial, higher compensation of the charges of the hydrophilic blocks through counter ions can lead to stronger agglomeration of particles (80,81,83); and last but not least, the pH affects the stability and size, depending on the chemical properties of the guest amino acid in the fourth position of the basic pentamer (VPGXG) of the hydrophilic block. In the case of cationic amino acids the charge is reduced at high pH, on the other hand, anionic amino acids show the same behavior at low pH (80). Moreover, more specific sensors for changes in salt concentrations have been designed. For instance, the introduction of a calcium selective sequence amplified the influence of calcium concentration, by reducing the transition temperature of the corresponding ELR from 70°C to 35°C (86). Even when the general shape of homogenous micelles is round, it can be tuned to more anisotropic cylindrical shapes by varying the architecture of the ELRs introducing amphiphilic blocks of different sizes in the protein sequence (87). In principle, each ELR has one clear transition temperature, but in the case of amphiphilic ELRs with different blocks, long enough to develop an own intrinsic transition, the effect of temperature on the particles shows two temperature-induced changes. First, the rearrangement of the hydrophobic core, driven by a change in the secondary structure from random coil and β–sheets to type-II β-turns. This change as well corresponds with the exhibition of a cylindrical shape of the

particles. This effect is also known as critical micelle temperature (CMT). The second and more prominent change is due to the collapse of the hydrophilic part, which is responsible for the coalescence, agglomeration and precipitation of the micelles (75). Other reported rearrangements describe the change from micelles to vesicles by reorganizations of the hydrophobic blocks. Here, vesicles could be obtained either by an increase of the length of the hydrophilic block, or by addition of another hydrophilic block to a triblock copolymer of the structure hydrophilic-hydrophobic-hydrophilic (48).

3.2. ELR-coatings and films

The generation of ELR coatings has a great interest for the creation of either antimicrobial, anti-fibrotic coatings, or for the deposition of a bioinductive layer that allows cellular interaction driving to a good implant integration within the surrounding tissues. In theory, there are two ways to accomplish a coating: physisorption by intermolecular interactions (hydrophobic and/or electrostatic interactions), or a grafting approach by covalent binding (Figure 3). For completion, a third possibility could be possible, which is the creation of elastin-like brushes by a grafting approach, but due to the relatively high molecular weight of ELRs, and the related cost to generate such proteins in a synthetic way, this approach is still a hypothetical option. Additionally, these proteins would not be ELRs since they are not obtained by recombinant techniques so they should be classified as ELPs (8,19,88,89).

Physisorption of ELRs has been deeply studied and applied in different works. It was described by Srokowski et al. that longer ELRs formed more stable coatings by physisorption than ELRs with lower MWs (90). Another approach targets on the endothelialization of CoCr alloys, that could be enhanced by physically adsorbed or covalently bond ELRs that bear a REDV sequence (91). ELR coatings also proved to reduce platelet activation and smoothening of surface topographies when coated PTFE substrates by a layer-by-layer approach (92). This was corroborated by other studies that showed that longer ELR sequences not only have a better deposition, but also decrease platelet activation more than short ELRs (90). In an earlier study, the patency time of non-thrombogenic ELR coatings could be more than doubled (93), and thrombus formation reduced (94).

Further micelle solutions have been used to adsorb ELRs to surfaces under retention of their nano- and microtopography. For the generation of surfaces that induce bone mineralization nanotopographies, it was performed a coating with an ELR containing a human salivary statherin sequence (95). The coating of previously generated orientated electrospun fibers with ELRs led to a conserved orientation in the scaffold, which guided human vocal fold fibroblasts (96). The transition temperature of the ELRs was also used to enhance the physisorption by thermally induced deposition. Here, surfaces with a low RGD concentration were formed, high enough to allow cell adhesion, but too little to form a cellular monolayer. Thus cells were forced to cluster and semi-functional pseudoislets could be formed (97). The good mechanical performance of SELR hybrids further led to the development of

coatings for osteochondral applications (98). Besides the deposition of ELRs in order to induce or avoid attachment of cells or proteins, the ability of the ELRs themselves to influence the microenvironment by temperature changes is of great interest, for example for biosensors, or drug delivery systems. By changing the temperature, features like the wettening of the surface (77), the release kinetics of drugs embedded in the coating (84), or the accessibility of active groups inside the ELR sequence in swelling and deswelling ELR/RGD brushes (99), can be controlled.

3.3. ELR-based hydrogels

In tissue engineering, hydrogels have been the predominant matrices for application in the human body in the last 40 years (100). A high water content leads to convenient mechanical properties and stimuli-responsiveness, which in many cases chimes with the properties of natural tissues (101,102). ELRs, inspired in a natural protein such as elastin, are excellent candidates for many researchers focused on the generation of artificial matrices that can be used as scaffolds for biomedical applications. The ECM is a very complex system in which the physical properties (elasticity, stiffness), the nano-topography, the presence of signaling molecules, protease-sensitive sites and adhesion domains are of great importance, and gathering as many of these properties as possible is a major requirement that have to be demanded to any material that might be used in tissue engineering. The generation of hydrogels from linear ELRs requires paying special attention to the mechanism that will drive the cross-linking of different ELRs molecules. These cross-linking methods can be either of covalent or

physical nature and the position of cross-linking points along the ELR backbone can be fully controlled through genetic engineering to get a precise tuning of the mechanical properties. Polypeptide-based block-copolypeptides, for example, manage to self-assemble into stable hydrogels (103), which can be further stabilized when flanked by protein segments with coiled-coil secondary structure (104,105). Another approach is the use of recombinant segments of elastin, silk and collagen (106-108). In contrast to general methods for the formation of hydrogels by radically or photo-polymerized acrylate cross-links, ELR hydrogels can be thoroughly controlled (e.g. chain and segment length, number of cross-links per chain). This leads to more homogeneous matrices, and to the reduction of artifacts, which could impair the mechanical properties of the resulting hydrogels (109).

Cross-linking mechanisms for ELRs can be as versatile as ELRs themselves: ionic or hydrophobic interactions, reaction of complementary groups, or enzymatically induced cross-links (Figure 4) (110,111). All these strategies can provide a very tight control over the length and the molecular weight of the proteins by the selection of the cross-linking sites, which usually correspond to lysine groups (112,113). Besides the control of the cross-linking, aforementioned bioactivities can be introduced into ELRs, so that the matrix is able to interact with the organism, improving the good integration of the generated tissue. The basic ELR sequence (VPGXG) is biocompatible, but lacks cellular adhesion sites. Nevertheless, the possibility of a tailored genetic design permits changes in the transition temperature, integration of protease-

sensitive sites (114,115), cellular adhesion motifs (59,116), or biological triggers (117-119).

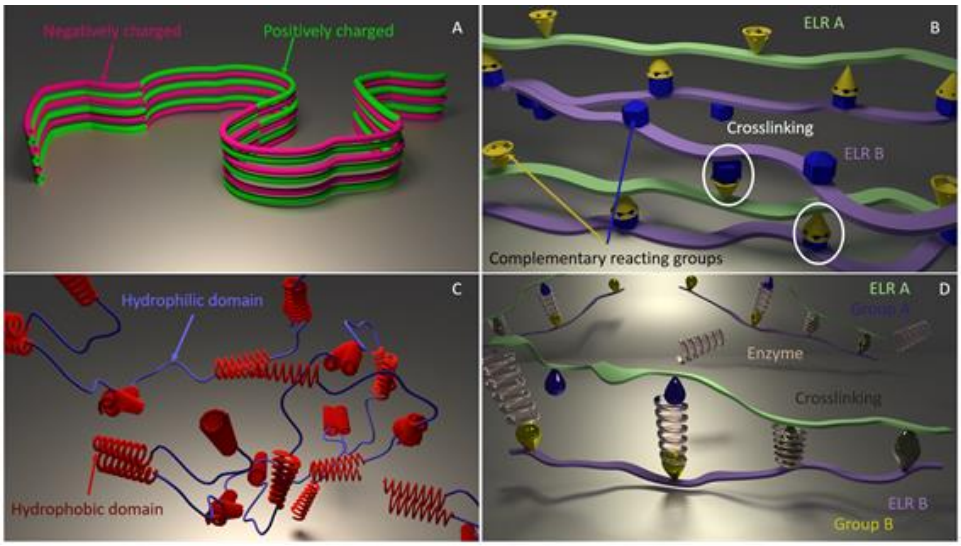

Figure 4. Common ELR crosslinking strategies: A) ionic interaction, B) chemical crosslinking, C) hydrophobic interactions, D) enzyme triggered crosslinking.

Physical cross-linking of ELRs can be obtained by several strategies. One approach is a cross-linking based on ionic interactions by segments of opposite charge (e.g. cationic and anionic amino acids in the X position of the ELR). Even though ionic interactions are relatively weak, an specific design of complementary charged strands (120,121) helps to a better strengthening of these interactions which leads to obtain stable ELR hydrogels at room temperature and physiological pH (122). Potentially, the presence of ions could trigger the formation of hydrogels, since some ELRs are sensible to salts concentration changes, especially to chelating ions like calcium (121). More advanced approaches including ELR/chitosan blends, could be stabilized by sodium ions (123), and modification with

monosaccharide side chains allowed a complexation with pottassium (124). A second way of physical cross-linking is obtained by the introduction of self-assembling motifs, i.e. amphiphilic blocks, or interaction of protein secondary structures (β-sheets, leucine zippers). The self-organization is basically driven by aggregation of different segments. In the case of amphiphilic block ELRs this self-assembling is due to the aggregation process of the hydrophobic segments. On the other hand, the interaction of secondary structures is triggered by the aggregation of β-sheets or pairing of leucine zippers.

Hydrophobic blocks are generated when the ELR sequence has several hydrophobic amin oacids (like alanine (Ala), leucine (Leu), isoleucine (Ile), valine (Val), phenylalanine (Phe), tryptophan (Trp), tyrosine (Tyr) or methionine (Met)) on the X position. This results in segments of distinct polarity within the same protein chain and leads to mutual repulsion between the different blocks, that tend to segregate. The segregation is locally constrained by the "forced cohabitation" of the blocks within the same ELR chain, resulting in a separation into different domains, which as a consequence, self-assemble into periodic nanostructures (125). Amphiphilic blocks can be designed to form stable hydrogels that even persist *in vivo*. One way to enhance stability is to create longer sequences with several blocks of alternating polarity (108,126,127).

The interaction of intermolecular secondary structures, on the other hand, follows the key-lock-principle with the assembly of matching structures of similar polarity. From the tailor perspective, almost any protein secondary structure that is able to form a stable

link with itself or contrary groups could be implemented. It has to be considered that in one component systems gelation can occur easily, and solvation is limited. Furthermore, the effect on the ELRs T_t has to be considered.

The recent approaches to include physical cross-linking cues into ELRs are inspired by natural silk sequences that enable crystalline-like β-sheets formation with unique mechanical properties (128-132). The repetitive sequence responsible for the β-sheet formation and for the intrinsic strength is the GAGAGS hexapeptide (*Bombyx mori* silkworm) (133). In this silkworm the blocks are stabilized by hydrophilic compartments within the protein and a complex mixture of stabilizing agents (134). The integration into ELRs needs to consider the stability of the resulting bonds and the amount of silk domains govern the manipulation of the material. Silk-ELR (SELR) hybrid materials reveal a two-step gelation process when heated above the T_t. The ELR transition occurs first, enabling the thermodinamically driven annealing of silk sequences, hence forming stable physically cross-linked hydrogels *in situ* (108). SELRs are biocompatible and performed well in *in vivo* studies (135-137). Moreover, they have been forged into a variety structures like hydrogels, films, 3D porous matrices and submicron to macroscale fibers (138).

Lately, ELRs physically cross-linked by leucine zipper domains (139-145) gained interest. The leucine zippers are capable to dimerize with other leucine zipper domains driven by hydrophobic interactions (139,146-148), and ionic interactions (149-151). On account of its novelty, ELRs with leucine zipper motifs have been less explored than SELRs, and the complete potential

remains to be discovered. Nevertheless, the human origin of the domain and the conserved nature of the structure alleviate concerns regarding the biocompatibility. First studies on ELR-Zippers support the biocompatibility and showed enhanced stability when compared to pure amphiphilic block ELRs (61). Furthermore, a recent *in vivo* study regarding zipper-based scaffolds revealed no foreign body reaction (152).

The introduction of amino acids bearing functional groups in the X position can be used for subsequent reactions without losing the pH and temperature sensitivity of the ELRs. The majority of published works used the free ε-amine of lysine residues within the ELR chain for chemical modification due to its reactivity. (153,154) Regarding the cross-linking process, the MW, concentration and the number of cross-links are important to form stable hydrogels (155). ELRs with high molecular weight have a higher entanglement and are more prone to establish sufficient number of cross-links to stabilize the hydrogel network. Due to the tailored design of the ELR sequence, the number of cross-linking sites and the segment length between cross-links can be precisely controlled, enabling the tuning of relevant features such as pore size, gelation time, stiffness and degradability. Functionalization of ELRs aims to introduce bioactive sequences, adhesion sites, inhibitors, antibodies or anchor and signaling molecules (156). Degradation can be further controlled through the introduction of protease-sensitive sequences, or through introduction of labile chemical linkages (157).

One drawback of common chemical linkages is that they are reactive under conditions that require organic solvents or other

chemical reagents to avoid hydrolysis. To elude removal of this undesired components, the typical cross-linking of hydrogels is based on the reaction of complementary groups (158), enzymatic cross-linking (159-161), condensation reactions (162), or high-energy irradiation (163). The classical cross-linking reactions of ELRs are solvent dependent, in organic solvents, due to the absence of a lower critical solution temperature (LCST). The obtained hydrogels are very homogenous, whereas in water the diffusion of active sites is limited above the LCST (112). The fusion of several ELR strands by cross-linking results in stable hydrogels, which remain stable when cooled below the ELRs T_t. Using enzymatic cross-links, hybrid protein hydrogels of ELR and other functional proteins can be obtained. Mild covalent cross-linking strategies without organic solvents and cytotoxic reactants have some important advantages, such as that the gelation can be performed in the implantation site, without further purification *in situ*, without the diffusion out of the injection site. Ravi *et al.* showed that an ELR/fibronectin gel cross-linked by genipin performed well *in vitro*. (164) Moreover, the Huisgen reaction has been introduced in the past years to form ELR networks in water (165,166). The reaction of complementary groups can be used further to fuse ELRs of different bioactivity together (167), and to generate hybrid materials. This method has been used for the creation of non-thrombogenic stents (165).

4. ELASTIN-LIKE RECOMBINAMERS: APPLICATIONS

4.1. ELRs for gene delivery applications

Gene therapy provides a unique approach to deliver a therapeutic gene into specific human tissues or cells; the modification of patient's altered gene expression can be performed by gene addition, gene correction, gene knockdown or their combination (168,169). The concept of gene therapy is based on nucleic acids being used as pharmaceutical products to obtain *in vivo* production or silencing of therapeutic proteins (170,171); the therapeutic material can be integrated into the host chromosome or remained as an episomal plasmid with transient expression (168,172). The successful expression of the deficient gene product at physiological levels (168,173) is based on an appropriate delivery system (174). The most important properties that a delivery vector must have are the biocompatibility and the ability to release the cargo into a specific target.

Gene delivery systems can be divided into two categories: viral and non-viral vectors. Despite approximately 65% of clinical trials use a viral vector for DNA delivery (175), non-viral vectors have been widely studied over the past few years and constitute the most promising alternative for overcoming the immunogenicity problems inherent to viral vectors; moreover, they are easier to produce on a large scale (176,177). Cationic polymers can form a complex with DNA by electrostatic interactions with the negatively charged phosphates from nucleic acids. The formed polyplex, is able

to protect the genetic material from degradation by nucleases (178). PEI (polyethylenimine), PEG (polyethyleneglycol), PLL (poly-L-lysine), chitosan, PLGA (polylactic-coglycolic acid), and PDMAEMA (polydimethylaminoethyl methacrylate) are some of the most widely used non-viral gene delivery vehicles (169,179-181). The cytocompatible nature of the biomaterial forming the polyplexes and their ability to be internalized into the cell, determine the success of the system (177,179,182-184). Nevertheless, most of the cationic polymers mentioned above are not ideal for drug delivery application. For instance, the main problem of PEI is its cytotoxicity, causing cell apoptosis in a wide number of human cell lines (185). Regarding PEG, not only hypersensitivity reactions occur when it is injected intravenously, but also cutaneous application can cause allergic reactions, such as contact dermatitis (186).

Thus, it is required a new design of gene delivery vectors able to address the individual rate-limiting steps along the gene delivery process (187). ELRs have grown in popularity in the field of protein-inspired biomimetic materials, and they are becoming increasingly important in different fields of biomedicine (165,188-190). ELRs are non-immunogenic, and according with their biodegradability and biocompatibility for human tissue, blood, and other fluids, they can play a key role as carriers in delivery systems (189,191,192). ELRs have been previously used as oligo-lysine carriers by Furgerson's group to deliver an EGFP–plasmid inside cells in *in vitro* assays (193). The use of specifically designed ELRs joined to functional peptides as agents shows promising results for delivering genes *in vitro* (190). Moreover, cellular transfection can be

improved through the formation of charged polyplexes and their further interaction with the negatively charged components on the cell membrane, such as proteoglycans and cell-surface receptors (194,195). In this study, taking advantage of the recombinant DNA technology to design and produce ELRs, functional motifs were incorporated into a basic ELR sequence. Then, imidazole groups were covalently bound, obtaining stable polyplexes composed of plasmid DNA and ELRs (190). Several studies have demonstrated the use of ELRs fused to a cell penetrating peptide (CPP) as a drug delivery vector for solid tumors (182,196,197). In this sense, a similar combination of ELRs fused to CPPs was utilized to deliver therapeutic peptides into target tumor cells (198). Finally, Piña *et al.*, specifically designed a lysine-enriched ELR in order to complex and protect the therapeutic DNA, forming stable polyplexes. In this work, for the first time, cancer-specific aptamers were incorporated into ELR polyplexes with potential application in the treatment of breast cancer (199).

4.2. ELRs as vaccine delivery systems

In the past recent years, due to the increasing knowledge about the mechanisms of protective immune responses, and about new biotechnology techniques, newer vaccine designs have been considered. For instance, a novel approach based on genetic engineering in order to obtain non-pathogenic vaccine strains, naked plasmid DNA vaccines, or for the preparation of relevant recombinant proteins that may lead to adequate immunity (199). Certainly, the ability to isolate and produce pure proteins and peptide antigens that are safer than traditional vaccines has

enhanced the vaccine efficacy (201-203). However, a limiting factor with antigens made by recombinant DNA technology is that they are often weakly immunogenic on their own, thus it is often required the inclusion of immune adjuvants to enhance the resultant immune responses (204,205). Adjuvants have the ability to activate antigen-presenting cells (APCs), and despite their clear relevance and essential role, only adjuvants that induce minimal adverse effects are acceptable for standard prophylactic immunization in healthy individuals.

Certainly, the relative lack of antigenic carriers approved for the usage in humans suggests that better materials and new strategies are needed to generate successful nanovaccines. As it has been already described, biomaterials play a key role in the therapeutic field regarding vaccine development. The engineering of materials that can modulate the immune system, known as immunobioengineering, is playing an increasingly important part for the development of new particulate vaccines and adjuvants carrying the desired epitopes for immunization (201,206,207). Therefore, because of one of the most powerful strategies to form very small particles is based on self-assembled di-block co-polymers, many different materials displaying stimuli-responsiveness with different molecular architectures have been investigated (207).

Several factors such as particle size, surface properties, particle shape, and hydrophobicity (201,208,209), affect the nature of the immune response caused by biomaterial-based nano-objects. It has been shown that the particles themselves are intrinsically recognized as a sign of danger (210), and considering that the

particle size is the primary control parameter, a particulate vaccine can target several pathways depending on its size. Biomaterial particles can include specific functional domains such as targeting ligands that are able to bind specific receptors for endocytosis, promoting an increase of specific cellular uptake (204,211). In addition, another important parameter is the hydrophilicity in the nanoformulation, that can modulate the amount of proteins adsorbed onto the surface of nanoparticles after the administration, increasing their residence time in circulating blood (212).

ELRs play a key role in several biomedical applications due to the ability to control and manipulate the interface between them and the biological components. In this sense, the American Society for Analysis of Materials (ASTM) has demonstrated their extraordinary biocompatibility, while the feasibility of tuning and controlling the shape and topology of ELRs has been previously explored (213,214). In addition, elastin-like block co-recombinamers (ELbcRs) are able to form multimeric nanoparticles by self-assembling, and considering the ability to control their hydrophobicity, molecular weight and block rearrangement, ELRs are exceptional candidates as carriers in vaccine-delivery approaches (191,215). The recombinant production of ELRs allows obtaining a highly monodisperse, multivalent and biocompatible properties of the resulting constructions by a simple, affordable, reproducible and easy to scale up process of bioproduction (216,217). Furthermore, ELbcRs can be subjected to secondary processes such as sterilization, drying, packaging, and reconstitution of the resulting dried powder (126) (218).

Another advantage of the ELRs about the vaccine formulation regards the possibility to develop a single-gene product that self-assembles into a nanoparticle with the desired antigenic sequence. Therefore, thanks to the fusion strategy to produce ELR-based constructions, it is not required the use of bioconjugate chemistry to fuse other proteins to the nanoparticles. It has been already described the potential use of this strategy for many biomedical applications such as protein purification (219) or as drug and gene delivery systems (216).

Previous works (48,51,216) describe the nanoparticle structure of an ELbcR obtained by recombinant process, having the antigenic sequence(s) at the hydrophilic terminus gene(s); the genetically encoded synthesis does not affect the assembly of the nanoparticles, in fact, the elastin contribution serves as hidden support, whereas the antigen molecule(s) is oriented towards the outside of the particle. García-Areválo *et al.*, developed a new ELbcR-based vaccine carrier that self-assembles into highly monodisperse and stable nanovesicles that can be used to present low antigenic peptides, for example, from the bacterium *M. tuberculosis* (189). In another work, it was described the expression and immunogenicity of a construct produced by combining plant-based production and the ELR fusion strategy in order to produce a potential vaccine candidate containing two major antigens from *M. tuberculosis* (220).

4.3. ELR-based hydrogels for tissue engineering applications

Widely defined, tissue engineering is the process of restoring, maintaining, or enhancing living, physiological, three-dimensional tissues and organs utilizing specific combinations of cells, scaffolds, and/or signals, both chemical and physical. The process involves mainly four components: a material scaffold, functional cells, biomolecules (e.g. growth factors, extracellular matrix (ECM) molecules, and other biological), and dynamic forces (221). Thanks to the recombinant DNA technology, ELRs allow the tailoring at the genetic level of the mechanical and biological properties to satisfy end-user application, thus offering numerous choices for the development of cell culture matrices for a specific tissue (222). Several studies have shown how different types of ELRs can be addressed over the most challenging fields in tissue regeneration, such as cardiovascular, ocular prosthesis and osteochondral applications, among others.

Biofunctional materials require advanced design and preparation with the purpose of matching the sophisticated recognition ability of biological systems. The biocompatibility of any biomaterial has a critical importance and must be assessed prior to any clinical trial. As regards the purity of the biomaterial, any contamination with (globular) proteins entails one of the greater risks, namely the development of immunological responses that preclude their application in regenerative medicine and tissue engineering. Thus, the biomaterial is required to pass the

toxicological test that take into account the duration and the type of tissue in contact with the tested one.

As it has previously mentioned, ELRs have been used for the development of novel protein peptide biomaterials obtained through recombinant DNA technology that are playing an increasingly important role in a diverse range of applications such as drug delivery, tissue engineering, biosensors and a wide variety of 'smart' systems. Sallach *et al.* have described the production of a recombinant elastin-mimetic triblock copolymer and the further application *in vivo* for more than 1 year. During this time, the ELR-based hydrogel showed a minimal inflammatory response, confirming its high and extraordinary biocompatibility (127).

Considering the ability of the ELRs to self-assemble into different structures such as hydrogels, and taking into account that ELRs completely fulfill the prerequisites of biocompatibility and bioactivity, ELRs play a key role for the development of scaffolds and advanced systems for application in the fields of regenerative medicine and tissue engineering. In this sense, specific requirements of ELRs, such as topographic, chemical configuration and viscoelastic patterns, determine the hydrogel properties. Hence, they can be tuned specifically to match proteins at the nanometer scale and cells at the micrometer scale. In light of this, numerous reports have largely demonstrated requests from *in vitro* experiments (192,223,224).

In vascular tissue, elastin is an essential extracellular matrix protein that plays an important biomechanical and biological signaling role. Elastin-like recombinamers are able to mimic the structure and function of native elastin, representing a practical

alternative to the native elastic fiber (which is difficult to extract from tissues) for vascular applications. Several studies have demonstrated that stent surface endothelialization is a well-known methodology to inhibit restenosis and thrombosis (91,225-227). The use of active ELR coatings with endothelial cell adhesion sequences onto stents surfaces is a great strategy to recover a healthy endothelium. *In vivo* studies have demonstrated how ELR scaffolds support the neovascularization in the total absence of an immune response (91). In this sense, González de Torre *et al*. have shown the applicability of recently developed ELRs as a coating for vascular stents with the ultimate goal of producing a new endovascular device (165). The ELR applied on the stent gain a full endothelialization in a short time (2 weeks), showing a high biocompatibility and a reduced response of the immune system. Finally another approach by Weber *et al.* was to generate tissue-engineered heart valves (TEHVs) by multi-step injection molding using ELR as a hybrid system with fibrin (228).

In 2015, Mata's group demonstrated the supramolecular interaction between peptides and ELRs to generate complex 3D architectures through a dynamic self-assembly system, forming a stable multilayer membrane. This membrane can be spatiotemporally controlled and can be used to form bioactive tubular scaffolds which may support and lead the growth of different cell lines (229). This tubular morphogenesis could play an important role in tissue engineering applications that requires the formation of tubular structures that usually are complex to obtain in the milli- and micro scale.

According to the elastin-like nature of the hydrogel and the high percentage of elastin present in the native chondral matrix, ELR-based hydrogels are likely to simulate the properties of hyaline cartilage (230,231). The hyaline articular cartilage is a highly specialized tissue characterized by its unique mechanical features and it is formed by a matrix that embeds chondrocytes. Considering that the articular hyaline cartilage does not repair itself and that the generally regenerated fibrocartilage is unable to maintain the biomechanical characteristics of articular cartilage (232,233), ELR hydrogels could be used as scaffolds for osteochondral tissue engineering. As it has been previously described above, ELRs show thermosensitivity, on that regard is possible to form hydrogels stable at body temperature, whenever the transition temperature (T_t) of the ELR is lower than the body temperature. Moreover, ELRs containing bioactive sequences, such as the well-known RGD cell-adhesion sequence found in fibronectin, which promotes specific cell attachment via integrins (162), are able to form a bioactive scaffold that improves the regenerative potential of the implanted hydrogel.

Vila *et al.* showed how ELR coatings are able to improve the well-known biocompatible and bone regeneration properties of calcium phosphate-based materials (234).

Due to the development of novel tissue-engineering methods (52,235), it has been considered the use of mesenchymal stromal cell (MSC) therapy (236,237) for the treatment of musculoskeletal lesions (238,239). For articular defect applications, the use of a hydrogel serves as vehicle for the MSCs to acquire a 3D structure that could mimic the properties of the ECM providing a cell-friendly

environment in order to increase the persistence of the implanted cells at the site of injury. According with ELRs properties, a homogeneous embedding of MSCs in the ELR solution can be achieved at a temperature below T_t, and further applied as a cell-scaffold system for injectable therapies (Figure 5).

Figure 5. ELR-based injectable hydrogel for osteochondral applications.

Moreover, ELRs might also have beneficial applications in the field of ocular tissue engineering. Cornea wound healing requires cell adhesion and proliferation on a substrate with ligands such as fibronectin, secreted by corneal epithelial cells and stromal fibroblasts during the first steps of corneal wound healing (240). Nevertheless, the ocular surface, unwounded cornea and conjunctiva do not express elastin. Therefore, several metalloproteinases (MMPs) have been described in pathological ocular processes such as dry eye (241) or conjunctivochalasis (242), while some other MMP present at the ocular surface are able to degrade elastin fibers (241). Thus, ELRs are a potential candidate for Bruch´s membrane prosthesis. Martínez-Osorio *et al.* showed how a blend of ELRs was able to promote epithelial cell adhesion from human conjunctiva-derived primary cells (192). Finally, ELRs application as ocular implants was studied by Srivastasa *et al.*,

which confirmed ELRs as a suitable carrier for the transplantation of autologous RPE cells for the treatment of age-related macular degeneration (AMD) (243).

4.4. ELRs for surface bio-functionalization

The ELRs properties of elasticity and self-assembling allow the formation of a wide range of biomaterial-based constructs such as aggregates (51), films (77), fibers (224), micelles (48,244), nanoparticles (245), and hydrogels (246). Another advantage of this recombinant biomaterial is the capacity to form hybrid systems with materials having different origins, in order to obtain several morphologies and functional possibilities for a diverse range of applications such as functionalized surfaces, fibers, and drug delivery. Therefore, the recombinant technologies by which ELRs are obtained, allow a perfect control of their sequence, length and stereochemistry; moreover, for functionalized surfaces even a nanometric control of their position displayed by these systems is possible.

Chilkoti's group has created what they refer to as the "Thermodynamically Reversible Addressing of Proteins" (TRAP) (247), where an ELR is covalently micropatterned onto a glass surface obtaining a spatial-temporal system for protein binding that can be applied as a microsensor for detecting single biomolecules in bioanalytical applications. Additionally, different approaches based on controllable properties (stimuli-responsive) of the biofunctionalized surfaces have been studied in order to obtain a cell sheet harvesting system from a culture dish. In this sense Okano *et al.*, have developed a smart surface with PIPAAm polymer (and

its derivates) that can switch between a cell-adherent and non-adherent state as a result of a change in temperature (248). Despite this approach led a significant progress in this field (249-251), PIPAAm polymer lacks specific bioactivity, meaning that cellular membrane proteins, such as integrins, are not able to directly bind to the surface. To address this issue, Pierna *et al.* developed a smart surface system by covalent coupling of tailored ELRs onto glass surfaces by click chemistry methods. This cell sheet harvesting system leads to the exposition of the bioactive RGD motif to the water interface at physiological temperature, producing a cell adherent surface (252) (Figure 6). Na *et al.* also took advantage of the rapid response to external stimuli of a smart material surface created by adsorption of ELRs for use in cell-based biochips. The smart transition of ELR-based micropatterns between a hydrophilic and a hydrophobic surface glass at T_t allows to revert cell adhesion by way of the incubation temperature (253).

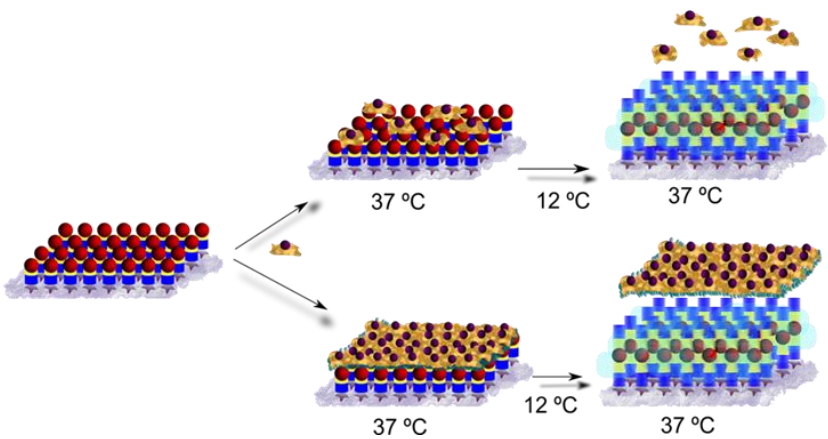

Figure 6. Schematic representation of a system based on ELRs for cell sheet harvesting.

Layer-by-layer (LbL) techniques are one of the most versatile and easy-to-apply of the numerous surface-modification tools. They

are based on the spontaneous adsorption of materials onto a substrate, generally a polymer, biomolecule, or inorganic particle, and allow the sequential formation of a nanostructured film, hence having a great interest in tissue-engineering applications (254-257). A layer-by-layer deposition of alternating ELR-polyelectrolytes generated a bioactive surfaces (258). In this work, it was developed a thermoresponsive thin coating by electrostatic self-assembly (ESA); the deposition of an ELR containing the bioactive RGD motif can be exploited for tunable cell adhesion and controlled protein adsorption by nanoscale surface tailoring (77). Another example of biomimetic surface-modification regards the chemical functionalization of ELRs in order to obtain metallic (Commercial pure titanium, Cp Ti) dental implants with osteostimulative capabilities by the covalent immobilization of biomolecules on the Cp Ti (259). Finally, Costa *et al*. demonstrated the feasibility of LbL synthesis using natural marine-based polysaccharides (chitosan and alginate) and ELRs (260) for possible application in wound dressings and drug-delivery systems (261,262). Furthermore, ELR molecules can be used for the functionalization of surfaces in order to obtain stronger and faster cell responses on the tissue–biomaterial interface, thus promoting better implant integration than short peptides functionalization; for instance, ELRs have been used to enhance the properties of poly-methylmethacrylate (PMMA) surfaces. Although PMMA has a great usage in several biomedical applications (263-269), this study showed that ELR-functionalized PMMA surfaces can enhance the cellular attachment efficiency and the cell anchorage strength (270). Finally, ELRs were thoroughly investigated as biocompatible vasculogenic surface

coatings and smooth muscle cells (SMC) showed enhanced attachment under retention of their contractile phenotype on similar ELR-coated electrospun fibers (271).

Abbreviations

A	Alanine
Ala	Alanine
AMD	Age-related macular degeneration
APCs	Antigen-presenting cells
ASTM	American Society for Analysis of Materials
C	Cysteine
CMT	critical micelle temperature
CPPs	Cell penetrating peptides
D	Aspartic Acid
DNA	Deoxyribonucleic acid
E	Glutamic Acid
E. coli	*Escherichia coli*
ECM	Extracellular matrix
EGFP	Enhanced green fluorescent protein
ELbcR	Elastin-like block co-recombinamer
ELP	Elastin-like polymer
ELR	Elastin-like recombinamer
ESA	Electrostatic self-assembly
G	Glycine
Gly	Glycine
IL	Interleukin
Ile	Isoleucine
IPTG	Isopropylthio-β-D-galactoside
ITC	Inverse transition cycle
ITT	Inverse temperature transition
LB	Luria Broth
LbL	Layer by layer
LCST	Lower critical solution temperature
Leu	Leucine
M. tuberculosis	*Mycobacterium tuberculosis*
Met	Methionine
MMPs	Matrix metalloproteinases
MSCs	Mesenchymal stromal cells

Mw	Molecular weight
nts	Nucleotides
P	Proline
P. pastoris	*Pichia pastoris*
PDMAEMA	Poly(2-dimethylamino-ethylmethacrylate)
PEG	Polyethylenglycol
PEI	Polyethylenimine
Phe	Phenylalanine
PIPAAm	poly(N-isopropylacrylamide)
PLGA	Poly(Lactide-co-Glycolide)
PLGA	Polylactic-coglycolic acid
PLL	Polylysine
PMMA	Polymethyl methacrylate
Pre-RDL	Plasmid reconstruction-recursive directional ligation
Pro	Proline
PTFE	Polytetrafluoroethylene
R	Arginine
RDL	Recursive directional ligation
RPE	Retinal pigment epithelium
SELR	Silk Elastin like recombinamer
SEM	Scanning electron microscopy
SMCs	Smooth muscle cells
T	Threonine
TB	Terrific Broth
TEHVs	Tissue engineering heart valves
TNF	Tumor necrosis factor
TRAP	Thermodynamically Reversible Addressing of Proteins
Trp	Tryptophan
T_t	Transition temperature
Tyr	Tyrosine
V	Valine
Val	Valine

References

1. P. E. Watson, I. D. Watson and R. D. Batt. *The American Journal of Clinical Nutrition* **33**, 27-39 (1980).

2. E. Petersen, F. WÃ¥gberg and K. A. A. Angquist. *European journal of vascular and endovascular surgery : the official journal of the European Society for Vascular Surgery* **24**, 440-444 (2002).

3. S. M. Mithieux and A. S. Weiss. Elastin. In: David ADP, John MS, editors. Advances in Protein Chemistry: Academic Press; 2005. p. 437-461.

4. F. W. Keeley, C. M. Bellingham and K. A. Woodhouse. *Philosophical Transactions of the Royal Society B: Biological Sciences* **357**, 185-189 (2002).

5. D. W. Urry. *J Protein Chem* **7**, 1-34 (1988).

6. A. M. Tamburro, V. Guantieri, A. Scopa and J. M. Drabble. *Chirality* **3**, 318-323 (1991).

7. M. A. Morelli, M. DeBiasi, A. DeStradis and A. M. Tamburro. *J Biomol Struct Dyn* **11**, 181-90 (1993).

8. H. Reiersen, A. R. Clarke and A. R. Rees. *Journal of molecular biology* **283**, 255-64 (1998).

9. D. W. Urry. *Angewandte Chemie-International Edition in English* **32**, 819-841 (1993).

10. D. W. Urry. *What sustains life? Consilient mechanisms for protein-based machines and materials*. Springer-Verlag, New York, 2006.

11. D. W. Urry. *J Protein Chem* **7**, 81-114 (1988).

12. D. Urry and K. P. D. Williams. Syntheses, Characterizations and Medical Uses of the Polypentapeptide of Elastin and its Analogs. In: Williams DF, editor. Biocompatibility of Tissue Analogues: CRC Press, Inc; 1985. p. 27.

13. D. T. McPherson, C. Morrow, D. S. Minehan, J. Wu, E. Hunter and D. W. Urry. *Biotechnol Prog* **8**, 347-52 (1992).

14. W. R. Gray, L. B. Sandberg and J. A. Foster. *Nature* **246**, 461-466 (1973).

15. L. D. Muiznieks, A. S. Weiss and F. W. Keeley. *Biochemistry and Cell Biology* **88**, 239-250 (2010).

16. B. Vrhovski and A. S. Weiss. *European Journal of Biochemistry* **258**, 1-18 (1998).

17. D. W. Urry, W. D. Cunningham and T. Ohnishi. *Biochemistry* **13**, 609-16 (1974).

18. V. Renugopalakrishnan, M. A. Khaled, R. S. Rapaka and D. W. Urry. *Biochim Biophys Acta* **536**, 421-8 (1978).

19. D. W. Urry, K. Okamoto, R. D. Harris, C. F. Hendrix and M. M. Long. *Biochemistry* **15**, 4083-9 (1976).

20. D. K. Chang and D. W. Urry. *Chemical Physics Letters* **147**, 395-400 (1988).

21. J. Cappello, J. Crissman, M. Dorman, M. Mikolajczak, G. Textor, M. Marquet and F. Ferrari. *Biotechnology Progress* **6**, 198-202 (1990).

22. U.S. Pat. WO/1988/003533 (1988), F. A. Ferrari, C. Richardson, J. Chambers, S. C. Causey and T. J. Pollock (to Google Patents).

23. D. A. Tirrell, M. J. Fournier and T. L. Mason. *MRS Bulletin* **16**, 23-28 (1991).

24. K. A. Padgett and J. A. Sorge. *Gene* **168**, 31-5 (1996).

25. R. A. McMillan, T. A. T. Lee and V. P. Conticello. *Macromolecules* **32**, 3643-3648 (1999).

26. D. E. Meyer and A. Chilkoti. *Biomacromolecules* **3**, 357-367 (2002).

27. J. R. McDaniel, J. A. Mackay, F. G. Quiroz and A. Chilkoti. *Biomacromolecules* **11**, 944-52 (2010).

28. J. C. Rodriguez-Cabello, A. Girotti, A. Ribeiro and F. J. Arias. *Methods in molecular biology* **811**, 17-38 (2012).

29. O. S. Rabotyagova, P. Cebe and D. L. Kaplan. *Biomacromolecules* **12**, 269-289 (2011).

30. D. T. McPherson, C. Morrow, D. S. Minehan, J. Wu, E. Hunter and D. W. Urry. *Biotechnology Progress* **8**, 347-52 (1992).

31. D. T. McPherson, J. Xu and D. W. Urry. *Protein expression and purification* **7**, 51-7 (1996).

32. C. Guda, X. Zhang, D. T. McPherson, J. Xu, J. H. Cherry, D. W. Urry and H. Daniell. *Biotechnology Letters* **17**, 745-750 (1995).

33. K. D. Tartof and C. A. Hobbs. *Bethesda Res. Lab. Focus* **9**, 12-16 (1987).

34. D. C. Chow, M. R. Dreher, K. Trabbic-Carlson and A. Chilkoti. *Biotechnology Progress* **22**, 638-46 (2006).

35. R. Machado, J. Azevedo-Silva, C. Correia, T. Collins, F. J. Arias, J. C. Rodriguez-Cabello and M. Casal. *AMB Express* **3**, 11 (2013).

36. T. Collins, M. Barroca, F. Branca, J. Padrao, R. Machado and M. Casal. *Biomacromolecules* **15**, 2701-8 (2014).

37. R. W. Herzog, N. K. Singh, D. W. Urry and H. Daniell. *Applied microbiology and biotechnology* **47**, 368-72 (1997).

38. R. Schipperus, R. L. M. Teeuwen, M. W. T. Werten, G. Eggink and F. A. de Wolf. *Applied Microbiology and Biotechnology* **85**, 293 (2009).

39. R. E. Sallach, V. P. Conticello and E. L. Chaikof. *Biotechnology Progress* **25**, 1810-1818 (2009).

40. R. Schipperus, G. Eggink and F. A. de Wolf. *Biotechnology Progress* **28**, 242-247 (2012).

41. X. Zhang, C. Guda, R. Datta, R. Dute, D. W. Urry and H. Daniell. *Biotechnology Letters* **17**, 1279-1284 (1995).

42. X. Zhang, D. W. Urry and H. Daniell. *Plant Cell Reports* **16**, 174-179 (1996).

43. R. Heppner, N. Weichert, A. Schierhorn, U. Conrad and M. Pietzsch. *International Journal of Molecular Sciences* **17**, 1687 (2016).

44. J. C. Rodriguez-Cabello, S. Prieto, J. Reguera, F. J. Arias and A. Ribeiro. *Journal of biomaterials science. Polymer edition* **18**, 269-86 (2007).

45. D. W. Urry. *The Journal of Physical Chemistry B* **101**, 11007-11028 (1997).

46. E. R. Wright and V. P. Conticello. *Advanced Drug Delivery Reviews* **54**, 1057-1073 (2002).

47. T. A. T. Lee, A. Cooper, R. P. Apkarian and V. P. Conticello. *Advanced Materials* **12**, 1105-1110 (2000).

48. L. Martín, E. Castro, A. Ribeiro, M. Alonso and J. C. Rodríguez-Cabello. *Biomacromolecules* **13**, 293-298 (2012).

49. D. E. Meyer and A. Chilkoti. *Biomacromolecules* **5**, 846-851 (2004).

50. J. R. McDaniel, D. C. Radford and A. Chilkoti. *Biomacromolecules* **14**, 2866-72 (2013).

51. A. Ribeiro, F. J. Arias, J. Reguera, M. Alonso and J. C. Rodríguez-Cabello. *Biophysical Journal* **97**, 312-320 (2009).

52. A. Girotti, D. Orbanic, A. Ibáñez-Fonseca, C. Gonzalez-Obeso and J. C. Rodríguez-Cabello. *Advanced Healthcare Materials* **4**, 2423-2455 (2015).

53. A. Nagarsekar, J. Crissman, M. Crissman, F. Ferrari, J. Cappello and H. Ghandehari. *Biomacromolecules* **4**, 602-607 (2003).

54. Q. Wang, X. Xia, W. Huang, Y. Lin, Q. Xu and D. L. Kaplan. *Advanced Functional Materials* **24**, 4303-4310 (2014).

55. A. Bracalello, V. Santopietro, M. Vassalli, G. Marletta, R. Del Gaudio, B. Bochicchio and A. Pepe. *Biomacromolecules* **12**, 2957-2965 (2011).

56. A. Panitch, T. Yamaoka, M. J. Fournier, T. L. Mason and D. A. Tirrell. *Macromolecules* **32**, 1701-1703 (1999).

57. A. Girotti, J. Reguera, J. C. Rodríguez-Cabello, F. J. Arias, M. Alonso and A. M. Testera. *Journal of Materials Science: Materials in Medicine* **15**, 479-484 (2004).

58. M. D. Pierschbacher and E. Ruoslahti. *Nature* **309**, 30-33 (1984).

59. A. Nicol, D. Channe Gowda and D. W. Urry. *Journal of Biomedical Materials Research* **26**, 393-413 (1992).

60. J. C. Liu, S. C. Heilshorn and D. A. Tirrell. *Biomacromolecules* **5**, 497-504 (2004).

61. A. Fernández-Colino, F. J. Arias, M. Alonso and J. C. Rodríguez-Cabello. *Biomacromolecules* **16**, 3389-3398 (2015).

62. W.-B. Zhang, F. Sun, D. A. Tirrell and F. H. Arnold. *Journal of the American Chemical Society* **135**, 13988-13997 (2013).

63. T. Christensen, M. Amiram, S. Dagher, K. Trabbic-Carlson, M. F. Shamji, L. A. Setton and A. Chilkoti. *Protein Science* **18**, 1377-1387 (2009).

64. T. Christensen, W. Hassouneh, K. Trabbic-Carlson and A. Chilkoti. *Biomacromolecules* **14**, 1514-1519 (2013).

65. D. E. Meyer and A. Chilkoti. *Nat Biotech* **17**, 1112-1115 (1999).

66. M. R. Banki, L. Feng and D. W. Wood. *Nat Meth* **2**, 659-662 (2005).

67. W. Hassouneh, T. Christensen and A. Chilkoti. Elastin-Like Polypeptides as a Purification Tag for Recombinant Proteins. Current Protocols in Protein Science: John Wiley & Sons, Inc.; 2001.

68. W.-J. Liu, Q. Wu, B. Xu, X.-Y. Zhang, X.-L. Xia and H.-C. Sun. *Protein Expression and Purification* **98**, 18-24 (2014).

69. J. Patel, H. Zhu, R. Menassa, L. Gyenis, A. Richman and J. Brandle. *Transgenic Research* **16**, 239-249 (2007).

70. U. Conrad, I. Plagmann, S. Malchow, M. Sack, D. M. Floss, A. A. Kruglov, S. A. Nedospasov, S. Rose-John and J. Scheller. *Plant Biotechnology Journal* **9**, 22-31 (2011).

71. A. Kaldis, A. Ahmad, A. Reid, B. McGarvey, J. Brandle, S. Ma, A. Jevnikar, S. E. Kohalmi and R. Menassa. *Plant Biotechnology Journal* **11**, 535-545 (2013).

72. F. Hu, T. Ke, X. Li, P. H. Mao, X. Jin, F. L. Hui, X. D. Ma and L. X. Ma. *Applied Biochemistry and Biotechnology* **160**, 2377-2387 (2010).

73. D. A. Sousa, K. C. L. Mulder, K. S. Nobre, N. S. Parachin and O. L. Franco. *Journal of Biotechnology* **234**, 83-89 (2016).

74. D. W. Urry. *Methods Enzymol* **82 Pt A**, 673-716 (1982).

75. S. M. Janib, M. Pastuszka, S. Aluri, Z. Folchman-Wagner, P.-Y. Hsueh, P. Shi, Yi-An, H. Cui and J. A. Mackay. *Polymer chemistry* **5**, 1614-1625 (2014).

76. M. H. Misbah, L. Quintanilla, M. Alonso and J. C. Rodríguez-cabello. *Polymer* **81**, 37-44 (2015).

77. R. R. Costa, C. A. Custodio, A. M. Testero, F. J. Arias, J. C. Rodriguez-Cabello, N. M. Alves and J. F. Mano. *Advanced Functional Materials* **19**, 3210-3218 (2009).

78. X. X. Xia, M. Wang, Y. Lin, Q. Xu and D. L. Kaplan. *Biomacromolecules* **15**, 908-914 (2014).

79. M. R. Dreher, A. J. Simnick, K. Fischer, R. J. Smith, A. Patel, M. Schmidt and A. Chilkoti. *Journal of the American Chemical Society* **130**, 687-694 (2008).

80. A. Ghoorchian, K. Vandemark, K. Freeman, S. Kambow, N. B. Holland and K. A. Streletzky. *Journal of Physical Chemistry B* **117**, 8865-8874 (2013).

81. G. Pinedo-martín, M. Santos, A. M. Testera, M. Alonso and J. C. Rodríguez-cabello. *Polymer* **55**, 5314-5321 (2014).

82. R. E. Sallach, M. Wei, N. Biswas, V. P. Conticello, S. Lecommandoux, R. A. Dluhy and E. L. Chaikof. *Journal of the American Chemical Society* **128**, 12014-12019 (2006).

83. A. Ghoorchian, J. T. Cole and N. B. Holland. *Macromolecules* **43**, 4340-4345 (2010).

84. N. U. Patel, C. A. Purser, R. C. Baker and A. V. Janorkar. *Biomacromolecules* **14**, 2891-2899 (2013).

85. G. Pinedo-martin, E. Castro, L. Martin, M. Alonso and J. C. Rodr. *Langmuir* **30**, 8 (2014).

86. W. Hassouneh, M. L. Nunalee, M. C. Shelton and A. Chilkoti. *Biomacromolecules* **14**, 2347-2353 (2013).

87. J. R. McDaniel, I. Weitzhandler, S. Prevost, K. B. Vargo, M. S. Appavou, D. A. Hammer, M. Gradzielski and A. Chilkoti. *Nano Letters* **14**, 6590-6598 (2014).

88. R. M. Senior, G. L. Griffin, R. P. Mecham, D. S. Wrenn, K. U. Prasad and D. W. Urry. *The Journal of Cell Biology* **99**, 870-874 (1984).

89. M. R. Banki and D. W. Wood. *Microbial Cell Factories* **4**, 32 (2005).

90. E. M. Srokowski and K. A. Woodhouse. *Journal of Biomedical Materials Research - Part A* **102**, 540-551 (2014).

91. M. I. Castellanos, A.-S. Zenses, A. Grau, J. C. Rodríguez-Cabello, F. J. Gil, J. M. Manero and M. Pegueroles. *Colloids and Surfaces B: Biointerfaces* **127**, 22-32 (2015).

92. S. W. Jordan, C. A. Haller, R. E. Sallach, R. P. Apkarian, S. R. Hanson and E. L. Chaikof. *Biomaterials* **28**, 1191-1197 (2007).

93. K. A. Woodhouse, P. Klement, V. Chen, M. B. Gorbet, F. W. Keeley, R. Stahl, J. D. Fromstein and C. M. Bellingham. *Biomaterials* **25**, 4543-4553 (2004).

94. A. Waterhouse, S. G. Wise, M. K. Ng and A. S. Weiss. *Tissue engineering. Part b* **17**, 93-99 (2011).

95. Y. Li, X. Chen, A. J. Ribeiro, E. D. Jensen, K. V. Holmberg, J. C. Rodriguez-cabello and C. Aparicio. *advanced Healthcare Materials* **3**, 1638-1647 (2014).

96. L. A. Hughes, J. Gaston, K. McAlindon, K. A. Woodhouse and S. L. Thibeault. *Acta Biomaterialia* **13**, 111-120 (2015).

97. K. M. Lee, G. S. Jung, J. K. Park, S. K. Choi and W. B. Jeon. *Acta Biomaterialia* **9**, 5600-5608 (2013).

98. J. Scheller, D. Henggeler, A. Viviani and U. Conrad. *Transgenic Research* **13**, 51-57 (2004).

99. M. Pierna, M. Santos, F. J. Arias, M. Alonso and J. C. Rodríguez-Cabello. *Biomacromolecules* **14**, 1893-1903 (2013).

100. J. Kopeček. *Biomaterials* **28**, 5185-5192 (2007).

101. N. A. Peppas. *Journal of Controlled Release* **68**, 135 (2000).

102. A. S. Hoffman. *Advanced Drug Delivery Reviews* **54**, 3-12 (2002).

103. A. P. Nowak, V. Breedveld, L. Pakstis, B. Ozbas, D. J. Pine, D. Pochan and T. J. Deming. *Nature* **417**, 424-428 (2002).

104. C. Xu, V. Breedveld and J. Kopecek. *Biomacromolecules* **6**, 1739-1749 (2005).

105. W. A. Petka, J. L. Harden, K. P. Mcgrath, D. Wirtz and D. A. Tirrell. *Science* **281**, 389-392 (1998).

106. D. W. Urry. *The Journal of Physical Chemistry B* **101**, 11007-11028 (1997).

107. J. T. Prince, K. P. McGrath, C. M. DiGirolamo and D. L. Kaplan. *Biochemistry* **34**, 10879-10885 (1995).

108. A. Fernandez-Colino, F. J. Arias, M. Alonso and J. Carlos Rodriguez-Cabello. *Biomacromolecules* **15**, 3781-3793 (2014).

109. J. Kopeček and J. Yang. *Polymer International* **56**, 1078-1098 (2007).

110. D. Campoccia, P. Doherty, M. Radice, P. Brun, G. Abatangelo and D. F. Williams. *Biomaterials* **19**, 2101-2127 (1998).

111. G. D. Prestwich, D. M. Marecak, J. F. Marecek, K. P. Vercruysse and M. R. Ziebell. *Journal of Controlled Release* **53**, 93-103 (1998).

112. R. A. McMillan and V. P. Conticello. *Macromolecules* **33**, 4809-4821 (2000).

113. R. A. McMillan, K. L. Caran, R. P. Apkarian and V. P. Conticello. *Macromolecules* **32**, 9067-9070 (1999).

114. A. J. Alix. *Journal de la Socie´te´ de biologie* **195**, 181-93 (2001).

115. A. Girotti, J. Reguera, J. C. Rodríguez-Cabello, F. J. Arias, M. Alonso and A. M. Testera. *Journal of Materials Science: Materials in Medicine* **15**, 479-484 (2004).

116. D. W. Urry, A. Pattanaik, J. Xu, T. C. Woods, D. T. McPherson and T. M. Parker. *Journal of biomaterials science. Polymer edition* **9**, 1015-48 (1998).

117. T. Miyata, N. Asami and T. Uragami. *Nature* **399**, 766-9 (1999).

118. C. Wang, J. Kopecek and R. J. Stewart. *Biomacromolecules* **2**, 912-20 (2001).

119. K. Ulbrich, J. Strohalm and J. Kopecek. *Biomaterials* **3**, 150-154 (1982).

120. T. C. Holmes, S. de Lacalle, X. Su, G. Liu, A. Rich and S. Zhang. *Proceedings of the National Academy of Sciences* **97**, 6728-6733 (2000).

121. S. Zhang. *Nature Biotechnology* **21**, 1171-1178 (2003).

122. B. Ozbas, J. Kretsinger, K. Rajagopal, J. P. Schneider and D. J. Pochan. *Macromolecules*, (2004).

123. R. R. Costa, C. A. Custódio, F. J. Arias, J. C. Rodríguez-Cabello and J. F. Mano. *Small* **7**, 2640-2649 (2011).

124. G. C. Yeo, F. W. Keeley and A. S. Weiss. *Advances in Colloid and Interface Science* **167**, 94-103 (2011).

125. M. Li and C. K. Ober. *Materials Today* **9**, 30-39 (2006).

126. J. C. Rodríguez-Cabello, L. Martín, A. Girotti, C. García-Arévalo, F. J. Arias and M. Alonso. *Nanomedicine (London, England)* **6**, 111-122 (2011).

127. R. E. Sallach, W. Cui, F. Balderrama, A. W. Martinez, J. Wen, C. A. Haller, J. V. Taylor, E. R. Wright, R. C. Long Jr and E. L. Chaikof. *Biomaterials* **31**, 779-791 (2010).

128. T. Asakura, J. Yao, T. Yamane, K. Umemura and A. S. Ulrich. (2002).

129. Y. Takahashi, M. Gehoh and K. Yuzuriha. *Journal of Polymer Science Part B: Polymer Physics* **29**, 889-891 (1991).

130. Y. Takahashi, M. Gehoh and K. Yuzuriha. *International Journal of Biological Macromolecules* **24**, 127-138 (1999).

131. K. Shimura, A. Kikuchi, K. Ohtomo, Y. Katagata and A. Hyodo. *Journal of biochemistry* **80**, 693-702 (1976).

132. F. G. Omenetto and D. L. Kaplan. *Science (New York, N.Y.)* **329**, 528-31 (2010).

133. K. Tanaka, S. Inoue and S. Mizuno. *Insect Biochemistry and Molecular Biology* **29**, 269-276 (1999).

134. J. G. Hardy, L. M. Römer and T. R. Scheibel. *Polymer* **49**, 4309-4327 (2008).

135. J. Zhou, C. Cao, X. Ma, L. Hu, L. Chen and C. Wang. *Polymer Degradation and Stability* **95**, 1679-1685 (2010).

136. B. Panilaitis, G. H. Altman, J. Chen, H.-J. Jin, V. Karageorgiou and D. L. Kaplan. *Biomaterials* **24**, 3079-3085 (2003).

137. H. Fan, H. Liu, S. L. Toh and J. C. H. Goh. *Biomaterials* **30**, 4967-4977 (2009).

138. B. Kundu, R. Rajkhowa, S. C. Kundu and X. Wang. *Advanced Drug Delivery Reviews* **65**, 457-470 (2013).

139. P. B. Harbury, T. Zhang, P. S. Kim and T. Alber. *Science (New York, N.Y.)* **262**, 1401-7 (1993).

140. J. R. Litowski and R. S. Hodges. *The Journal of Peptide Research* **58**, 477-492 (2001).

141. G. De Crescenzo, J. R. Litowski, R. S. Hodges and M. D. O'Connor-McCourt. *Biochemistry* **42**, 1754 (2003).

142. C. Vinson, M. Myakishev, A. Acharya, A. A. Mir, J. R. Moll and M. Bonovich. *Molecular and cellular biology* **22**, 6321-35 (2002).

143. C. R. Vinson, P. B. Sigler and S. L. McKnight. *Science (New York, N.Y.)* **246**, 911-6 (1989).

144. T. Abel and T. Maniatis. *Nature* **341**, 24-25 (1989).

145. D. N. Woolfson. *Advances in Protein Chemistry* **70**, 79-112 (2005).

146. J. Yang, C. Xu, P. Kopečková and J. Kopeček. *Macromolecular Bioscience* **6**, 201-209 (2006).

147. J. Moitra, L. Szilak, D. Krylov and C. Vinson. *Biochemistry* **36**, 12567-12573 (1997).

148. B. Tripet, K. Wagschal, P. Lavigne, C. T. Mant and R. S. Hodges. *Journal of Molecular Biology* **300**, 377-402 (2000).

149. D. Krylov, I. Mikhailenko and C. Vinson. *The EMBO journal* **13**, 2849-61 (1994).

150. T. Alber. *Current opinion in genetics & development* **2**, 205-10 (1992).

151. D. Krylov, J. Barchi and C. Vinson. *Journal of Molecular Biology* **279**, 959-972 (1998).

152. C.-C. Huang, S. Ravindran, Z. Yin and A. George. *Biomaterials* **35**, 5316-5326 (2014).

153. J. C. Rodríguez-Cabello, J. Reguera, A. Girotti, M. Alonso and A. M. Testera. *Progress in Polymer Science* **30**, 1119-1145 (2005).

154. J. C. Rodríguez-Cabello, M. Alonso, L. Guiscardo, V. Reboto and A. Girotti. *Advanced Materials* **14**, 1151-1154 (2002).

155. K. Trabbic-Carlson, L. A. Setton and A. Chilkoti. *Biomacromolecules* **4**, 572-580 (2003).

156. E. Ruoslahti and M. D. Pierschbacher. *Cell* **44**, 517-518 (1986).

157. W. E. Hennink and C. F. van Nostrum. *Advanced Drug Delivery Reviews* **54**, 13-36 (2002).

158. T. R. Hoare and D. S. Kohane. *Polymer* **49**, 1993-2007 (2008).

159. Y. Garcia, N. Hemantkumar, R. Collighan, M. Griffin, J. C. Rodriguez-Cabello and A. Pandit. *Tissue engineering. Part A* **15**, 887-899 (2009).

160. E. Westhaus and P. B. Messersmith. *Biomaterials* **22**, 453-462 (2001).

161. Y. Garcia, R. Collighan, M. Griffin and A. Pandit. *Journal of Materials Science: Materials in Medicine* **18**, 1991-2001 (2007).

162. A. E. J. de Nooy, G. Masci and V. Crescenzi. *Macromolecules* **32**, 1318-1320 (1999).

163. M. R. Huglin. *British Polymer Journal* **21**, 184-184 (1989).

164. S. Ravi, J. M. Caves, A. W. Martinez, C. A. Haller and E. L. Chaikof. *Journal of Biomedical Materials Research Part A* **101A**, 1915-1925 (2013).

165. A. M. Testera, A. Girotti, I. G. de Torre, L. Quintanilla, M. Santos, M. Alonso and J. C. Rodríguez-Cabello. *Journal of Materials Science: Materials in Medicine* **26**, 105 (2015).

166. J. Patterson, M. M. Martino and J. A. Hubbell. *Materials Today* **13**, 14-22 (2010).

167. I. G. de Torre, M. Santos, L. Quintanilla, A. Testera, M. Alonso and J. C. Rodríguez Cabello. *Acta Biomaterialia* **10**, 2495-2505 (2014).

168. D. J. Glover, H. J. Lipps and D. A. Jans. *Nature Reviews Genetics* **6**, 299-310 (2005).

169. M. Ramamoorth and A. Narvekar. *Journal of Clinical and Diagnostic Research : JCDR* **9**, GE01-GE06 (2015).

170. M. D. Brown, A. G. Schätzlein and I. F. Uchegbu. *International Journal of Pharmaceutics* **229**, 1-21 (2001).

171. J. M. Bergen, I.-K. Park, P. J. Horner and S. H. Pun. *Pharmaceutical Research* **25**, 983-998 (2008).

172. K. Van Craenenbroeck, P. Vanhoenacker and G. Haegeman. *European Journal of Biochemistry* **267**, 5665-5678 (2000).

173. M. A. Kay. *Nat Rev Genet* **12**, 316-328 (2011).

174. Z. Liu, Z. Zhang, C. Zhou and Y. Jiao. *Progress in Polymer Science* **35**, 1144-1162 (2010).

175. D. Putnam. *Nat Mater* **5**, 439-451 (2006).

176. H. Yin, R. L. Kanasty, A. A. Eltoukhy, A. J. Vegas, J. R. Dorkin and D. G. Anderson. *Nat Rev Genet* **15**, 541-555 (2014).

177. P. Midoux, C. Pichon, J.-J. Yaouanc and P.-A. Jaffrès. *British Journal of Pharmacology* **157**, 166-178 (2009).

178. M. A. Mintzer and E. E. Simanek. *Chemical Reviews* **109**, 259-302 (2009).

179. M. S. Al-Dosari and X. Gao. *The AAPS Journal* **11**, 671 (2009).

180. X. Gao, K.-S. Kim and D. Liu. *The AAPS Journal* **9**, E92-E104 (2007).

181. M. W. Konstan, P. B. Davis, J. S. Wagener, K. A. Hilliard, R. C. Stern, L. J. H. Milgram, T. H. Kowalczyk, S. L. Hyatt, T. L. Fink, C. R. Gedeon, S. M. Oette, J. M. Payne, O. Muhammad, A. G. Ziady, R. C. Moen and M. J. Cooper. *Human Gene Therapy* **15**, 1255-1269 (2004).

182. J. J. Thomas, M. R. Rekha and C. P. Sharma. *Molecular Pharmaceutics* **9**, 121-134 (2012).

183. M. R. Rekha and C. P. Sharma. *Acta Biomaterialia* **7**, 370-379 (2011).

184. C. L. Grigsby and K. W. Leong. *Journal of The Royal Society Interface* **7**, S67 (2009).

185. A. C. Hunter. *Advanced Drug Delivery Reviews* **58**, 1523-1531 (2006).

186. K. Knop, R. Hoogenboom, D. Fischer and U. S. Schubert. *Angewandte Chemie International Edition* **49**, 6288-6308 (2010).

187. N. L. Goeden-Wood, V. P. Conticello, S. J. Muller and J. D. Keasling. *Biomacromolecules* **3**, 874-879 (2002).

188. J. R. McDaniel, S. R. MacEwan, M. Dewhirst and A. Chilkoti. *Journal of Controlled Release* **159**, 362-367 (2012).

189. C. García-Arévalo, J. F. Bermejo-Martín, L. Rico, V. Iglesias, L. Martín, J. C. Rodríguez-Cabello and F. J. Arias. *Molecular Pharmaceutics* **10**, 586-597 (2013).

190. J. C. Rodríguez-Cabello, M. J. Piña, A. Ibáñez-Fonseca, A. Fernández-Colino and F. J. Arias. *Bioconjugate Chemistry* **26**, 1252-1265 (2015).

191. S. R. Ong, K. A. Trabbic-Carlson, D. L. Nettles, D. W. Lim, A. Chilkoti and L. A. Setton. *Biomaterials* **27**, 1930-1935 (2006).

192. H. Martínez-Osorio, M. Juárez-Campo, Y. Diebold, A. Girotti, M. Alonso, F. J. Arias, J. C. Rodríguez-Cabello, C. García-Vázquez and M. Calonge. *Current Eye Research* **34**, 48-56 (2009).

193. T.-H. H. Chen, Y. Bae and D. Y. Furgeson. *Pharmaceutical Research* **25**, 683-691 (2008).

194. W. Shen, M. A. van Dongen, Y. Han, M. Yu, Y. Li, G. Liu, M. M. Banaszak Holl and R. Qi. *European Journal of Pharmaceutics and Biopharmaceutics* **88**, 658-663 (2014).

195. S. Blau, T. T. Jubeh, S. M. Haupt and A. Rubinstein. *Critical Reviews in Therapeutic Drug Carrier Systems* **17**, 41 (2000).

196. H. Lee, J. H. Jeong and T. G. Park. *Journal of Controlled Release* **79**, 283-291 (2002).

197. L. Walker, E. Perkins, F. Kratz and D. Raucher. *International Journal of Pharmaceutics* **436**, 825-832 (2012).

198. G. L. Bidwell and D. Raucher. *Advanced drug delivery reviews* **62**, 1486-1496 (2010).

199. M. J. Piña, A. Girotti, M. Santos, J. C. Rodríguez-Cabello and F. J. Arias. *Molecular Pharmaceutics* **13**, 795-808 (2016).

200. M. T. Dertzbaugh. *Plasmid* **39**, 100-113 (1998).

201. J. A. Hubbell, S. N. Thomas and M. A. Swartz. *Nature* **462**, 449-460 (2009).

202. K. S. Jones. *Biotechnology Progress* **24**, 807-814 (2008).

203. O. A. Ali, N. Huebsch, L. Cao, G. Dranoff and D. J. Mooney. *Nat Mater* **8**, 151-158 (2009).

204. S. T. Reddy, M. A. Swartz and J. A. Hubbell. *Trends in Immunology* **27**, 573-579 (2006).

205. M. O. Oyewumi, A. Kumar and Z. Cui. *Expert Review of Vaccines* **9**, 1095-1107 (2010).

206. A. Travesset. *Science* **334**, 183-184 (2011).

207. M. A. C. Stuart, W. T. S. Huck, J. Genzer, M. Muller, C. Ober, M. Stamm, G. B. Sukhorukov, I. Szleifer, V. V. Tsukruk, M. Urban, F. Winnik, S. Zauscher, I. Luzinov and S. Minko. *Nat Mater* **9**, 101-113 (2010).

208. P. L. Mottram, D. Leong, B. Crimeen-Irwin, S. Gloster, S. D. Xiang, J. Meanger, R. Ghildyal, N. Vardaxis and M. Plebanski. *Molecular Pharmaceutics* **4**, 73-84 (2007).

209. A. Verma, O. Uzun, Y. Hu, Y. Hu, H.-S. Han, N. Watson, S. Chen, D. J. Irvine and F. Stellacci. *Nat Mater* **7**, 588-595 (2008).

210. F. A. Sharp, D. Ruane, B. Claass, E. Creagh, J. Harris, P. Malyala, M. Singh, D. T. O'Hagan, V. Petrilli, J. Tschopp, L. A. O'Neill and E. C. Lavelle. *Proc Natl Acad Sci U S A* **106**, 870-5 (2009).

211. S. D. Xiang, A. Scholzen, G. Minigo, C. David, V. Apostolopoulos, P. L. Mottram and M. Plebanski. *Methods* **40**, 1-9 (2006).

212. D. J. Bharali, V. Pradhan, G. Elkin, W. Qi, A. Hutson, S. A. Mousa and Y. Thanavala. *Nanomedicine: Nanotechnology, Biology and Medicine* **4**, 311-317 (2008).

213. L. Martin, M. Alonso, M. Moller, J. C. Rodriguez-Cabello and P. Mela. *Soft Matter* **5**, 1591-1593 (2009).

214. R. Sivakumar. *Bulletin of Materials Science* **22**, 647-655 (1999).

215. D. W. Urry, T. M. Parker, M. C. Reid and D. C. Gowda. *Journal of Bioactive and Compatible Polymers* **6**, 263-282 (1991).

216. G. Sun, P.-Y. Hsueh, S. M. Janib, S. Hamm-Alvarez and J. Andrew MacKay. *Journal of Controlled Release* **155**, 218-226 (2011).

217. J. C. Rodríguez-Cabello, S. Prieto, F. J. Arias, J. Reguera and A. Ribeiro. *Nanomedicine* **1**, 267-280 (2006).

218. A. Chilkoti, M. R. Dreher and D. E. Meyer. *Advanced Drug Delivery Reviews* **54**, 1093-1111 (2002).

219. D. E. Meyer, K. Trabbic-Carlson and A. Chilkoti. *Biotechnology Progress* **17**, 720-728 (2001).

220. D. M. Floss. *Journal of Biomedicine and Biotechnology* **Volume 2010 (2010)**, 14 pages (2010).

221. D. S. W. Benoit, M. P. Schwartz, A. R. Durney and K. S. Anseth. *Nat Mater* **7**, 816-823 (2008).

222. T. Johnson and P. Koria. *BioDrugs* **30**, 117-127 (2016).

223. J. Andrew MacKay, M. Chen, J. R. McDaniel, W. Liu, A. J. Simnick and A. Chilkoti. *Nat Mater* **8**, 993-999 (2009).

224. C. Garcia-Arevalo, M. Pierna, A. Girotti, F. J. Arias and J. C. Rodriguez-Cabello. *Soft Matter* **8**, 3239-3249 (2012).

225. Y. Wei, Y. Ji, L.-L. Xiao, Q.-k. Lin, J.-p. Xu, K.-f. Ren and J. Ji. *Biomaterials* **34**, 2588-2599 (2013).

226. L. G. Melo, M. Gnecchi, A. S. Pachori, D. Kong, K. Wang, X. Liu, R. E. Pratt and V. J. Dzau. *Arteriosclerosis, Thrombosis, and Vascular Biology* **24**, 1761-1774 (2004).

227. T. Inoue, K. Croce, T. Morooka, M. Sakuma, K. Node and D. I. Simon. *JACC: Cardiovascular Interventions* **4**, 1057-1066 (2011).

228. M. Weber, I. Gonzalez de Torre, R. Moreira, J. Frese, C. Oedekoven, M. Alonso, C. J. Rodriguez Cabello, S. Jockenhoevel and P. Mela. *Tissue Engineering Part C: Methods* **21**, 832-840 (2015).

229. K. E. Inostroza-Brito, E. Collin, O. Siton-Mendelson, K. H. Smith, A. Monge-Marcet, D. S. Ferreira, R. P. Rodríguez, M. Alonso, J. C. Rodríguez-Cabello, R. L. Reis, F. Sagués, L. Botto, R. Bitton, H. S. Azevedo and A. Mata. *Nat Chem* **7**, 897-904 (2015).

230. B. Kinikoglu, J. C. Rodriguez-Cabello, O. Damour and V. Hasirci. *J Mater Sci Mater Med* **22**, 1541-54 (2011).

231. B. Kinikoglu, J. C. Rodriguez-Cabello, O. Damour and V. Hasirci. *Biomaterials* **32**, 5756-64 (2011).

232. J. A. Vega Álvarez, O. García-Suárez, D. Fernández Monjil and M. E. del Valle Soto *Revista Española de Cirugía Ortopédica y Traumatología* **46**, 391-400 (2002).

233. T. Minas and L. Peterson. *Operative Techniques in Orthopaedics* **7**, 323-333 (1997).

234. M. Vila, A. García, A. Girotti, M. Alonso, J. C. Rodríguez-Cabello, A. González-Vázquez, J. A. Planell, E. Engel, J. Buján, N. García-Honduvilla and M. Vallet-Regí. *Acta Biomaterialia* **45**, 349-356 (2016).

235. J. T. Kerker, A. J. Leo and N. A. Sgaglione. *Sports Medicine and Arthroscopy Review* **16**, 208-216 (2008).

236. J. Vaquero and F. Forriol. *Injury* **43**, 694-705 (2012).

237. S. Vijayan, W. Bartlett, G. Bentley, R. W. J. Carrington, J. A. Skinner, R. C. Pollock, M. Alorjani and T. W. R. Briggs. *a two- to eight-year follow-up study* **94-B**, 488-492 (2012).

238. S. Trattnig, A. Ba-Ssalamah, K. Pinker, C. Plank, V. Vecsei and S. Marlovits. *Magnetic Resonance Imaging* **23**, 779-787 (2005).

239. M. W. Kessler, G. Ackerman, J. S. Dines and D. Grande. *Sports Medicine and Arthroscopy Review* **16**, 246-254 (2008).

240. L. S. Fujikawa, C. S. Foster, T. J. Harrist, J. M. Lanigan and R. B. Colvin. *Lab Invest* **45**, 120-9 (1981).

241. F. Bian, F. S. A. Pelegrino, S. C. Pflugfelder, E. A. Volpe, D.-Q. Li and C. S. de Paiva. *Investigative Ophthalmology & Visual Science* **56**, 4908-4918 (2015).

242. D. Meller, D. Q. Li and S. C. G. Tseng. *Investigative Ophthalmology & Visual Science* **41**, 2922-2929 (2000).

243. G. K. Srivastava, L. Martín, A. K. Singh, I. Fernandez-Bueno, M. J. Gayoso, M. T. Garcia-Gutierrez, A. Girotti, M. Alonso, J. C. Rodríguez-Cabello and J. C. Pastor. *Journal of Biomedical Materials Research Part A* **97A**, 243-250 (2011).

244. M. R. Dreher, A. J. Simnick, K. Fischer, R. J. Smith, A. Patel, M. Schmidt and A. Chilkoti. *Journal of the American Chemical Society* **130**, 687-694 (2008).

245. S. Roberts, M. Dzuricky and A. Chilkoti. *FEBS Letters* **589**, 2477-2486 (2015).

246. A. M. Testera, A. Girotti, I. G. de Torre, L. Quintanilla, M. Santos, M. Alonso and J. C. Rodríguez-Cabello. *Journal of Materials Science: Materials in Medicine* **26**, 105 (2015).

247. N. Nath and A. Chilkoti. *Analytical Chemistry* **74**, 504-509 (2002).

248. T. Okano, N. Yamada, M. Okuhara, H. Sakai and Y. Sakurai. *Biomaterials* **16**, 297-303 (1995).

249. H. Imen Elloumi, Y. Masayuki and O. Teruo. *Biofabrication* **1**, 022002 (2009).

250. M. Hirose, M. Yamato, O. H. Kwon, M. Harimoto, A. Kushida, T. Shimizu, A. Kikuchi and T. Okano. *Yonsei Med J* **41**, 803-813 (2000).

251. J. Yang, M. Yamato, T. Shimizu, H. Sekine, K. Ohashi, M. Kanzaki, T. Ohki, K. Nishida and T. Okano. *Biomaterials* **28**, 5033-5043 (2007).

252. M. Pierna, M. Santos, F. J. Arias, M. Alonso and J. C. Rodríguez-Cabello. *Biomacromolecules* **14**, 1893-1903 (2013).

253. K. Na, J. Jung, O. Kim, J. Lee, T. G. Lee, Y. H. Park and J. Hyun. *Langmuir* **24**, 4917-4923 (2008).

254. T. Boudou, T. Crouzier, K. Ren, G. Blin and C. Picart. *Advanced Materials* **22**, 441-467 (2010).

255. V. Gribova, R. Auzely-Velty and C. Picart. *Chemistry of materials : a publication of the American Chemical Society* **24**, 854-869 (2012).

256. H. S. Silva and P. B. Miranda. *The Journal of Physical Chemistry B* **113**, 10068-10071 (2009).

257. Z. Tang, Y. Wang, P. Podsiadlo and N. A. Kotov. *Advanced Materials* **18**, 3203-3224 (2006).

258. M. Swierczewska, C. S. Hajicharalambous, A. V. Janorkar, Z. Megeed, M. L. Yarmush and P. Rajagopalan. *Acta Biomaterialia* **4**, 827-837 (2008).

259. C. Aparicio, E. Salvagni, M. Werner, E. Engel, M. Pegueroles, C. Rodriguez-Cabello, F. Munoz, J. A. Planell and J. Gil. *Journal of Medical Devices* **3**, 027555-027555 (2009).

260. R. R. Costa, A. M. Testera, F. J. Arias, J. C. Rodríguez-Cabello and J. F. Mano. *The Journal of Physical Chemistry B* **117**, 6839-6848 (2013).

261. J. S. Boateng, K. H. Matthews, H. N. E. Stevens and G. M. Eccleston. *Journal of Pharmaceutical Sciences* **97**, 2892-2923 (2008).

262. M. George and T. E. Abraham. *Journal of Controlled Release* **114**, 1-14 (2006).

263. R. Q. Frazer, R. T. Byron, P. B. Osborne and K. P. West. *Journal of Long-Term Effects of Medical Implants* **15**, 629-639 (2005).

264. B. Wang, Q. Lin, C. Shen, J. Tang, Y. Han and H. Chen. *Journal of Colloid and Interface Science* **431**, 1-7 (2014).

265. B.-S. Yu, Z.-K. Yang, Z.-M. Li, L.-W. Zeng, L.-B. Wang and W. W. Lu. *Clinical Spine Surgery* **24**, E49-E56 (2011).

266. J. Jaberi, K. Gambrell, P. Tiwana, C. Madden and R. Finn. *Journal of Oral and Maxillofacial Surgery* **71**, e81-e88 (2013).

267. K. Sawakami, A. Yamazaki, S. Ishikawa, T. Ito, K. Watanabe and N. Endo. *Clinical Spine Surgery* **25**, E28-E35 (2012).

268. G. Lemperle, H. Ott, U. Charrier, J. Hecker and M. Lemperle. *Annals of Plastic Surgery* **26**, 57-63 (1991).

269. N. M. Goodger, J. Wang, G. W. Smagalski and B. Hepworth. *Journal of Oral and Maxillofacial Surgery* **63**, 1048-1051 (2005).

270. X. Punet, R. Mauchauffé, J. C. Rodríguez-Cabello, M. Alonso, E. Engel and M. A. Mateos-Timoneda. *Regenerative Biomaterials*, (2015).

271. P. H. Blit, K. G. Battiston, M. Yang, J. Paul Santerre and K. A. Woodhouse. *Acta Biomaterialia* **8**, 2493-2503 (2012).

CHAPTER 2

BIOCOMPATIBILITY OF TWO MODEL ELASTIN-LIKE RECOMBINAMER-BASED HYDROGELS FORMED THROUGH PHYSICAL OR CHEMICAL CROSSLINKING FOR VARIOUS APPLICATIONS IN TISSUE ENGINEERING AND REGENERATIVE MEDICINE

Arturo Ibáñez-Fonseca,[†] Teresa L. Ramos,[‡§] Israel González de Torre,[†] Luis Ignacio Sánchez-Abarca,[‡§] Sandra Muntión,[‡§] Francisco Javier Arias,[†] María Consuelo del Cañizo,[‡§] Matilde Alonso,[†] Fermín Sánchez-Guijo,[‡§] José Carlos Rodríguez-Cabello[†*]

[†] BIOFORGE Lab, University of Valladolid – CIBER-BBN, Valladolid, Spain

[‡] Instituto de Investigación Biomédica de Salamanca (IBSAL). Hospital Universitario de Salamanca, Salamanca, Spain

[§] Unidad de Terapia Celular. Servicio de Hematología. Hospital Universitario de Salamanca, Salamanca, Spain

A. Ibáñez-Fonseca, T.L. Ramos, I. González de Torre, L.I. Sánchez-Abarca, S. Muntión, F.J. Arias, M.C. del Cañizo, M. Alonso, F. Sánchez-Guijo, J.C. Rodríguez-Cabello. *Journal of Tissue Engineering and Regenerative Medicine* (2017). In press. doi: 10.1002/term.2562

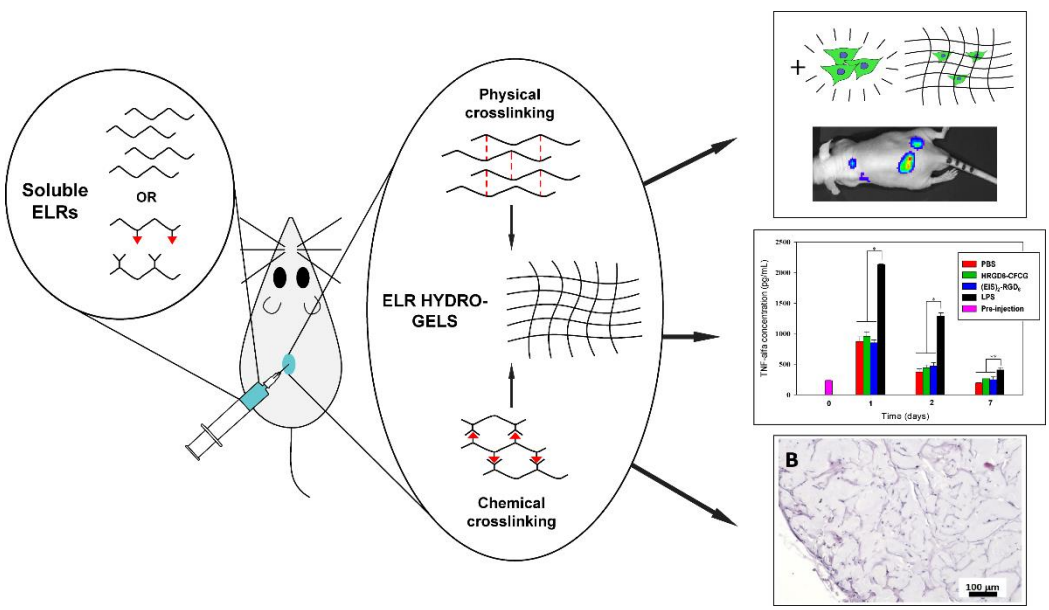

Abstract

Biocompatibility studies, especially innate immunity induction, *in vitro* and *in vivo* cytotoxicity, and fibrosis, are often lacking for many novel biomaterials including recombinant protein-based ones, such as elastin-like recombinamers (ELRs), and has not been extensively explored in the scientific literature, in contrast to traditional biomaterials. Herein we present the results from a set of experiments designed to elucidate the preliminary biocompatibility of two types of ELRs that are able to form extracellular matrix-like hydrogels through either physical or chemical crosslinking, both of which are intended for different applications in tissue engineering and regenerative medicine (TERM). Initially we present *in vitro* cytocompatibility results obtained upon culturing HUVECs on ELR substrates, showing optimal proliferation up to 9 days. Regarding *in vivo* cytocompatibility, luciferase-expressing hMSCs were viable for at least 4 weeks in terms of bioluminescence emission when embedded in ELR hydrogels and injected subcutaneously into immunosuppressed mice. Furthermore, both types of ELR-based hydrogels were injected subcutaneously in immunocompetent mice and serum TNFα, IL-1β, IL-4, IL-6 and IL-10 concentrations were measured by ELISA, confirming the lack of inflammatory response, as also observed upon macroscopic and histological evaluation. All these findings suggest that both types of ELRs possess broad biocompatibility, thus making them very promising for TERM-related applications.

Keywords: biocompatibility; cytocompatibility; elastin-like recombinamers; Catalyst-Free Click Gels; silk-elastin multiblock co-recombinamers; tissue engineering; regenerative medicine

1. INTRODUCTION

There is an increasing interest in developing bioactive materials with applications in tissue engineering and regenerative medicine (TERM). Many of these materials are designed as multi-purpose biomaterials that can be used to promote the regeneration of different tissues or organs and, as such, initially lack a specific target. Despite this, general preliminary biocompatibility studies are often overlooked. Various families of biomaterials have traditionally been employed as matrices in TERM applications, including natural polymers, such as alginate (Lee and Mooney, 2012), chitosan (Croisier and Jérôme, 2013) and silk fibroin (Melke *et al.*, 2016), and synthetic ones, like PEG (Engebretson and Sikavitsas, 2012) and PNIPAAM (Navaei *et al.*, 2016). However, all these materials possess some limitations in terms of biocompatibility, such as the absence of functionalization that may improve their interaction with the host, although some progress has been made as a result of the incorporation of bioactive sequences and polypeptides into natural and synthetic polymers (Wohlrab *et al.*, 2012, Zhu, 2010).

Novel biomaterials with a different nature and origin are currently being designed to overcome these issues (Veiseh *et al.*, 2015). Among them, we can identify recombinant protein-based biomaterials, which promise a significant improvement in the functionality thereof that has already been demonstrated in many cases (Girotti *et al.*, 2015). Although these materials have been evaluated in terms of physicochemical and mechanical properties, and in some cases *in vitro* cytotoxicity, their biocompatibility has

not been extensively studied. Hence, it is important to determine the degree of biocompatibility (in terms of *in vivo* cell survival, inflammation and foreign body response) of these biomaterials by way of wide-ranging preliminary studies as their implementation in the biomedical field depends highly on this feature rather than just on their advanced functionality.

Herein we aim to investigate the cyto- and biocompatibility of two recently developed families of hydrogels based on elastin-like recombinamers (ELRs) (Rodríguez-Cabello *et al.*, 2009), both of which are designed as a multi-purpose approach for different TERM applications, such as bone (Coletta *et al.*, 2017) and osteochondral regeneration (Pescador *et al.*, 2017), or to improve the traceability of ELR-based hydrogels through the recombinant conjugation of fluorescent proteins (Ibáñez-Fonseca *et al.*, 2017), among others. ELRs are genetically engineered protein-based materials whose composition is inspired by the primary sequence found in natural elastin, specifically the VPGXG pentapeptide, where X can be any amino acid except L-proline. Moreover, they show thermosensitivity, as characterized by a reversible phase transition associated with a temperature known as the transition temperature (T_t). In an aqueous medium, the ELR chains remain soluble below their T_t, while above that temperature ELRs self-assemble hydrophobically and adopt a regular, non-random structure stabilized by the presence of type II β-turns (Urry, 1993). The first of these families of hydrogels is based on ELR-catalyst-free click gels (ELR-CFCGs) (Gonzalez de Torre *et al.*, 2014), and the second type is based on a silk-elastin-based injectable multiblock co-recombinamer (SELR) that spontaneously forms stable physical

nanofibrillar hydrogels under physiological conditions as a result of the fusion of short silk-like peptides taken from the sequence of silk fibroin from the silkworm *Bombyx mori* to the ELR gene (Fernandez-Colino *et al.*, 2014). This SELR has been genetically modified in this work to include the Arg-Gly-Asp (RGD) cell-adhesion sequence (Ruoslahti and Pierschbacher, 1986) in order to improve its bioactivity and to more closely mimic the extracellular matrix (ECM) environment; this motif has already been included in the ELR used to form ELR-CFCGs. Both families of ELRs have been physicochemically characterized previously (Fernandez-Colino *et al.*, 2014, Gonzalez de Torre *et al.*, 2014), although herein we present the characterization of the novel RGD-containing SELR. Furthermore, ELR-CFCGs have demonstrated certain properties that point to a potentially good biocompatibility, especially their very low *in vitro* thrombogenicity (Gonzalez de Torre *et al.*, 2015). However, apart from those scarce and *ad hoc* tests, the cyto- and biocompatibility of these two representative families of hydrogels have not been tested *in vitro* or *in vivo* to date.

In this study we present results from *in vitro* cell-proliferation assays and from the *in vivo* viability of luciferase-expressing cells at different time-points by bioluminescence detection (Jang *et al.*, 2010, Kim *et al.*, 2015) when embedded inside either ELR-CFCGs or SELR-based hydrogels that were subsequently injected subcutaneously into mice. Moreover, we performed an *in vivo* inflammatory evaluation that involved measuring the concentration of an array of cytokines (TNFα, IL-1β, IL-4, IL-6 and IL-10), all of which are produced and secreted during inflammation (Turner *et al.*, 2014, Zhang and An, 2007), by

enzyme-linked immunosorbent assay (ELISA). Finally, macroscopic and histological results after long-term (1, 3 and 6 months) subdermal injection of both types of hydrogels in mice are presented. These experiments are intended to demonstrate the preliminary biocompatibility of two types of ELR hydrogels formed through either physical or chemical crosslinking, which is of paramount importance due to their huge potential in cutting-edge fields such as tissue-engineering and regenerative medicine.

2. MATERIALS AND METHODS

2.1. Ethical approval

Experimental procedures involving the use of animals were approved by the Animal Care and Use Committee of the University of Valladolid in accordance with Directive 2010/63/EU of the European Union and Spanish Royal Decree RD 53/2013.

Collection of the hMSCs specified below was approved by the Ethical Committee of the University Hospital of Salamanca and was also in accordance with the Helsinki Declaration of 1975, as revised in 2000. Informed consent was obtained from all subjects included in the study.

2.2. ELR biosynthesis, characterization and modification

The genetic construction of the ELRs used in this work, which were bioproduced and supplied by Technical Proteins Nanobiotechnology, S.L. (TPNBT, S.L., Spain), was performed as described elsewhere (Rodriguez-Cabello *et al.*, 2012). Briefly, they

were biosynthesized in a 15-L bioreactor and purified using several cooling and heating purification cycles (Inverse Temperature Cycling) taking advantage of the ability of these recombinamers to precipitate above their transition temperature. Further centrifugation steps led to a highly pure product, which was dialyzed against ultra-pure water, filtered through 0.22 μm filters (Nalgene) to obtain a sterile solution, and freeze-dried prior to storage. This process allowed the production of different ELRs, namely the previously described HRGD6 (TP71254, TPNBT, S.L., Spain) (Costa *et al.*, 2011), which was subsequently modified for chemical crosslinking, and $(EIS)_2$-RGD6 (TP20736, TPNBT, S.L., Spain), which is also known as a silk-elastin-like recombinamer (SELR). This latter recombinamer is able to establish physical interactions between isoleucine-containing hydrophobic domains that are further stabilized by the inclusion of two silk-like motifs per molecule, thus allowing the formation of hydrogels that remain unalterable over time, as described in a previous study (Fernandez-Colino *et al.*, 2014). Both ELRs contain six RGD cell-adhesion sequences per molecule to permit cell attachment and proliferation. They were found to contain less than two endotoxin units (EU)/mg of ELR, as determined using the limulus amebocyte lysate assay with the Endosafe®-PTS system (Charles River Laboratories).

The characterization techniques used for the novel $(EIS)_2$-RGD6 included sodium dodecyl sulfate polyacrylamide gel electrophoresis (SDS-PAGE) and matrix-assisted laser desorption/ionization time-of-flight (MALDI-TOF) for purity and molecular weight evaluation compared to the theoretical value of 121 012 Da; HPLC to calculate the amino acid composition;

differential scanning calorimetry (DSC) to determine the transition temperature; and nuclear magnetic resonance (NMR) to provide recombinamer fingerprint data.

Chemical modification of the HRGD6 elastin-like recombinamer was achieved by transformation of the ε-amine group in the side chain of the lysine residues to bear cyclooctyne and azide groups, as reported previously (Gonzalez de Torre *et al.*, 2014), thus giving rise to HRGD6-N_3 (TP71254, TPNBT, S.L., Spain) and HRGD6-cyclooctyne (TP70254, TPNBT, S.L., Spain) recombinamers, which were characterized by NMR and FTIR to assess the degree of modification.

2.3. Gel formation

Since chemical crosslinking of the azide- and cyclooctyne-modified recombinamers takes place without the need for a catalyst, such as copper, the hydrogels obtained upon combining the two components are termed catalyst-free click gels (CFCG). The two recombinamers were dissolved separately in an aqueous solution (ultra-pure water, MilliQ, Millipore; PBS or culture medium) at the final concentration and kept at 4 °C for at least 24 hours. ELR-CFCGs were obtained by mixing the solutions at 4 °C. Gels were formed after 15 minutes.

For the SELR, physically crosslinked hydrogels were obtained by dissolving the polymer in an aqueous solution at the desired concentration for 24 h at 4 °C. Gels were then formed by casting the cold solution into the appropriate molds, depending on the expected applications.

2.4. Cell cultures

Commercially available human umbilical vein endothelial cells (HUVEC, ATCC CRL-1730) at passage 2-5 were used. Medium 200 (Gibco) supplemented with the antibiotics gentamicin/amphotericin (1%, Gibco) and low serum growth supplement (LSGS, Gibco) were utilized to maintain cell culture at 37 °C and 5% CO_2, with medium replacement every two days until 80% confluence, at which point the medium was replaced every day. When required, cells were detached using a solution of 0.05% Trypsin-EDTA (Gibco), centrifuged and re-suspended at the desired concentration.

The human mesenchymal stromal cells (hMSCs) used for subcutaneous injection of the cell-ELR mixture were obtained from the bone marrow of healthy donors at the Hospital Universitario de Salamanca (Salamanca, Spain). First, mononucleated cells (MNCs) still not identified as MSCs were isolated through a density gradient using Ficoll (Sigma-Aldrich), seeded in culture flasks at a concentration of 10^6 MNC/cm^2 and cultured at 37 °C, 5% CO_2 until 80-90% confluence was reached, with medium replacement every 3-4 days. At that stage the cells were trypsinized and seeded into new flasks at 5 000 cells/cm^2. After passage 3, the cells were confirmed as hMSCs according to the International Society for Cellular Therapy (ISCT) minimum criteria (Dominici *et al.*, 2006). hMSCs were expanded in DMEM supplemented with 1% penicillin/streptomycin and 10% FBS (Gibco). Further modification of these cells was achieved by lentiviral transduction of the pLV-CMV-Luc2-IRES-GFP, with the modification being confirmed by

flow cytometry. These transduced genes led to the expression of luciferase and GFP, thus allowing the hMSCs to be tracked non-invasively *in vivo*.

2.5. Cell proliferation experiments

HUVEC proliferation when cultured on both ELR-CFCG hydrogels and SELR adsorbed onto the well plate was evaluated at 1, 5 and 9 days after cell seeding. ELR-CFCGs were formed at 75 mg/mL by adding 15 μL of each solution into the well of a 96-well tissue culture plate (TCP, Fisher), while SELR was adsorbed (in order to avoid hydrogel auto-fluorescence that may hinder fluorescence measurements) onto the well surface (0.33 cm^2) of non-adherent 96-well plates (Fisher) by incubation of a 5 mg/mL solution at 4 °C for at least 24 h prior to cell culture. Previously formed hydrogels or adsorbed recombinamers were exposed to UV light for 3 h for surface sterilization, and then washed with minimum cell culture medium for at least 2 h, even for non-coated TCPs. 2 500 HUVECs suspended in 100 μL of complete culture medium (25 000 cells/mL) were seeded on each recombinamer and allowed to grow in the appropriate media. A quantitative Calcein-AM assay (Molecular Probes) was performed at each time point according to the manufacturer's instructions, and fluorescence intensity was measured at 530 nm using a plate reader (SpectraMax M2e, Molecular Devices). This fluorescence intensity, which corresponded to live cells, was then used to calculate cell numbers using calibration curves obtained with different known quantities of cells (from 1 000 to 15 000 cells per well) seeded on black 96-well plates with a clear bottom 24 h before the measurement. Cell-free

ELR substrates were used as blank, except for the case of cells cultured on non-coated TCP. Each condition was performed in triplicate and three experiments were performed for each.

2.6. Determination of hMSC bioluminescence *in vivo*

To assess the potential use of these hydrogels as scaffolds for cell therapy, the transduced hMSCs described above were embedded in HRGD6-N_3 and SELR solutions in penicillin/streptomycin-supplemented DMEM at a final concentration of 10^6 cells/mL. A 100 μL aliquot of each suspension was used for subcutaneous injection in nude Swiss nu/nu mice (Charles River Laboratories). For the ELR-CFCGs, HRGD6-N_3 containing hMSCs and HRGD6-cyclooctyne solutions were mixed in a 1:1 ratio (50 μL of each) immediately prior to injection for optimal homogenization. Solutions of hydrogel-forming ELRs were injected at various concentrations in four different points of the same animal (n = 3). The final concentration values used in the case of ELR-CFCGs were 25, 50, 75 and 100 mg/mL, whereas for SELR gels they were 75, 100, 125 and 150 mg/mL. These concentrations will be referred to as 1, 2, 3 and 4, respectively, for each kind of recombinamer. Cells were tracked through space and over time by luminescence measurements (see below). All procedures were performed under sterile conditions in facilities with positive pressure and laminar flow cabinets. Animals were stored in filtered air racks.

Luciferase-expressing hMSCs were tracked using the Xenogen IVIS 50 bioluminescence system (Xenogen Corporation, Caliper Life Science). Briefly, animals were anesthetized with

isoflurane and then injected intraperitoneally with 15 μg luciferin/g body weight. They were then introduced into the IVIS chamber 10 minutes post-injection, which was found to be the most appropriate moment for obtaining reproducible results. Images were analyzed using the Living Image 2.50.1 software (Xenogen Corporation, Caliper Life Science) by determining the number of photons emitted per second from a selected region of interest (ROI). Bioluminescence was measured at day 1 and then weekly over 4 weeks.

2.7. Subcutaneous implantation and ELISA *in vivo*

Three albino Swiss mice (male) per group were used for the subcutaneous injection of 100 μL of each hydrogel-forming ELR solution. In the case of ELR-CFCGs, 50 μL HRGD6-N_3 and 50 μL HRGD6-cyclooctyne cold solutions (75 mg/mL in PBS) were mixed immediately prior to subdermal implantation. The SELR was dissolved at 150 mg/mL in cold PBS. The solutions used to obtain both kinds of gels were injected using a 20G needle and a 1 mL syringe at one side of the spinal cord. Chemically or physically crosslinked hydrogels were formed instantaneously and could be observed as a small bulge under the skin. These same animals were also employed for blood harvesting to obtain data about the acute inflammatory response that these recombinamers could trigger, using PBS and bacterial lipopolysaccharide (LPS, Sigma-Aldrich) at 3 mg/kg (Lehner *et al.*, 2001) (1 endotoxin unit = 100 pg of LPS), as negative and positive controls, respectively. Hence, four groups were used in this experiment to study the inflammatory response by ELISA.

Five different cytokines, namely TNFα, IL-1β, IL-4, IL-6 and IL-10 (product reference EMTNFA, EM2IL1B, EMIL4, EM2IL6 and EM2IL10, respectively; Thermo Fisher), were quantitatively studied to evaluate the acute inflammatory response towards ELR hydrogels. Approximately 250 μL of blood was collected in Microvette CB 300 K2E treated capillary tubes (Sarstedt) by tail clipping following by centrifugation at 2 000 rcf for 10 minutes at room temperature to finally obtain a cleared serum, which was subsequently ultra-frozen at -80 °C until assay. The process was repeated at days 1, 2 and 7 post-injection.

Sera were thawed in ice and undiluted samples were used. ELISAs were performed in duplicate, as recommended in the guidelines for each anti-mouse cytokine kit. Colorimetric results, measured using a plate reader (SpectraMax M2e, Molecular Devices), were translated into protein concentration values with the help of a standard curve obtained using known quantities of the recombinant cytokines included in each kit. The amounts used for the calibration curve varied for each, but they always ranged between the lowest and highest ELISA sensitivity thresholds.

2.8. Long-term hydrogel stability *in vivo*

For the evaluation of long-term stability, ELR-CFCG and SELR hydrogels were injected as cold solutions at 75 and 150 mg/mL in PBS, respectively, into three albino Swiss mice (male) per group, in a similar manner to the ELRs used in the subcutaneous injection for ELISA experiments. Mice were euthanized by cervical dislocation at 1, 3 and 6 months post-injection, as recommended in standard procedures. The hydrogels

were then extracted to determine their long-term stability. Macroscopic assessment of the hydrogels and of the surrounding tissues was performed, along with microscopic observations after histological processing of the hydrogels.

2.9. Histological processing

Hydrogels were extracted from the mice and immersed in paraformaldehyde at 4% in PBS using 10-fold the gel volume. Samples were stored at 4 °C for at least 24 h and dehydrated by immersion in ethanol solutions of increasing concentration (75%, 95% and 100%) with a final dehydration step in xylene (Sigma-Aldrich). Finally, hydrogels were embedded in paraffin (Sigma-Aldrich) and cut with a microtome (Leica) to obtain sections with a thickness of 10 μm. These were placed in slides and deparaffinized, with subsequent immersion in xylene, ethanol solutions of decreasing concentration (100%, 95%, and 75%) and, finally, in water.

Hematoxylin-eosin staining was performed following a previously described method (Fischer *et al.*, 2008). Briefly, slides were dipped in hematoxylin stain for 30 seconds and rinsed in water for 1 minute. A 1% eosin solution was then used for staining during 30 seconds, with shaking, and samples were dehydrated by immersion in ethanol solutions and xylene. Finally, mounting medium was used to cover the sample on the slide with a microscope coverslip. Images were taken using a bright field microscope (Nikon Eclipse 80i) coupled to a color camera (Nikon Digital Sight DS-Fi1) with different magnifications.

2.10. Statistical analysis

Data are reported as mean ± SD (n = 3). Statistical analysis was performed using a one-way analysis of variance using the Holm–Sidak method. A p-value of less than 0.05 was considered to be statistically significant. $^{*}P < 0.05$, $^{**}P < 0.01$, $^{***}P < 0.001$; $P > 0.05$ indicates no significant differences (n.s.d.).

3. RESULTS AND DISCUSSION

3.1. ELR bioproduction and characterization

Both ELRs were provided by TPNBT after characterization for internal batch control using standardized methods. Nonetheless, full characterization of the RGD-containing SELR (namely, $(EIS)_2$-RGD6) was performed since it was produced for the first time in this study (see Table S2 for the amino acid sequence and molecular weight). The experimental molecular weight was found to be similar to the estimated value (120.4 vs. 121.0 kDa), as confirmed by SDS-PAGE and MALDI-TOF (Figure S1, Supporting Information). Furthermore, the T_t was found to be 16.8 °C in PBS (Figure S2, Supporting Information), which is 2.4 °C higher than the T_t reported for $(EIS)_2$, i.e. the non-RGD-containing SELR, in the same solvent (Fernandez-Colino *et al.*, 2014). This result is consistent with those reported in other studies, which predict an increase in the T_t when hydrophilic (poly)peptides are fused to the ELR sequence (Christensen *et al.*, 2013), which is the case of the RGD motif comprising several polar amino acids. In addition, ^{1}H

NMR data and amino acid analysis showed good agreement with the expected values (Figure S3 and Table S1, Table S3, respectively).

3.2. HUVEC proliferation on ELR substrates

In order to shed light on the proliferation of cells on SELR and ELR-CFCG substrates, HUVECs were seeded on previously ELR-coated TCPs. Non-coated TCPs were used as control. This cell line is widely used to test the cytocompatibility and suitability of vascular devices. In this case, we chose HUVECs due to the previously described use of ELR-CFCGs in cardiovascular applications, for example the development of heart valves in combination with fibrin (Weber *et al.*, 2015).

Given the presence of RGD-containing domains along the ELR molecules, a specific interaction between this 12-mer peptide, which includes the RGD tripeptide, and cell membrane integrins was expected, thus conferring a favorable environment for cell spreading and proliferation. For this purpose, TCPs were covered with the hydrogel-forming ELRs as described above (see Materials and Methods) to form hydrogels (ELR-CFCGs) or to adsorb ELR molecules on the well surface of non-adherent well plates (SELRs) prior to cell seeding.

Cells were found to be adhered to the modified plates for ELR-CFCGs, similarly to the TCP control, thus meaning that they promote cell adhesion. Moreover, a rapid proliferation was observed for this condition (Figure 1), with a high cell number at day 4, similar to the one observed at day 9. On the other hand, a lower cell number was observed at day 1 on SELR substrates, showing significant differences with ELR-CFCGs and non-coated

TCPs ($P < 0.001$), while cells were not found attached to surfaces coated with a SELR that does not contain RGD sequences at day 1 ($P < 0.001$, Figure S4, Supporting Information). Consequently, cell number at day 4 was also significantly lower for SELRs, compared to the other two substrates ($P < 0.001$), although cell number was similar to the expected value (approximately 2400 cells), taking into account the number of cell divisions between day 1 and day 4 (2 cell divisions at the most). However, there were not significant differences between all the conditions at day 9, indicating that HUVECs were able to proliferate to confluence on both ELR-CFCGs and SELR-coated non-adherent TCPs.

Differences in cell adhesion at day 1 can be explained by the variation in RGD density on ELR-coated well plates (Chollet *et al.*, 2009, Patel *et al.*, 2007). In the case of the ELR used for the formation of ELR-CFCGs, namely HRGD6, its molecular weight is 66 kDa and possesses six RGD sequences per molecule, while SELR maintains the same number of RGD domains, but the molecular weight is 121 kDa. This means that a SELR-coated surface will expose less RGD motifs in the same area than an ELR-CFCG-coated one, since a lower number of molecules will be present covering the surface. Similarly, the proliferation rate might be also affected by this difference in RGD density, explaining the faster cell growth observed in the case of ELR-CFCGs (Larsen *et al.*, 2006, Lin *et al.*, 2001). Nevertheless, according to the data showed in this work, the amount of RGD domains in SELR substrates is enough to support an initial minimum cell attachment and a subsequent cell growth *in vitro*.

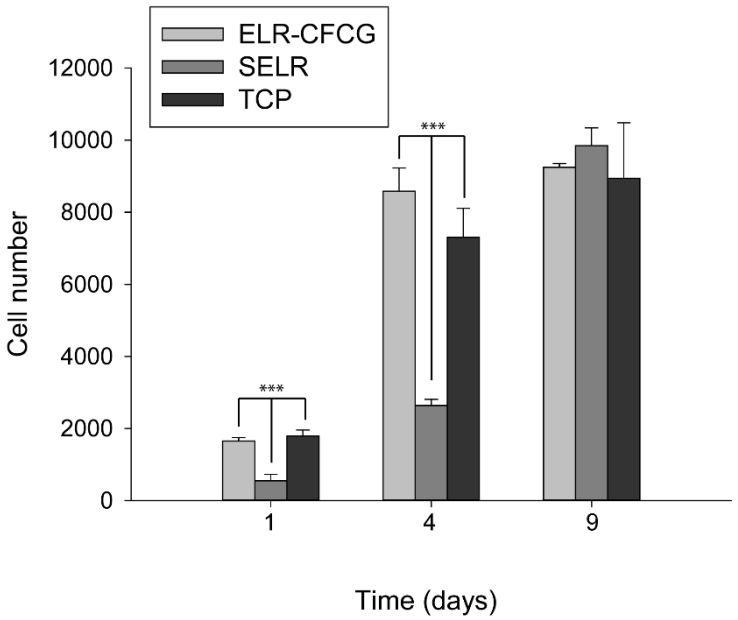

Figure 1. HUVEC total number at different time points after seeding on substrates based on ELR-CFCGs (pale grey) and SELRs (dark grey). Non-coated TCPs were used as controls (dark bars). ***$P < 0.001$ (n = 3).

3.3. *In vivo* cell tracking and viability of hMSCs in ELR-based hydrogels

To obtain information about the viability of cells embedded in both types of ELR hydrogels at different concentrations after *in vivo* implantation, we used luciferase-expressing hMSCs, a multipotent cell type widely used in regenerative medicine that often shows poor retention and viability if injected without a scaffold (Martens *et al.*, 2009, Roche *et al.*, 2014). Our aim was to assess the viability of hMSCs inside the ELR hydrogels *in vivo*, thereby simulating the therapeutic conditions. Cells were initially mixed with solutions of each type of ELR at low temperatures (below the T_t). The resulting ELR-cell suspensions were then injected subcutaneously in mice and hydrogels were formed

instantaneously, as reported previously *in vitro* (Fernandez-Colino *et al.*, 2014, Gonzalez de Torre *et al.*, 2014), and confirmed by the observation of a protuberance under the skin of the animals, which was not seen when PBS alone was injected. This is also in good agreement with previous *in vitro* studies regarding the gelation kinetics of SELRs (Fernandez-Colino *et al.*, 2014) and ELR-CFCGs (Gonzalez de Torre *et al.*, 2014). In the first case, a rapid gelation process was observed by rheological measurements upon increasing the temperature above the T_t, whereas for chemically cross-linked hydrogels, these were formed in a few seconds upon mixing ELR-azide and ELR-cyclooctine solutions, as observed macroscopically.

With regard to the SELRs, bioluminescence signals were observed for hMSCs embedded in hydrogels at SELR concentrations of 100 and 125 mg/mL for three weeks (label 2 and 3 in Figure 2C, respectively), whereas they could be observed up to the fourth week for a concentration of 100 mg/mL (label 2, Figure 2D). For the ELR-CFCGs implanted with cells, bioluminescence was detected for all concentrations tested up to the end of the experiment at week 4 (images E, F, G and H in Figure 2).

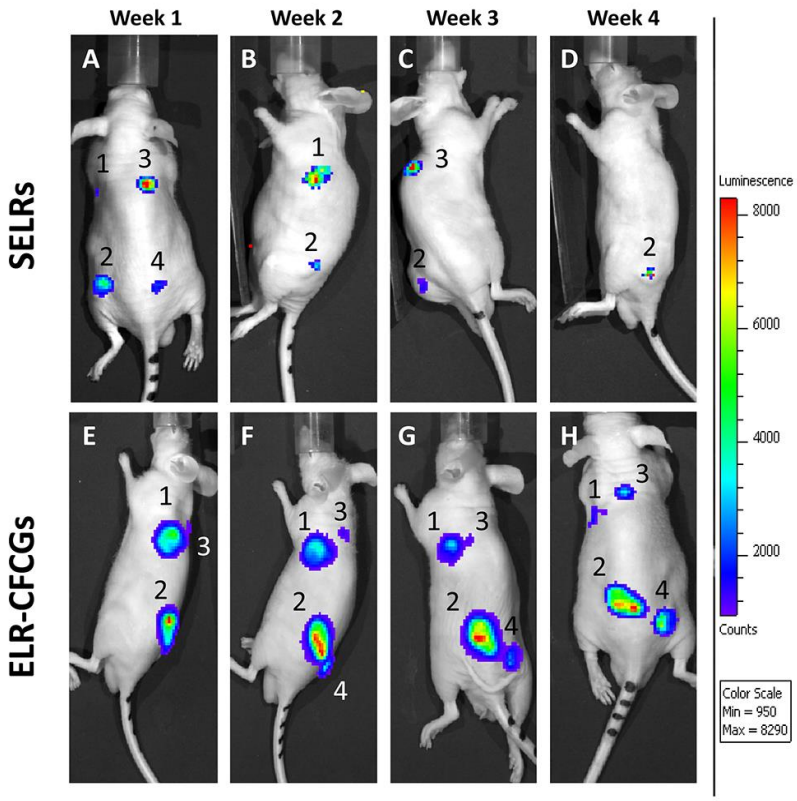

Figure 2. *In vivo* images of hMSCs embedded in the two ELR-based hydrogels at different times post-implantation by means of light emission after luciferin injection. Top and bottom pictures correspond to SELR and ELR-CFCG hydrogels, respectively. Bioluminescence is measured as photon counts and represented as a "Hot/Cold" colormap.

The differences between the two groups may be due to the easier migration of cells from SELR-based hydrogels, which are physically crosslinked, thus meaning that the network is stabilized mainly by hydrophobic interactions and H-bonds, whereas ELR-CFCGs form covalent bonds that may hinder cell migration, thus meaning that hMSCs remain in this type of hydrogel for longer.

Luciferin-mediated bioluminescence was observed in cells embedded in at least one of the hydrogel concentrations used at

every time, thus indicating that hMSCs express luciferase and that cells remaining inside the scaffolds were alive for up to 4 weeks, since the luminescence signal coincides with the protuberances observed under the skin, which correspond to ELR hydrogels. This result strongly highlights the ability of physically or chemically crosslinked ELR-based hydrogels to sustain cells embedded in them when injected *in vivo*, hence providing an excellent approach for the development of ECM-like scaffolds for cell delivery in different applications in regenerative medicine.

3.4. Evaluation of the inflammatory response mediated by ELR hydrogels *in vivo*

With the aim of elucidating whether ELR hydrogels induced an innate immune response, namely an inflammatory reaction, or not, we injected ELR solutions (below the T_t) subcutaneously into mice to form hydrogels instantaneously. Blood samples were then collected at different timepoints and sera were obtained after centrifugation. These sera were used to measure the concentration of different cytokines, namely the pro-inflammatory TNFα, IL-1β and IL-6, and the anti-inflammatory IL-4 and IL-10, all of which are expressed during inflammation, as discussed above (see Introduction).

The cytokine analyses are presented in Figure 3. The results of these studies showed that LPS triggered an innate immune response in terms of acute inflammation, as expected. On the other hand, lower concentrations of each cytokine were found for both types of ELR-based hydrogels (ELR-CFCG and SELR) than those for the positive control (LPS) ($P < 0.05$), with some exceptions. For

instance, the concentration of IL-6 for the LPS group at day 2 did not differ significantly from that for the SELR group, with this also being observed at day 7 for LPS with every other group, including the negative control (PBS). Moreover, the cytokine concentrations for the SELR and ELR-CFCG groups were similar to that for the PBS group in every case (n.s.d.), apart from the IL-6 levels for SELR-based hydrogels at day 1.

The cytokine concentrations for the ELR-CFCG and SELR groups were therefore similar to those observed for the negative control (PBS), thus allowing us to conclude that the injection of ELR-based hydrogels does not trigger an acute inflammatory response. These results support the findings observed in previous studies (Rincón *et al.*, 2006, Urry *et al.*, 1998), although they assessed biocompatibility mainly on the basis of histological findings. Furthermore, we were able to confirm the absence of active bacterial LPS residues (widely known as endotoxins) in any of the ELRs, which addresses one of the main fears regarding the use of recombinant proteins produced in *E. coli*.

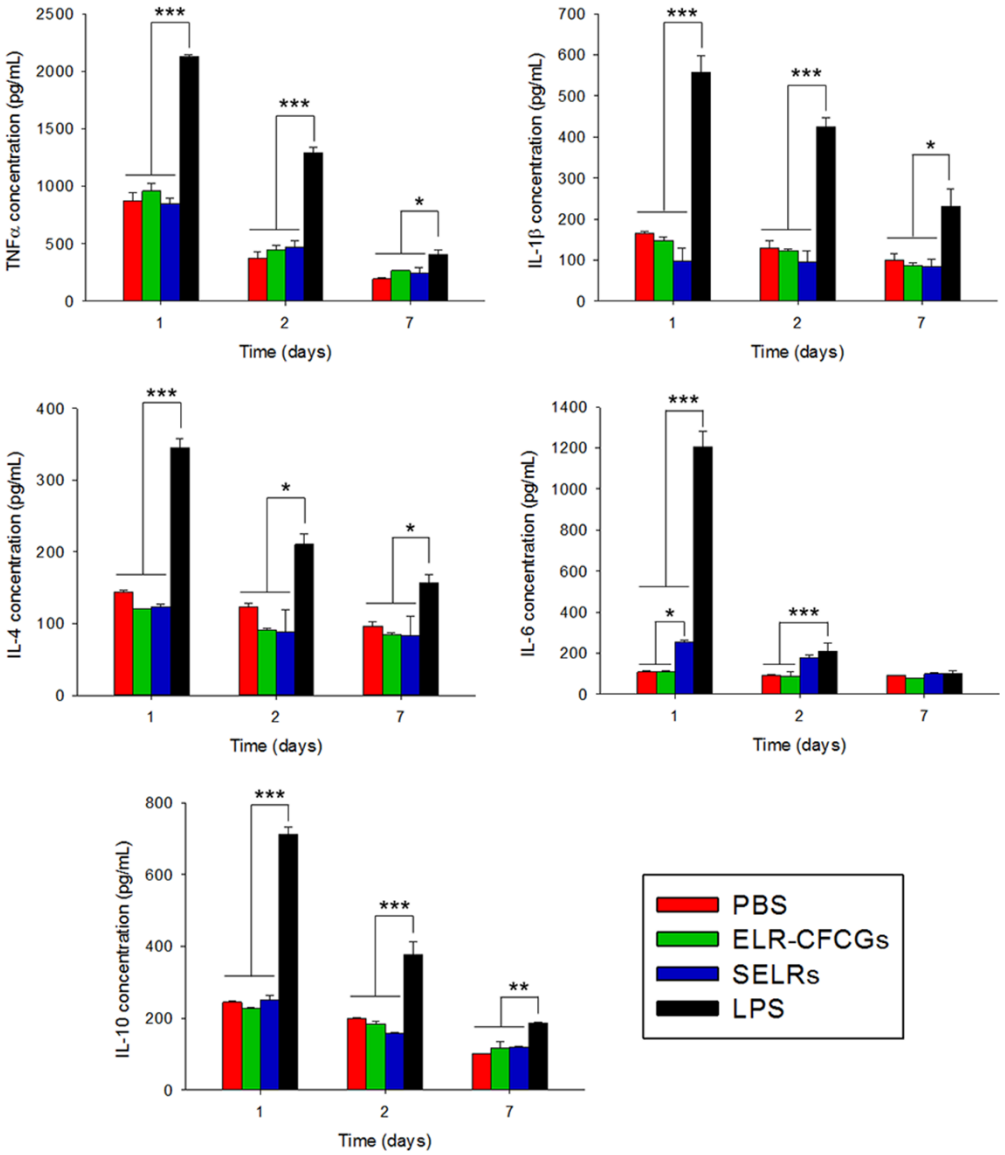

Figure 3. Cytokine concentrations determined using sera obtained after blood collection in mice at different times post-injection of both ELRs [ELR-CFCGs (green) and SELRs (blue)] compared to the negative (PBS, red) and positive (LPS, black) controls (*$P < 0.05$, **$P < 0.01$, ***$P < 0.001$, n = 3).

3.5. Macroscopic evaluation of the long-term stability of ELR-based hydrogels *in vivo*

Long-term stability after injection of the ELRs was evaluated by extracting the subcutaneous implants at different timepoints (1, 3 and 6 months). Both gels (ELR-CFCGs and SELRs) were easily found attached to the hypodermis in the three mice used in each group at every timepoint (Figure 4). This result highlights that both types of ELR hydrogels are very stable when implanted subdermally *in vivo*, even when the hydrogel network is only stabilised via non-covalent interactions, which is the case of the SELR. This is in good agreement with previous findings for this type of recombinamer *in vitro* (Fernandez-Colino *et al.*, 2014) and suggests that additional biodegradation domains should be included in the amino acid sequence of the ELRs if a temporary implant is needed. However, the good stability over time observed here is relevant for both tissue-engineering applications and for the development of drug-delivery systems since the formation of a stable system could be crucial for achieving the long-lasting effects required in many of these applications.

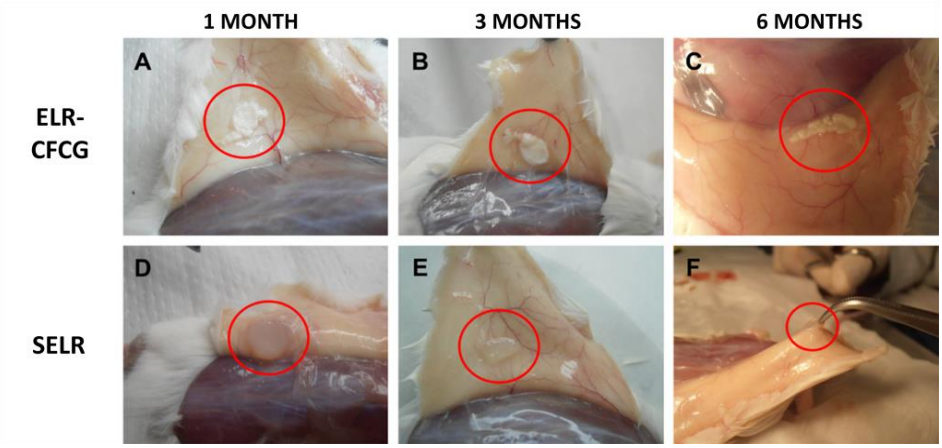

Figure 4. Hydrogels attached to mice hypodermis at 30 (A, D), 90 (B, E) and 180 days (C, F) post-injection for the two hydrogel-forming ELRs [ELR-CFCG (A, B and C) and SELR (D, E and F)].

Furthermore, no encapsulation of ELR hydrogels by fibrotic tissue, or signs of inflammation, redness or swelling of the tissues surrounding the hydrogels, was observed macroscopically, although some vascularization close to the implant area could be detected. The edges of the hydrogels were well defined and no macroscopic debris was found at any time point.

With regard to the morphology of the hydrogels, clear differences were seen in the color and general appearance of the two types of hydrogels. Thus, whereas ELR-CFCGs are white and have a "granular" appearance, the SELRs are more transparent and homogeneous. The explanation for these differences resides in the different composition of the backbone of the ELRs and in the different crosslinking methods used to obtain the hydrogels. For instance, the modified ELR molecules used to form ELR-CFCGs undergo a phase transition above the T_t, therefore resulting in the shrinking of the hydrogels and an increase in opacity. On the other hand, SELR molecules possess a block structure, with hydrophilic

blocks (containing glutamic acid as guest residue) and hydrophobic ones (containing isoleucine), having different T_t (Urry *et al.*, 1992). Hence, the hydrophilic blocks retain water molecules, even above the T_t, which is mainly influenced by the hydrophobic blocks. This results in an increasing of the transparency of the hydrogels. In any case, their appearance did not change over time while implanted, as can be seen in Figure 4.

3.6. Histological evaluation of ELR-based hydrogels injected subcutaneously

Histological analysis was performed on both SELR hydrogels and ELR-CFCGs extracted at six months post-implantation, with hematoxylin-eosin staining used to add information to the macroscopic evaluation of the behavior of ELR-based hydrogels when implanted *in vivo*. This study revealed no presence of macrophages or giant cells that could indicate a chronic inflammatory process (Figure 5). Furthermore, a thin layer of connective tissue was observed surrounding the ELR-based gels, which might be considered a very mild reaction where cells are interacting with the hydrogels in a biocompatible manner, thus indicating a lack of encapsulation or a fibrotic response. Moreover, these connective tissue layers were irrigated by blood vessels in both types of hydrogels (Figure 5D and Figure 5H, black arrows).

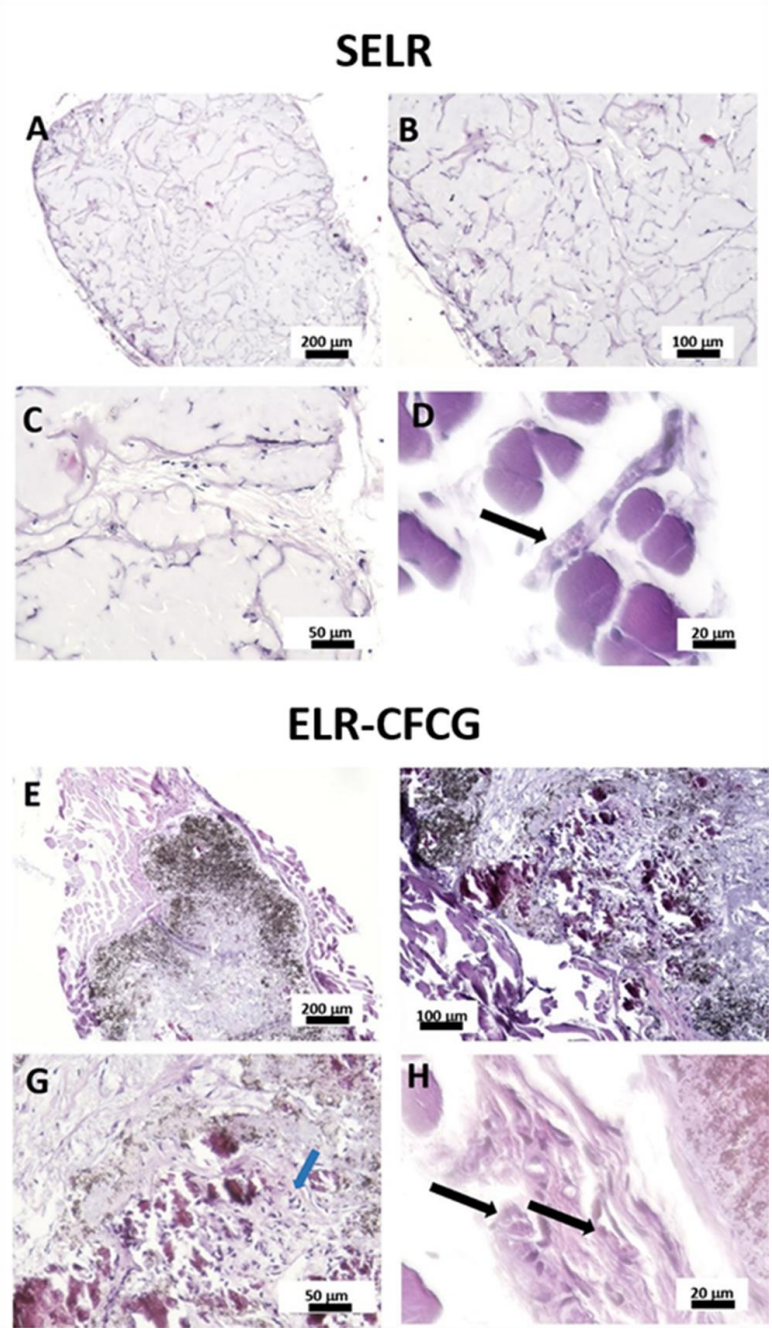

Figure 5. Hematoxylin-eosin staining of sections of both SELR-based hydrogels (A-D) and ELR-CFCGs (E-H) extracted from mice at 6 months post-subcutaneous injection observed by bright field microscopy with different magnifications. Black arrows denote blood vessels.

The infiltration of cells inside the scaffold was also observed in the case of the SELR hydrogels, whereas this was not so obvious for ELR-CFCGs due to the differences in staining, probably because of the composition (lysine (ELR-CFCG) instead of glutamic acid (SELR) residues) and the granular structure, which results in a darker staining of the hydrogel in some areas. Nevertheless, many cells were found at the edges of the chemically crosslinked hydrogels, i.e. ELR-CFCGs, and, to a lesser extent, in their inner structure, as shown in Figure 5 (blue arrow). This cell colonization is probably enhanced by the presence of the RGD amino acid sequence, which allows cell attachment (as confirmed by HUVEC proliferation experiments) and thus provides an ECM-mimetic scaffold that can be invaded by endogenous cells. Moreover, due to their high stability over time and their optimal biocompatibility, both types of ELR-based hydrogels have been shown to be suitable for long-term testing to investigate possible chronic inflammation reactions or cytotoxic effects induced by drugs or other agents via the incorporation thereof into the scaffolds.

It should be noted that the different concentrations of the ELR solution used to form both types of hydrogels have a crucial effect on the final structure of the gels. This difference can be explained by the diverse mechanism of gelification: more and larger ELR molecules (thus a higher concentration) are needed to establish a physically crosslinked stable network, as is the case of SELR hydrogels, while a lower concentration is sufficient for chemically crosslinked ELR-CFCGs if sufficient anchoring points are present within the ELR molecules. As such, SELRs with a concentration of 150 mg/mL produced a denser and more

continuous structure than ELR-CFCGs with a concentration of only 75 mg/mL, which showed a granular structure, as can be seen from the histological pictures (Figure 5), thus confirming the previously observed macroscopic findings (Figure 4).

4. CONCLUSIONS

We have presented the results obtained upon combining different methods with the aim of assessing the preliminary wide-ranging biocompatibility of two recently developed types of ELR-based hydrogels formed via either chemical (ELR-CFCGs) or physical (SELR hydrogels) crosslinking. HUVEC proliferation on ELR substrates evaluated over 9 days was found to be optimal, i.e. similar to that for the non-coated TCP control. Cell viability inside ELR-CFCGs and SELR hydrogels was also confirmed since bioluminescence could be detected from luciferase-expressing hMSCs for up to 4 weeks. Furthermore, we found an absence of an early acute immune response, namely inflammation, as confirmed by the values obtained for the concentration of relevant cytokines (TNFα, IL-1β, IL-4, IL-6 and IL-10) in mice blood samples after subcutaneous injection of ELR-based hydrogels, which were similar to the concentrations obtained for the negative control (PBS). This was further corroborated by the macroscopic and histological evaluation of ELR-based hydrogels and their surroundings after long-term subcutaneous injection, which revealed an excellent stability up to 6 months, and a very low immune response in terms of foreign body response. Specifically, histological analysis revealed the growth of a thin layer of newly formed connective tissue around the hydrogels, even showing the presence of small blood vessels.

Moreover, an invasion of the hydrogels by host cells was observed, with this being most clearly seen in the case of SELR hydrogels.

In summary, this work confirms the preliminary biocompatibility of two types of multi-purpose ELR-based hydrogels and is thus the first step towards the use of both types of ELRs in different applications in the field of tissue engineering and regenerative medicine.

Conflict of interest

The authors declare no competing financial interest.

Acknowledgments

The authors are grateful for funding from the European Commission (NMP-2014-646075, HEALTH-F4-2011-278557, PITN-GA-2012-317306 and MSCA-ITN-2014-642687), MINECO of the Spanish Government (MAT2016-78903-R, MAT2016-79435-R, MAT2015-68901-R, MAT2013-42473-R, MAT2013-41723-R and MAT2012-38043), Centro en Red de Medicina Regenerativa y Terapia Celular de Castilla y León, and Junta de Castilla y León (VA244U13 and VA313U14). Teresa L. Ramos is supported by a fellowship from the Portuguese Fundação para a Ciência e Tecnologia (SFRH/BD/86451/2012). Sandra Muntión is supported by grant RD12/0019/0017 from the Instituto de Salud Carlos III.

References

Coletta DJ, Ibáñez-Fonseca A, Missana LR, *et al.* 2017, Bone regeneration mediated by a bioactive and biodegradable ECM-like hydrogel based on elastin-like recombinamers, *Tissue Engineering Part A*.

Costa RR, Custódio CA, Arias FJ, *et al.* 2011, Layer-by-Layer Assembly of Chitosan and Recombinant Biopolymers into Biomimetic Coatings with Multiple Stimuli-Responsive Properties, *Small*, **7**: 2640-2649.

Croisier F, Jérôme C. 2013, Chitosan-based biomaterials for tissue engineering, *European Polymer Journal*, **49**: 780-792.

Chen YM, Ogawa R, Kakugo A, *et al.* 2009, Dynamic cell behavior on synthetic hydrogels with different charge densities, *Soft Matter*, **5**: 1804-1811.

Chollet C, Chanseau C, Remy M, *et al.* 2009, The effect of RGD density on osteoblast and endothelial cell behavior on RGD-grafted polyethylene terephthalate surfaces, *Biomaterials*, **30**: 711-720.

Christensen T, Hassouneh W, Trabbic-Carlson K, *et al.* 2013, Predicting Transition Temperatures of Elastin-Like Polypeptide Fusion Proteins, *Biomacromolecules*, **14**: 1514-1519.

Dominici M, Le Blanc K, Mueller I, *et al.* 2006, Minimal criteria for defining multipotent mesenchymal stromal cells. The International Society for Cellular Therapy position statement, *Cytotherapy*, **8**: 315-317.

Engebretson B, Sikavitsas VI. 2012, Long-Term In Vivo Effect of Peg Bone Tissue Engineering Scaffolds, **22**: 211-218.

Fernandez-Colino A, Arias FJ, Alonso M, *et al.* 2014, Self-organized ECM-mimetic model based on an amphiphilic multiblock silk-elastin-like corecombinamer with a concomitant dual physical gelation process, *Biomacromolecules*, **15**: 3781-3793.

Fischer AH, Jacobson KA, Rose J, *et al.* 2008, Hematoxylin and eosin staining of tissue and cell sections, *CSH protocols*, **2008**: pdb prot4986.

Girotti A, Orbanic D, Ibáñez-Fonseca A, *et al.* 2015, Recombinant Technology in the Development of Materials and Systems for Soft-Tissue Repair, *Adv Healthc Mater*, **4**: 2423-2455.

Gonzalez de Torre I, Santos M, Quintanilla L, *et al.* 2014, Elastin-like recombinamer catalyst-free click gels: characterization of poroelastic and intrinsic viscoelastic properties, *Acta Biomater*, **10**: 2495-2505.

Gonzalez de Torre I, Wolf F, Santos M*, et al.* 2015, Elastin-like recombinamer-covered stents: Towards a fully biocompatible and non-thrombogenic device for cardiovascular diseases, *Acta Biomater*, **12**: 146-155.

Ibáñez-Fonseca A, Alonso M, Arias FJ*, et al.* 2017, Förster Resonance Energy Transfer-Paired Hydrogel Forming Silk-Elastin-Like Recombinamers by Recombinant Conjugation of Fluorescent Proteins, *Bioconjugate Chemistry*, **28**: 828-835.

Jang K-S, Lee K-S, Yang S-H*, et al.* 2010, In vivo Tracking of Transplanted Bone Marrow-Derived Mesenchymal Stem Cells in a Murine Model of Stroke by Bioluminescence Imaging, *J Korean Neurosurg Soc*, **48**: 391-398.

Kim JE, Kalimuthu S, Ahn B-C. 2015, In Vivo Cell Tracking with Bioluminescence Imaging, *Nucl Med Mol Imaging*, **49**: 3-10.

Larsen CC, Kligman F, Kottke-Marchant K*, et al.* 2006, The effect of RGD fluorosurfactant polymer modification of ePTFE on endothelial cell adhesion, growth, and function, *Biomaterials*, **27**: 4846-4855.

Lee KY, Mooney DJ. 2012, Alginate: Properties and biomedical applications, *Progress in Polymer Science*, **37**: 106-126.

Lehner MD, Ittner J, Bundschuh DS*, et al.* 2001, Improved Innate Immunity of Endotoxin-Tolerant Mice Increases Resistance to Salmonella enterica Serovar Typhimurium Infection despite Attenuated Cytokine Response, *Infect Immun*, **69**: 463-471.

Lin Y-S, Wang S-S, Chung T-W*, et al.* 2001, Growth of Endothelial Cells on Different Concentrations of Gly-Arg-Gly-Asp Photochemically Grafted in Polyethylene Glycol Modified Polyurethane, *Artificial Organs*, **25**: 617-621.

Liu D, Wang T, Liu X*, et al.* 2014, Cell proliferation and cell sheet detachment from the positively and negatively charged nanocomposite hydrogels, *Biopolymers*, **101**: 58-65.

Martens TP, Godier AFG, Parks JJ*, et al.* 2009, Percutaneous Cell Delivery Into the Heart Using Hydrogels Polymerizing In Situ, *Cell Transplant*, **18**: 297-304.

Melke J, Midha S, Ghosh S, *et al.* 2016, Silk fibroin as biomaterial for bone tissue engineering, *Acta Biomater*, **31**: 1-16.

Navaei A, Truong D, Heffernan J, *et al.* 2016, PNIPAAm-based biohybrid injectable hydrogel for cardiac tissue engineering, *Acta Biomater*, **32**: 10-23.

Patel S, Tsang J, Harbers GM, *et al.* 2007, Regulation of endothelial cell function by GRGDSP peptide grafted on interpenetrating polymers, *Journal of Biomedical Materials Research Part A*, **83A**: 423-433.

Pescador D, Ibáñez-Fonseca A, Sánchez-Guijo F, *et al.* 2017, Regeneration of hyaline cartilage promoted by xenogeneic mesenchymal stromal cells embedded within elastin-like recombinamer-based bioactive hydrogels, *Journal of Materials Science: Materials in Medicine*, **28**: 115.

Rincón AC, Molina-Martinez IT, de las Heras B, *et al.* 2006, Biocompatibility of elastin-like polymer poly(VPAVG) microparticles: in vitro and in vivo studies, *J Biomed Mater Res A*, **78A**: 343-351.

Roche ET, Hastings CL, Lewin SA, *et al.* 2014, Comparison of biomaterial delivery vehicles for improving acute retention of stem cells in the infarcted heart, *Biomaterials*, **35**: 6850-6858.

Rodriguez-Cabello JC, Girotti A, Ribeiro A, *et al.* 2012, Synthesis of genetically engineered protein polymers (recombinamers) as an example of advanced self-assembled smart materials, *Methods Mol Biol*, **811**: 17-38.

Rodríguez-Cabello JC, Martín L, Alonso M, *et al.* 2009, "Recombinamers" as advanced materials for the post-oil age, *Polymer (Guildf)*, **50**: 5159-5169.

Ruoslahti E, Pierschbacher MD. 1986, Arg-Gly-Asp: A versatile cell recognition signal, *Cell*, **44**: 517-518.

Turner MD, Nedjai B, Hurst T, *et al.* 2014, Cytokines and chemokines: At the crossroads of cell signalling and inflammatory disease, *Biochim Biophys Acta*, **1843**: 2563-2582.

Urry DW. 1993, Molecular Machines - How Motion and Other Functions of Living Organisms Can Result from Reversible Chemical-Changes, *Angew Chem Int Ed Engl*, **32**: 819-841.

Urry DW, Gowda DC, Parker TM, *et al.* 1992, Hydrophobicity scale for proteins based on inverse temperature transitions, *Biopolymers*, **32**: 1243-1250.

Urry DW, Pattanaik A, Xu J, *et al.* 1998, Elastic protein-based polymers in soft tissue augmentation and generation, *J Biomater Sci Polym Ed*, **9**: 1015-1048.

Veiseh O, Doloff JC, Ma M, *et al.* 2015, Size- and shape-dependent foreign body immune response to materials implanted in rodents and non-human primates, *Nat Mater*, **14**: 643-651.

Weber M, Gonzalez de Torre I, Moreira R, *et al.* 2015, Multiple-Step Injection Molding for Fibrin-Based Tissue-Engineered Heart Valves, *Tissue Eng Part C Methods*, **21**: 832-840.

Wohlrab S, Müller S, Schmidt A, *et al.* 2012, Cell adhesion and proliferation on RGD-modified recombinant spider silk proteins, *Biomaterials*, **33**: 6650-6659.

Zhang J-M, An J. 2007, Cytokines, Inflammation and Pain, *Int Anesthesiol Clin*, **45**: 27-37.

Zhu J. 2010, Bioactive modification of poly(ethylene glycol) hydrogels for tissue engineering, *Biomaterials*, **31**: 4639-4656.

Supporting information

Additional supporting information may be found in the online version of this article at the publisher's website.

Supporting figures and tables: different figures and tables are shown regarding the full characterization of the SELR used in this work, namely SDS-PAGE analysis, MALDI-TOF spectrum, DSC spectra, ^{1}H NMR spectra and table summarizing results, amino acid composition, comparison of cell adhesion and proliferation on SELRs with and without RGD cell adhesion sequences.

5. SUPPORTING INFORMATION

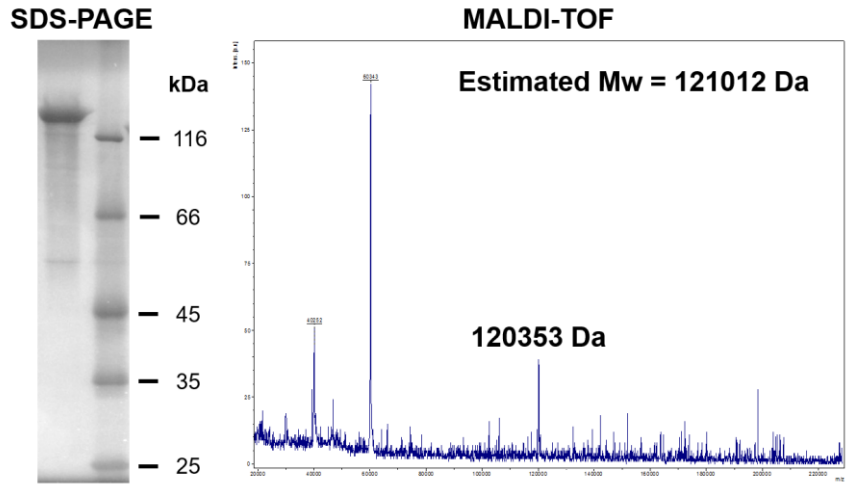

Figure S1. Molecular weight and purity assessment by SDS-PAGE and MALDI-TOF mass spectrometry for $(EIS)_2$-RGD6 (also termed SELR). MALDI-TOF spectra represent non-quantitative intensity (a.u.) against m/z (mass divided by net charge of the molecule) of the ELR.

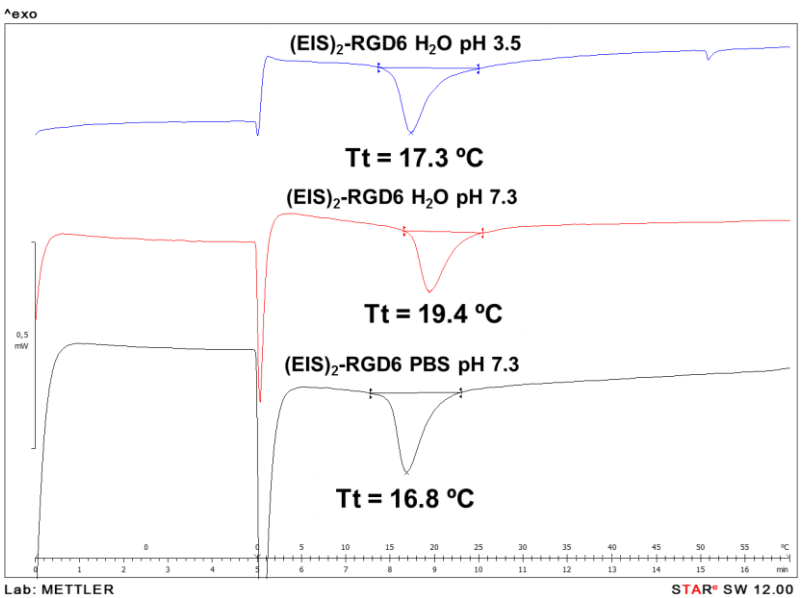

Figure S2. DSC graphs of $(EIS)_2$-RGD6 (SELR) showing the experimental T_t in different solvents (water and PBS) and at different pH values.

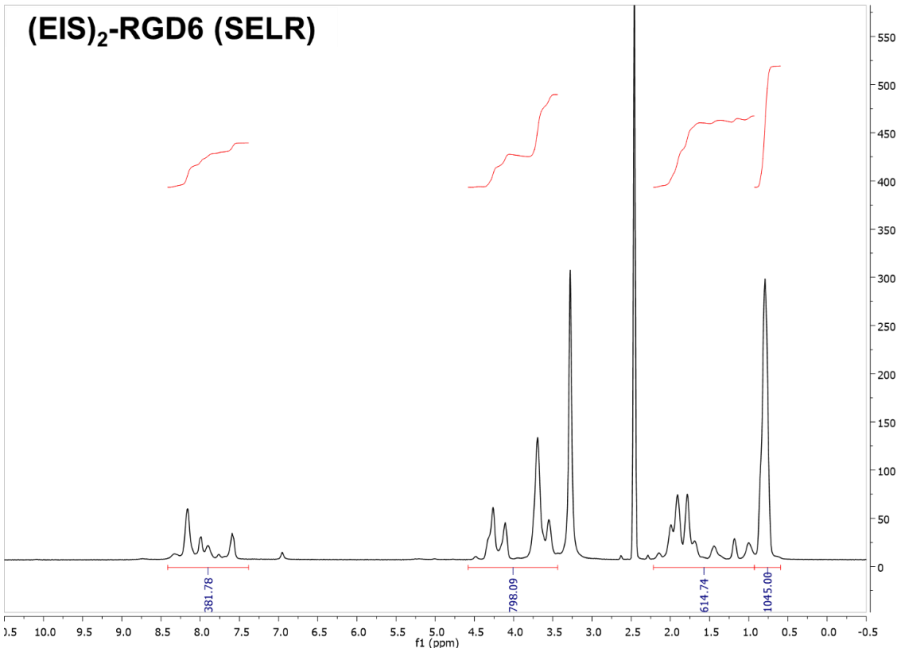

Figure S3. ^{1}H-NMR spectrum of $(EIS)_2$-RGD6 (SELR) showing the integration of the peaks corresponding to the different types of hydrogens.

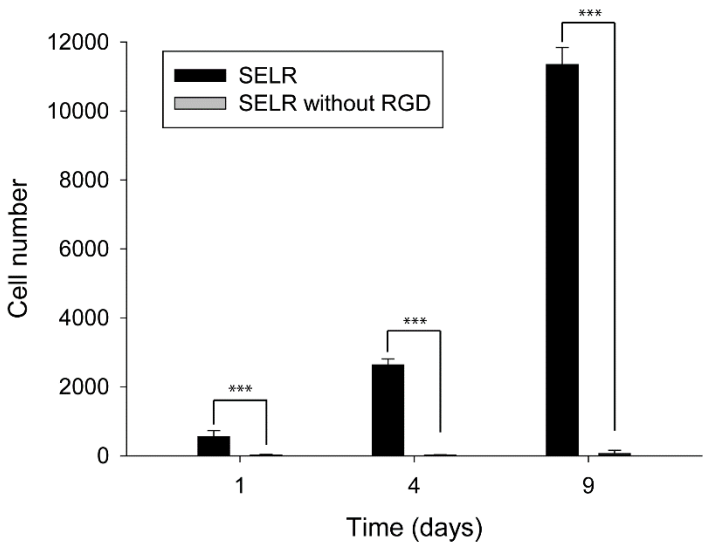

Figure S4. Comparison of HUVEC proliferation seeded on non-adherent plates coated either with SELR (black) or SELR without RGD (grey) at 1, 4 and 9 days.

Table S1. Comparison between the predicted value of each type of hydrogen in $(EIS)_2$-RGD6 (SELR) and the experimental values found by integration of each peak in the corresponding ^{1}H-NMR spectrum.

Type of hydrogen	Predicted value	Measured value
-C<u>H</u>$_3$	1045	Reference
-C<u>H</u>- and -C<u>H</u>$_2$-	1531	1403.83
-N<u>H</u>$_2$	408	381.78

Table S2. Abbreviated amino acid sequence and molecular weight of the SELR used in this work.

ELR	Abbreviated amino acid sequence	Molecular weight (Da)
$(EIS)_2$-RGD6	MESLLP-{[$(VPGVG)_2$-VPGEG-$(VPGVG)_2$]$_{10}$-$(VGIPG)_{60}$-[V$(GAGAGSG)_5$]$_2$G}-[$(VPGIG)_5$-AVTGRGDSPASS]$_6$-V	121 012
HRGD6 (used for the formation of ELR-CFCGs	MGSSHHHHHHSSGLVPRGSHMESLLP-{[$(VPGIG)_2$-(VPGKG)-$(VPGIG)_2$]$_2$-AVTGRGDSPASS-[$(VPGIG)_2$-(VPGKG)-$(VPGIG)_2$]$_2$}$_6$V	60 660

Table S3. Comparison between the predicted number of each amino acid in $(EIS)_2$-RGD6 (SELR) and the experimental values.

Amino acid	Predicted	Experimental
ASP+ASN	6+0	5.40
GLU+GLN	21	25.92

SER	39	30.63
HIS	-	-
GLY	574	575.99
THR	6	5.50
ARG	6	4.91
ALA	52	50.47
TYR	-	-
CYS	-	-
VAL	341	339.33
MET	1	1.08
TRP	-	-
PHE	-	-
ILE	150	154.44
LEU	2	2.36
LYS	-	-
PRO	257	257.24

CHAPTER 3

BONE REGENERATION MEDIATED BY A BIOACTIVE AND BIODEGRADABLE ECM-LIKE HYDROGEL BASED ON ELASTIN-LIKE RECOMBINAMERS

Dante J. Coletta, MD,[1#] Arturo Ibáñez-Fonseca, MSc,[2#] Liliana R. Missana, PhD,[3,4#] María V. Jammal, PhD,[3,4] Ezequiel J. Vitelli, MD,[1] Mariangeles Aimone, BSc,[1] Facundo Zabalza, BSc,[1] João P. Mardegan Issa, PhD,[5] Matilde Alonso, PhD,[2] José Carlos Rodríguez-Cabello, PhD,[2] and Sara Feldman, PhD[1]

[1] LABOATEM. Osteoarticular Biology, National Rosario University, Rosario, Argentina.

[2] BIOFORGE Lab, University of Valladolid, CIBER-BBN, Valladolid, Spain.

[3] Experimental Pathology & Tissue Engineering Laboratory, Dental School, National Tucumán University, Tucumán, Argentina.

[4] Tissues Laboratory, Proimi-Biotechnology-Conicet, Tucumán, Argentina.

[5] Ribeirão Preto School of Dentistry, University of São Paulo, São Paulo, Brazil.

D.J. Coletta, A. Ibáñez-Fonseca, L.R. Missana, M.V. Jammal, E.J. Vitelli, M. Aimone, F. Zabalza, J.P. Mardegan Issa, M. Alonso, J.C. Rodríguez-Cabello, S. Feldman. *Tissue Engineering Part A* (2017). In press. doi: 10.1089/ten.tea.2017.0047

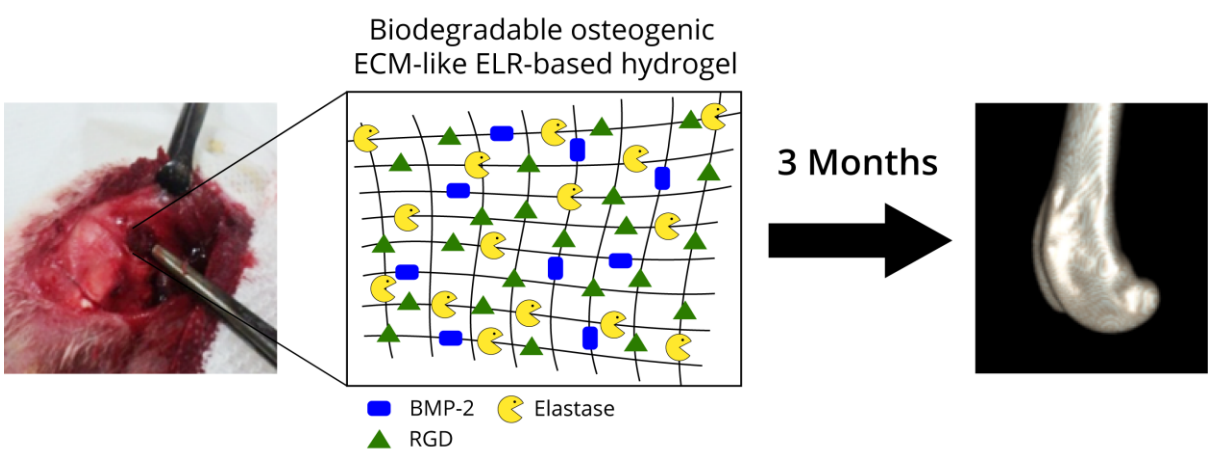

Abstract

The morbidity of bone fractures and defects is steadily increasing due to changes in the age pyramid. As such, novel biomaterials that are able to promote the healing and regeneration of injured bones are needed in order to overcome the limitations of auto-, allo-, and xenografts, while providing a ready-to-use product that may help to minimize surgical invasiveness and duration. In this regard, recombinant biomaterials, such as elastin-like recombinamers (ELRs), are very promising as their design can be tailored by genetic engineering, thus allowing scalable production and batch-to-batch consistency, amongst others. Furthermore, they can self-assemble into physically cross-linked hydrogels above a certain transition temperature, in this case body temperature, but are injectable below this temperature, thereby markedly reducing surgical invasiveness. Herein we have developed two bioactive hydrogel-forming ELRs, one including the osteogenic and osteoinductive BMP-2 and the other the RGD cell-adhesion motif. The combination of these two novel ELRs results in a BMP-2-loaded extracellular matrix-like hydrogel. Moreover, elastase-sensitive domains were included in both ELR molecules, thereby conferring biodegradation as a result of enzymatic cleavage and avoiding the need for scaffold removal after bone regeneration. Both ELRs and their combination showed excellent cytocompatibility, and the culture of cells on RGD-containing ELRs resulted in optimal cell adhesion. In addition, hydrogels based on a mixture of both ELRs were implanted in a pilot study involving a femoral bone injury model in New Zealand White rabbits, showing complete

regeneration in six out of seven cases, with the other showing partial closure of the defect. Moreover, bone neo-formation was confirmed using different techniques, such as radiography, computed tomography and histology. This hydrogel system therefore displays significant potential in the regeneration of bone defects, promoting self-regeneration by the surrounding tissue with no involvement of stem cells or osteogenic factors other than BMP-2, which is released in a controlled manner by elastase-mediated cleavage from the ELR backbone.

Keywords: bone regeneration, elastin-like recombinamers, bioactive hydrogels, BMP-2.

1. INTRODUCTION

It is well known that dental, maxillofacial, and other orthopedic surgeries often require the use of different biomaterials for the treatment of injuries and other diseases through tissue engineering, including osteoporosis (1-6). In addition, changes of the age pyramid towards an older population have led to an increasing number of bone fractures (7-11). Despite the availability of numerous biomaterials for tissue regeneration, autologous bone is usually the first option for the replacement of injured bone tissue. However, a large number of different types of biomaterials and bone grafts have been employed to date for the healing of bone defects (12). These biomaterials should be: a) osteoinductive, hence promoting stem cell differentiation to osteoblasts, b) osteoconductive, thereby inducing growth of the surrounding healthy bone, and c) osseointegrative, merging with the nearby bone (13-15). They should also stimulate an optimal cell response and be liable to be replaced by *de novo* formed tissue, acting as a provisional substitute (1, 16, 17).

Engineered biomaterials, in combination with growth factors, have been shown to be an effective approach in bone tissue engineering since they can act both as a scaffold and as a drug-delivery system to promote bone repair and regeneration (18, 19). For instance, the osteoinductive bone morphogenetic protein-2 (BMP-2) (20, 21) has been shown to enhance the formation of bone tissue in situations that lead to bone degradation, such as alcohol dependence (22) and osteometabolic diseases (23). Due to the high cost and rapid release of BMP-2 when placed at the site of injury, it

is often associated with carrier matrices that act as drug-delivery systems to increase its half-life and to avoid the adverse effects associated to high doses of BMP-2 (24-27).

On the other hand, protein-based recombinant biomaterials, such as resilin-, silk-, collagen- and elastin-like polypeptides, have been developed over the last few decades with the aim of improving the features of traditional biomaterials in terms of ease of design and synthesis, biocompatibility and bioactivity (28). As an example, elastin-like recombinamers (ELRs), thus named due to their polymeric and recombinant nature (29), have been shown to be a potential tool for the development of biomedical devices for regenerative medicine due to their thermosensitivity. This smart behavior is a result of their composition, which is based on repetitions of the Val-Pro-Gly-X-Gly (VPGXG) pentapeptide, in which X (guest residue) is any amino acid except L-proline. Moreover, it is characterized by a transition temperature (T_t) which itself depends on the polarity of the side chain in the guest residue. Thus, in an aqueous medium, the ELR chains remain soluble below their T_t while above that T_t (e.g. physiologic temperature) the ELR self-assembles hydrophobically, undergoing a phase transition (30). In this study, two different ELRs have been developed, based on a previously described hydrogel-forming ELR (31). Taking advantage of the recombinant nature of these biomolecules, one of the novel ELRs designed in this work has been genetically engineered to include Arg-Gly-Asp (RGD) motifs to enhance cell adhesion via cell-membrane integrins (32), whereas the other ELR was designed to include BMP-2. Both ELRs also contain elastase-sensitive domains resulting from repetition of the VGVAPG

hexapeptide (33) to improve the enzymatic biodegradability of the biomaterial.

In order to study the potential of these novel ELRs in bone regeneration, we have used a previously developed model of femoral bone injury (FBI) in New Zealand White rabbits. This involves the creation of a defect 6 mm in diameter in a femoral condyle 8 mm in diameter (34, 35). This animal model allows the study of the defect by computed tomography (CT) and by radiological studies given the size of the bone.

The aim of this work was to evaluate whether novel bioactive ELRs are cytocompatible and degradable, while being able to form extracellular matrix (ECM)-like hydrogels and promoting bone regeneration after implantation into an FBI in rabbits, as a preliminary step for their use in humans. For this purpose, the cytocompatibility and biodegradation ability were assessed *in vitro*, and a highly reproducible model was subsequently used to carry out a pilot *in vivo* study.

2. MATERIALS AND METHODS

2.1. Ethical approval

Experimental procedures regarding the use of animals were approved by the Bioethics Committee of Rosario National University (Resolution No. 150/2015). Its regulations include well-established guidelines for animal care and manipulation to decrease pain and suffering of the animal, according to the 3Rs (replacement, reduction and refinement), and are in accordance with international laws concerning the use of animals.

2.2. ELR biosynthesis and characterization

The genetic construction of the ELRs used in this work was performed as described elsewhere (36). Briefly, their DNA sequences were obtained by genetic engineering techniques and cloned into a pET-25b(+) vector for expression in *Escherichia coli*. ELRs were biosynthesized in a 15-L bioreactor and purified by several cooling and heating purification cycles (Inverse Transition Cycling) taking advantage of the ability of these recombinamers to precipitate above their transition temperature. Further centrifugation steps led to a pure product, which was dialyzed against ultra-pure water, filtered through 0.22 μm filters (Nalgene, Thermo Fisher, USA) to obtain a sterile solution, and freeze-dried prior to storage. The ELRs were found to contain less than two endotoxin units (EU)/mg of ELR, as determined using the limulus amebocyte lysate assay with the Endosafe®-PTS system (Charles River Laboratories). This process allowed the production of two different ELRs, both of which were derived from a previously synthesized block co-recombinamer (31). Further information can be obtained in Supplementary Methods (Supplementary Information).

The characterization techniques used included sodium dodecyl sulfate polyacrylamide gel electrophoresis (SDS-PAGE) and matrix-assisted laser desorption/ionization time-of-flight (MALDI-TOF) spectrometry for purity and molecular weight (*Mw*) evaluation compared to the theoretical values of 113,556 Da for ELR-E-RGD and 107,752 Da for ELR-E-BMP-2; differential scanning calorimetry (DSC) to determine the transition

temperature; HPLC to determine the amino acid composition of both ELRs (Table S1 and Table S2, Supplementary Information), and nuclear magnetic resonance (NMR) to provide recombinamer fingerprint data (Figure S3 and Figure S4; Table S3 and Table S4, Supplementary Information). The procedure for the measurement of the mechanical properties of ELR-based hydrogels is described in Supplementary Methods (Supplementary Information).

2.3. Elastase-mediated cleavage of the ELR in solution

Different quantities (1.2, 1.8 and 2.4 U) of porcine pancreas elastase (4 mg/mL, 6.8 U/mg) (Sigma-Aldrich, USA) were added to solutions of the mixture of both ELRs (98% (w/w) ELR-E-RGD and 2% (w/w) ELR-E-BMP-2) at a final concentration of 1 mg/mL dissolved in ultra-pure water in order to evaluate the biodegradation rate for each quantity of enzyme. The quantity of elastase used was 2000-, 3000- and 4000-times the amount needed to cleave the mixture of ELRs used as substrate in 30 minutes, since preliminary experiments showed that larger quantities than those calculated are required to observe an actual effect of the enzyme *in vitro*. Samples were incubated at 37 ºC and collected at various time points (10, 20, 30, 45, 60, 90 and 120 minutes), then stored frozen at –20 ºC until further use. A negative control, namely an ELR molecule lacking elastase-sensitive sequences but with the same elastin-like structure as the two ELRs designed for this work (31), was also treated with 1.2 U of elastase for further comparisons. Methods concerning the evaluation of the biodegradation are

explained in Supplementary Methods (Supplementary Information).

2.4. *In vitro* cell culture

Bone marrow derived human mesenchymal stem cells (hMSCs) were extracted and isolated as described elsewhere (37) and were generously provided as a gift by Citospin S.L. (Spain). They were cultured for expansion in DMEM low glucose (1 g/L) (Gibco, USA) supplemented with 10% fetal bovine serum (FBS) (Gibco, USA) and 1% Penicillin/Streptomycin (P/S) (Gibco, USA).

All cells were used at passage 3-5 in subsequent experiments. They were detached from the wells using a Trypsin-EDTA solution (0.25%, Gibco, USA) and counted using a hematocytometer.

2.5. Cell viability

Human MSCs were used to determine the *in vitro* viability using the Calcein AM assay (Molecular Probes, USA) when cultured in DMEM supplemented with 10 mg/mL of the different ELRs or the mixture of them (98% (w/w) ELR-E-RGD and 2% (w/w) ELR-E-BMP-2) for 3 days. This assay was performed in a black, 96-well plate with clear-bottom (Greiner Bio One, USA) according to the manufacturer's instructions and the fluorescence intensity measured at 530 nm using a plate reader (SpectraMax M2e, Molecular Devices, USA). The intensity measured at this wavelength, corresponding to live cells, was then used to calculate cell numbers by using calibration curves obtained with different known quantities of cells (from 1000 to 10,000 cells per well) seeded

on 96-well plates 24 h before the measurement. Each condition was performed in triplicate, with four experiments for each (n = 4).

2.6. Cell adhesion on ELR-coated tissue culture plates

96-well plates were used for the coating of different wells with both ELRs separately and combined (98% (w/w) ELR-E-RGD and 2% (w/w) ELR-E-BMP-2). Briefly, a 5 mg/mL solution of the recombinamers in ultra-pure water was placed in the well and allowed to adsorb to the surface for 24 h at 4 ºC. The wells were washed twice with 1x PBS (Gibco) and blocked with 1% BSA for 2 h at 37 ºC, then rinsed again and, finally, 3000 cells per well were seeded onto the modified surfaces to study cell adhesion after 24 hours. The number of cells in each well was determined using the Calcein AM assay as described above.

2.7. Dissolution of the ELRs for the *in vivo* experiments

A mixture of both ELRs (98% (w/w) ELR-E-RGD and 2% (w/w) ELR-E-BMP-2) was prepared and dissolved in sterile tubes (one per animal) at 300 mg/mL with 1x sterile phosphate buffered saline (PBS) (Gibco, USA) by incubation at 4 ºC for 24 h. A 2% (w/w) ELR-E-BMP-2 solution at 300 mg/mL gives a similar amount of BMP-2 in our device ($5.57 \cdot 10^{-5}$ M) as in INFUSE® Bone Graft ($5.77 \cdot 10^{-5}$ M, Medtronic, USA) (38). This solution was kept in an ice bath during surgery until implantation.

2.8. *In vivo* experiments

Adult female New Zealand white rabbits (n = 7) with an average weight of 3.5 kg were used for the creation and treatment of bone defects. These animals were kept in individual cages with food (ACA Cooperativas, Argentina) and water *ad libitum*.

Antibiotic prophylaxis, anesthetic treatment and surgical techniques were performed according to a previously described procedure (34, 35). Further details regarding the surgical procedure can be found in Supplementary Methods (Supplementary Information). Three months post-surgery, the animals were euthanized using three doses of anaesthesia, as previously described (34, 39). The femora were then collected to perform different experiments to assess bone regeneration (see below).

2.9. Multi-slice computed tomography (MSCT)

Multi-slice computed tomography was performed on the seven right femurs of the rabbits using a Toshiba Alexion apparatus with 16 detectors and a thickness of 0.5 mm. Coronal, sagittal and axial slices were obtained and the images were processed using Alexion Advance Edition software with the Adaptive Iterative Dose Reduction (AIDR 3D) algorithm, thus obtaining the 3D reconstruction for every sample. All images were analyzed together for an optimal comparison.

2.10. Bone histopathology

Femoral bone samples were evaluated by way of radiographic studies using a conventional dental X-ray machine

with dental occlusal films (Eastman Kodak, USA) to determine the implant position to guide the histological procedures. The femoral epiphysis was cut 4 cm below the metaphysis using a carborundum-disk cutter (Dochem, China) attached to a dental drill under irrigation with distilled water. The implanted area was marked with Indian ink. Two samples were selected for decalcification using modified Morse solution (Okayama University Dental School) and embedded in paraffin following well-established protocols. The samples were serial cut (7 μm thick) using a manual rotary microtome (Micron-Zeiss, Germany), and stained with Hematoxylin & Eosin (H&E). All specimens were examined by light microscopy and evaluated by a single pathologist. Subsequently, another pathologist (certified by the Argentinean Ministry of Health No. 31455) performed an independent review to verify microscopic observations. The reported results reflect the mutually-agreed-upon diagnoses by both pathologists. Photomicrographs were taken from slides of each specimen using a Sony digital camera fitted to an Olympus CH30 microscope with an Olympus stereo zoom SZ51.

2.11. Statistical analysis

Data for the *in vitro* experiments are reported as mean ± SD (n = 4). Statistical analysis of data following a normal distribution was performed using a one-way analysis of variance and the Holm–Sidak method. A p-value of less than 0.05 was considered to be statistically significant, while $p > 0.05$ indicates no significant differences (n.s.d.). (*) $p < 0.05$, (**) $p < 0.01$.

3. RESULTS

3.1. ELR biosynthesis and characterization

Both ELRs were obtained as a lyophilized product in a yield of approximately 200 mg/L (ELR/culture volume). Their molecular weights and purities were confirmed as satisfactory by SDS-PAGE and MALDI-TOF (Figure 1), while the T_t calculated by DSC for the ELRs dissolved in PBS (pH 7.4) was found to be 15.8 ºC and 15.3 ºC for ELR-E-RGD and ELR-E-BMP-2, respectively (Figure S2, Supplementary Information).

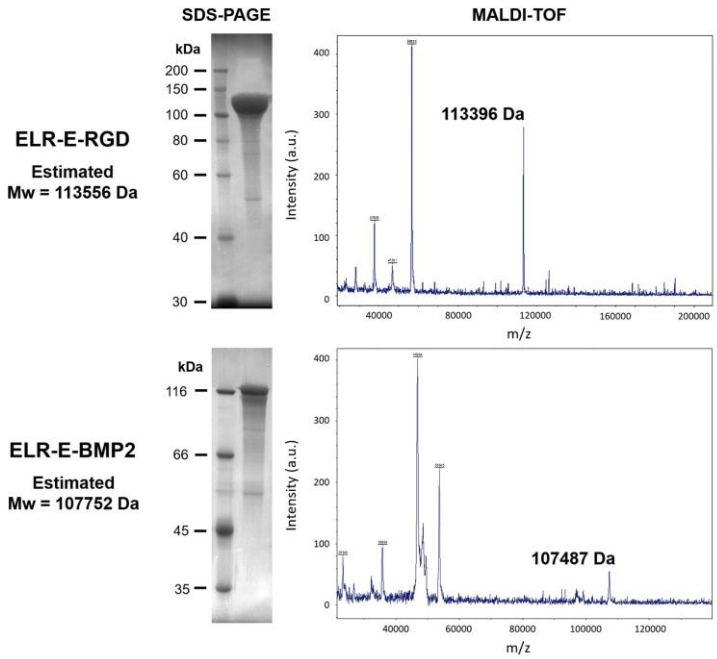

Figure 1. Molecular weight and purity assessment by SDS-PAGE and MALDI-TOF mass spectrometry for ELR-E-RGD and ELR-E-BMP2. MALDI-TOF spectra represent non-quantitative intensity (a.u.) against m/z (mass divided by net charge of the molecule) of the ELRs.

As regards the mechanical characterization, the storage modulus (G') of the ELR-based hydrogel at a concentration of 300 mg/mL (98% ELR-E-RGD and 2% ELR-E-BMP-2) was found to be approximately 1600 Pa at 37ºC (Figure S5, Supplementary Information). In addition, hydrogels were formed above the T_t, as observed macroscopically (Figure S6, Supplementary Information).

3.2. Enzymatic cleavage of ELR molecules by elastase digestion

Due to the incorporation of elastase-sensitive domains in the ELR molecules designed for this work, we aimed to verify whether elastase was able to cleave these ELRs. Hence, a mixture of them (98% ELR-E-RGD and 2% ELR-E-BMP-2) was dissolved at 1 mg/mL, and ELRs were found to be cleaved *in vitro* in solution when different quantities of elastase were added. As observed in Figure 2, and as expected, the ELRs are sensitive to the quantity of elastase, therefore biodegradation was slower when only 1.2 U of elastase was added to the ELR solution (Figure 2a), whereas an increase in the biodegradation rate was observed if 1.8 U (Figure 2b) or 2.4 U (Figure 2c) of elastase were supplemented. In contrast, no elastase-mediated cleavage was observed in the negative control (non-elastase sensitive ELR, named $(EI)_2$ in Tabla 2 and in Table S6) at any sample collection time (Figure 2d).

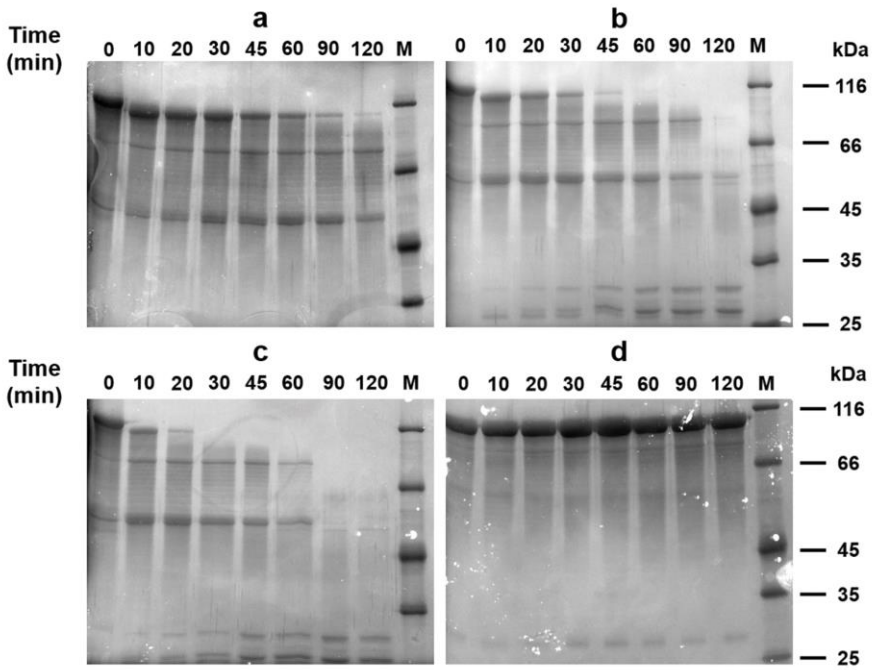

Figure 2. SDS-PAGE images showing the biodegradation of the mixture of ELR-E-RGD (98%) and ELR-E-BMP-2 (2%) in solution at 1 mg/mL mediated by a) 1.2 U, b) 1.8 U and c) 2.4 U of elastase, at different sample collection times, as indicated above each picture (0, 10, 20, 30, 45, 60, 90 and 120 minutes after addition of the specific quantity of elastase). Picture d) shows the lack of elastase-mediated biodegradation in the case of the non-sensitive ELR (named $(EI)_2$ in **Tabla 2** of "Resumen" and in **Table S6**). M represents the protein molecular weight marker.

The disappearance of the larger bands at 113.6 and 107.8 kDa was further studied by image analysis, and the results are summarized in **Figure 3**. This figure clearly reinforces the statement made above regarding the biodegradation rate, namely that biodegradation is faster as more elastase is added to the solution.

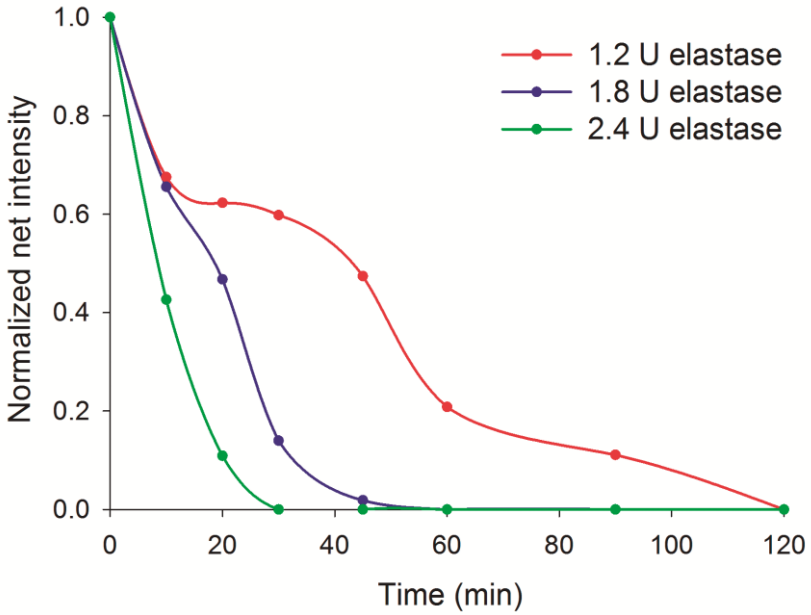

Figure 3. Graph showing the elastase-mediated cleavage rate of the highest molecular weight band with data obtained from analysis of the SDS-PAGE gels from Figure 2. The net intensity of this double band at 113.6 and 107.8 kDa is represented at different sampling times.

As regards the nascent bands observed by SDS-PAGE (Figure 2), we expected to obtain bands in three different molecular weight ranges, namely 65.5-66.5, 46.7-48.2, and 12-12.9 kDa, as by-products of ELR-E-RGD/BMP-2 digestion since there are two different elastase-sensitive domains at different points in the ELR-E-BMP-2 molecule. However, the molecular weight of the higher bands was found to be 80.8 and 54.2 kDa, respectively, while the band at 12-12.9 kDa could not be observed due to the limitations of SDS-PAGE in terms of resolution. Nevertheless, these results correlate well with previous studies that reported a 20% increase in the apparent molecular weight for different ELRs (40, 41). As such, we estimated the *Mw* plus 20% and the values showed good

agreement with those found empirically, with the experimental values for the nascent bands being 80.8 and 54.2 kDa, while the expected values of *Mw* + 20% were 78.6-79.8 and 56.0-57.8 kDa, respectively (Table S5, Supplementary Information).

3.3. hMSCs viability and integrin-mediated cell adhesion

The viability of the cells after culture for 3 days in media supplemented with the ELRs was found to be similar to that for the negative control, i.e. medium without supplementation, as can be observed in Figure 4. Since no significant differences were observed, we can conclude that the ELRs alone, or the mixture thereof, do not affect cell viability.

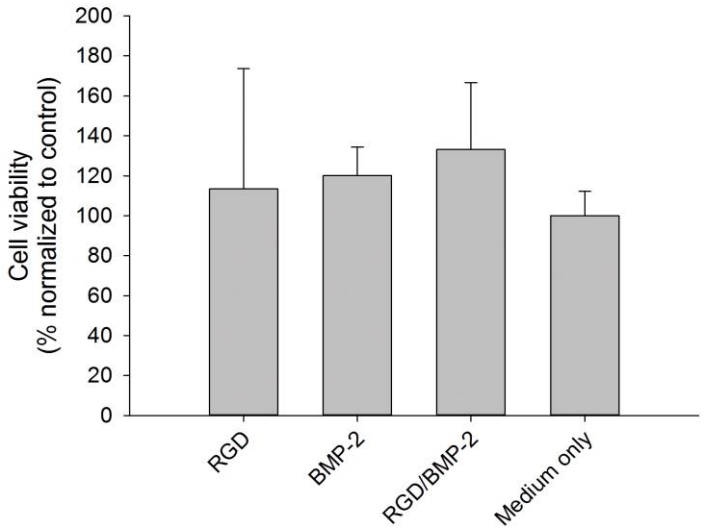

Figure 4. Graph showing hMSCs viability results after 3 days of culture in terms of cell number as measured using the Calcein AM assay for different ELR supplements in medium at 10 mg/mL: ELR-E-RGD (represented as RGD), ELR-E-BMP-2 (BMP-2), the mixture of both (98%

(w/w) ELR-E-RGD and 2% (w/w) ELR-E-BMP-2, RGD/BMP-2) and supplement-free medium (medium only). No significant differences ($p > 0.05$) were found in any case.

Furthermore, the evaluation of cell adhesion in ELR-coated tissue culture plates (TCP) showed good results in the case of ELR-E-RGD and the mixture of both. This finding was in agreement with our expectations since the mixture contains 98% ELR-E-RGD. However, coating only with ELR-E-BMP-2 led to statistically significantly lower levels of attachment due to the lack of cell-adhesion domains in the recombinamer (Figure 5).

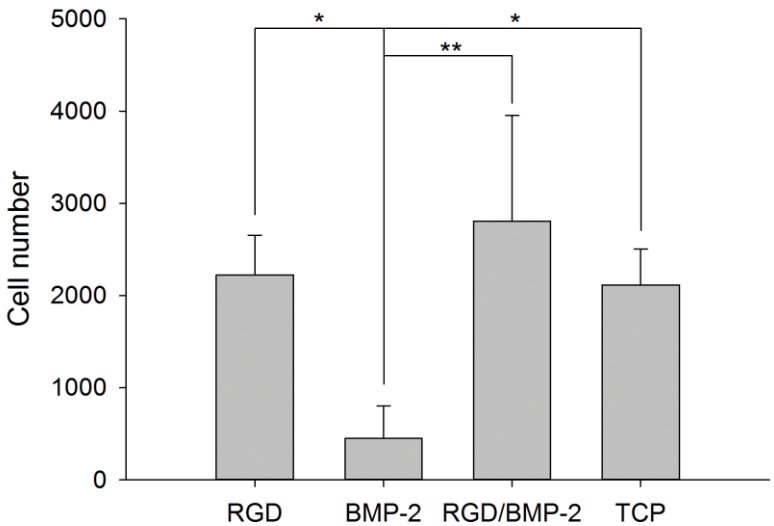

Figure 5. Graph showing the number of hMSCs attached to the ELR-coated well-plates as measured using the Calcein AM assay for different ELR coatings absorbed at 5 mg/mL: ELR-E-RGD (represented as RGD), ELR-E-BMP-2 (BMP-2), the mixture of both (98% (w/w) ELR-E-RGD and 2% (w/w) ELR-E-BMP-2, RGD/BMP-2) and non-coated tissue culture plates (TCP) ($n = 4$). (*) $p < 0.05$, (**) $p < 0.01$.

3.4. Biochemical and clinical results

The welfare of the animals in the first two days post-implantation was slightly affected, with disrupted walking, as expected. After seven days, treated animals behaved similarly to their non-operated control counterparts. The temperature values, food intake and all the biochemical parameters measured were similar between animals from control groups at every time point studied (n.s.d., $p > 0.05$).

3.5. MSCT studies

MSCT studies showed bone healing in the defect area. A closer examination of the distal metaepiphysis region, in the medial cortical plane, showed total closure of the defect in most of the coronal and sagittal slices for all of the samples analyzed. However, it was possible to identify the persistence of a small defect with a diameter of 1 mm in the medial cortical plane of the lesion site in one of the femora extracted, although only in one coronal slice and two axial ones (Figure 6a and Figure 6b, white arrow). These results were confirmed by radiological studies (Figure S7, Supplementary Information).

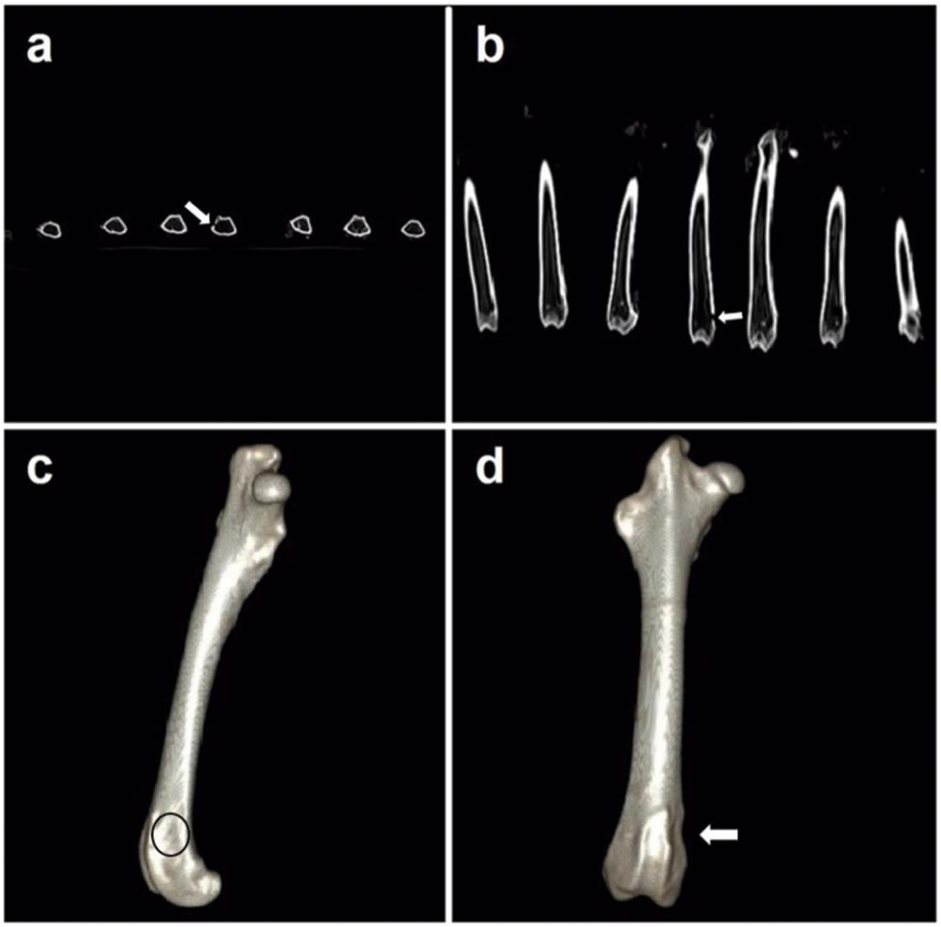

Figure 6. a) Axial computed tomography of right rabbit femora showing full cortical medial regeneration in six out of seven samples. The fourth sample from the left shows persistence in the cortical defect at the injury site (white arrow). b) Axial computed tomography of right rabbit femora showing a coronal slice of the samples. From left to right, in the fourth sample, the persistence of a cortical defect approximately 1 mm in size can be observed in the distal metaphysis (white arrow). c) Medial view of the 3D reconstruction of a rabbit right femur. The restitution of cortical bone at the distal metaphysis can be observed (black circumference). d) Medial view of the 3D reconstruction of a rabbit right femur. In this case, the sample with the remaining partial defect shows a small hollow with continuity (white arrow).

Bone restitution in the distal femoral metaphysis was also observed in the 3D reconstructions of all samples, and the created defect could not be detected (injury site indicated with a black circle; Figure 6c), even in the case of the sample that showed a small defect remaining in the axial and coronal slices. This 3D reconstruction showed a tiny hollow (white arrow), but the processed signal correlates to cortical bone (Figure 6d).

3.6. Histopathology results

The histological analytical results obtained for experimental samples showed *de novo* bone formation in the experimental femoral injury (EFI) region. The new bone formed was thick and comprised lamellar bone. In addition, it showed numerous vascular channels of different calibers and was surrounded by various osteoblast layers (Figure 7a). Each bone layer was deposited on the remaining ELR hydrogel in a disorganized fashion (Figure 7b), resembling pagetoid-like bone (Figure 7c), in which cellular activity produces a mosaic pattern rather than the normal linear lamellar pattern.

Remnants of non-biodegraded ELR hydrogels were observed inside the EFI center, showing a network or mesh shape and surrounded by micro-hemorrhages and congestive vessels. Rounded, triangular, rhomboid or even amorphous structures were found inside the network, showing an eosinophil, granular and mineralized pattern. These mineralized structures were surrounded by osteoblast-like cells, with osteocyte-like cells being found inside them, and angiogenesis could also be observed (Figure 7d).

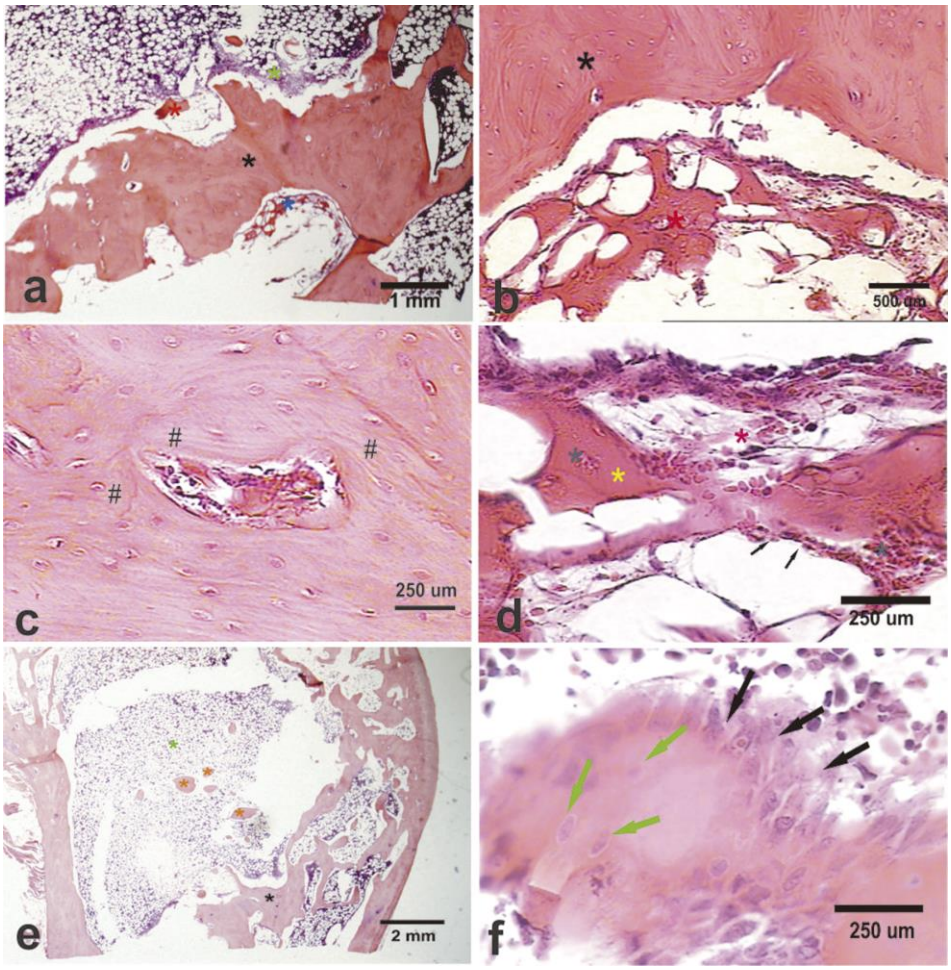

Figure 7. Microphotographs taken from decalcified femoral bone sections stained with hematoxylin and eosin. a) Thick lamellar bone showing numerous vascular blood channels (black asterisk), remnants of the ELR hydrogel (blue asterisk), hematopoietic bone marrow and osteoblast layers (green asterisk) are observed in the EFI region. Magnification 46.6x, bar = 1 mm. b) The high magnification images show the interface between new lamellar bone (black asterisk) and the ELR hydrogel (red asterisk), with a network aspect acting as a guide for cells. Magnification 233.4x, bar = 500 μm. c) At high magnification, a few vascular channels are observed in new lamellar bone at the EFI. Each layer of bone is deposited in the form of a "mosaic pattern", resembling pagetoid-like bone. Magnification 700.2x, bar= 250 μm. d) At high magnification the ELR hydrogel shows mineralized amorphous regions surrounded by osteoblast-like cells (black arrows). Micro-hemorrhage

(red asterisk) and congestive vessels (grey asterisk) are also observed. Magnification 700.2x bar= 250 μm. e) At low magnification, a panoramic microphotography of the femoral epiphysis and metaphysis shows new bone formed in the EFI region (black asterisk). This bone is surrounded by hematopoietic bone marrow (green asterisk) with a few trabeculae (orange asterisk). Magnification 80x, bar = 2 mm. f) A few bone nodules surrounding the EFI region are lined by several layers of prominent osteoblasts (black arrows). Osteocytes (green arrows) are observed inside a nodule. Magnification 700.2x, bar = 250 μm.

Hematopoietic bone marrow was observed surrounding the newly formed bone in the EFI, with scattered, rounded, nodule-like trabecular bone (Figure 7e). This new trabecular bone was covered by two, three or even more layers of prominent osteoblasts. Osteocyte cells were observed in the inner region (Figure 7f). Furthermore, several congestive vessels were observed close to each trabecula.

4. DISCUSSION

In order to address the main aim of this work, namely the regeneration of a femoral bone injury (FBI) in three-year-old female New Zealand white rabbits, two different bioactive ELRs have been developed and characterized to meet the requirements of novel biomaterials commonly used for that purpose. These novel ELRs were specifically designed to be osteoinductive, by fusing BMP-2 to one of them, and osteoconductive, by fusing RGD domains that promote cell adhesion, thus allowing surrounding cells to interact with the hydrogel and possibly promote bone formation even from inside the scaffold.

Initially it was shown that the T_t is lower than body temperature, which may permit the formation of hydrogels once the

ELR solution is injected into the body. In addition, this T_t is similar to that described previously for the non-bioactive ELR, which was found to be 13.0 ºC (42), although an increase of 2.8 and 2.3 ºC was observed for ELR-E-RGD and ELR-E-BMP-2, respectively. This can be explained by the lower hydrophobicity of the ELR molecule when other, more hydrophilic peptides or proteins containing charged residues are fused to it (43, 44).

As regards the rheological data, although this system is intended to be used for bone regeneration and the storage modulus is very low in comparison with bone tissue, this hydrogel was designed to be able to promote cell invasion and proliferation inside itself, acting as a temporary soft tissue that promotes optimal regeneration in a manner whereby the implanted scaffold is substituted by host tissue. As such, although it may not be useful on its own for treating large bone defects, it has been shown to be very suitable in the FBI model used in this work since the hydrogel remains free from significant mechanical stress (45).

Biodegradation of the ELR molecules in solution has been confirmed *in vitro*, thus showing that this process can also be controlled by varying the quantity of elastase used. Although this fails to imitate *in vivo* conditions, it sheds light onto the biodegradation kinetics. The use of elastase-sensitive sequences should also allow the slow release of BMP-2 from the ELR molecule to exert its biological effect. Consequently, the ELR-based hydrogel acts as a drug-delivery system. Despite the fact that there are other examples in which rhBMP-2 and ELRs are combined as an encapsulation system (46), this approach allows a more efficient

production and application by taking advantage of recombinant DNA technology.

The excellent cell adhesion found on surfaces coated with ELR-E-RGD was similar to that obtained in other studies using RGD-containing ELRs (47). As such, this work demonstrates that the inclusion of RGD sequences in the final ELR molecule by genetic-engineering methods promotes cell attachment and therefore provides a more ECM-mimetic environment that is also osteoconductive. ELR-E-BMP-2-coated substrates did not support cell adhesion due to the absence of cell-adhesion motifs in the ELR itself and in BMP-2. With regard to cell viability, the lack of differences between the negative control (medium only) and the media supplemented with the recombinamers is in agreement with previous studies in which a cell-culture medium was supplemented with ELRs (48).

As regards the clinical and biochemical results of the implant process, although initially affected by the surgery *per se*, animal gait recovered rapidly to normal conditions. The lack of change in the biochemical parameters showed that neither the surgical procedure nor the subsequent possible matrix biodegradation had any effect on the animals, thus showing good biocompatibility.

The images obtained in the tomographic study with 3D reconstruction of the samples show promising results since the signal patterns processed in this work are correlated to bone tissue with similar characteristics to the surrounding tissue, with complete closure of the defect being achieved in six out of seven samples. Although a defect approximately 1 mm in diameter was still visible in the remaining animal, this was only the case in three

tomographic slices and may simply be a consequence of a lack of time for the regeneration process in this particular animal. However, the bone formed had the same characteristics as the other samples, therefore it can be concluded that these ELR-based matrices have a high osteogenic potential to restitute a bone defect of 6 mm diameter and 6 mm depth *ad integrum* in 90 days, most probably due to fusion of the BMP-2 protein to the ELR, which results in a BMP-2-loaded hydrogel.

The histological analyses showed that the FBI was replaced by dense, new lamellar bone. Although a few remnants of the ELR were observed at 90 days post-implantation, they were surrounded by congestive vessels and dense laminar bone. This supports the accepted knowledge whereby new bone is only formed in the presence of blood irrigation (49). This new bone is arranged randomly, with an irregular arrangement in various different directions, thus suggesting that the ELR-based hydrogels act as a carrier for BMP-2, with osteoprogenitor cells colonizing these hydrogels, depositing osteoid matrix and mineralizing as pagetoid-like bone, probably driven by the network arrangement of the ELR-based hydrogels (50). The new trabeculae obtained show a peculiar shape, as if they were obtained by the confluence of rounded isolated bone formations. The numerous layers of prominent osteoblasts and various shapes observed, which appear to simulate pseudo-stratification, could be a result of the activity of BMP-2 (22, 51, 52).

As observed *in vivo* from the microscopic results, the ELR-based hydrogel was found to be biodegraded as bone formation occurred since the cells involved in this phenomenon were

stimulated by the BMP-2 released into the microenvironment, probably slowly enough to allow the differentiation of stem and progenitor cells. As such, in this situation, elastase (MMP-12) secretion by osteoclasts might be increased as a consequence of matrix remodeling due to the formation of *de novo* bone tissue, as suggested before (53). This could lead to degradation of the ELR-based hydrogel, which is sensitive to MMP-12 as a result of inclusion of the VPVAPG sequence, as described previously (54). On the other hand, ELRs without cleavable domains are not supposed to be biodegraded. In this regard, Sallach *et al*. reported a long-term stability (up to 1 year) of a physically cross-linked ELR-based hydrogel, similar to the one used in our work, when implanted *in vivo* (55). In our case, biodegradation might happen simultaneously with bone regeneration, thus resulting in a resorbable matrix that maintains bone integrity until full regeneration. In addition, the peptides resulting from the degradation of VPVAPG have been reported to exhibit a strong cell-proliferation activity that may promote tissue repair, as described previously (56). Furthermore, RGD sequences provide anchoring points for cells that help them to migrate and proliferate inside the scaffold, thereby promoting self-regeneration of the damaged tissue.

Although several approaches have been developed in the field of tissue engineering, to the best of our knowledge this is the first work describing the use of ELR-based hydrogels for the successful regeneration of a bone defect *in vivo*. Previous examples make use of ELRs in combination with other materials (57, 58), and most of them have only been tested *in vitro*, although with promising results (59). Besides, the ELR-based hydrogel described

in this study overcomes different issues regarding the use of biomaterials in bone tissue engineering. For instance, BMP-2 is not only loaded inside the hydrogel, but it is part of it. Hence, there is no need to add this osteogenic factor during the preparation of the scaffold, in contrast to other works (60), reducing its cost. In addition, this acellular system has shown to be able to promote optimal bone regeneration, while other studies report good outcomes only in the presence of mesenchymal stromal cells (61, 62). On the other hand, another acellular scaffold has been described, showing its usefulness in bone regeneration (63). However, this system is not injectable, and thus requires the use of invasive methods for its implantation. Moreover, the adaptation of this scaffold to the shape of the defect depends on the mold used in its development, reducing its versatility.

In conclusion, this work shows that a mixture of the originally designed ELRs is able to self-assemble into an appropriate BMP-2 carrier, namely an injectable and biodegradable hydrogel, which allows the slow release of this osteogenic factor, thereby stimulating progenitor and stem cell differentiation and osteoblast proliferation. Furthermore, the resulting ELR-based hydrogels also demonstrated an osteoconductive behavior since they provide an ECM-like environment as a result of the inclusion of RGD sequences. These two bioactivities (RGD and BMP-2), together with elastase-sensitiveness were easily included in the final ELR molecules in a controlled manner, due to their recombinant nature. Endogenous cells were able to migrate and proliferate into these hydrogels, thereby favouring bone neo-formation at the

femoral injury, as confirmed by computed tomography, radiography and histology.

Acknowledgements

The authors are grateful for funding from the European Commission (NMP-2014-646075, HEALTH-F4-2011-278557, PITN-GA-2012-317306 and MSCA-ITN-2014-642687), the MINECO of the Spanish Government (MAT2013-42473-R and MAT2013-41723-R), the Junta de Castilla y León (VA244U13 and VA313U14) and the Centro en Red de Medicina Regenerativa y Terapia Celular de Castilla y León. Dante J. Coletta has been funded by the Consejo Nacional de Investigaciones de Ciencia y Tecnología de la Nación (CONICET, Argentina). We would also like to thank Dr. Pedro Esbrit, from the Jiménez Díaz Foundation.

Author disclosure statement

No competing financial interests exist.

References

1. Amini, A.R., Laurencin, C.T., and Nukavarapu, S.P. Bone Tissue Engineering: Recent Advances and Challenges. Critical reviews in biomedical engineering **40**, 363, 2012.

2. Khademhosseini, A., and Langer, R. A decade of progress in tissue engineering. Nat Protocols **11**, 1775, 2016.

3. Yoseph, B.-C. Biomimetics. Biomimetics: CRC Press; 2005. pp. 495.

4. Costa, H.S., Mansur, A.A.P., Pereira, M.M., and Mansur, H.S. Engineered Hybrid Scaffolds of Poly(vinyl alcohol)/Bioactive Glass for Potential Bone

Engineering Applications: Synthesis, Characterization, Cytocompatibility, and Degradation. Journal of Nanomaterials **2012**, 16, 2012.

5. Santolini, E., West, R., and Giannoudis, P.V. Risk factors for long bone fracture non-union: a stratification approach based on the level of the existing scientific evidence. Injury **46 Suppl 8**, S8, 2015.

6. Chrcanovic, B.R., Albrektsson, T., and Wennerberg, A. Dental implants inserted in male versus female patients: a systematic review and meta-analysis. Journal of oral rehabilitation **42**, 709, 2015.

7. Cointry, G.R., Capozza, R.F., Feldman, S., Reina, P., and Ferretti, J.L. Estructura y biomecánica ósea. In: E. A., ed. Osteoporosis en Iberoamérica (2ª Ed). México DF (México): El Manual Moderno; 2012. pp. 33.

8. Compston, J. Osteoporosis: social and economic impact. Radiologic clinics of North America **48**, 477, 2010.

9. Curran, D., Maravic, M., Kiefer, P., Tochon, V., and Fardellone, P. Epidemiology of osteoporosis-related fractures in France: a literature review. Joint, bone, spine : revue du rhumatisme **77**, 546, 2010.

10. Cointry, G.R., Capozza, R.F., Feldman, S., Reina, P., Grappiolo, I., Ferretti, S.E., Mortarino, P., Chiappe, M.A., and Ferretti, J.L. Los huesos son estructuras genéticas, metabólicas, biomecánicas, o todo a la vez. Actualizaciones en Osteología **5**, 184, 2009.

11. Melton, L.J., 3rd, Achenbach, S.J., Atkinson, E.J., Therneau, T.M., and Amin, S. Long-term mortality following fractures at different skeletal sites: a population-based cohort study. Osteoporosis international : a journal established as result of cooperation between the European Foundation for Osteoporosis and the National Osteoporosis Foundation of the USA **24**, 1689, 2013.

12. Kremenetzky, A., Kremenetzky, L., and Feldman, S. Aplicación de aloinjerto óseo como cemento biológico. Revista de la Asociación Argentina de Ortopedia y Traumatología **71**, 61, 2006.

13. Alghazali, K.M., Nima, Z.A., Hamzah, R.N., Dhar, M.S., Anderson, D.E., and Biris, A.S. Bone-tissue engineering: complex tunable structural and biological

responses to injury, drug delivery, and cell-based therapies. Drug metabolism reviews **47**, 431, 2015.

14. Zhang, S., Zhang, X., Cai, Q., Wang, B., Deng, X., and Yang, X. Microfibrous beta-TCP/collagen scaffolds mimic woven bone in structure and composition. Biomedical materials **5**, 065005, 2010.

15. Arealis, G., and Nikolaou, V.S. Bone printing: new frontiers in the treatment of bone defects. Injury **46 Suppl 8**, S20, 2015.

16. Salgado, A.J., Oliveira, J.M., Martins, A., Teixeira, F.G., Silva, N.A., Neves, N.M., Sousa, N., and Reis, R.L. Chapter One - Tissue Engineering and Regenerative Medicine: Past, Present, and Future. In: Stefano Geuna I.P.P.T., Bruno B., eds. International Review of Neurobiology: Academic Press; 2013. pp. 1.

17. Detsch, R., and Boccaccini, A.R. The role of osteoclasts in bone tissue engineering. Journal of tissue engineering and regenerative medicine **9**, 1133, 2015.

18. van der Stok, J., Lozano, D., Chai, Y.C., Amin Yavari, S., Bastidas Coral, A.P., Verhaar, J.A.N., Gómez-Barrena, E., Schrooten, J., Jahr, H., Zadpoor, A.A., Esbrit, P., and Weinans, H. Osteostatin-Coated Porous Titanium Can Improve Early Bone Regeneration of Cortical Bone Defects in Rats. Tissue Engineering Part A **21**, 1495, 2015.

19. Romagnoli, C., D'Asta, F., and Brandi, M.L. Drug delivery using composite scaffolds in the context of bone tissue engineering. Clinical Cases in Mineral and Bone Metabolism **10**, 155, 2013.

20. Inoda, H., Yamamoto, G., and Hattori, T. Histological investigation of osteoinductive properties of rh-BMP2 in a rat calvarial bone defect model. Journal of Cranio-Maxillofacial Surgery **32**, 365, 2004.

21. Chen, D., Zhao, M., and Mundy, G.R. Bone morphogenetic proteins. Growth factors **22**, 233, 2004.

22. G. dos S. Kotake, B., M. P. Salzedas, L., Ervolino, E., A. J. Calzzani, R., Sebald, W., and P. M. Issa, J. Bone Recuperation After rhBMP-2 Insertion in Alcoholic Animals-Experimental Study. Current Pharmaceutical Design **21**, 3557, 2015.

23. Siéssere, S., de Sousa, L.G., Issa, J.P.M., Iyomasa, M.M., Pitol, D.L., Barbosa, A.P.A., Semprini, M., Sebald, W., Bentley, M.V.B., and Regalo, S.C.H. Application of Low-Level Laser Irradiation (LLLI) and rhBMP-2 in Critical Bone Defect of Ovariectomized Rats: Histomorphometric Evaluation. Photomedicine and Laser Surgery **29**, 453, 2011.

24. Abdala, P.M.F., Iyomasa, M.M., Sato, S., Bentley, M.V.L.B., Pitol, D.L., Regalo, S.C.H., Siéssere, S., and Issa, J.P.M. Osteoinductivity potential of rhBMP-2 associated with two carriers in different dosages. Anatomical Science International **85**, 181, 2010.

25. Issa, J.P.M., do Nascimento, C., Bentley, M.V.L.B., Del Bel, E.A., Iyomasa, M.M., Sebald, W., and de Albuquerque Jr, R.F. Bone repair in rat mandible by rhBMP-2 associated with two carriers. Micron **39**, 373, 2008.

26. Haidar, Z.S., Hamdy, R.C., and Tabrizian, M. Delivery of recombinant bone morphogenetic proteins for bone regeneration and repair. Part A: Current challenges in BMP delivery. Biotechnology Letters **31**, 1817, 2009.

27. Schmidmaier, G., Schwabe, P., Strobel, C., and Wildemann, B. Carrier systems and application of growth factors in orthopaedics. Injury **39**, S37, 2008.

28. Girotti, A., Orbanic, D., Ibáñez-Fonseca, A., Gonzalez-Obeso, C., and Rodríguez-Cabello, J.C. Recombinant Technology in the Development of Materials and Systems for Soft-Tissue Repair. Advanced Healthcare Materials **4**, 2423, 2015.

29. Rodríguez-Cabello, J.C., Martín, L., Alonso, M., Arias, F.J., and Testera, A.M. "Recombinamers" as advanced materials for the post-oil age. Polymer **50**, 5159, 2009.

30. Urry, D.W. Molecular Machines: How Motion and Other Functions of Living Organisms Can Result from Reversible Chemical Changes. Angewandte Chemie International Edition in English **32**, 819, 1993.

31. Martin, L., Arias, F.J., Alonso, M., Garcia-Arevalo, C., and Rodriguez-Cabello, J.C. Rapid micropatterning by temperature-triggered reversible gelation of a recombinant smart elastin-like tetrablock-copolymer. Soft Matter **6**, 1121, 2010.

32. Ruoslahti, E., and Pierschbacher, M.D. Arg-Gly-Asp: a versatile cell recognition signal. Cell **44**, 517, 1986.

33. Lombard, C., Arzel, L., Bouchu, D., Wallach, J., and Saulnier, J. Human leukocyte elastase hydrolysis of peptides derived from human elastin exon 24. Biochimie **88**, 1915, 2006.

34. Goy, D.P., Gorosito, E., Costa, H.S., Mortarino, P., Pedemonte, N.A., Toledo, J., Mansur, H.S., Pereira, M.M., Battaglino, R., and Feldman, S. Hybrid matrix grafts to favor tissue regeneration in rabbit femur bone lesions. The open biomedical engineering journal **6**, 85, 2012.

35. Coletta, D.J., Lozano, D., Rocha-Oliveira, A.A., Mortarino, P., Bumaguin, G.E., Vitelli, E., Vena, R., Missana, L., Jammal, M.V., Portal-Nunez, S., Pereira, M., Esbrit, P., and Feldman, S. Characterization of Hybrid Bioactive Glass-polyvinyl Alcohol Scaffolds Containing a PTHrP-derived Pentapeptide as Implants for Tissue Engineering Applications. The open biomedical engineering journal **8**, 20, 2014.

36. Rodríguez-Cabello, J.C., Girotti, A., Ribeiro, A., and Arias, F.J. Synthesis of Genetically Engineered Protein Polymers (Recombinamers) as an Example of Advanced Self-Assembled Smart Materials. In: Navarro M., Planell J.A., eds. Nanotechnology in Regenerative Medicine: Methods and Protocols. Totowa, NJ: Humana Press; 2012. pp. 17.

37. Orozco, L., Munar, A., Soler, R., Alberca, M., Soler, F., Huguet, M., Sentis, J., Sanchez, A., and Garcia-Sancho, J. Treatment of knee osteoarthritis with autologous mesenchymal stem cells: a pilot study. Transplantation **95**, 1535, 2013.

38. McKay, W.F., Peckham, S.M., and Badura, J.M. A comprehensive clinical review of recombinant human bone morphogenetic protein-2 (INFUSE® Bone Graft). International Orthopaedics **31**, 729, 2007.

39. Feldman, S., Cointry, G.R., Leite Duarte, M.a.E., Sarrió, L., Ferretti, J.L., and Capozza, R.F. Effects of hypophysectomy and recombinant human growth hormone on material and geometric properties and the pre- and post-yield behavior of femurs in young rats. Bone **34**, 203, 2004.

40. Meyer, D.E., and Chilkoti, A. Genetically Encoded Synthesis of Protein-Based Polymers with Precisely Specified Molecular Weight and Sequence by Recursive Directional Ligation: Examples from the Elastin-like Polypeptide System. Biomacromolecules **3**, 357, 2002.

41. McPherson, D.T., Xu, J., and Urry, D.W. Product Purification by Reversible Phase Transition Following Escherichia coli Expression of dGenes Encoding up to 251 Repeats of the Elastomeric Pentapeptide GVGVP. Protein Expression and Purification **7**, 51, 1996.

42. Fernandez-Colino, A., Arias, F.J., Alonso, M., and Rodriguez-Cabello, J.C. Self-organized ECM-mimetic model based on an amphiphilic multiblock silk-elastin-like corecombinamer with a concomitant dual physical gelation process. Biomacromolecules **15**, 3781, 2014.

43. Christensen, T., Hassouneh, W., Trabbic-Carlson, K., and Chilkoti, A. Predicting Transition Temperatures of Elastin-Like Polypeptide Fusion Proteins. Biomacromolecules **14**, 1514, 2013.

44. Ibáñez-Fonseca, A., Alonso, M., Arias, F.J., and Rodríguez-Cabello, J.C. Förster Resonance Energy Transfer-Paired Hydrogel Forming Silk-Elastin-Like Recombinamers by Recombinant Conjugation of Fluorescent Proteins. Bioconjugate Chemistry 2017.

45. Gibbs, D.M.R., Black, C.R.M., Dawson, J.I., and Oreffo, R.O.C. A review of hydrogel use in fracture healing and bone regeneration. Journal of tissue engineering and regenerative medicine **10**, 187, 2016.

46. Bessa, P.C., Machado, R., Nurnberger, S., Dopler, D., Banerjee, A., Cunha, A.M., Rodriguez-Cabello, J.C., Redl, H., van Griensven, M., Reis, R.L., and Casal, M. Thermoresponsive self-assembled elastin-based nanoparticles for delivery of BMPs. Journal of controlled release : official journal of the Controlled Release Society **142**, 312, 2010.

47. de Torre, I.G., Wolf, F., Santos, M., Rongen, L., Alonso, M., Jockenhoevel, S., Rodriguez-Cabello, J.C., and Mela, P. Elastin-like recombinamer-covered stents: Towards a fully biocompatible and non-thrombogenic device for cardiovascular diseases. Acta biomaterialia **12**, 146, 2015.

48. Pina, M.J., Girotti, A., Santos, M., Rodriguez-Cabello, J.C., and Arias, F.J. Biocompatible ELR-Based Polyplexes Coated with MUC1 Specific Aptamers and Targeted for Breast Cancer Gene Therapy. Molecular pharmaceutics **13**, 795, 2016.

49. Tomlinson, R.E., and Silva, M.J. Skeletal Blood Flow in Bone Repair and Maintenance. Bone Research **1**, 311, 2013.

50. Missana, L., Nagai, N., and Kuboki, Y. Comparative histological studies of bone and cartilage formations induced by various BMP-carrier composites. Journal of Oral Biosciences **36**, 9, 1994.

51. Issa, J.P.M., Defino, H.L.A., Netto, J.C., Volpon, J.B., Regalo, S.C.H., Iyomasa, M.M., Siéssere, S., and Tiossi, R. Evaluation of rhBMP-2 and Natural Latex as Potential Osteogenic Proteins in Critical Size Defects by Histomorphometric Methods. The Anatomical Record: Advances in Integrative Anatomy and Evolutionary Biology **293**, 794, 2010.

52. Issa, J.P.M., Do Nascimento, C., Lamano, T., Iyomasa, M.M., Sebald, W., and De Albuquerque Jr, R.F. Effect of recombinant human bone morphogenetic protein-2 on bone formation in the acute distraction osteogenesis of rat mandibles. Clinical Oral Implants Research **20**, 1286, 2009.

53. Hou, P., Troen, T., Ovejero, M.C., Kirkegaard, T., Andersen, T.L., Byrjalsen, I., Ferreras, M., Sato, T., Shapiro, S.D., Foged, N.T., and Delaissé, J.-M. Matrix metalloproteinase-12 (MMP-12) in osteoclasts: new lesson on the involvement of MMPs in bone resorption. Bone **34**, 37, 2004.

54. Taddese, S., Weiss, A.S., Jahreis, G., Neubert, R.H.H., and Schmelzer, C.E.H. In vitro degradation of human tropoelastin by MMP-12 and the generation of matrikines from domain 24. Matrix Biology **28**, 84, 2009.

55. Sallach, R.E., Cui, W., Balderrama, F., Martinez, A.W., Wen, J., Haller, C.A., Taylor, J.V., Wright, E.R., Long Jr, R.C., and Chaikof, E.L. Long-term biostability of self-assembling protein polymers in the absence of covalent crosslinking. Biomaterials **31**, 779, 2010.

56. Rodriguez-Cabello, J., Ribeiro, A., Reguera, J., Girotti, A., and Testera, A. 14 - Elastin-like systems for tissue engineering. Natural-Based Polymers for Biomedical Applications: Woodhead Publishing; 2008. pp. 374.

57. Tejeda-Montes, E., Klymov, A., Nejadnik, M.R., Alonso, M., Rodriguez-Cabello, J.C., Walboomers, X.F., and Mata, A. Mineralization and bone regeneration using a bioactive elastin-like recombinamer membrane. Biomaterials **35**, 8339, 2014.

58. Prieto, S., Shkilnyy, A., Rumplasch, C., Ribeiro, A., Arias, F.J., Rodríguez-Cabello, J.C., and Taubert, A. Biomimetic Calcium Phosphate Mineralization with Multifunctional Elastin-Like Recombinamers. Biomacromolecules **12**, 1480, 2011.

59. Vila, M., García, A., Girotti, A., Alonso, M., Rodríguez-Cabello, J.C., González-Vázquez, A., Planell, J.A., Engel, E., Buján, J., García-Honduvilla, N., and Vallet-Regí, M. 3D silicon doped hydroxyapatite scaffolds decorated with Elastin-like Recombinamers for bone regenerative medicine. Acta biomaterialia **45**, 349, 2016.

60. Perez, R.A., Kim, J.-H., Buitrago, J.O., Wall, I.B., and Kim, H.-W. Novel therapeutic core–shell hydrogel scaffolds with sequential delivery of cobalt and bone morphogenetic protein-2 for synergistic bone regeneration. Acta biomaterialia **23**, 295, 2015.

61. Jo, S., Kim, S., Cho, T.H., Shin, E., Hwang, S.J., and Noh, I. Effects of recombinant human bone morphogenic protein-2 and human bone marrow-derived stromal cells on in vivo bone regeneration of chitosan–poly(ethylene oxide) hydrogel. Journal of Biomedical Materials Research Part A **101A**, 892, 2013.

62. Ren, Z., Wang, Y., Ma, S., Duan, S., Yang, X., Gao, P., Zhang, X., and Cai, Q. Effective Bone Regeneration Using Thermosensitive Poly(N-Isopropylacrylamide) Grafted Gelatin as Injectable Carrier for Bone Mesenchymal Stem Cells. ACS Applied Materials & Interfaces **7**, 19006, 2015.

63. Nguyen, T.B.L., and Lee, B.-T. A Combination of Biphasic Calcium Phosphate Scaffold with Hyaluronic Acid-Gelatin Hydrogel as a New Tool for Bone Regeneration. Tissue Engineering Part A **20**, 1993, 2014.

5. SUPPLEMENTARY INFORMATION

5.1. Supplementary Methods

5.1.1. ELR biosynthesis and characterization

The block co-polymer that constitutes the ELR backbone was designed to comprise a hydrophobic block (containing isoleucine as the guest residue), known as I_{60}, which is able to establish physical interactions above the T_t, i.e. at physiological temperature. Moreover, it includes a hydrophilic block (containing glutamic acid with a carboxylic group), termed E_{50}, which remains hydrated at physiological temperature. Both the ELRs designed and used in this work include an elastase cleavage sequence for biodegradation, as described above. One of them was genetically engineered to include a RGD domain for cell attachment, while the other one included the BMP-2 domain to enhance osteogenesis, thus giving ELR-Elastase-RGD (ELR-E-RGD) and ELR-Elastase-BMP-2, respectively (Figure S1, Supplementary Information).

The mechanical properties of the hydrogels formed by the ELRs above the T_t were assessed by rheological testing in a controlled stress rheometer (AR2000ex, TA Instruments) equipped with a Peltier plate for control of the temperature and a 12 mm plate diameter for the shear stress. To that end, a mixture of both ELRs (98% (w/w) ELR-E-RGD and 2% (w/w) ELR-E-BMP-2, see below) was dissolved in PBS at 300 mg/mL and 4 ºC for 24 h. Hydrogels were then formed *in situ* by depositing 200 μL of the solution onto the cold Peltier plate and increasing the temperature to 37 ºC. Time

sweep experiments were conducted at a constant strain of 0.5% and a frequency of 1 Hz.

5.1.2. Elastase-mediated cleavage of the ELR in solution

SDS-PAGE was performed to evaluate the biodegradation of the samples incubated with elastase, comparing those taken at different time points with the original sample at the beginning of the experiment. Gels were prepared at a polyacrylamide (Acryl/Bis™, Amresco, USA) concentration of 10%. The protein molecular weight marker used was Pierce Unstained Protein MW Marker (Thermo Fisher, USA). Images were obtained using the Gel Logic 100 Imaging System (Eastman Kodak, USA) and analyzed using Kodak 1D Image Analysis software (Eastman Kodak, USA).

5.1.3. *In vivo* experiments

5.1.3.1. Pre-surgical preparation

Antibiotic prophylaxis was carried out prior to the surgical procedure by applying cefazolin at a dose of 50 mg/kg/day, administered intramuscularly.

The anesthetic treatment was performed by combining three drugs, which were administered intramuscularly, namely Ketamine Hydrochloride at 35 mg/kg/day, Xylazine Hydrochloride (2.0%) at 18 mg/kg, and Acepromazine Maleate (1.0%) at 1 mg/kg, achieving complete relaxation of the animal. This anesthetic effect lasted for 45-60 minutes.

5.1.3.2. Surgical procedure

The area was shaved with an electric shaver, brushed with a 10% povidone-iodine solution, and immediately covered with fenestrated drapes. The intervention began with a longitudinal cutaneous incision of 4 cm in the internal lateral distal metaphysis of the femur, immediately above the medial condyle.

Both the medial and lateral flaps were separated, and a non-muscular aponeurotic plane was opened until the desired bone area had been reached through the divulsion in said tissues. The central point of the perforation was marked with a bradawl, and the first hole was cut immediately, using a drill with a 3 mm diameter bit attached to a sterile electric motor. Milling was subsequently continued using a 6 mm diameter bit to obtain the desired bone defect of no more than 3 mm in depth. The bone defect was washed with a sterile physiological solution to eliminate detritus, and hemostasis of the lesion was performed using a sterile swab plus gauze. The area was then dried with a sterile gauze and filled with the chilled ELR solution to form a hydrogel *in situ*. To this end, 100 μL of the solution was placed into the hole created in the bone using an automatic pipette and sterile tips, which were stored at 4 ºC to avoid gelification of the ELR before and during implantation. The aponeurotic plane was first sutured using resorbable material type 3/0, then the skin was sutured with 3/0 Nylon, and disinfected with povidone-iodine.

5.1.3.3. Post-surgical clinical studies

During the study period, the overall status, mobility and food intake of the animals were monitored daily. Body temperature was measured daily during the first week, and then weekly thereafter. Biochemical parameters (complete blood count) were evaluated using standard procedures at days 0, 2, 30 and at the end of the study. Total serum proteins, albumin, alanine aminotransferase (ALT) and aspartate aminotransferase (AST) were evaluated using standard commercial kits (Wiener lab Group, Argentina) (data not shown).

5.2. Supplementary Figures and Tables

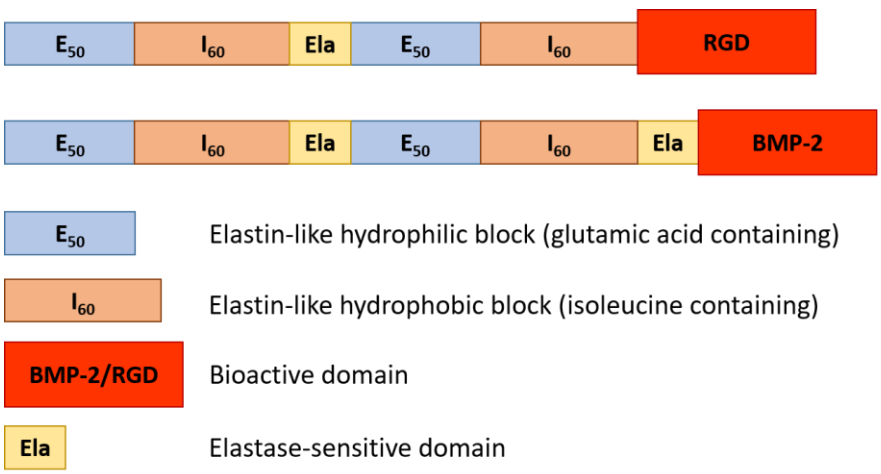

Figure S1. Original scheme of the design of the ELRs engineered for this work, ELR-E-RGD and ELR-E-BMP-2, respectively.

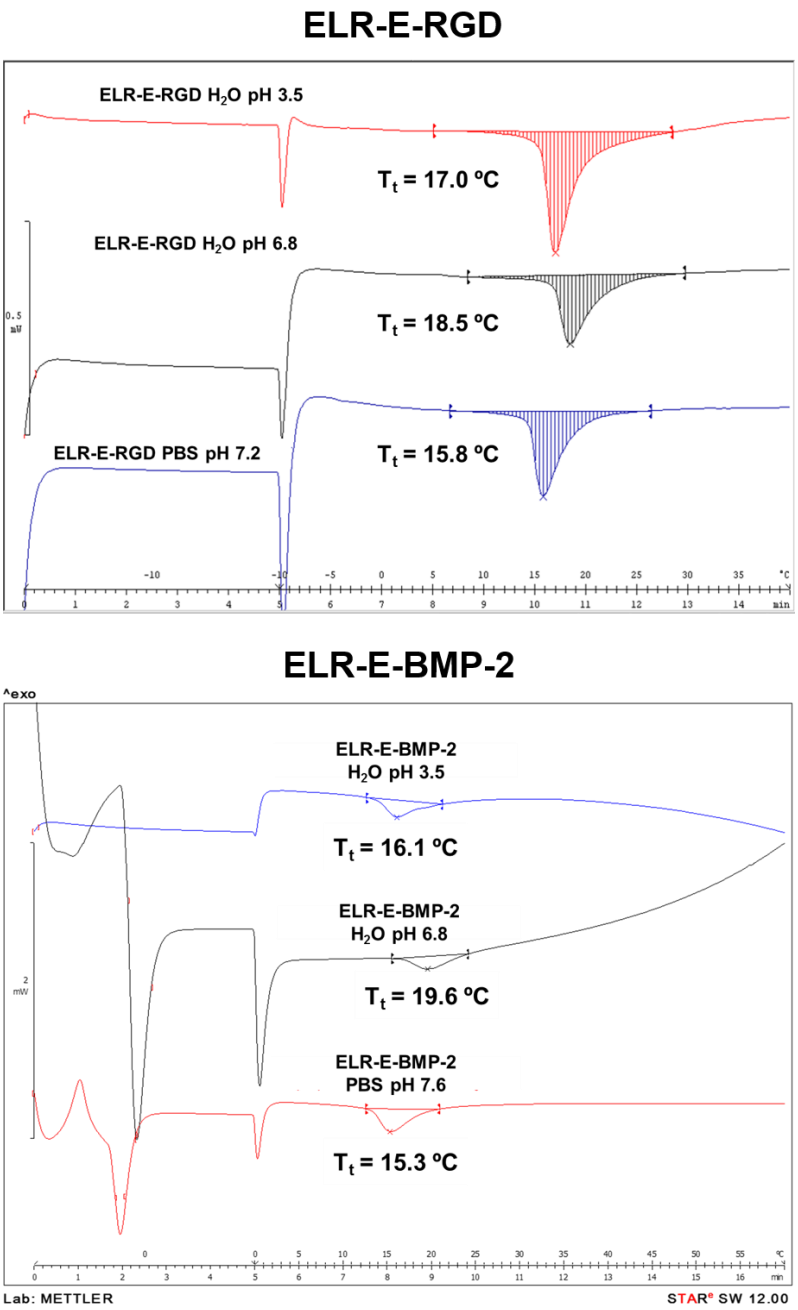

Figure S2. DSC graphs of ELR-E-RGD (top) and ELR-E-BMP-2 (bottom) showing the T_t of both ELRs in different solvents (water and PBS) and at different pH values.

Table S1. Comparison between the predicted number of each amino acid in ELR-E-RGD and the experimental values.

Amino acid	Predicted	Experimental
ASP+ASN	2+0	2.47
GLU+GLN	21	25.54
SER	7	5.34
HIS	-	-
GLY	530	533.99
THR	2	2.30
ARG	2	1.13
ALA	7	6.01
TYR	-	-
CYS	-	-
VAL	350	344.22
MET	1	0.66
TRP	-	-
PHE	-	-
ILE	160	158.98
LEU	2	2.32
LYS	-	-
PRO	266	267.47

Table S2. Comparison between the predicted number of each amino acid in ELR-E-BMP-2 and the experimental values.

Amino acid	Predicted	Experimental
ASP+ASN	6+7	10.30
GLU+GLN	26+2	34.82
SER	9	6.54
HIS	5	3.38
GLY	457	463.15
THR	3	3.01
ARG	2	5.79
ALA	12	14.94
TYR	5	8.43
CYS	7	7.32
VAL	325	313.03
MET	3	2.31
TRP	2	-
PHE	3	2.92
ILE	124	121.54
LEU	10	10.29
LYS	6	3.74
PRO	234	233.16

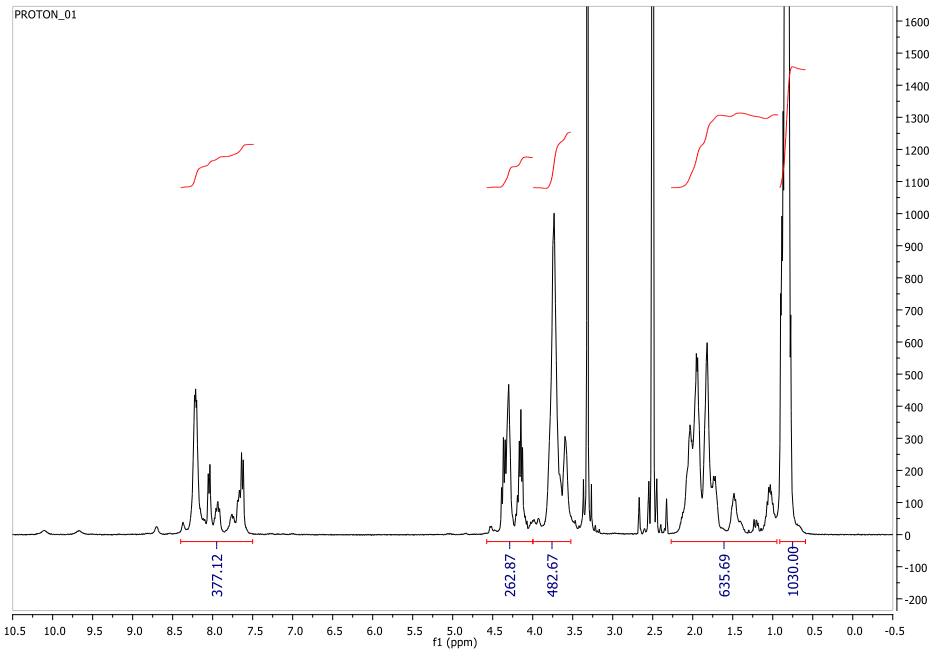

Figure S3. ^{1}H-NMR spectrum of ELR-E-RGD showing the integration of the peaks corresponding to the different types of hydrogens.

Table S3. Comparison between the predicted value of each type of hydrogen in ELR-E-RGD and the experimental values found by integration of each peak in the corresponding ^{1}H-NMR spectrum.

Type of hydrogen	Predicted value	Measured value
-C<u>H</u>$_3$	1030	Reference
-C<u>H</u>- and -C<u>H</u>$_2$-	1475	1381.2
-N<u>H</u>$_2$	363	377.1

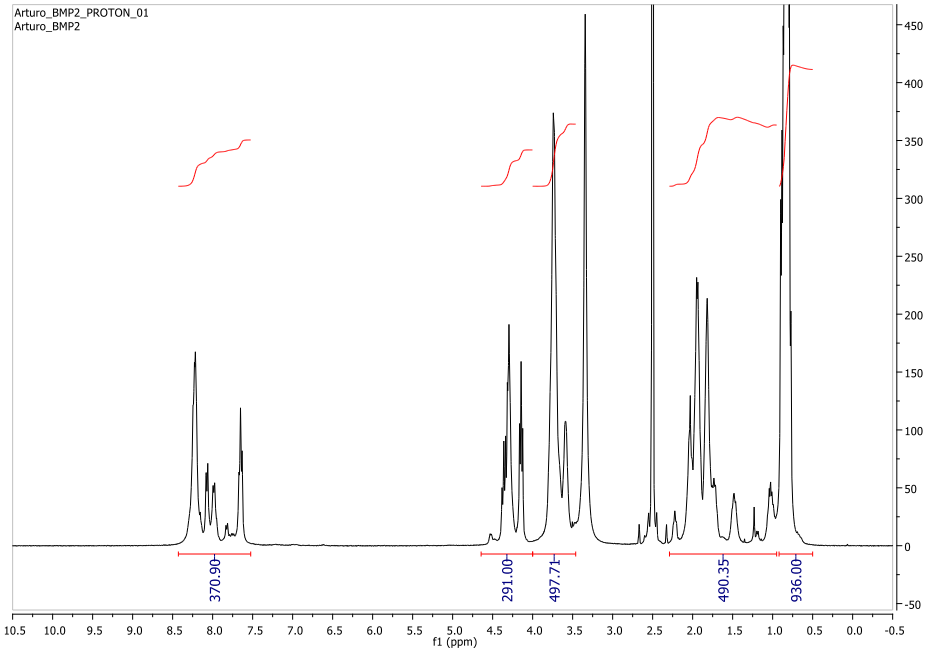

Figure S4. ^{1}H-NMR spectrum of ELR-E-BMP-2 showing the integration of the peaks corresponding to the different types of hydrogens.

Table S4. Comparison between the predicted value of each type of hydrogen in ELR-E-BMP-2 and the experimental values found by integration of each peak in the corresponding ^{1}H-NMR spectrum.

Type of hydrogen	Predicted value	Measured value
-C<u>H</u>$_3$	936	Reference
-C<u>H</u>- and -C<u>H</u>$_2$-	1370	1279.1
-N<u>H</u>$_2$	355	370.9

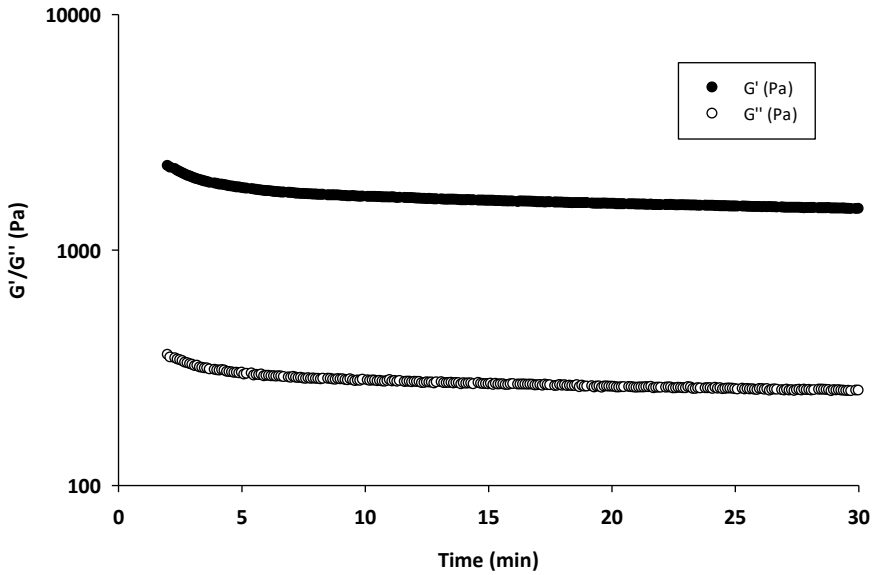

Figure S5. Graph showing the mechanical properties of a hydrogel made of a mixture of ELR-E-RGD (98% (w/w)) and ELR-E-BMP-2 (2% (w/w)) at 300 mg/mL in PBS.

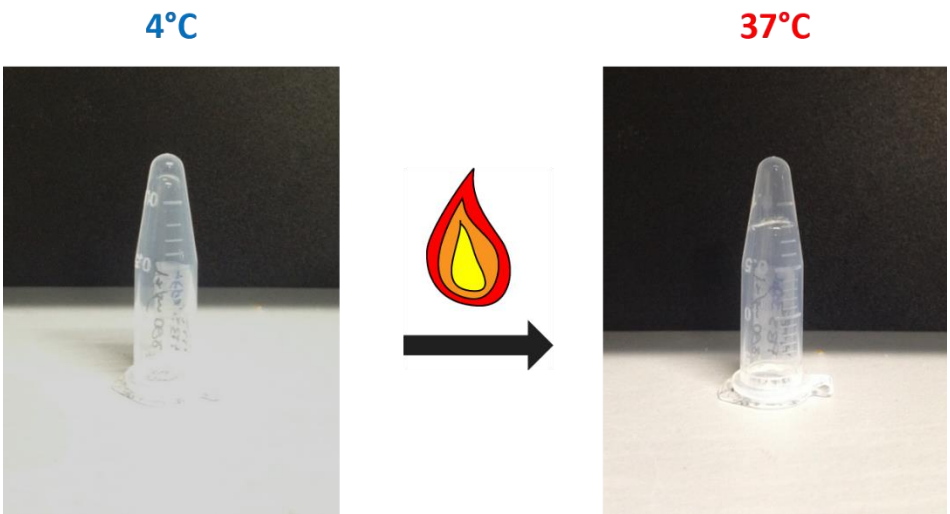

Figure S6. Hydrogel formation due to a temperature increase above the T_t of a mixture of ELR-E-RGD (98% (w/w)) and ELR-E-BMP-2 (2% (w/w)) at 300 mg/mL in PBS. The solution was first kept in an ice bath until

complete dissolution. Then, it was incubated at 37ºC for 5 minutes to allow the formation of the hydrogel.

Table S5. Table showing the expected molecular weight, the molecular weight plus 20%, and the calculated (experimental) *Mw* of the bands appearing upon elastase-mediated degradation.

Nascent bands	Expected *Mw* (kDa)	Expected *Mw* + 20% (kDa)	Calculated *Mw* (kDa)
Nascent band 1	66.5-65.5	79.8-78.6	80.8
Nascent band 2	48.2-46.7	57.8-56.0	54.2

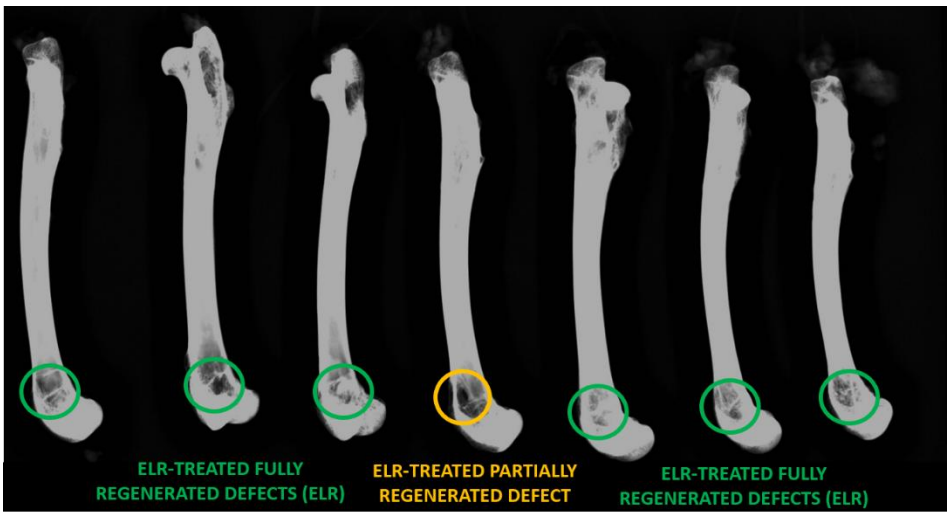

Figure S7. Radiography showing the seven femora extracted at the end of the experiment. Green circles correspond to fully regenerated defects (six out of seven samples) and the yellow circle to a partially regenerated defect.

Table S6. Abbreviated amino acid sequence and molecular weight of the different ELRs used in this work.

ELR	Abbreviated amino acid sequence	Molecular weight (Da)
ELR-E-RGD	MESLLP-[(VPGVG)$_2$-VPGEG-(VPGVG)$_2$]$_{10}$-(VGIPG)$_{60}$-(VGVAPG)$_3$-[(VPGVG)$_2$-VPGEG-(VPGVG)$_2$]$_{10}$-(VGIPG)$_{60}$-[(VPGIG)$_{10}$-AVTGRGDSPASS-(VPGIG)$_{10}$]$_2$V	113556
ELR-E-BMP-2	MESLLP-[(VPGVG)$_2$-VPGEG-(VPGVG)$_2$]$_{10}$-(VGIPG)$_{60}$-(VGVAPG)$_3$-[(VPGVG)$_2$-VPGEG-(VPGVG)$_2$]$_{10}$-(VGIPG)$_{60}$-(VGVAPG)$_3$-VKSSCKRHPLYVDFSDVGWND WIVAPPGYHAFYCHGECPFPLA DHLNSTNHAIVQTLVNSVNSKIP KACCVPTELSAISMLYLDENEKV VLKNYQDMVVEGCGCRV	107752
(EI)$_2$ (non-elastase sensitive ELR)	MESLLP-[(VPGVG)$_2$-VPGEG-(VPGVG)$_2$]$_{10}$-(VGIPG)$_{60}$-[(VPGVG)$_2$-VPGEG-(VPGVG)$_2$]$_{10}$-(VGIPG)$_{60}$-V	93158

CHAPTER 4

FÖRSTER RESONANCE ENERGY TRANSFER-PAIRED HYDROGEL FORMING SILK-ELASTIN-LIKE RECOMBINAMERS BY RECOMBINANT CONJUGATION OF FLUORESCENT PROTEINS

Arturo Ibáñez-Fonseca, Matilde Alonso, Francisco Javier Arias, José Carlos Rodríguez-Cabello*

BIOFORGE Lab, University of Valladolid — CIBER-BBN, Valladolid, Spain.

A. Ibáñez-Fonseca, M. Alonso, F.J. Arias, J.C. Rodríguez-Cabello. *Bioconjugate Chemistry* (2017), 28 (3), 828–835. doi: 10.1021/acs.bioconjchem.6b00738

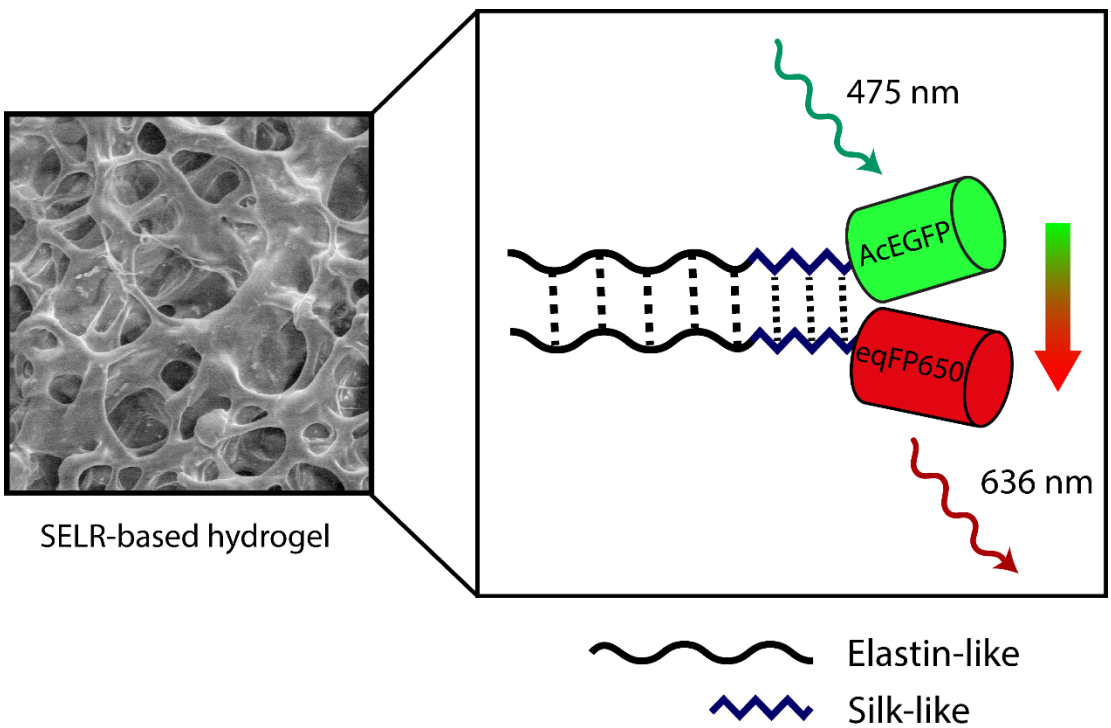

Abstract

In the last decades, recombinant structural proteins have become very promising in addressing different issues like the lack of traceability of biomedical devices or the design of more sensitive biosensors. Among them, we find elastin-like recombinamers (ELRs), which can be designed to self-assemble into diverse structures, like hydrogels. Furthermore, they might be combined with other protein polymers, such as silk, to give silk-elastin-like recombinamers (SELRs), holding the properties of both proteins. In this work, due to their recombinant nature, we have fused two different fluorescent proteins (FPs), i.e. the green *Aequorea coerulescens* EGFP and the near-infrared eqFP650, to a SELR able to form irreversible hydrogels through physical cross-linking. These recombinamers showed an emission of fluorescence similar to the single FPs, and they were capable of forming hydrogels with different stiffness (G' = 60-4000 Pa), by varying the concentration of the SELR-FPs. Moreover, the absorption spectrum of SELR-eqFP650 showed a peak greatly overlapping the emission spectrum of the SELR-AcEGFP, hence enabling Förster resonance energy transfer (FRET) upon the interaction between two SELR molecules, each one containing a different FP, due to the stacking of silk domains at any temperature and to the aggregation of elastin-like blocks above the transition temperature. This effect was studied by different methods and a FRET efficiency of 0.06-0.2 was observed, depending on the technique used for its calculation. Therefore, innovative biological applications arise from the combination of SELRs with FPs, such as enhancing the traceability of hydrogels

based on SELRs intended for tissue engineering, the development of biosensors, and the prediction of FRET efficiencies of novel FRET pairs.

1. INTRODUCTION

The combination of peptides and proteins holding specific properties with other molecules may lead to the engineering of novel materials with improved features that can be exploited in different biological applications. This can be achieved through the chemical conjugation of (poly)peptides to other molecules able to form diverse types of structures.[1] However, recombinant protein-based materials are much more interesting in terms of conjugation to other proteins, since the fusion protein can be obtained by genetic engineering methods and further expression in a heterologous host.[2]

Regarding specific recombinant polymers, elastin-like recombinamers (ELRs), a terminology that highlights the recombinant nature of elastin-like polypeptides first described by Urry *et al.*,[3] have been extensively used for the development of different materials in the recent years.[4-6] ELRs comprise repetitive units of the Val-Pro-Gly-X-Gly $(VPGXG)_n$ pentapeptide in which X (guest residue) is any amino acid except L-proline. Moreover, they show thermosensitivity due to the change of the protein conformation above the so-called transition temperature (T_t), which itself depends on the polarity of the side chain in the guest residue.[7] Therefore, the T_t can be tuned depending on the amino acid chosen in the X position of the pentapeptide.[8,9] Furthermore, ELRs can be designed so the phase transition occurring above the T_t is translated into a hydrophobically-driven self-assembly of the molecules towards supramolecular structures such as particles,[10] micelles and vesicles,[11] electrospun fibers[12] and hydrogels,[13] among

others. In addition, ELRs can be fused to repeated amino acid sequences derived from other structural proteins like the GAGAGS hexapeptide found in *Bombyx mori* silk fibroin, hence giving rise to silk-elastin-like recombinamers (SELR),[14] to form more complicated structures, e.g. hydrogels, that incorporate the properties of both polypeptides.[15]

In this work, we have fused two different fluorescent proteins (FPs) to a previously described amphiphilic SELR[15] based on two types of elastin-like domains, one hydrophilic and the other one hydrophobic, by including glutamic acid and isoleucine as guest residues, respectively. This SELR is able to self-assemble into hydrogels that are injectable below the T_t, through the transition mechanism due to the hydrophobic ELR blocks, while the formed network is further stabilized by the silk domains. First, we have fused a green-emitting FP to the SELR used in this study, namely *Aequorea coerulescens* enhanced green fluorescent protein (AcEGFP).[16,17] In another molecule maintaining the same SELR structure, we have cloned the near-infrared-emitting eqFP650, which was previously described as the brightest FP above 635 nm.[18] Furthermore, this protein was shown to behave as a dimer, which could be a disadvantage in the case of fusion proteins, since it may hamper dimerization and efficient emission of fluorescence. However, we intended to assess if this kind of oligomeric FPs kept their fluorescence when used to improve the properties of protein-based materials, such as ELRs or SELRs. For instance, there exist many dimeric and tetrameric far-red and infrared FPs that are very useful in *in vivo* applications as they avoid the drawbacks that arise from the use of GFP, YFP or orange FPs, like a low signal-to-noise

ratio due to the excitation and emission of auto-fluorescence by endogenous molecules, such as hemoglobin, at the wavelength ranges of these FPs.[19] Both fluorescent SELRs (SELR-FPs) were characterized by physicochemical methods and the mechanical properties of the hydrogels based on these recombinamers were also evaluated.

Moreover, with the aim of exploring novel approaches beyond simple fluorescence emission, we studied Förster resonance energy transfer (FRET).[20] High FRET efficiencies are achieved when the distance between the donor and the acceptor is in the range of 1-10 nm, they have a favourable dipole-dipole alignment, and there is a significant spectral overlap of the donor emission and acceptor excitation (or absorption) spectra.[21] Hence, the study of FRET between both SELR-FPs by spectroscopy (donor quenching) and confocal microscopy (acceptor photobleaching) allowed us to get information about the interaction between SELR molecules varying from low to high concentration solutions, at which they self-assemble into particles and hydrogels, respectively, as described for the SELR itself.[15] Although a previous work described a FRET effect between ELR molecules fused to fluorescent proteins, this was only feasible if other polypeptides forming a specific protein complex were included in the final protein.[22] In our case, our hypothesis relies on the ability of SELR molecules of establishing stacking interactions at mid and high concentrations that are able to minimize the distance between the two FPs, hence enabling FRET. Moreover, the formation of SELR-FPs-based hydrogels increases the potential of this FRET system in different applications. In

addition, this is the first time that FRET is described for this pair of FPs, to our best knowledge.

This work aimed to show the development of novel fluorescent SELRs and the study of the features inherent to the SELR, to the FPs and to their combination. The results described below provide the basis for further studies regarding the potential applications of the hydrogel-forming SELR-FPs designed and bioproduced in this work as biosensors,[23] taking advantage of their recombinant nature. Thereby, peptides/proteins that bind to different targets may be included in the SELR sequence, such as glucose,[24] LPS,[25] or metal ions,[26] thus showing an enormous potential in the field of biosensors. Furthermore, the use of FRET could considerably increase the sensitivity of these SELR-based biosensors due to the measurement through ratiometric instead of intensiometric measurements.[27] Likewise, SELR-FPs might be used to enhance the traceability of biomedical devices made of themselves or in combination with other ELRs or silk-based materials.

2. RESULTS AND DISCUSSION

2.1. Fluorescent SELRs design, bioproduction and physicochemical characterization

The genes of the SELRs designed for the purpose of this work were successfully synthetized (see Figure S1 for a schematic representation of both SELR-FPs and Table S1 for the full abbreviated amino acid sequence) and all the cloning steps were carefully evaluated by agarose gel electrophoresis and DNA

sequencing methods (data not shown). Further expression of SELRs in *E. coli* was confirmed by SDS-PAGE, and a final yield of 133 and 120 mg/L of lyophilized product was obtained for the SELR-AcEGFP and the SELR-eqFP650, respectively. These results are lower than the one found previously for the SELR itself,[15] hence indicating that the fusion of both FPs hinders the expression and/or the purification of the SELR.

The purity and molecular weight (*Mw*) of the final products were assessed by SDS-PAGE and MALDI-TOF (Figure S2 and Figure S3, respectively). As regards the purity, it was found to be ≥ 95% for both recombinamers. In the case of the *Mw*, the experimental values, obtained from the m/2z value, (126.9 and 128.9 kDa for SELR-AcEGFP and SELR-eqFP650, respectively) were very similar to the expected values (128.7 and 128.1 kDa) for both SELR-FPs. Additional characterization included H-NMR spectroscopy (Figure S4 and Table S6 and Table S7) and amino acid composition by HPLC (Table S2 and Table S3 for SELR-AcEGFP and SELR-eqFP650, respectively), confirming the absence of undesired contaminants. Furthermore, the transition process was studied by DSC and SELR-AcEGFP and SELR-eqFP650 showed a T_t of 16.8 and 17.2ºC, respectively, in PBS at neutral pH (Figure S5). This temperature is more than 2ºC higher than the one found for the SELR alone (14.4ºC),[15] since the hydrophilic FPs fused to this recombinamer increase the overall hydrophilicity of the final protein, and therefore the T_t raises, in agreement with a previous work by Chilkoti and co-workers.[28] Moreover, DSC results show that both SELR-FPs meet the requirements to be used in biomedical applications, since the transition of the recombinamers at body temperature (37ºC) will

give rise to hydrogels at high concentrations of the SELR-FPs, as shown below.

2.2. Mechanical properties of hydrogels based on SELR-FPs

The formation of SELR hydrogels is described in depth by Fernández-Colino *et al.*[15] Briefly, hydrophobic interactions between elastin-like blocks initiate the formation of the hydrogel network once the temperature is raised above the T_t. This brings silk-like domains together, allowing the hydrogen bonding between them in a process termed "annealing", which leads to an increase of the stiffness and to a complete stabilization of the hydrogels over time.

As observed in Figure 1, both SELR-FPs show a decrease in the storage modulus (*G'*) in comparison to the SELR alone at the same molar concentration.[15] For instance, *G'* for SELR-based hydrogels at 1.13 mM are 2.6-, 2.3- and 2.4-fold higher compared to SELR-AcEGFP, SELR-eqFP650 and the 1:1 molar mixture, respectively. On the other hand, the increase at 1.73 mM is 1.3- and 1.4-fold for SELR-AcEGFP and for both SELR-eqFP650 and the 1:1 molar mixture, respectively (see Table S4). These results can be explained by the steric effect due to the high volume occupied by either AcEGFP or eqFP650 that impedes the tight stacking of elastin-like blocks above the T_t and the formation of hydrogen bonds between silk domains that stiffen the hydrogels. However, this effect is counteracted by increasing the concentration of SELR-FPs solutions to form the hydrogels. The differences between SELR-AcEGFP and SELR-eqFP650 are very slight, being more noticeable at higher concentrations (1.94 mM), i.e. *G'* of 4055 and 3354 Pa,

respectively. This might be due to the higher steric effect in the case of the eqFP650 (and the 1:1 molar mixture) because this FP tends to form dimers.

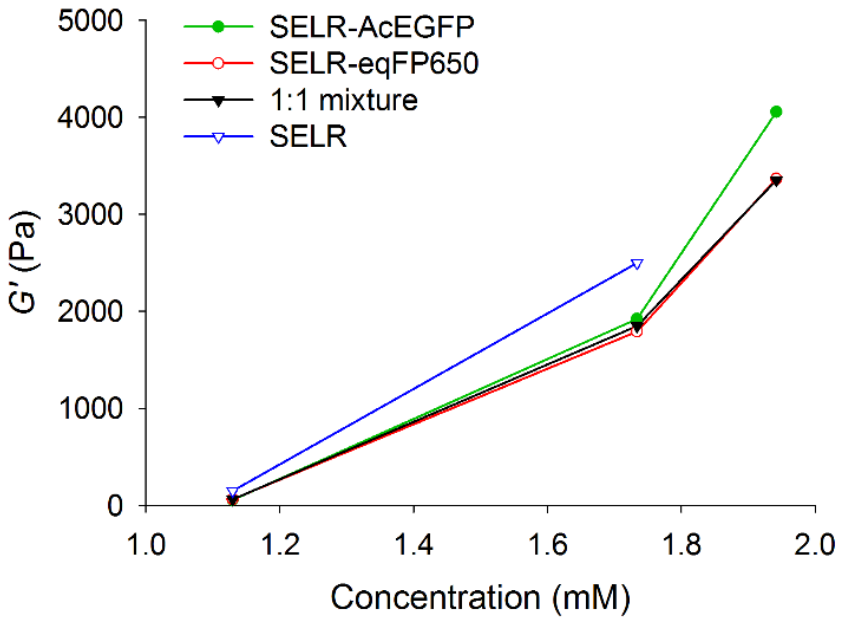

Figure 1. Graph showing the mechanical properties of SELR-FPs-based hydrogels compared to SELR-based ones, in terms of storage modulus (*G*) at three different concentrations (1.13, 1.73 and 1.94 mM). Data corresponding to SELR only was obtained from Fernández-Colino *et al.*[15]

In addition, results show that it is possible to obtain hydrogels with different grades of stiffness depending on the concentration, hence being suitable for diverse applications in tissue engineering.[29] For example, very soft hydrogels with a *G'* of ~60 Pa were achieved at 1.13 mM, while at 1.94 mM (250 mg/mL) a *G'* of ~3700 Pa is observed. Below 145 mg/mL, hydrogels were not formed above the T_t as confirmed by visual evaluation through the inversion of tubes containing the SELR-FPs solutions at this concentration.

2.3. Fluorescence characterization of SELR-FPs by spectroscopy

The extinction coefficient (ε) of both SELR-FPs was calculated as stated in the experimental section, following Equation 1. The absorbance (A) was obtained from the absorption spectra at the wavelength of its maximum (λ_{max}), i.e. A = 0.548 for SELR-AcEGFP at 488 nm, while A = 0.800 for SELR-eqFP650 at 589 nm (peak 2 in absorption spectrum, Figure S6). With these values, we calculated ε (see

Table 1) and it was found to be 21.7% and 15.8% of the corresponding non-fused FPs, for SELR-AcEGFP and SELR-eqFP650, respectively. We describe two excitation and emission maxima for SELR-eqFP650 due to the two peaks observed in its absorption spectrum (Figure S6), as described below. Hence, in Table 1, excitation peaks 1 and 2 are correlated to emission peaks 1 and 2, respectively.

Table 1. Key properties of SELR-FPs compared to the corresponding single FPs.

properties	AcGFP1 (Clontech)	SELR-AcEGFP	eqFP650 (TurboFP650, Evrogen)	SELR-eqFP650
Excitation peak (nm)	475	475	592	Peak 1 – 516 Peak 2 – 587
Emission peak (nm)	505	510	650	Peak 1 – 540 Peak 2 – 636
Molar extinction coefficient (ε, M^{-1} cm^{-1}) at	32,500	7,046	65,000	10,243

excitation maximum				
Fluorescence quantum yield (QY)	0.82	0.34	0.24	0.10
Brightness[a] (a.u.)	26,650	2,396	15,600	1,024
Brightness related to AcGFP1	1	0.09	0.59	0.04
Reference	Commercial brochure	This work	18	This work

[a] Calculated as the product of ε and QY.

Furthermore, the brightness, as calculated here, taking other works as references, is very low compared to SELR-FPs counterparts. However, it should be noticed that a great amount of molecules is present in a SELR-FP-based hydrogel, so it will be clearly visible by *in vivo* imaging systems or other instruments dedicated to detect fluorescence.

Moreover, the excitation and emission spectra of both SELR-FPs (Figure 2) were in good agreement with those found in the literature for AcGFP and other derivatives,[16,17] and for eqFP650.[18] Nevertheless, in the latter case, excitation and emission λ_{max} were found slightly shifted for SELR-eqFP650, meaning that the fusion to SELR may impede correct maturation or dimerization of the FP, hence changing chromophore conformation and, consequently, excitation and emission behavior.

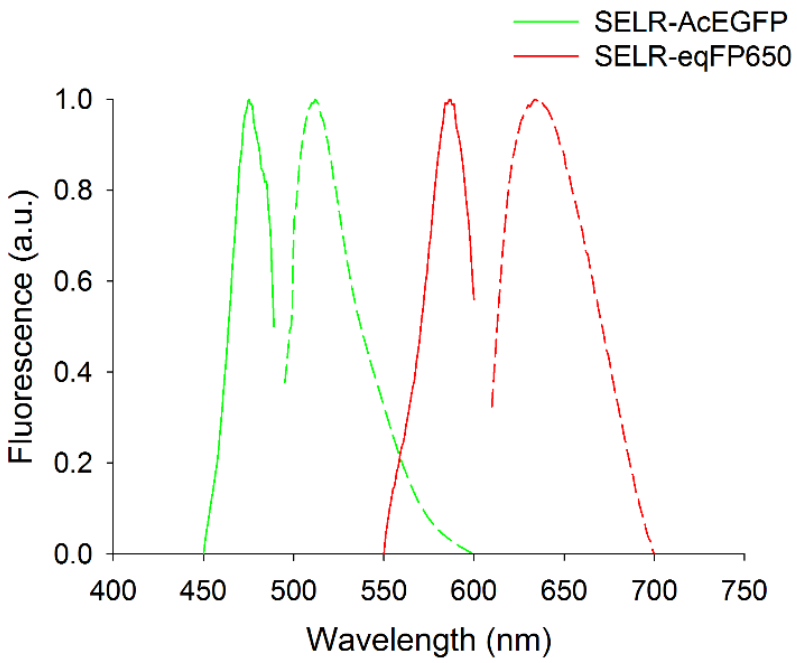

Figure 2. Excitation and emission spectra for SELR-AcEGFP (green solid and dotted lines) and SELR-eqFP650 (red solid and dotted lines).

However, although not observed in the excitation spectrum of SELR-eqFP650 in Figure 2 due to the settings used for its calculation, we observed a peak at 521 nm in the absorbance spectrum of SELR-eqFP650 (Figure S6). The appearance of this peak might be due to an incomplete dimerization or incorrect folding of the far-red FP, which would be hindered by the high molecular weight of the SELR fused to it. This peak presents a high overlap with the one found in the emission spectrum of SELR-AcEGFP (see Figure 3 for a more clear comparison). Therefore, we hypothesized that it may exist a FRET effect between both SELR-FPs, and different studies were performed in this regard, as shown below.

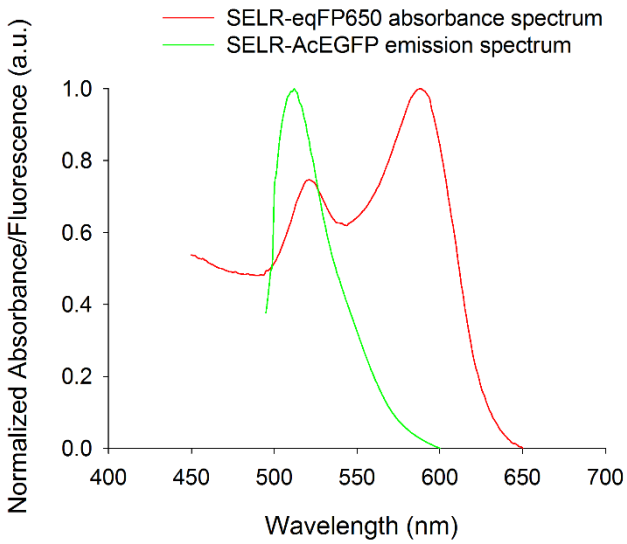

Figure 3. Overlay of the absorbance spectrum of SELR-eqFP650 and the emission spectrum of SELR-AcEGFP showing the high overlap occurring between them.

2.4. Calculation of FRET efficiency in SELR-FPs mixtures by spectroscopy (donor quenching)

The experimental determination of the FRET efficiency (E) by spectroscopy was achieved through the comparison of the fluorescence intensity emitted by SELR-AcEGFP in the presence and in the absence of SELR-eqFP650. It is widely described that quenching on the fluorescence emitted by the donor of a FRET pair occurs in the presence of the acceptor.[20] In order to obtain E accurately, we prepared samples containing the same amount of SELR-FPs, separately, than the quantity used to prepare the 1:1 molar mixture. First, spectra were obtained above T_t setting λ_{ex} at 475 nm, i.e. SELR-AcEGFP maximum, at different concentrations. Then, data from SELR-eqFP650 were subtracted from the ones of the mixture and a direct comparison was performed by representing

spectra from SELR-AcEGFP only and from the mixture, as it can be seen in Figure 4.

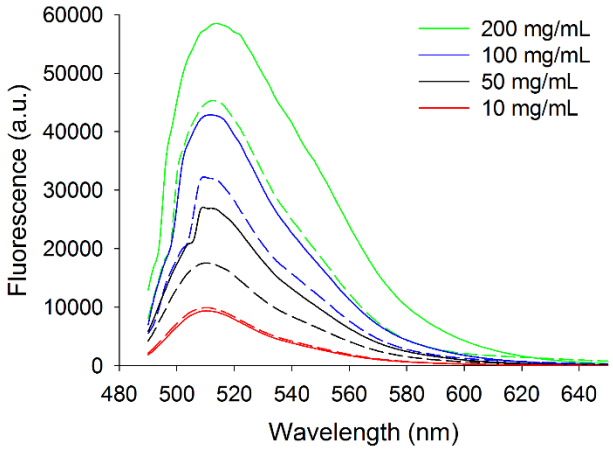

Figure 4. Emission spectra (λ_{ex} = 475 nm) of SELR-AcEGFP (solid lines) and of a 1:1 molar mixture (dotted lines) of both SELR-FPs at different concentrations.

It can be observed that fluorescence intensity is clearly reduced in the case of the mixture (dotted lines) when compared to the SELR-AcEGFP only (solid lines) for every concentration excepting 10 mg/mL, which was the lowest concentration tested. This result indicates that a FRET effect, by means of donor quenching, takes place at mid and high concentrations, probably due to the increased proximity (1-10 nm) between the FPs conjugated to the SELRs.

Concerning *E* values obtained by this technique, we studied the FRET behavior of SELR-FPs at two different temperatures, namely 15 and 37ºC, which are below and above the T_t, respectively. The results (Figure 5) show that FRET is non-existent for the 1:1 molar mixture at 10 mg/mL, as expected by the observation of

spectra in Figure 4. Furthermore, there are not significant differences between the FRET efficiencies obtained for the different concentrations and temperatures ($p > 0.05$), excepting between 10 mg/mL and the rest of concentrations. The exact values of E obtained for each sample are shown in Table S5.

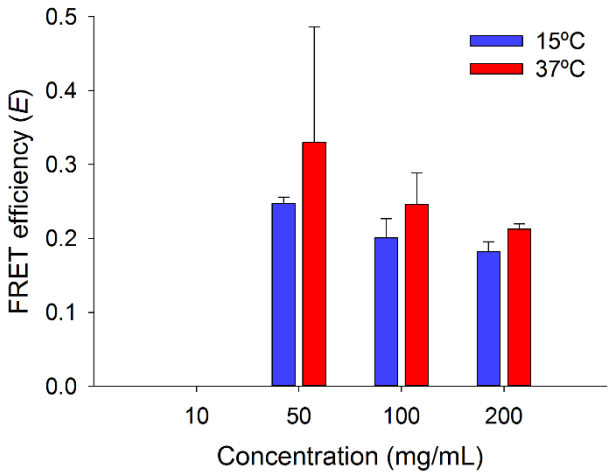

Figure 5. FRET efficiencies calculated by spectroscopy (donor quenching) below (15ºC, blue bars) and above (37ºC, red bars) the T_t, at different concentrations. Data are represented as mean ± SD (n = 2).

The lack of dissimilarities between the different conditions tested suggests that once a minimum concentration is reached, the distance between SELR-FPs molecules is low enough to enable FRET (1-10 nm), independently of the aggregation of the elastin-like blocks above the T_t. Nevertheless, silk-like domains are able to establish interactions between them at any temperature and may help molecules to stack and remain closer even at temperatures below the T_t. Moreover, even though p-values do not indicate significant differences, it can be observed an increase in E above T_t

because of the hydrophobic interaction of the elastin-like blocks included in the SELR-FPs.

The evaluation of *E* in further combinations of elastin- and silk-like domains, and FPs, e.g. including both FPs in the same molecule, may shed light into the structure of particles and hydrogels based on SELRs, since FRET is critically influenced by the distance between the fluorophores.

2.5. Calculation of FRET efficiency in a SELR-FP mixture by confocal microscopy (acceptor photobleaching)

In order to calculate *E* by confocal microscopy, hydrogels were prepared in the wells of a slide optimized for this technique and allowed to gel at room temperature (approximately 23ºC, not significant differences with spectroscopy data than for 37ºC, Table S5 and Figure S7) overnight. Figure 6 shows the images of a field of view (FOV) within the hydrogel before (Pre) and after (Post) performing photobleaching of the acceptor at its maximum λ_{ex}. As it can be seen, the intensity of the pixels for the green channel (corresponding to SELR-AcEGFP) inside the photobleached ROI increases after achieving a 93.8 ± 0.3% reduction of the intensity in the red channel (SELR-eqFP650). This is more clearly observed in the FRET (Post – Pre) picture obtained by subtraction of the Post picture from the Pre one.

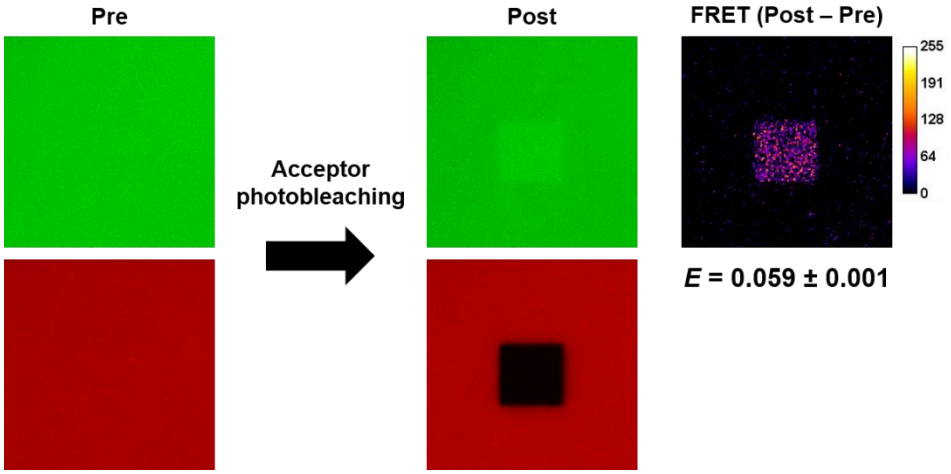

Figure 6. Diagram showing the results of SELR-AcEGFP de-quenching by photobleaching of SELR-eqFP650 through confocal microscopy. The calculated efficiency by this method was performed using Equation 4 (see Materials and Methods), and it was found to be 0.059 ± 0.001 (mean ± SD, n = 3). However, the picture showing the subtraction of the pre image from the post one does not represent exactly that efficiency, since images are not corrected.

However, the direct calculation of E by the Post – Pre subtraction leads to an underestimation due to partial bleaching of the whole FOV during image acquisition. For this reason, we proposed the correction of the mean intensity of the pixels inside the ROI by using another ROI close to the former, but not including that area. Then, a ratio was performed as stated in Equation 4. By this method, it was calculated E = 0.059 ± 0.001 (mean ± SD, n = 3), which is lower than the efficiencies found for other FPs by microscopy methods.[30] Nevertheless, it must be taken into account the large distance between the donor λ_{em} and the acceptor λ_{ex}, which might give different advantages like avoiding bleed through or overcoming limitations derived from live fluorescence imaging due to tissue auto-fluorescence.

The discrepancy between the *E* value obtained by spectroscopy and the one calculated by acceptor photobleaching is difficult to explain and could be related to the methods used for its determination. For the calculation of FRET by spectroscopy, we relied on Equation 2, which is obtained from the simplification of more complex formulas. With this simplification, it is assumed that the excitation light intensity absorbed by the donor (SELR-AcEGFP) and all the measurement parameters are identical for both samples (donor in the absence and in the presence of acceptor, i.e. SELR-eqFP650).[31] Since both measurements were obtained simultaneously, all the settings were similar. However, the first assumption could not be confirmed due to spectral overlap between the absorption spectra of SELR-AcEGFP and the one of SELR-eqFP650 in the mixture. Hence, we relied on precise sample preparation and duplicates to avoid artifacts, which may not be completely eradicated. As regards confocal microscopy, a 100% of acceptor photobleaching was not achieved, and thereby the *E* found by this technique might not be as high as it actually is. These results can serve as an example for future works concerning FRET, in which extraordinary care must be taken in choosing the methods used for the determination of the FRET efficiency.

3. CONCLUSIONS

We have developed two fluorescent SELRs able to form injectable hydrogels through the genetic fusion of two different fluorescent proteins: AcEGFP and eqFP650. Physicochemical characterization reported a thermosensitive behavior and hydrogels showed tunable mechanical properties, depending on

SELR-FP concentration, hence being suitable for different applications. Furthermore, solutions and hydrogels based on these SELR-FPs showed fluorescence emission similar to the FPs on their own, except for some differences in eqFP650 excitation and emission maximum and global spectra, probably due to uncompleted maturation and/or dimerization. However, the finding of a green-shifted peak in the absorption spectrum of SELR-eqFP650, not described in the literature for the specific FP, led us to determine the FRET effect between both SELR-FPs. We calculated *E* by different methods giving dissimilar results possibly because of artifacts derived from the techniques. Furthermore, *E* values were similar for the conditions tested, hence being independent of the concentration (over a specific mid one) and of the temperature (above or below the T_t).

To our knowledge, this is the first work describing FRET between AcEGFP, or any of its derivatives, and eqFP650. Hence, we propose this system as a good model to study the FRET efficiency of novel FRET pairs. In addition, several applications may arise from this work, such as the study of self-assembled ELR-based structures (e.g. particles) and the development of hydrogels with improved traceability for tissue engineering. Similarly, SELR-FPs may find their use as biosensors, either by themselves or as FRET-pairs, thanks to the feasible addition of binding domains, e.g. to metals or cell structures, due to their recombinant nature.

4. MATERIALS AND METHODS

4.1. SELR-FPs design and bioproduction

In order to achieve a green emitting SELR, the AcEGFP (GenScript) was cloned and fused to the SELR. For the development of a near-infrared emitting SELR, eqFP650 gene was synthesized (NZYTech) and genetically fused to the gene encoding the recombinamer.

Cloning and heterologous expression of the SELRs used in this work were performed as described elsewhere.[32] Briefly, their full-length DNA sequences, including FPs, were obtained by the iterative recursive method through several cloning steps in XL-1 Blue Competent Cells (Agilent) and cloned into a pET-25b(+) vector to be expressed in *Escherichia coli* (BLR strain). SELRs were biosynthesized in a 15-L bioreactor (Applikon Biotechnology) and purified by several cooling and heating purification cycles (Inverse Transition Cycling) taking advantage of the ability of these recombinamers to aggregate above their transition temperature. Further centrifugation steps led to a pure product, which was dialyzed against ultra-pure water, filtered through 0.22 μm filters (Nalgene) to obtain a sterile solution, and freeze-dried prior to storage.

4.2. Physicochemical characterization of pure SELR-FPs

Characterization techniques included sodium dodecyl sulfate polyacrylamide gel electrophoresis (SDS-PAGE) and matrix-

assisted laser desorption/ionization time-of-flight (MALDI-TOF) for purity and molecular weight (*Mw*) evaluation compared to the theoretical values of 128,737 Da for SELR-AcEGFP and 128,048 Da for SELR-eqFP650; differential scanning calorimetry (DSC) to determine the T_t, i.e. the thermosensitivity of the recombinamers; HPLC to determine the amino acid composition of both SELRs after acid hydrolysis, and nuclear magnetic resonance (NMR) to provide recombinamer fingerprint data.

4.3. Rheology of SELR-FP-based hydrogels

The mechanical properties of the hydrogels formed by the SELRs above the T_t were assessed by rheological tests in a controlled stress rheometer (AR2000ex, TA Instruments) equipped with a Peltier plate for the control of the temperature and a 12 mm plate diameter for the shear stress. The procedure followed for the mechanical study was previously described.[15] SELRs were dissolved separately at 4ºC for 24 h in PBS at different concentrations, namely 1.13, 1.73 and 1.94 mM (145, 222 and 250 mg/mL, respectively). Hydrogels were formed *in situ* by depositing 200 μL of the solution on the Peltier plate (12 mm diameter) below the T_t (5ºC), and rapidly increasing the temperature to 37ºC. Time sweep experiments were run at a constant strain of 0.5% and a frequency of 1 Hz. Furthermore, the mechanical properties of a 1:1 molar mixture of both SELRs at the same concentrations were also evaluated following the same protocol.

4.4. Fluorescence spectroscopy of SELR-FPs

A multi-mode microplate reader (SpectraMax M2e, Molecular Devices) was used for the characterization of the two SELR-FPs in terms of absorption and fluorescence emission. Molar extinction coefficients (ε) were calculated using Lambert-Beer's law and the absorbance (A) of a solution of each SELR-FP at their maximum at a concentration (C) of 10 mg/mL in PBS, in a 1-cm light path (l) cuvette, at 37ºC (Equation 1). A solution of SELR without FPs was used as reference at the same concentration.

$$(1)\ A = \varepsilon \cdot l \cdot C$$

In the case of the absorption spectra, SELR-FPs were dissolved in ultra-pure water instead of PBS (same concentration), since all the experiments that did not require comparison with the specific FPs alone were carried out in this solvent.

Emission spectrum was obtained for each SELR-FP setting the excitation wavelength at the maximum of absorption with 50 μL of a solution prepared as described above, in black half-area 96-well plates (Corning). Excitation spectra were acquired with the experimental emission λ_{max} obtained from the previous experiment: 510 nm for SELR-AcEGFP, and 636 nm for SELR-eqFP650. A 1-nm step was used in every case. All the measurements were performed at 37ºC.

Quantum yields (QY) were obtained by comparison of the emission spectra of the SELR-FPs (475 nm and 587 nm excitation for AcEGFP and eqFP650, respectively) with those of the FPs by themselves, using the free software a|e - UV-Vis-IR Spectral

Software 2.2 (FluorTools, www.fluortools.com). AcGFP1 (QY = 0.82, supplier data) was obtained from Clontech, while eqFP650 (QY = 0.24)[18] was purchased from Evrogen as TurboFP650 (commercial name). The brightness of each SELR-FP was calculated by the product of the ε and the QY and expressed relative to AcGFP1.

4.5. FRET efficiency calculation through spectroscopy (donor quenching)

Data for the calculation of FRET efficiency were collected with three different types of samples: donor only (SELR-AcEGFP) at the same molar concentration than in the mixture, acceptor only (SELR-eqFP650) at the same molar concentration than in the mixture, and a 1:1 molar mixture of both components. SELRs were prepared at different concentrations, namely 10, 50, 100 and 200 mg/mL, in cold ultra-pure water. In order to avoid biases related to the properties of the recombinamer by itself, SELR-FPs were diluted in a solution of SELR at the same concentration. Emission spectra were obtained with the multi-mode microplate reader (SpectraMax M2e, Molecular Devices) mentioned above. Single measurements at 475/510 ($\lambda_{ex}/\lambda_{em}$) were also performed on every sample below (15ºC) and above (37ºC) the T_t.

FRET efficiency (E) was calculated by the following equation (Equation 2):[20]

$$(2)\ E = 1 - \frac{F_{DA}}{F_D}$$

where F_{DA} and F_D are the fluorescence intensities of the donor at its λ_{max} of excitation and emission (475/510 nm), in the presence and

in the absence of the acceptor, respectively. Due to the emission of fluorescence by the acceptor at those λ_{max} settings, data were corrected prior to application of Equation 2 by subtracting the emission spectrum of the acceptor only sample to that of the 1:1 molar mixture.

4.6. FRET efficiency calculation through confocal microscopy (acceptor photobleaching)

In order to evaluate further the FRET efficiency, confocal microscopy was performed on hydrogels based on a 1:1 molar mixture of both SELR-FPs. For that purpose, recombinamers were dissolved at 200 mg/mL in cold ultra-pure water overnight at 4ºC. Hydrogels were formed by depositing 250 μL of the cold SELR-FPs mixture on different wells of a μ-Slide 8 Well Glass Bottom (ibidi) to allow confocal microscopy visualization through the bottom with a coverslip-like thickness.

Confocal images were obtained at 25ºC (above the T_t) with a Leica TCS SP5 confocal microscope controlled by the LAS software. Regarding donor fluorescence, an Argon laser was used for excitation, and emission was collected at 499-559 nm. On the other hand, a white laser couple to a monochromator was used for excitation of the acceptor at 587 nm, and emission was collected at 595-700 nm.

With the aim of calculating FRET efficiency through acceptor photobleaching (AB), a region of interest (ROI) was drawn on the chosen field and the following pictures were taken sequentially: 1) Pre-bleaching donor excitation and emission; 2) Pre-bleaching acceptor excitation and emission; 3) Post-bleaching donor

excitation and emission; 4) Post-bleaching acceptor excitation and emission. AB was accomplished setting the white laser at λ_{ex} = 600 and 90% intensity, performing 100 laser scans inside the ROI (approximately 5 minutes of bleaching time). Calculated AB was 93.8 ± 0.3% for the SELR-eqFP650, in every case.

To calculate FRET efficiency, mean intensities of the ROI in the pre- and the post-bleaching pictures of the donor were used in the following equation (Equation 3):[33]

$$(3)\ E = 1 - \frac{I_{pre}}{I_{post}}$$

However, because of the unwanted bleaching of both donor and acceptor outside the ROI, mean intensities were corrected using the mean intensity of another ROI that did not include the photobleached area. Hence, I_{pre} and I_{post} were a result of the relation of the mean intensity in the photobleached (I_p) and in the non-photobleached (I_{np}) ROIs, therefore giving the following equation (Equation 4):

$$(4)\ E = 1 - \frac{\left(\frac{I_p}{I_{np}}\right)_{pre}}{\left(\frac{I_p}{I_{np}}\right)_{post}}$$

Acknowledgments

The authors are grateful for the funding from the European Commission (NMP-2014-646075, HEALTH-F4-2011-278557, PITN-GA-2012-317306 and MSCA-ITN-2014-642687), MINECO of the Spanish Government (MAT2016-78903-R, MAT2016-79435-R,

MAT2013-42473-R, MAT2013-41723-R and MAT2012-38043), Junta de Castilla y León (VA244U13 and VA313U14) and Centro en Red de Medicina Regenerativa y Terapia Celular de Castilla y León. We also want to thank Cristina Sánchez Vicente for her help in acquiring and processing confocal images.

Supporting Information

Supporting information is available free of charge on the ACS Publications Website. Schematic representation of SELR-FPs, physicochemical characterization data regarding SELR-FPs, comparison of the mechanical properties with SELR only and absorbance spectra of both SELR-FPs.

Conflicts of interest

The authors declare no competing financial interest.

List of abbreviations

ELR: elastin-like recombinamer

SELR: silk-elastin-like recombinamer

FP: fluorescent protein

AcEGFP: *Aequorea coerulescens* enhanced green fluorescent protein

FRET: Förster resonance energy transfer

Val: valine

Pro: proline

Gly: glycine

T_t: transition temperature

Mw: molecular weight

DSC: differential scanning calorimetry

ε: extinction coefficient

A: absorbance

QY: quantum yield

E: FRET efficiency

λ_{max}: wavelength at excitation/emission maximum

λ_{ex}: excitation wavelength

λ_{em}: emission wavelength

FOV: field of view

ROI: region of interest

F_{DA}: fluorescence intensity of donor at its λ_{max} of excitation in the presence of the acceptor

F_D: fluorescence intensity of donor at its λ_{max} of excitation in the absence of the acceptor

AB: acceptor photobleaching

I_{pre}: fluorescence intensity before acceptor photobleaching

I_{post}: fluorescence intensity after acceptor photobleaching

I_p: fluorescence intensity in a photobleached ROI

I_p: fluorescence intensity in a non-photobleached ROI

References

(1) Ahadian, S., Sadeghian, R. B., Salehi, S., Ostrovidov, S., Bae, H., Ramalingam, M., and Khademhosseini, A. (2015) Bioconjugated Hydrogels for Tissue Engineering and Regenerative Medicine. *Bioconjugate Chemistry 26*, 1984-2001.

(2) Girotti, A., Orbanic, D., Ibáñez-Fonseca, A., Gonzalez-Obeso, C., and Rodríguez-Cabello, J. C. (2015) Recombinant Technology in the Development of Materials and Systems for Soft-Tissue Repair. *Advanced Healthcare Materials 4*, 2423-2455.

(3) Urry, D. W., Cunningham, W. D., and Ohnishi, T. (1974) Studies on the conformation and interactions of elastin. Proton magnetic resonance of the repeating pentapeptide. *Biochemistry 13*, 609-16.

(4) Yeo, G. C., Aghaei-Ghareh-Bolagh, B., Brackenreg, E. P., Hiob, M. A., Lee, P., and Weiss, A. S. (2015) Fabricated Elastin. *Advanced Healthcare Materials 4*, 2530-2556.

(5) Kowalczyk, T., Hnatuszko-Konka, K., Gerszberg, A., and Kononowicz, A. K. (2014) Elastin-like polypeptides as a promising family of genetically-engineered protein based polymers. *World Journal of Microbiology and Biotechnology 30*, 2141-2152.

(6) Arias, F. J., Mercedes, S., Alicia, F.-C., Guillermo, P., and Alessandra, G. (2014) Recent Contributions of Elastin-Like Recombinamers to Biomedicine and Nanotechnology. *Current Topics in Medicinal Chemistry 14*, 819-836.

(7) Urry, D. W. (1993) Molecular Machines: How Motion and Other Functions of Living Organisms Can Result from Reversible Chemical

Changes. *Angewandte Chemie International Edition in English 32*, 819-841.

(8) Ribeiro, A., Arias, F. J., Reguera, J., Alonso, M., and Rodríguez-Cabello, J. C. (2009) Influence of the Amino-Acid Sequence on the Inverse Temperature Transition of Elastin-Like Polymers. *Biophysical Journal 97*, 312-320.

(9) McDaniel, J. R., Radford, D. C., and Chilkoti, A. (2013) A Unified Model for De Novo Design of Elastin-like Polypeptides with Tunable Inverse Transition Temperatures. *Biomacromolecules 14*, 2866-2872.

(10) Herrero-Vanrell, R., Rincón, A. C., Alonso, M., Reboto, V., Molina-Martinez, I. T., and Rodríguez-Cabello, J. C. (2005) Self-assembled particles of an elastin-like polymer as vehicles for controlled drug release. *Journal of Controlled Release 102*, 113-122.

(11) Martín, L., Castro, E., Ribeiro, A., Alonso, M., and Rodríguez-Cabello, J. C. (2012) Temperature-Triggered Self-Assembly of Elastin-Like Block Co-Recombinamers:The Controlled Formation of Micelles and Vesicles in an Aqueous Medium. *Biomacromolecules 13*, 293-298.

(12) Putzu, M., Causa, F., Nele, V., Torre, I. G. d., Rodriguez-Cabello, J. C., and Netti, P. A. (2016) Elastin-like-recombinamers multilayered nanofibrous scaffolds for cardiovascular applications. *Biofabrication 8*, 045009.

(13) Martín, L., Alonso, M., Girotti, A., Arias, F. J., and Rodríguez-Cabello, J. C. (2009) Synthesis and Characterization of Macroporous Thermosensitive Hydrogels from Recombinant Elastin-Like Polymers. *Biomacromolecules 10*, 3015-3022.

(14) Cappello, J., Crissman, J., Dorman, M., Mikolajczak, M., Textor, G., Marquet, M., and Ferrari, F. (1990) Genetic Engineering of Structural Protein Polymers. *Biotechnology Progress 6*, 198-202.

(15) Fernández-Colino, A., Arias, F. J., Alonso, M., and Rodríguez-Cabello, J. C. (2014) Self-Organized ECM-Mimetic Model Based on an Amphiphilic Multiblock Silk-Elastin-Like Corecombinamer with a Concomitant Dual Physical Gelation Process. *Biomacromolecules 15*, 3781-3793.

(16) Gurskaya, N. G., Fradkov, A. F., Pounkova, N. I., Staroverov, D. B., Bulina, M. E., Yanushevich, Y. G., Labas, Y. A., Lukyanov, S., and Lukyanov, K. A. (2003) A colourless green fluorescent protein homologue from the non-fluorescent hydromedusa Aequorea coerulescens and its fluorescent mutants. *Biochemical Journal 373*, 403-408.

(17) Cormack, B. P., Valdivia, R. H., and Falkow, S. (1996) FACS-optimized mutants of the green fluorescent protein (GFP). *Gene 173*, 33-38.

(18) Shcherbo, D., Shemiakina, I. I., Ryabova, A. V., Luker, K. E., Schmidt, B. T., Souslova, E. A., Gorodnicheva, T. V., Strukova, L., Shidlovskiy, K. M., Britanova, O. V.*, et al.* (2010) Near-infrared fluorescent proteins. *Nat Meth 7*, 827-829.

(19) Kobayashi, H., Ogawa, M., Alford, R., Choyke, P. L., and Urano, Y. (2010) New Strategies for Fluorescent Probe Design in Medical Diagnostic Imaging. *Chemical Reviews 110*, 2620-2640.

(20) Lakowicz, J. R. (2006) *Principles of Fluorescence Spectroscopy*, 3 ed., Springer US.

(21) Day, R. N., and Davidson, M. W. (2012) Fluorescent proteins for FRET microscopy: Monitoring protein interactions in living cells. *BioEssays 34*, 341-350.

(22) Fujita, Y., Funabashi, H., Mie, M., and Kobatake, E. (2007) Design of a Thermocontrollable Protein Complex. *Bioconjugate Chemistry 18*, 1619-1624.

(23) Obeng, E. M., Dullah, E. C., Danquah, M. K., Budiman, C., and Ongkudon, C. M. (2016) FRET spectroscopy-towards effective biomolecular probing. *Analytical Methods 8*, 5323-5337.

(24) Hsieh, H. V., Sherman, D. B., Andaluz, S. A., Amiss, T. J., and Pitner, J. B. (2012) Fluorescence Resonance Energy Transfer Glucose Sensor from Site-Specific Dual Labeling of Glucose/Galactose Binding Protein Using Ligand Protection. *Journal of Diabetes Science and Technology 6*, 1286-1295.

(25) Voss, S., Fischer, R., Jung, G., Wiesmüller, K.-H., and Brock, R. (2007) A Fluorescence-Based Synthetic LPS Sensor. *Journal of the American Chemical Society 129*, 554-561.

(26) Hussain, S. A., Dey, D., Chakraborty, S., Saha, J., Roy, A. D., Chakraborty, S., Debnath, P., and Bhattacharjee, D. (2015) Fluorescence Resonance Energy Transfer (FRET) sensor. *Journal of Spectroscopy and Dynamics 5*.

(27) Carlson, H. J., and Campbell, R. E. (2009) Genetically encoded FRET-based biosensors for multiparameter fluorescence imaging. *Current Opinion in Biotechnology 20*, 19-27.

(28) Christensen, T., Hassouneh, W., Trabbic-Carlson, K., and Chilkoti, A. (2013) Predicting Transition Temperatures of Elastin-Like Polypeptide Fusion Proteins. *Biomacromolecules 14*, 1514-1519.

(29) Pal, S. (2014) Mechanical Properties of Biological Materials, in *Design of Artificial Human Joints & Organs* pp 23-40, Springer US, Boston, MA.

(30) Suzuki, A., Badger, B. L., Haase, J., Ohashi, T., Erickson, H. P., Salmon, E. D., and Bloom, K. (2016) How the kinetochore couples microtubule force and centromere stretch to move chromosomes. *Nat Cell Biol 18*, 382-392.

(31) Hildebrandt, N. (2013) How to Apply FRET: From Experimental Design to Data Analysis, in *FRET – Förster Resonance Energy Transfer* pp 105-163, Wiley-VCH Verlag GmbH & Co. KGaA.

(32) Rodriguez-Cabello, J. C., Girotti, A., Ribeiro, A., and Arias, F. J. (2012) Synthesis of genetically engineered protein polymers (recombinamers) as an example of advanced self-assembled smart materials. *Methods in molecular biology 811*, 17-38.

(33) Bajar, B. T., Wang, E. S., Zhang, S., Lin, M. Z., and Chu, J. (2016) A Guide to Fluorescent Protein FRET Pairs. *Sensors (Basel, Switzerland) 16*.

5. SUPPORTING INFORMATION

Table of contents

Table S1. Abbreviated amino acid sequence of each SELR-FP.

Table S2. Theoretical and calculated amino acid composition of SELR-AcEGFP.

Table S3. Theoretical and calculated amino acid composition of SELR-eqFP650.

Table S4. Fold increase of the storage modulus (*G'*) of SELR-based hydrogels in comparison to each SELR-FP at two different concentrations.

Table S5. FRET efficiencies of SELR-FPs 1:1 molar mixtures at different concentrations and temperatures.

Table S6. Comparison between experimental and estimated data for the H-NMR spectrum of SELR-AcEGFP.

Table S7. Comparison between experimental and estimated data for the H-NMR spectrum of SELR-eqFP650.

Figure S1. Schematic representation of both SELR-FPs.

Figure S2. SDS-PAGE of both SELR-FPs.

Figure S3. MALDI-TOF spectra of both SELR-FPs.

Figure S4. H-NMR spectra of both SELR-FPs.

Figure S5. DSC spectra of both SELR-FPs.

Figure S6. Absorbance spectra of both SELR-FPs.

Figure S7. Comparison of FRET efficiencies at 200 mg/mL at different temperatures.

Table S1. Abbreviated amino acid sequence and molecular weight (*Mw*) of each SELR-FP. The sequence corresponding to elastin-like blocks is represented in blue, while the one for silk-like domains is denoted in purple. The sequence of each FP is written in green (AcEGFP) or red (eqFP650).

ELR	abbreviated amino acid sequence	*Mw* (Da)
SELR-AcEGFP	MESLLP-{[(VPGVG)$_2$-VPGEG-(VPGVG)$_2$]$_{10}$-(VGIPG)$_{60}$-[V(GAGAGSG)$_5$]$_2$G}-VMASKGEELFTGVVPILVELDGDVN GHKFSVSGEGEGDATYGKLTLKFICTTGKLPVPWPTLVTTL TYGVQCFSRYPDHMKQHDFFKSAMPEGYIQERTIFFEDDG NYKSRAEVKFEGDTLVNRIELTGTDFKEDGNILGNKMEYNY NAHNVYIMTDKAKNGIKVNFKIRHNIEDGSVQLADHYQQ NTPIGDGPVLLPDNHYLSTQSALSKDPNEKRDHMILLEFVT AAGITHGMDELYKV	128,737
SELR-eqFP650	MESLLP-{[(VPGVG)$_2$-VPGEG-(VPGVG)$_2$]$_{10}$-(VGIPG)$_{60}$-[V(GAGAGSG)$_5$]$_2$G}-VMGEDSELISENMHMKLYMEGTVN GHHFKCTSEGEGKPYEGTQTAKIKVVEGGPLPFAFDILATSF MYGSKTFINHTQGIPDFFKQSFPEGFTWERITTYEDGGVLTA TQDTSLQNGCLIYNVKINGVNFPSNGPVMQKKTLGWEAST EMLYPADSGLRGHSQMALKLVGGGYLHCSLKTTYRSKKPAK NLKMPGFYFVDRKLERIKEADKETYVEQHEMAVARYCDLPS KLGHSV	128,048

Table S2. Theoretical and calculated absolute amino acid composition of SELR-AcEGFP. Data regarding Cys (C) and Trp (W) are missing due to experimental issues.

amino acid	theoretical	calculated	difference (%)
D+N	18+14	21.53	-32.7
E+Q	38+7	49.00	8.9
S	31	24.74	-20.2
H	9	6.30	-30.0
G	524	562.18	7.3
T	18	11.66	-35.2
R	6	7.49	24.8
A	50	50.55	1.1
Y	11	8.68	-21.1
C	2	-	-

V	321	329.23	2.6
M	8	7.73	-3.4
W	1	-	-
F	12	8.44	-29.7
I	133	136.07	2.3
L	21	18.91	-10.0
K	18	13.68	-24.0
P	231	231.93	0.4
TOTAL	**1473**	**1488.12**	**1.0**

Table S3. Theoretical and calculated absolute amino acid composition of SELR-eqFP650.

amino acid	theoretical	calculated	difference (%)
D+N	9+9	18.69	3.8
E+Q	39+8	52.19	11.0
S	36	33.13	-8.0
H	8	5.50	-31.3
G	528	547.70	3.7
T	18	15.31	-14.9
R	6	10.63	77.2
A	51	52.51	3.0
Y	11	8.63	-21.5
C	4	4.56	14.0
V	317	315.42	-0.5
M	11	10.63	-3.4
W	2	1.97	-1.5
F	12	8.38	-30.2
I	129	127.02	-1.5
L	20	18.38	-8.1
K	20	15.25	-23.8
P	232	232.17	0.1
TOTAL	**1470**	**1478.07**	**0.5**

Table S4. Fold increase of the storage modulus (*G'*) of SELR-based hydrogels in comparison to each SELR-FP at two different concentrations.

concentration (mM)	*G'* fold increase compared to SELR only		
	SELR-AcEGFP	SELR-eqFP650	1:1 mixture
1.13	2.63	2.35	2.36
1.73	1.30	1.36	1.40

Table S5. FRET efficiencies of SELR-FPs 1:1 molar mixtures at different concentrations and temperatures. FRET efficiencies are represented as mean ± SD (n = 2).

concentration (mg/mL)	temperature (ºC)	FRET efficiency (mean ± SD)
	15	0
	37	0
	15	0.247 ± 0.008
	37	0.330 ± 0.156
	15	0.201 ± 0.026
	37	0.246 ± 0.043
	15	0.182 ± 0.014
	23	0.185 ± 0.012
	37	0.212 ± 0.007

Table S6. Comparison between the predicted value of each type of hydrogen in SELR-AcEGFP and the experimental values found by integration of each peak in the corresponding H-NMR spectrum (see Figure S4).

type of hydrogen	predicted value	measured value
-CH3	1026	Reference
-CH- and -CH2-	1591	1383
-NH2	454	371

Table S7. Comparison between the predicted value of each type of hydrogen in SELR-eqFP650 and the experimental values found by integration of each peak in the corresponding H-NMR spectrum (see Figure S4).

type of hydrogen	predicted value	measured value
-CH3	1012	Reference
-CH- and -CH2-	1594	1330
-NH2	451	413

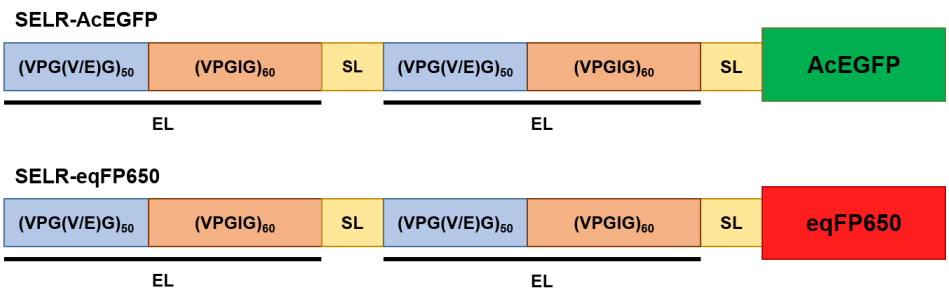

Figure S1. Schematic representation of both SELR-FPs. SL stands for silk-like, while EL means elastin-like.

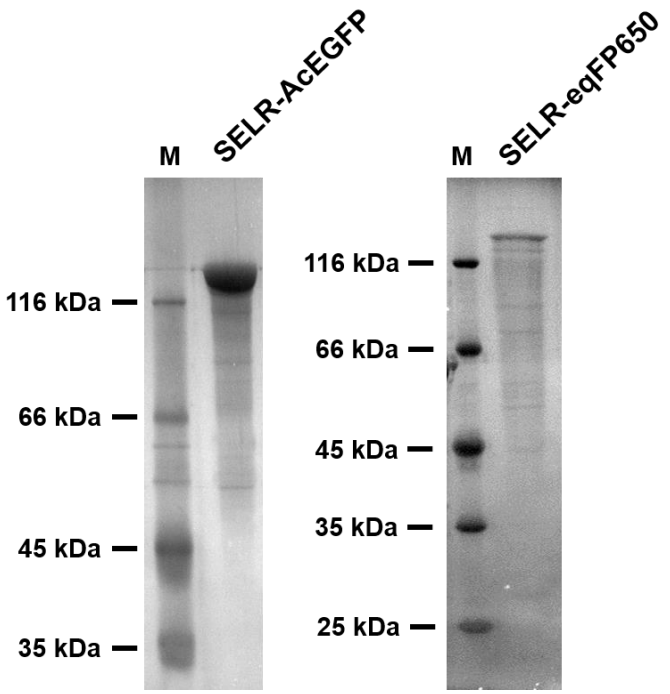

Figure S2. SDS-PAGE of both SELR-FPs showing a good correlation between the observed M_w and the theoretical one: 128.7 and 128.1 kDa for SELR-AcEGFP and SELR-eqFP650, respectively.

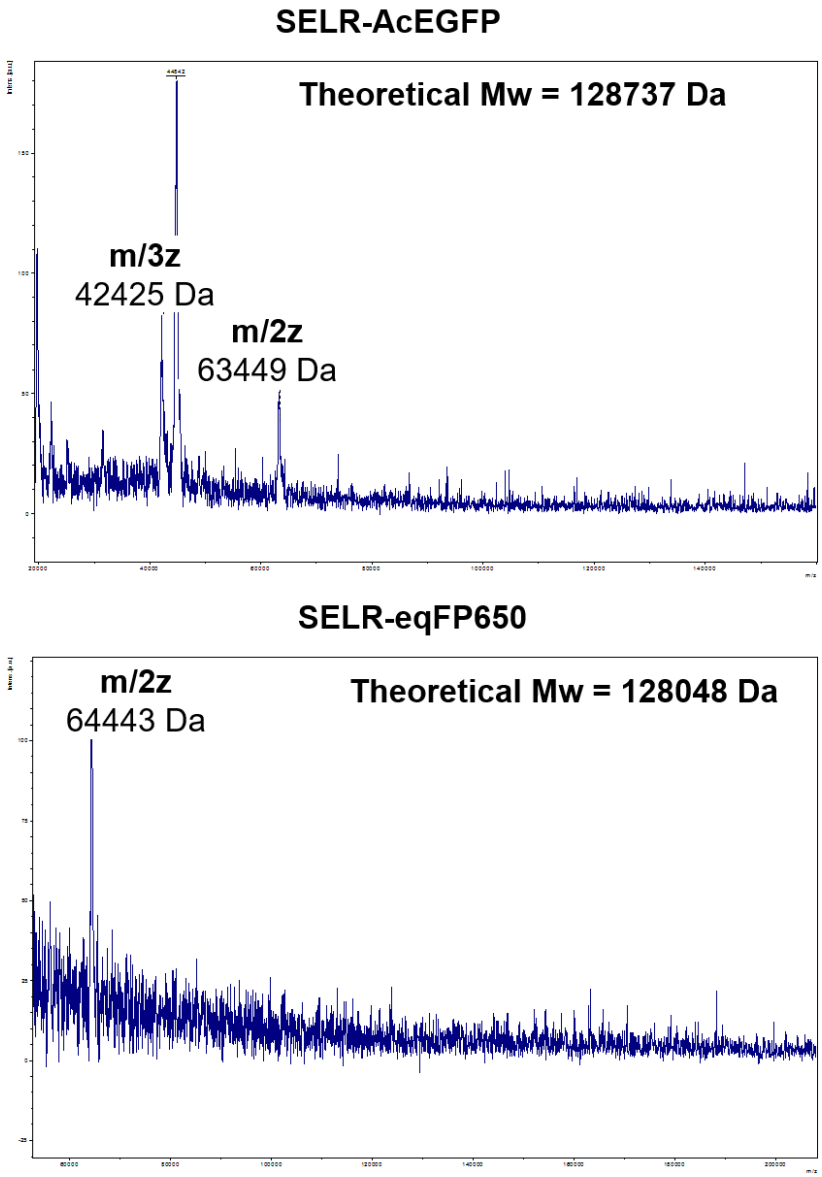

Figure S3. MALDI-TOF spectra of both SELR-FPs. It can be observed that only the doubly charged recombinamers were detected, but it confirms the agreement between the experimental and the expected M_w.

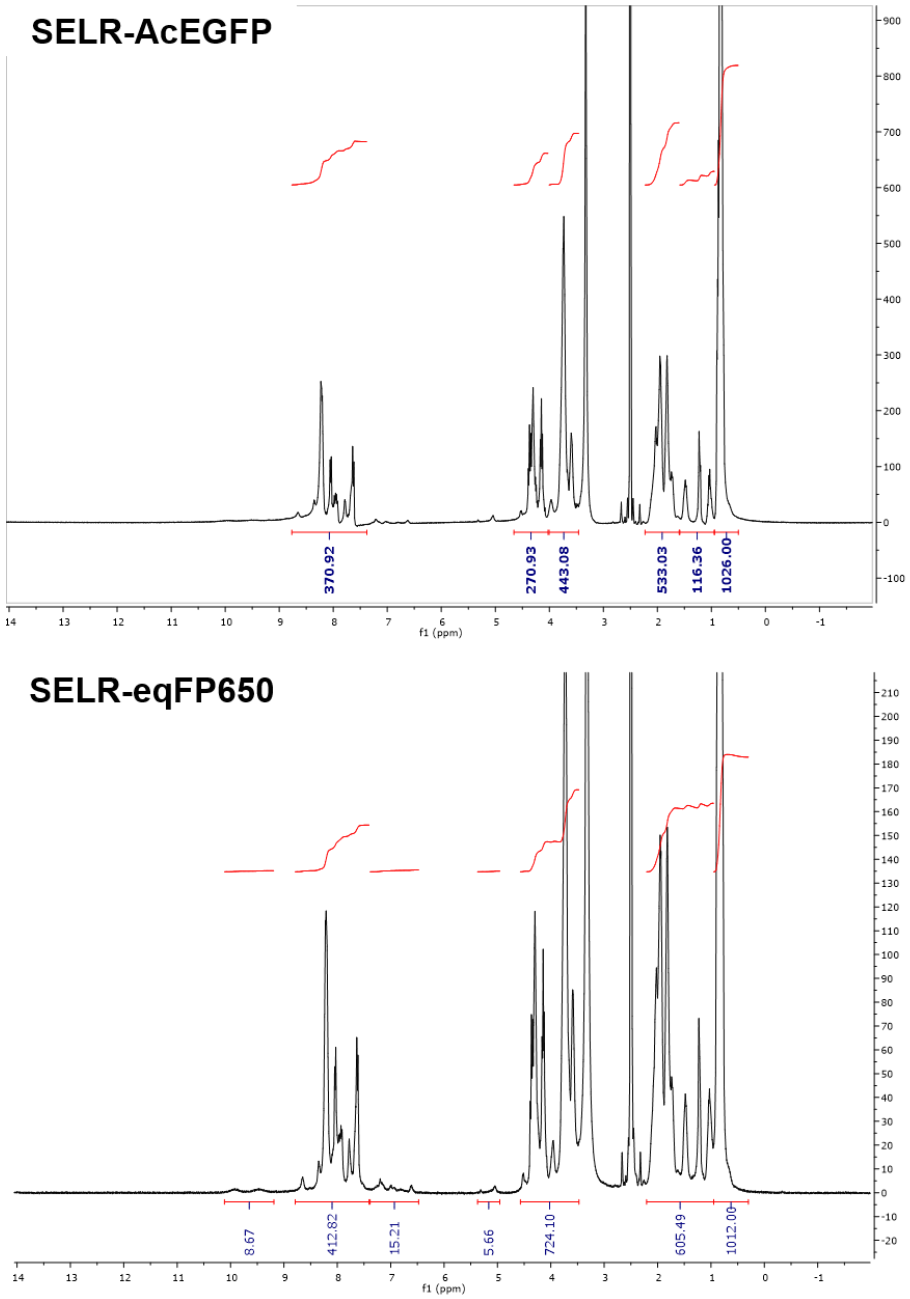

Figure S4. H-NMR spectra of both SELR-FPs. The peak corresponding to protons in -CH_3 groups (0.5-0.95 ppm) is used as integration reference by assigning the theoretical proton number. No contaminants derived from the bioproduction and purification processes could be observed in any case.

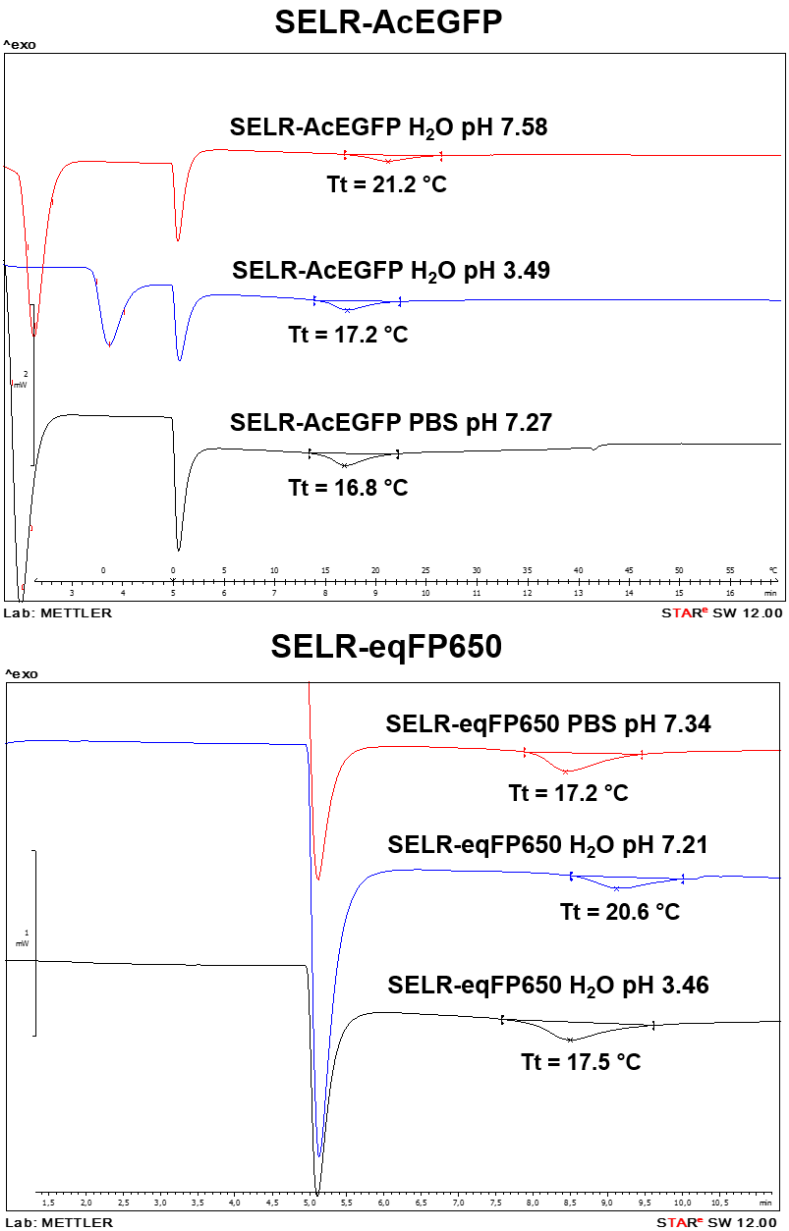

Figure S5. DSC spectra of both SELR-FPs indicating the T_t at 50 mg/mL and different solvent conditions. As expected, the T_t is lower at acid pH in ultra-pure water due to protonation of the carboxyl group present in glutamic acid residues included in the elastin-like blocks. This result was also observed for the SELRs dissolved in the presence of salts (PBS, 137 mM NaCl, 10 mM Na_2HPO_4, 1.8 mM KH_2PO_4, and 2.7 mM KCl) due to the salting out effect.

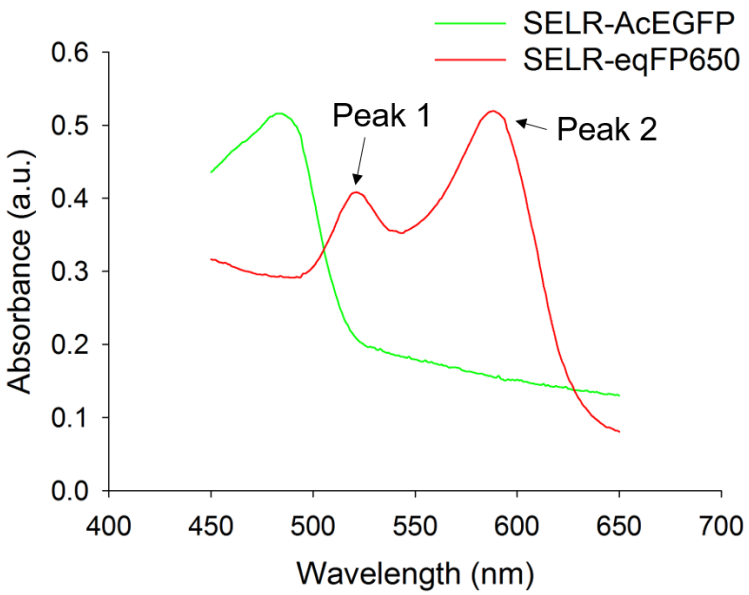

Figure S6. Absorbance spectra of both SELR-FPs dissolved in ultra-pure water at 10 mg/mL ($7.77 \cdot 10^{-5}$ and $7.81 \cdot 10^{-5}$ M for SELR-AcEGFP and SELR-eqFP650, respectively). Both measurements were performed in 1-cm light path cuvettes at 37ºC. SELR without fusion to FPs was used as reference.

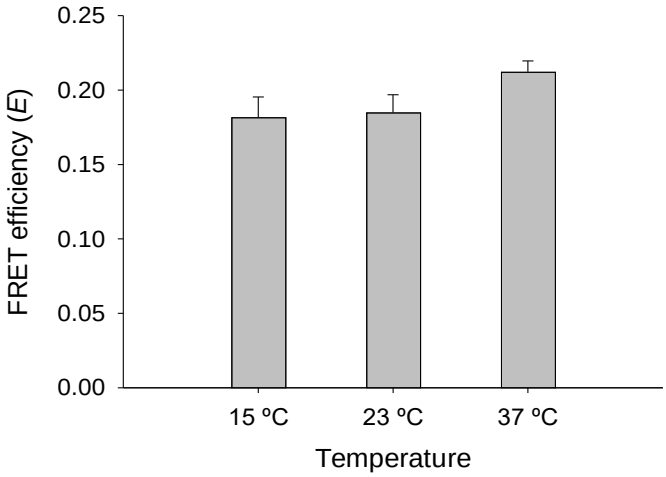

Figure S7. Comparison of FRET efficiencies at 200 mg/mL at different temperatures, below (15ºC) and above the T_t (23 and 37ºC). Not significant differences were found in every case.

FUTURE DIRECTIONS AND CONCLUSIONS

Future directions

1. ELR-based hydrogels for skeletal muscle regeneration

Once the biocompatibility of both physically and chemically cross-linked ELR-based hydrogels has been confirmed, and taking into account the good outcomes found in the regeneration of bone tissue, new opportunities arise regarding the use of hydrogel-forming ELRs for the regeneration of other different tissues, such as skeletal muscle. This tissue may suffer diverse types of injuries, including volumetric muscle loss (VML), which implies losing at least the 20% of the total muscle mass (1). The complexity of the regeneration process of VML defects, including immunological regulation, might lead to an imbalance in which too much collagen deposition induces the formation of a non-functional scar-like fibrotic tissue, which hinders nutrient diffusion and myoblast migration and differentiation to form myofibers (2). Current therapies involve the use of autologous muscle to fill VML injuries, which presents several limitations, such as lack of availability of tissue for transplantation and the high co-morbidity of the donor tissue (3). Therefore, novel therapeutic approaches have been developed recently, including the use of stem cells, biomaterials (including hydrogels), or a combination of both of them, to promote an optimal skeletal muscle regeneration (4). In our case, we aim to elucidate the ability of ELR-based hydrogels, combined or not with MSCs, to improve muscle regeneration after the creation of a defect in the tibialis anterior muscle of rats (5).

Preliminary results concerning the use of biodegradable and non-biodegradable hydrogels based on ELRs, stabilized either by physical or chemical cross-linking, loaded or not with hMSCs (8 different conditions, Table 1), showed the formation of new myogenic fibers after 14 days, by the calculation of the percentage of cells with internal nuclei after hematoxylin-eosin staining (Figure 1), which is known to be characteristic of growing myofibers (6).

Table 1. Summary of the treatments used in preliminary studies regarding ELR-mediated skeletal muscle regeneration.

Treatment	Cross-linking	Biodegradable	hMSCs
A	Chemical	No	Yes
B	Chemical	No	No
C	Physical	No	Yes
D	Physical	No	No
E	Chemical	Yes	Yes
F	Chemical	Yes	No
G	Physical	Yes	Yes
H	Physical	Yes	No

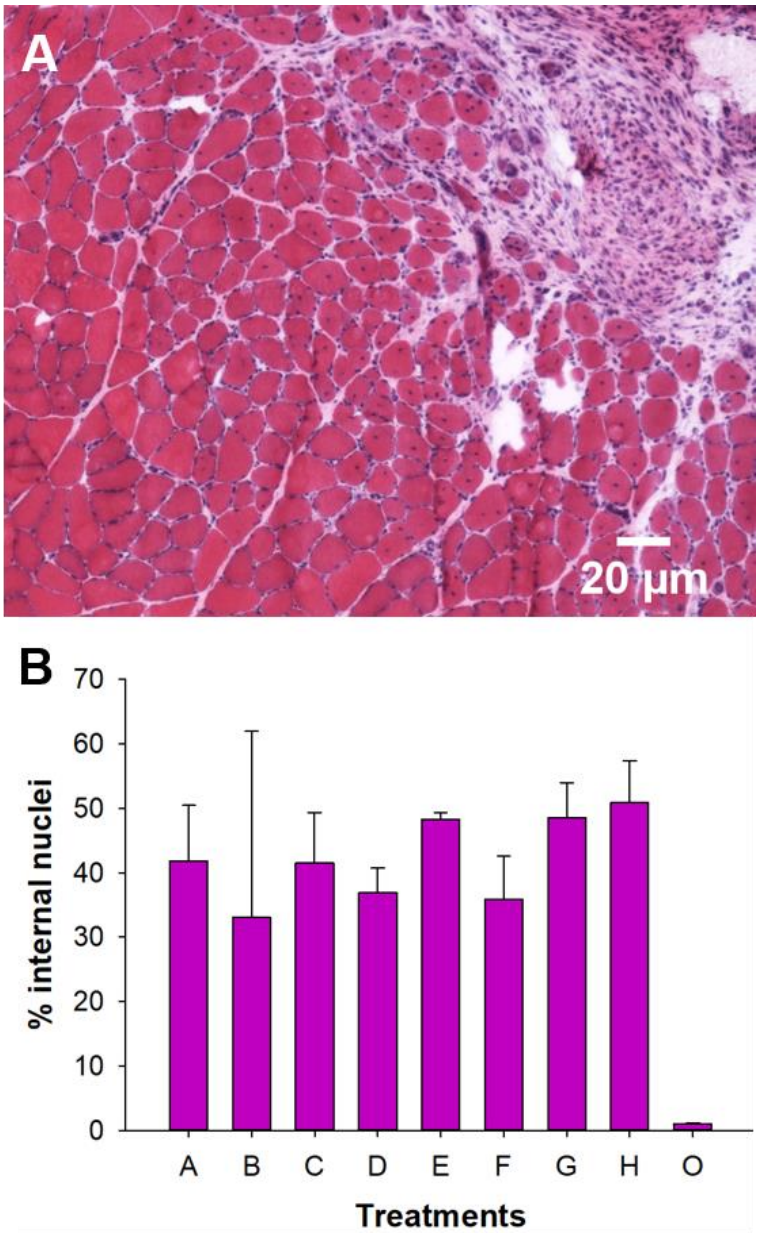

Figure 1. A) Microphotograph showing the interface area between regenerating muscle and remaining defect after 14 days. B) Percentage of cells containing internal nuclei in the defect site after 14 days.

Furthermore, non-biodegradable hydrogels were clearly observed after 14 days, and the defect was partially filled with

myofibers, still containing a high volume of hydrogel (Figure 2). On the other hand, biodegradable ELR-based hydrogels were not so obviously identified, but the defect was almost filled by muscle tissue in most of the samples.

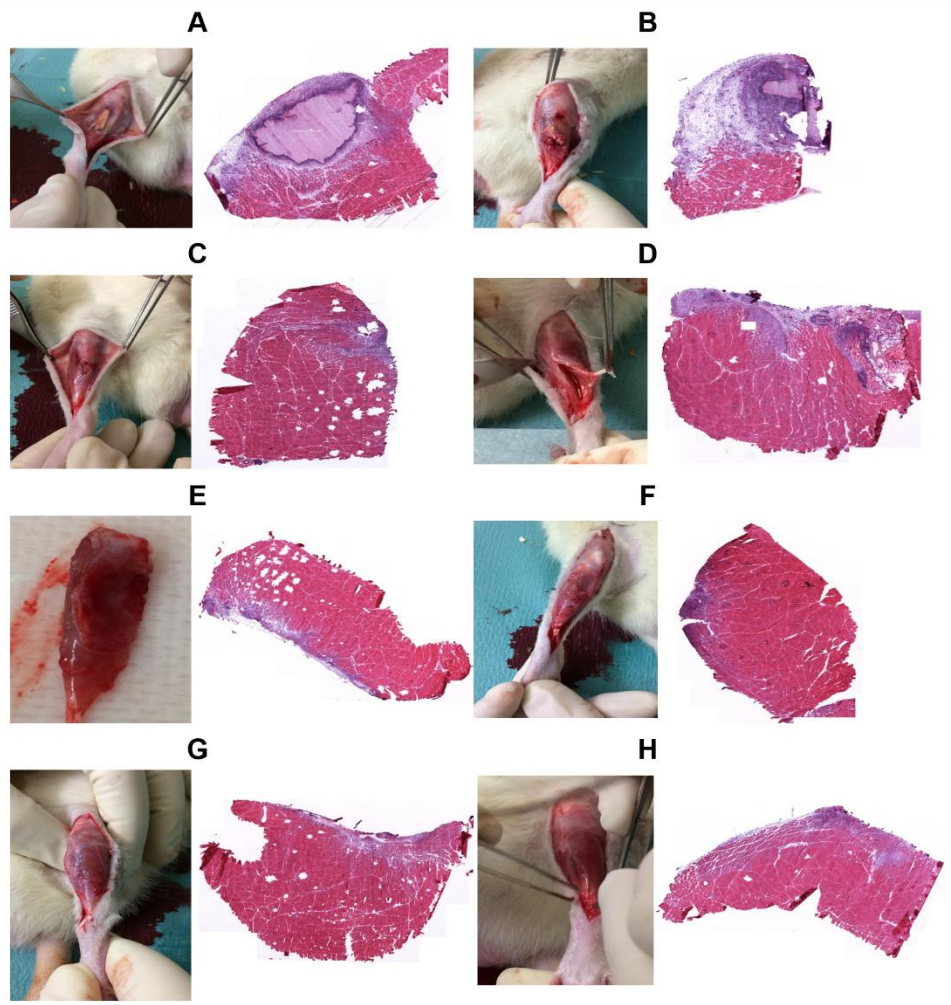

Figure 2. Photographs of the muscles during extraction (left) and microphotographs of hematoxilin-eosin stained sections (right) for every condition (A-H) at 14 days post-surgery.

In conclusion, these preliminary results show that skeletal muscle regeneration might be enhanced by the treatment of VML

defects with ELR-based hydrogels. Furthermore, no differences were observed after 14 days between MSC-laden and empty hydrogels, hence suggesting that tissue repair could be driven by endogenous progenitor cells, such as $Pax7^+$, that could be able to migrate inside the hydrogels and to differentiate into novel myofibers within them. However, further experiments should be performed in order to corroborate these results, including appropriate controls, and to shed light on the role of the immune response during regeneration, i.e. the balance between M1 and M2 macrophages, and on the functionality of the restored muscle.

2. Investigation of pore dynamics in SELR-based hydrogels

Recently, porosity and pore size have been proposed as key parameters in the design of hydrogels for tissue engineering and regenerative medicine (7). In this regard, it is widely accepted that hydrogels require a high porosity and interconnectivity to achieve a homogeneous cell distribution and cell proliferation (7). For instance, ECM secretion has been shown to increase by incrementing the pore size of gelatin hydrogels (8). Finally, yet importantly, pore size has been found to influence vascularization (9), which is a fundamental event in tissue regeneration. Therefore, many methods have been developed in order to modulate pore size and global porosity of different scaffolds to achieve a desired tissue/cell interaction (7). However, most of them require several cytotoxic steps that limit the feasibility of embedding cells inside the scaffolds, e.g. hydrogels, during their formation. Moreover, those methods may restrict critically the injectability of biomaterials.

In our case, we have found that a specific SELR construction was able to form hydrogels whose pores undergo an evolution over time, by increasing largely the pore size, as observed through fluorescence microscopy (Nikon Eclipse Ti-E coupled to a Nikon DS-2MBWc digital camera) when the SELR-based hydrogel was combined with a 2% of the SELR-AcEGFP described in Chapter 4 (Figure 3). This is thought to be a consequence of the different kinetics of the inverse temperature transition (ITT) undergone by the elastin-like domains, and the one of the β-sheet formation between silk-like motifs (10), which, eventually, stabilize the hydrogel network.

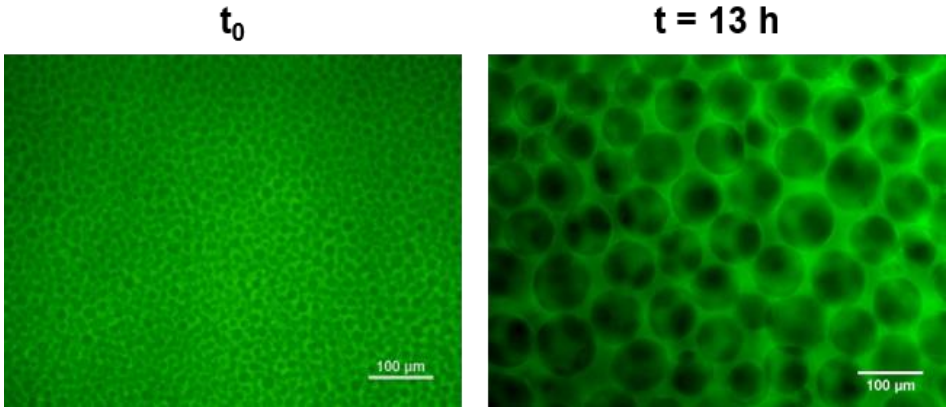

Figure 3. Start (left) and endpoint (right) of the gelation process undergone by a SELR-based hydrogel.

We hypothesize that this phenomenon is a result of a number of steps. First, a phase separation (namely, an ITT) happens above the T_t (also known as lower critical solution temperature, LCST). This involves an entropically driven transition of the SELR molecules leading to coacervation upon rupture of water-based clathrate-like structures surrounding apolar amino acids in the elastin-like blocks, which subsequently results in the hydrophobic

interaction between these apolar residues, as described before (11). On the other hand, this process can be also explained through spinodal decomposition, which implies that phase separation is merely driven by diffusional forces once the spinodal curve (defined as the points at a given temperature and solute concentration at which two phases coexist) has been surpassed (above the T_t or LCST) (12). Therefore, at this early stage, we can consider a liquid-liquid system, composed of water and coacervated SELR molecules (considered as a fluid), which tend to segregate due to thermodynamic instability caused by the difference in density and viscosity between both fluids, and by the hydrophobicity of the coacervate (12). Subsequently, late stages of spinodal decomposition involve a percolation-to-cluster transition, with the water phase forming a droplet morphology in order to reduce the interfacial tension/free energy of the system: less surface area (droplet or sphere) leads to a lower tension/free energy (13-15). Then, a confined growth happens, leading to an evolution of the microstructure by coarsening, mainly coalescence (driven by diffusion), of the water droplets inside the hydrogel (12). Finally, these water droplets become trapped at a non-equilibrium stage (meaning that they tend to segregate from the hydrogel network since they do not interact with it) due to “pinning” or “arresting” (12, 16) of the coarsening of the structure due to gelation (13), in this case as a consequence of silk annealing or crystallization (10). At the molecular level, this crystallization is due to the formation of hydrogen bonds, which leads to a β-sheet organization. Furthermore, it implies an increase in the enthalpy of the SELR-rich phase that forms the hydrogel network, which eventually

results in the creation of an enthalpic barrier that oppose diffusion of water droplets to coalesce, hampering further coarsening, thus "pinning" (stopping) the hydrogel structure (16).

Similarly, Glassman *et al*. have reported the formation of hydrogels through arrested phase separation of an ELR containing L-Alanine as guest residue, in combination with L-Isoleucine (17), although this effect is observed at the nanoscale by small angle neutron scattering (SANS), and it occurs fast enough to avoid coarsening, hence impeding the increase of pore size. Nevertheless, it supports the idea that an "arrester" or "pinner" is needed to stabilize the hydrogel network and to elude complete phase separation. In the mentioned work, this "arrester" is L-Ala, which leads to a plastic behaviour by the ELR, probably due to the formation of other non-covalent bonds than hydrophobic interactions (e.g. hydrogen bonds), whereas in our case silk-like domains act as "arresters". The slower kinetics of β-sheet formation by these latter motifs allows an evolution of the microstructure towards the formation of pores whose size increases over time through coarsening until full thermodynamic arrest. This also highlights the relation between the nano (i.e. formation of hydrogen bonds in β-sheets) and the microscale (i.e. pore size evolution).

Regarding the quantitative assessment of the evolution of pore size over time, the use of real-time fluorescence microscopy methods, taking advantage of the availability of fluorescent SELRs (see Chapter 4) that can be used as labels for other SELRs, extremely facilitates the study. Pictures may be analyzed with image processing softwares, such as ImageJ, and the procedure can be

easily automated by designing specific macros or plugins. A scheme of the image processing analysis might be observed in Figure 4.

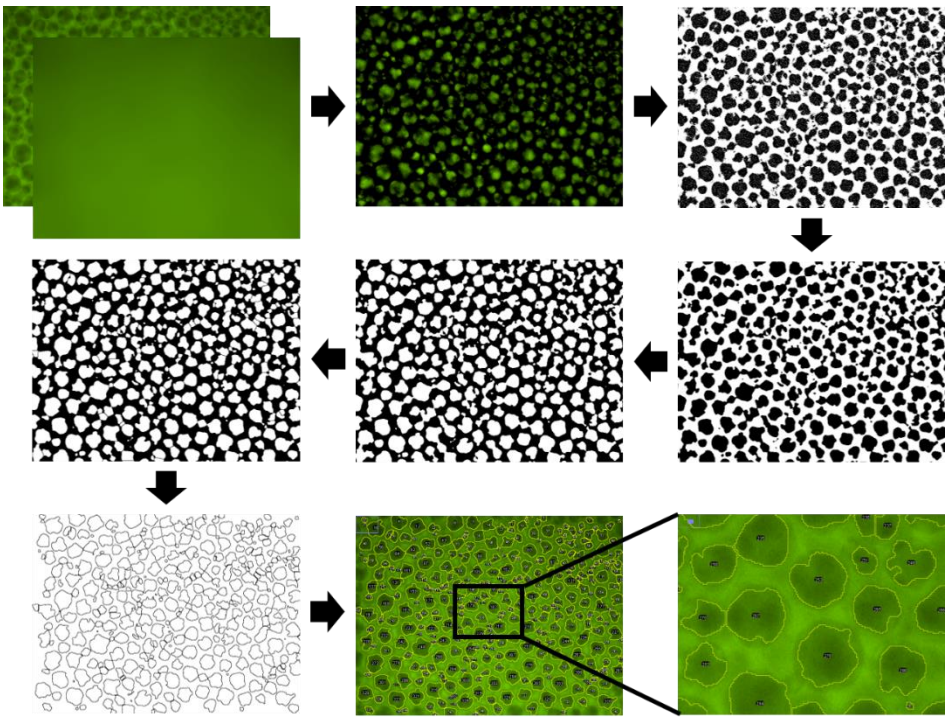

Figure 4. Schematic representation of the steps followed for the analysis of pore size in images showing hydrogel microstructure with a Fiji distribution of ImageJ (version 1.51p).

Furthermore, this automatic processing through real-time fluorescence microscopy and imaging software might permit the high-throughput screening of pore sizes at different conditions, such as SELR concentration, solvent, etc. Preliminarily, we have observed that at a concentration of 175 mg/mL, pore size increases from a few μm to approximately 70 μm over 16 h.

Ultimately, these hydrogels may be used in tissue engineering and regenerative applications, since they are able to support cell attachment (Figure 5), and presumably cell growth, due

to the inclusion of RGD cell-adhesion sequences within the SELR molecule.

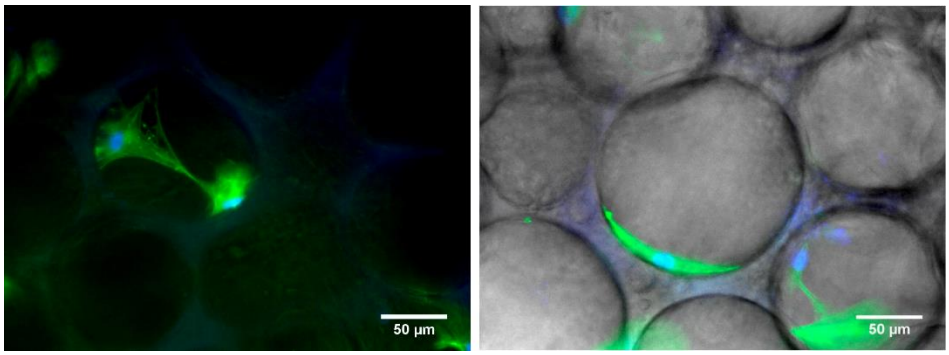

Figure 5. hMSCs attached to the walls of the pores of the SELR-based hydrogels 14 days post-seeding. Actin is stained in green with Phalloidin-Alexa Fluor® 488, while nuclei are stained in blue with DAPI.

In summary, biomimetic SELR-based hydrogels with evolving pore sizes can be of great utility to study the dual self-assembly of SELR molecules. This self-assembly is characterized by a rapid phase transition of the elastin-like blocks, followed by a partial arrest of the process and a gradual strengthen of the network through the formation of β-sheets between silk domains, until complete arrest. Moreover, this phenomenon can be studied by simple methods, such as real-time fluorescence microscopy, giving new insights about their formation. In addition, the modification of different parameters, like SELR concentration, temperature, etc., may lead to the formation of scaffolds with diverse controlled pore sizes. Further studies regarding silk crystallization should be performed in order to correlate empirically the evolution of the microstructure and the formation of β-sheets.

References

1. Turner NJ, Badylak SF. Regeneration of skeletal muscle. Cell and Tissue Research. 2012;347(3):759-74.

2. Souza Jd, Gottfried C. Muscle injury: Review of experimental models. Journal of Electromyography and Kinesiology. 2013;23(6):1253-60.

3. Beier JP, Stern-Straeter J, Foerster VT, Kneser U, Stark GB, Bach AD. Tissue Engineering of Injectable Muscle: Three-Dimensional Myoblast-Fibrin Injection in the Syngeneic Rat Animal Model. Plastic and Reconstructive Surgery. 2006;118(5):1113-21.

4. Longo UG, Loppini M, Berton A, Spiezia F, Maffulli N, Denaro V. Tissue Engineered Strategies for Skeletal Muscle Injury. Stem Cells International. 2012;2012:13.

5. Wu X, Corona BT, Chen X, Walters TJ. A Standardized Rat Model of Volumetric Muscle Loss Injury for the Development of Tissue Engineering Therapies. BioResearch Open Access. 2012;1(6):280-90.

6. Dubowitz V, Sewry C, Oldfors A. Muscle Biopsy: A Practical Approach. 4th ed. Philadelphia, USA: Saunders; 2013.

7. Annabi N, Nichol JW, Zhong X, Ji C, Koshy S, Khademhosseini A, et al. Controlling the Porosity and Microarchitecture of Hydrogels for Tissue Engineering. Tissue Engineering Part B: Reviews. 2010;16(4):371-83.

8. Lien S-M, Ko L-Y, Huang T-J. Effect of pore size on ECM secretion and cell growth in gelatin scaffold for articular cartilage tissue engineering. Acta Biomaterialia. 2009;5(2):670-9.

9. Chiu Y-C, Cheng M-H, Engel H, Kao S-W, Larson JC, Gupta S, et al. The role of pore size on vascularization and tissue remodeling in PEG hydrogels. Biomaterials. 2011;32(26):6045-51.

10. Fernandez-Colino A, Arias FJ, Alonso M, Rodriguez-Cabello JC. Self-organized ECM-mimetic model based on an amphiphilic multiblock silk-elastin-like corecombinamer with a concomitant dual physical gelation process. Biomacromolecules. 2014;15(10):3781-93.

11. Urry DW. What Sustains Life? Consilient Mechanisms for Protein-Based Machines and Materials. Boston (USA): Birkhäuser Boston; 2006.

12. Elbert DL. Liquid–liquid two-phase systems for the production of porous hydrogels and hydrogel microspheres for biomedical applications: A tutorial review. Acta Biomaterialia. 2011;7(1):31-56.

13. Lorén N, Altskär A, Hermansson A-M. Structure Evolution during Gelation at Later Stages of Spinodal Decomposition in Gelatin/Maltodextrin Mixtures. Macromolecules. 2001;34(23):8117-28.

14. Crist B, Nesarikar AR. Coarsening in Polyethylene-Copolymer Blends. Macromolecules. 1995;28(4):890-6.

15. Chandler D. Interfaces and the driving force of hydrophobic assembly. Nature. 2005;437(7059):640-7.

16. Crist B. On “Pinning” Domain Growth in Two-Phase Polymer Liquids. Macromolecules. 1996;29(22):7276-9.

17. Glassman MJ, Olsen BD. Arrested Phase Separation of Elastin-like Polypeptide Solutions Yields Stiff, Thermoresponsive Gels. Biomacromolecules. 2015;16(12):3762-73.

Conclusions

1. Genetic engineering, bioproduction and characterization of hydrogel-forming ELRs

In this thesis, it has been shown the development of several novel hydrogel-forming ELRs with improved bioactivity in terms of cell adhesion, osteogenesis and emission of fluorescence. Regarding cell attachment, a SELR containing RGD domains was designed and bioproduced to form ECM-like hydrogels. In the case of osteoinduction, an elastase-sensitive biodegradable ELR was fused to BMP-2. Finally, in order to achieve fluorescence emission, an SELR was genetically bioconjugated either to a GFP derivative, i.e. AcEGFP, or to eqFP650, a far-red fluorescent protein (FP). All these gene constructions were successfully achieved as evaluated by agarose gel electrophoresis and DNA sequencing. ELRs were further expressed in *Escherichia coli* for bioproduction, obtaining yields from 120 to 400 mg/L of culture media.

Characterization techniques, such as SDS-PAGE and MALDI-TOF, showed good agreement of the experimental molecular weight with the expected one. Moreover, the T_t of the ELRs was assessed through DSC, confirming that it was always below the physiological temperature, hence being able of forming hydrogels when injected *in vivo*. Other methods, like ^{1}H-NMR and HPLC for amino acid analysis reported acceptable results that confirm the purity of each batch of the different ELRs. In addition, the mechanical properties of the hydrogels were easily tunable by changing the concentration of the ELRs.

2. Biocompatibility of ELR-based hydrogels

The wide-ranging biocompatibility of physically or chemically cross-linked ELR-based hydrogels was evaluated through several methods, both *in vitro* and *in vivo*. Specifically, HUVECs were able to proliferate on ELR-coated surfaces over 9 days of culture. Moreover, luciferase-expressing hMSCs embedded within ELR-based hydrogels were injected subcutaneously in mice, and their viability was confirmed through bioluminescence upon injection of luciferin up to 4 weeks. In addition, the subcutaneous injection of ELR-based hydrogels did not promote an inflammatory response, as indicated by the concentrations of the different cytokines tested (TNFα, IL-1β, IL-4, IL-6 and IL-10) in comparison to the negative (PBS) and the positive (LPS) controls. The macroscopic and histological evaluation of ELR-based hydrogels injected *in vivo* further corroborated this outcome, showing optimal stability after 6 months. Besides, a very mild reaction was observed microscopically, showing the lack of a foreign body response for both types of hydrogels, with cell invasion and colonization in a biocompatible manner.

In summary, this work confirms the preliminary biocompatibility of two types of multi-purpose ELR-based hydrogels, being the first step towards the use of both types of ELRs in different applications in the field of tissue engineering and regenerative medicine.

3. Bone regeneration mediated by bioactive and biodegradable hydrogels based on ELRs

The ability of a bioactive and biodegradable ELR-based hydrogel to promote bone regeneration was evaluated. First, two different hydrogel-forming ELRs containing elastase sensitive domains were bioproduced, one containing RGD cell adhesion sequences and the other one including the osteogenic BMP-2. Afterwards, the biodegradation of the mixture of both ELRs was characterized *in vitro* by the enzymatic cleavage with elastase, confirming this feature. Furthermore, the lack cytotoxicity of the ELRs was corroborated by culturing hMSCs in ELR-supplemented culture medium, while cell adhesion on ELR-coated plates was also demonstrated. Finally, femoral bone defects were created in New Zealand rabbits, which were subsequently filled with the hydrogel based on the mixture of both ELRs. Then, samples were extracted after 3 months and the regeneration was assessed by different methods. 3D computed tomography showed complete closure of the defect, with bone calcification, in six out of seven samples, being the remaining one almost fully regenerated. The histological analysis showed the formation of lamellar (compact) bone *de novo* together with pagetoid-like areas with a less organized structure, probably due to the arrangement of the matrix guided by the hydrogel network. Some fragments of the ELR-based hydrogel were still visible, but it was mostly degraded by the action of elastase secreted within the remodeling phase during regeneration.

To conclude, this work confirms the ability of a bioactive and biodegradable hydrogel based on ELRs to regenerate bone tissue, being osteoinductive and osteoconductive.

4. Fluorescence and FRET evaluation of two different SELR-FPs

Two hydrogel-forming fluorescent SELRs have been developed within this thesis by the genetic bioconjugation of two different fluorescent proteins: AcEGFP and eqFP650, giving two different SELR-FPs. Regarding their fluorescence properties, excitation and emission spectra of both recombinamers were similar to the ones of the native FPs, except for some differences in eqFP650 excitation and emission maximum and global spectra, probably due to uncompleted maturation and/or dimerization. Specifically, the finding of a green-shifted peak in the absorption spectrum of SELR-eqFP650, not described in the literature for the native FP, and highly overlapping the emission spectrum of SELR-AcEGFP, motivated the evaluation of a FRET interaction between both SELR-FPs. Thus, the FRET efficiency (E) was calculated by different methods giving dissimilar results possibly because of artifacts derived from the techniques. Furthermore, E values were similar for the conditions tested, hence being independent of the concentration (over a specific mid one) and of the temperature (above or below the T_t).

This work shows evidence on how SELRs fused to different FPs could be used to study E for novel FRET pairs. Moreover, several applications may arise from this work, such as the study of self-assembled ELR-based structures (e.g. particles) and the

development of hydrogels with improved traceability for tissue engineering. Similarly, SELR-FPs may find their use as biosensors, either by themselves or as FRET-pairs, thanks to the feasible addition of binding domains, e.g. to metals or cell structures, due to their recombinant nature.

APPENDIX

Abbreviations

A: absorbance

AB: acceptor photobleaching

AcEGFP: *Aequorea coerulescens* enhanced green fluorescent protein

BMP-2: bone morphogenetic protein-2

CFCG: catalyst-free click gel

CT: computed tomography

DSC: differential scanning calorimetry

E: FRET efficiency

ECM: extracellular matrix

ELbcR: elastin-like block co-recombinamer

ELISA: enzyme-linked immunosorbent assay

ELP: elastin-like polymer

ELR: elastin-like recombinamers

EFI: experimental femoral injury

FBI: femoral bone injury

F_D: fluorescence intensity of donor at its λ_{max} of excitation in the absence of the acceptor

F_{DA}: fluorescence intensity of donor at its λ_{max} of excitation in the presence of the acceptor

FOV: field of view

FP: fluorescent protein

FRET: Förster resonance energy transfer

hMSCs: human mesenchymal stem cells

HPLC: high-performance liquid cromatography

HUVECs: human umbilical vein endothelial cells

H-E: hematoxylin-eosin

I_p: fluorescence intensity in a photobleached ROI

I_p: fluorescence intensity in a non-photobleached ROI

I_{pre}: fluorescence intensity before acceptor photobleaching

I_{post}: fluorescence intensity after acceptor photobleaching

ITC: inverse transition cycle

ITT: inverse temperature transition

LCST: lower critical solution temperature

LPS: lipopolysaccharide

MALDI-TOF: matrix-assisted laser desorption/ionization-time-of-flight

MCST: multi-slice computed tomography

MMP: matrix metalloproteinase

MQ: milliQ ultra-pure water

Mw: molecular weight

NMR: nuclear magnetic resonance

PBS: phosphate buffered saline

QY: quantum yield

ROI: region of interest

SDS-PAGE: sodium dodecyl sulfate-polyacrylamide gel electrophoresis

SELR: silk-elastin-like recombinamers

TCP: tissue culture plate

TERM: tissue engineering and regenerative medicine

TNFα: tumor necrosis factor α

T_t: transition temperature

ε: extinction coefficient

λ_{max}: wavelength at excitation/emission maximum

λ_{ex}: excitation wavelength

λ_{em}: emission wavelength

Table of standard amino acid abbreviations

Amino acid	3-letter code	1-letter code
Alanine	Ala	A
Arginine	Arg	R
Asparagine	Asn	N
Aspartic acid	Asp	D
Cysteine	Cys	C
Glutamic acid	Glu	E

Glutamine	Gln	Q
Glycine	Gly	G
Histidine	His	H
Isoleucine	Ile	I
Leucine	Leu	L
Lysine	Lys	K
Methionine	Met	M
Phenylalanine	Phe	F
Proline	Pro	P
Serine	Ser	S
Threonine	Thr	T
Tryptophan	Trp	W
Tyrosine	Tyr	Y
Valine	Val	V

Publications

2017

- A. Ibáñez-Fonseca, T.L. Ramos, I. González de Torre, L.I. Sánchez-Abarca, S. Muntión, F.J. Arias, M.C. del Cañizo, M.Alonso, F. Sánchez-Guijo, J.C. Rodríguez-Cabello. Biocompatibility of two model elastin-like recombinamer-

based hydrogels formed through physical or chemical crosslinking for various applications in tissue engineering and regenerative medicine. *Journal of Tissue Engineering and Regenerative Medicine* (**2017**). doi: 10.1002/term.2562. Just accepted.

- J.C. Rodriguez-Cabello, A. Ibáñez-Fonseca, M. Alonso, L. Poocza, F. Cipriani, I. González de Torre. Elastin-Like Polymers: Properties, Synthesis, and Applications. *Encyclopedia of Polymer Science and Technology*, 1–36 (**2017**). doi: 10.1002/0471440264.pst656

- D. Pescador, A. Ibáñez-Fonseca, F. Sánchez-Guijo, J.G. Briñón, F.J. Arias, S. Muntión, C. Hernández, A. Girotti, M. Alonso, M.C. del Cañizo, J.C. Rodríguez-Cabello, J.F. Blanco. Regeneration of hyaline cartilage promoted by xenogeneic mesenchymal stromal cells embedded within elastin-like recombinamer-based bioactive hydrogels. *Journal of Materials Science: Materials in Medicine*, 28(8):115 (**2017**). doi: 10.1007/s10856-017-5928-1

- J. Coletta, A. Ibáñez-Fonseca, L.R. Missana, M.V. Jammal, E.J. Vitelli, M. Aimone, F. Zabalza, J.P. Mardegan Issa, M. Alonso, J.C. Rodríguez-Cabello, S. Feldman. Bone regeneration mediated by a bioactive and biodegradable ECM-like hydrogel based on elastin-like recombinamers. *Tissue Engineering Part A* (**2017**). Ahead of print. doi: 10.1089/ten.tea.2017.0047

- A. Ibáñez-Fonseca, M. Alonso, F.J. Arias, J.C. Rodriguez-Cabello. FRET-paired hydrogel forming silk-elastin-like

recombinamers by recombinant conjugation of fluorescent proteins. *Bioconjugate Chemistry*, 28(3): 828–835 (**2017**). doi: 10.1021/acs.bioconjchem.6b00738

2016

- F.J. Arias, M. Santos, A. Ibáñez-Fonseca, M.J. Piña, S. Serrano. Elastin-like recombinamers as smart drug delivery systems. *Current Drug Targets*, 17:1-20 (**2016**) doi: 10.2174/1389450117666160201114617

2015

- J.C. Rodríguez-Cabello, M.J. Piña, A. Ibáñez-Fonseca, A. Fernández-Colino, and F.J. Arias. Nanotechnological Approaches to Therapeutic Delivery Using Elastin-Like Recombinamers. *Bioconjugate Chemistry*, 26(7):1252–1265 (**2015**), doi: 10.1021/acs.bioconjchem.5b00183.

- A. Girotti, D. Orbanic, A. Ibáñez-Fonseca, C. González-Obeso, J.C. Rodríguez-Cabello. Recombinant technology in the development of materials and systems for soft-tissue repair. *Advanced Healthcare Materials*, 4(16):2423-2455 (**2015**). doi: 10.1002/adhm.201500152.

Congresses and conferences

2017

- 28th Annual Conference of the European Society for Biomaterials (ESB), Athens (Greece). ORAL COMMUNICATION. Fluorescent hydrogel-forming silk-elastin-like recombinamers for improved traceability of biomedical devices.

- 6th China-Europe Symposium on Biomaterials in Regenerative Medicine (CESB2017), Porto (Portugal). ORAL COMMUNICATION. Development of FRET-paired hydrogel-forming SELRs.

2016

- XXXIX Congreso de la Sociedad Ibérica de Biomecánica y Biomateriales, León (Spain). ORAL COMMUNICATION. Compared biocompatibility of elastin-like recombinamer-based hydrogels formed through physical or chemical cross-linking.

- XIV Reunión del Grupo Especializado de Polímeros GEP (RSEQ, RSEF), Burgos (Spain). ORAL COMMUNICATION. Biocompatibility of hydrogels based on elastin-like recombinamers.

- European Chapter Meeting of the Tissue Engineering and Regenerative Medicine International Society 2016, Uppsala

(Sweden). ORAL COMMUNICATION. Bone regeneration of rabbit femur through the implant of a hydrogel based on novel bioactive elastin-like recombinamers (ELRs).

- 10th World Biomaterials Congress, Montréal (Canada). ORAL COMMUNICATION. 3D and 2D hMSCs spreading and proliferation in ECM-mimetic hydrogels based on elastin-like recombinamers. POSTER. Self-assembled ECM-like physically cross-linked hydrogels based on nature-derived recombinant biomaterials.

2015

- XXXIII Congreso Anual de la Sociedad Española de Ingeniería Biomédica, Madrid (Spain). ORAL COMMUNICATION. Regeneración ósea en fémur de conejo mediante el implante de una matriz bioactiva basada en recombinámeros de tipo elastina (ELRs).

- VI Congreso Iberoamericano de Ciencias Farmacéuticas, XLVII Reunión Científica Anual de la Sociedad Argentina de Farmacología Experimental y III Congreso Sudamericano de Biofarmacia y Farmacocinética, Córdoba (Argentina). ORAL COMMUNICATION. Terapia celular en medicina regenerativa: reparación del manguito rotador mediante la implantación *in situ* de ELR y rMSCs alogénicas.

- XXXII Reunión Anual de la Asociación Argentina de Osteología y Metabolismo Mineral, Sierra de la Ventana (Argentina). ORAL COMMUNICATION. Regeneración tisular ósea

mediante el implante de matriz obtenida por técnicas de ADN recombinante.

- 27th European Conference on Biomaterials of the European Society for Biomaterials, Krakow (Poland). ORAL COMMUNICATION. Fluorescent hydrogels for improved traceability of biomedical devices *in vivo*.

- XXXV Bienal de la Real Sociedad Española de Química, A Coruña (Spain). POSTER. Desarrollo de hidrogeles y nanopartículas fluorescentes.

2014

- 8vo Congreso Latinoamericano de Órganos Artificiales, Biomateriales e Ingeniería de Tejidos, Rosario (Argentina). POSTER. Hydrogels based on elastin-like recombinamers for bone regeneration.

- XXX Latinorum Investigatorum de Arteriis Colloquium, Valladolid (Spain). POSTER. Developing of a fluorescent silk-elastin-like recombinamer for enhanced tracking in tissue engineering applications.

- XXXVII Congreso de la Sociedad Ibérica de Biomecánica y Biomateriales, Madrid (Spain). ORAL COMMUNICATION. Síntesis de un recombinámero silk-elastin-like fluorescente para mejorar la trazabilidad de hidrogeles *in vivo*.

Other contributions

2016

- Co-supervision of the BSc thesis titled "Estudio de la degradabilidad de hidrogeles inyectables obtenidos a partir de biopolímeros de tipo elastina y con un alto interés en medicina regenerativa" by Edyta Penkiewicz in the Universidad de Valladolid (Spain).